MULTIPLE ENDOCRINE NEOPLASIA TYPE 2B: MODELLING THE DISEASE IN HUMAN CELLS AND AVIAN EMBRYOS

Kwaku Dad Abu-Bonsrah

Doctor of Philosophy

Generating human cell and avian models for the study of the pathogenesis of the MEN2B disease

Kwaku Dad Abu-Bonsrah

Submitted in total fulfilment of the requirements of the degree of Doctor of Philosophy to the Department of Paediatrics, The University of Melbourne

Supervisors: Dr. Donald Francis Newgreen & Dr. Mirella Dottori

Submission Date: 5th October 2017

ABSTRACT

Paediatric cancer initiation is difficult to study because the early stages are often prenatal. Patient cells at the time of detection already have complex genetic (including epigenetic) changes, and the cancer cell population is heterogeneous. One way to model cancer initiation at the organism level is to engineer the specific initiating mutation into the appropriate cell lineage of an experimental animal embryo. For the human cell context, an ideal cell model would start with the normal human cell of origin and create candidate initiating mutations.

Multiple Endocrine Neoplasia type 2B (MEN2B) is an autosomal dominant complex oncologic disease of the neural crest (NC) cell lineage, a so-called neurocristopathy. It presents with i) multiple mucosal ganglioneuromas including hyperplasia of the enteric (gut) nervous system leading to gastrointestinal disorders, ii) pheochromocytoma, with sympathoadrenal (SA) hyperplasia and catecholamine disturbance, and iii) medullary thyroid carcinoma with C-cell hyperplasia, elevated calcitonin and calcium metabolism disturbance. In addition, patients have marfanoid facial features. MEN2B results from de novo germline gain-of-function mutations in the gene *RET*, most often M918T. *RET* codes for the signalling receptor for the growth factor ligand GDNF, hence in MEN2B cells, *RET* signalling is divorced from GDNF availability. MEN2B is rare but it is often misdiagnosed especially early in life. This is due to the nature and diversity of the lineages affected; SA and enteric NC-lineage cells and thyroid C-cells, the latter being of foregut endodermal entero-endocrine lineage.

We were the first to successfully use CRISPR/Cas9 to mutate the developing chicken embryo in vivo, showing phenotypic abnormality. This included creating a single point mutation by homology directed repair in vivo in NC cells at the avian MEN2B homologous site (M910T).

For the human cell context, we combined the CRISPR/Cas9 technology and knowledge of embryo development and cell differentiation to create MEN2B M918T cells using the human embryonic stem cell (hESC) lines H9, HES3 and MEL2. We modified a hESC differentiation protocol to produce enteric NC-like cells, showing in vitro that these cells upregulated key NC and enteric genes. Functionally we also showed higher

proliferation and greater axon production in the MEN2B mutant cells: this is consistent with the ganglioneuroma phenotype. In addition, we developed a new differentiation protocol to produce human SA progenitors and medullary chromaffin-like cells, as marked by expression of key catecholamine genes TH and PNMT, and expression of adrenaline and noradrenaline by HPLC. These cells are affected in MEN2B patient pheochromocytoma. We then developed a novel differentiation protocol for thyroid C-cell-like cells from hESCs via Definitive Endodermal Cells. These cells produce Calcitonin and we validated their functionality by ELISA assay and compared the MEN2B clones with the control hESCs. These cells are affected in MEN2B patients resulting in medullary thyroid carcinoma.

LIST OF ABBREVIATIONS

β2M	Beta-2-microglobulin
BMP	Bone morphogenetic protein
CAM	Chorio-Allantoic Membranes
cDNA	Complementary DNA
CDKN1β	Cyclin Dependent Kinase Inhibitor 1B
CE8	Chick Embryonic day 8
CT	Threshold Cycle
DEPC	Diethyl pyrocarbonate
DGCR8	*DiGeorge syndrome* chromosomal [or critical] region 8
DM	Differentiation Medium
DMEM	Dulbecco's Modified Eagle's Medium
DNA	Deoxyribonucleic Acid
DNase	Deoxyribonuclease
EB	Embryoid Bodies
EDTA	Ethylenediaminetetraacetic acid
EZH2	Enhancer of zeste homolog 2
F-12	Ham's F12 medium
FBS	Foetal Bovine Serum
FGF	Fibroblast Growth Factor
FP	Forward Primer
GAPDH	Glyceraldehyde 3-phosphate dehydrogenase
hESC	Human Embryonic Stem Cell
HS	Horse Serum
IGF	Insulin-like growth Factor
iPSC	induced Pluripotent Stem Cells
IPTG	Isopropyl β-D-1-thiogalactopyranoside
ITS-A	Insulin-Transferrin-Selenium-Sodium Pyruvate
KO	Knockout
KSR	Knockout Serum Replacement
MEF	Mouse Embryonic Fibroblast
MBD3	Methyl-CpG-binding domain protein 3
NBM	Neurobasal Medium
NC	Neural Crest
NCPC	Neural Crest Progenitor Cell
NEAA	Non Essential Amino Acids
NGS	Normal Goat Serum
NSP	Neurospheres
OCT	optimum cutting temperature
CMF-PBS	Calcium-Magnesium Free Phosphate Buffered Saline
PCR	Polymerase Chain Reaction
PMA	Phorbol 12-myristate 13-acetate
PVA	Polyvinyl Alcohol
QE2	Quail Embryonic day 2
RA	Retinoic Acid
RNA	Ribonucleic Acid
RP	Reverse Primer
RPL32	Ribosomal Protein L32
RT-PCR	Real Time PCR
SAP	Sympathoadrenal Progenitors

sgRNA	Single guide RNA
SNP	single nucleotide polymorphism
ssODN	single-stranded oligodeoxynucleotides
TGFβ	transforming growth factor beta
TYRP1	Tyrosinase-related protein 1
Wnt	Wnt signalling pathway (Wingless-related integration site)

ACKNOWLEDGEMENTS

Above all praise is to God, the Almighty, on whom ultimately I depend and rely for grace to guide, sustain and urge me to succeed. Second, I am indebted to the International Postgraduate Scholarship and the Australian Postgraduate Award (International), now the Australian Government Research Training Program Scholarship, the MCRI Top Up Scholarship and the University of Melbourne for providing me with the opportunity to pursue my PhD studies and contributing to my career development. My deepest appreciation and immense gratitude then goes to my primary supervisor Dr. Donald Francis Newgreen for introducing me to the developmental biology (embryology) field, providing invaluable academic step-by-step guidance with full patience, and contributing to my personal and academic growth and helping to shape my career goals. I am also grateful to my co-supervisor: A/Prof Mirella Dottori for her immense support in the stem cells field and guidance during differentiation and also for providing the necessary equipment to make sure that my project did run very smoothly and also pushing my boundaries when the need arises. I would like to also thank my PhD advisory committee members: A/Prof Ed Stanley, Dr Gursharan Chana, and Dr Peter Farlie for their constructive advice and feedback throughout my PhD, and my laboratory mentors: Dr Dongcheng Zhang, for teaching me the essentials of embryo electroporation and graftings and also to Dr. Ben Rollo, Dr. Treve Menheniott, Dr Matthew Burton and Paul Lau, for their precious technical guidance and warm encouragements. Warm thanks also go to staff and my fellow students in the Embryology Department: Samiramis Ighaniyan, Centre for Neural Engineering: Ms Tejal Kulkarni, Ms Jan Barrett, Ms Serena Viventi, Ms Ting Ting, Ms Rachael Chatterton, Dr Ana Antonic, Ms Pegah Jamshidi, Dr Giovanna D'Abaco and several others for their support and sharing the experience. A special thanks goes to Jennifer Wintima Alenga (BA Political Science), Desmond Ofosu-Anim (Environmental Engineer), Richard Ofori-Asenso (Pharmacist), Akosua Adom (Pharmacist) and Edith Botchway (Neuropsychologist) for proof reading of my thesis. I wish to express my wholehearted gratitude to my family and friends, especially to my mother Stella Welbourne, my wife Jennifer Wintima Alenga and my son Delwinde Paa Kwasi Abu-Bonsrah, Delwinde's Godfamily Mr and Mrs Kwame Poku, without their

prayers, sacrifices, limitless support and constant encouragement, this would never have been achieved.

Last but not the least, I thank my reviewers for first agreeing and taking time despite their busy schedule to examine my PhD thesis.

PUBLICATIONS

Publications

Posters, Presentations and Awards

Kwaku Dad Abu-Bonsrah, Dongcheng Zhang, Donald F. Newgreen 2015. 'Efficient Genome Editing in Chicken by CRISPR-Targeted Homologous Recombination'.

Poster and a talk presented at the 48th Annual Meeting of the Japanese Society of Developmental Biology, Tsukuba, Japan.

Awarded the best student talk award.

Kwaku Dad Abu-Bonsrah, Dongcheng Zhang, Donald F. Newgreen 2016. 'Efficient Genome Editing in Chicken by CRISPR-Targeted Homologous Recombination'.

Poster presented at the Annual MCRI Student Symposium 2016, VIC, Australia.

Kwaku Dad Abu-Bonsrah, Dongcheng Zhang, Donald F. Newgreen 2016. 'Efficient Genome Editing in Chicken by CRISPR-Targeted Homologous Recombination'.

Talk presented at the ***Avian Model Systems 9*** conference, Taipei, Taiwan.

Awarded the best talk for students and early career research category.

Kwaku Dad Abu-Bonsrah, Dongcheng Zhang, Donald F. Newgreen 2016. 'Efficient Genome Editing in Chicken by CRISPR-Targeted Homologous Recombination'.

Poster presented at the Annual Australian Society for Medical Research (ASMR) Student Symposium 2016, VIC, Australia.

Publications

Zhang D, Osborne JM, **Abu-Bonsrah KD** (**Kwaku Dad Abu-Bonsrah**), Cheeseman BL, Landman KA, Jurkowicz B, Newgreen DF. 'Stochastic clonal expansion of "superstars" enhances the reserve capacity of enteric nervous system precursor cells'. Developmental Biology 2018

Kwaku Dad Abu-Bonsrah, Dongcheng Zhang, Mirella Dottori, Andrew Bjorksten, Donald F. Newgreen. 'Generation of Functional Adrenal Chromaffin-like Cells from Human Pluripotent Stem Cells'. Stem Cells Reports, 2018

Kwaku Dad Abu-Bonsrah, Dongcheng Zhang, Donald F. Newgreen. 'CRISPR/Cas9 Targets Chicken Embryonic Somatic Cells In Vitro and In Vivo and generates Phenotypic Abnormalities'. Scientific Reports, 2016

Cho HM, Kim PH, Chang HK, Shen YM, Bonsra K (**Kwaku Dad Abu-Bonsrah**), Kang BJ, Yum SY, Kim JH, Lee SY, Choi MC, Kim HH, Jang G, Cho JY. 'Targeted Genome Engineering to Control VEGF Expression in Human Umbilical Cord Blood-Derived Mesenchymal Stem Cells: Potential Implications for the Treatment of Myocardial Infarction.' Stem Cells Transl Med, 2017

Dad AB (**Kwaku Dad Abu-Bonsrah**), Ramakrishna S, Song M, Kim H. 'Enhanced gene disruption by programmable nucleases delivered by a minicircle vector.' Gene Therapy, 2014

Ramakrishna S, Kwaku Dad AB (**Kwaku Dad Abu-Bonsrah**), Beloor J, Gopalappa R, Lee SK, Kim H. 'Gene disruption by cell-penetrating peptide-mediated delivery of Cas9 protein and guide RNA.' Genome Research, 2014

TABLE OF CONTENTS

LIST OF FIGURES

both MEN2B clones (significant in the 2B6 clone) with an increase in TUBB3 expression only in the 2B6 clone. The expression of RET and PTEN remained unaltered with a slight decrease in CASP3 and CASP8 expression in both clones. Both clones had an increased expression of TOP2α mRNA expression. (B) Representative FACs plots show the high percentage of PI+ cells in the MEN2B clones when differentiated by RA only than the controls but this reduces more than 1.5-fold as compared to the controls when GDNF is added during differentiation. Cumulative graph showing the percentage of decrease after the addition of GDNF to the differentiation mix and a qPCR analysis showing the upregulation of apoptotic markers, CASP3 and CASP8 in RA only treated conditions as compared to RA plus GDNF conditions. N = 3 independent experiments; error bars represent mean ± SEM. ns- Not significant, *P < 0.05, **P < 0.01, ***P < 0.001, ****P < 0.0001…….132

LIST OF TABLES

PREFACE

Several others have contributed to the work described in this thesis. General contributions include:

- Dr Dongcheng Zhang assisted with the embryo electroporation, transplantations and CAM graftings in Chapter 3 and 4.
- A/Prof Andrew Bjorksten at the Department of Anaesthesia and Pain Management, The Royal Melbourne Hospital performed the HPLC analysis of the hESC-derived adrenal chromaffin-like cells in Chapter 4.
- Emily Gilbert did the RA concentration optimisation for the Vagal Neural Crest-like Cells differentiation from hESCs.
- A/Prof Alice Pebay provided control iPSC line 007.
- Ms Tejal Kalkarni, Ms Rachael Chatterton and Ms Pegah Jamshidi maintained iPSC lines.

DECLARATION

This is to certify that:

(I) This thesis comprises only my original work towards the PhD except where indicated in the preface,

(II) Due acknowledgement has been made in the text to all other material used,

(III) This thesis is fewer than 100,000 words in length, exclusive of tables, bibliographies and appendices.

1 LITERATURE REVIEW

1.1 Introduction

1.1.1 Neural Crest

During development, gastrulation gives rise to three germ layers-endoderm, mesoderm and ectoderm; to which the ectoderm is further subdivided into the neural and non-neural epidermal ectoderm. The laterally placed epidermal ectoderm develops into the skin, dermis and placodes whilst the medially placed neural ectoderm will give rise to the central nervous system (CNS). The region between the neural and epidermal domains is the neural border where progenitor cells are capable of differentiating into epidermal cells, craniofacial placodal cells, sensory neurons of the CNS (Groves and LaBonne 2014) and also into neural crest (NC) cells (Selleck and Bronner-Fraser 1995). NC cells are multipotent stem cells with a vast range of options for differentiation. NC cells differentiate to produce connective tissue including cartilage (cranial NC only) and most of the cells of the peripheral nervous system (PNS) (Le Douarin 1982; Le Douarin and Smith 1988). The PNS includes the sensory ganglia (e.g. cranial ganglia and dorsal root ganglia) and the autonomic nervous system (ANS). The largest division of the ANS is the enteric nervous system (ENS) (Yntema and Hammond 1954; Le Douarin and Teillet 1973; Sasselli et al. 2012) in the wall of the gastro-intestinal tract and comprising at least 15 types of neurons and 3 types of glia cells (Furness 2000). The ANS also includes the parasympathetic and sympathetic systems, the latter including catecholaminergic neurons and non-neuronal but biochemically related adrenal chromaffin cells (Chung et al. 2009; Furlan et al. 2017).

The specification of the NC within the ectoderm is governed by a gene regulatory network with Sox10 and FoxD3 playing an important role in the homeostatic regulation of self-renewal and differentiation (Kim et al. 2003; Mundell and Labosky 2011). The genes of this network are induced shortly after gastrulation by an interplay of patterning signals like the BMPs, FGFs, Wnt, RA and Delta-Notch which are involved in the specification and differentiation of NC (Mead and Yutzey 2012; Milet and Monsoro-Burq 2012; Stuhlmiller and Garcia-Castro 2012a; Stuhlmiller and Garcia-Castro 2012b).

During the early stages of development there are also major morphogenetic movements, and the neural plate epithelium rolls up to form the neural tube and the previously lateral epidermal domain now lies dorsal to the neural tube. After the initial specification, NC cells delaminate from the region between the dorsal neural tube and

overlying epidermal domain, by undergoing an epithelial-to-mesenchymal transition (EMT). These EMT cells migrate out towards the periphery along specific paths. Interaction of NC cells with cells and molecules on these paths are important in guiding their migration and in determining their later cell fates (Huang and Saint-Jeannet 2004; Gammill and Roffers-Agarwal 2010; Lim and Thiery 2012). The growth factors exposure includes the same factors involved in the initial specification. Knowledge of these factors and the sequence and timing of exposure derived from studies of normal development is crucial in designing induction protocols for NC-like cells from human pluripotent stem cells (Lee et al. 2007; Denham and Dottori 2011; Denham et al. 2015).

1.2 Multiple Endocrine Neoplasia

Multiple endocrine neoplasia (MEN) syndromes are autosomal dominant diseases that are categorised based on the germ-line inactivating mutations of the menin 1 gene (MEN1) of chromosome 11q13 or the germ-line activating mutations of the MEN 2 gene which was reported by genetic linkage analysis to be localised to the centromeric region of chromosome 10 in 1987 (Mathew et al. 1987). In 1993, Ponder's group reported activating germline point mutations of the *RET* (REarranged during transfection) proto-oncogene as causative events in MEN2A and Familial Medullary Thyroid Carcinoma (FMTC) (Mulligan et al. 1993*)* whilst in 1994, two different groups reported other mutations in *RET* as causative events in MEN2B (Eng et al. 1994; Hofstra et al. 1994). MEN syndromes as their name suggests involves the occurrence of tumours (neoplasia) in two or more endocrine tissues in a single patient and although these syndromes are known to be rare hereditary complex disorders, some cases arise as a result of spontaneous new mutations (sporadic form of disease) in the genes involved (Sakorafas et al. 2008; Wells et al. 2013). Although FMTC involves only one endocrine tissue, it is allied to MEN2 genetically because MTC occurs in both MEN2A and 2B.

The MEN2 subtypes including FMTC can be differentiated based on the mutated gene or nucleotide (genetics), age of onset, association with other diseases, aggressiveness of MTC, prognosis and sometimes the presence or absence of hyperparathyroidism (HPT) (Kouvaraki et al. 2005; Raue and Frank-Raue 2007; Raue and Frank-Raue 2009). The prevalence of MEN2 has been estimated to be 1:30,000 with MEN2A accounting for more than 80% of the cases; however, morbidity and mortality rates are higher in MEN2B patients (Marini et al. 2006). MEN2 can be diagnosed following the detection

of one or more MEN-related tumours (Medullary Thyroid Carcinoma (MTC), Pheochromocytoma (PHEO), primary Hyperparathyroidism (pHPT)) or by clinical features, especially in patients with MEN2B (Taieb et al. 2014). However, in the absence of a revealing tumour, acetylcholinesterase study of rectal mucosa and molecular analysis of *RET* on patients presenting with persistent gastrointestinal problems after only a few weeks of life serves as a standard diagnostic tool to detect potential *RET* mutations and thus the early diagnosis of MEN2B cases (Martucciello et al. 2012).

MEN2, an autosomal dominantly inherited cancer syndrome, was found to arise from and affect neural ectodermally derived tissues, specifically from the NC (Mulligan et al. 1993). However, recent findings on the derivation of thyroid C cells from foregut endoderm makes this syndrome a more complicated one in terms of cell lineage with further studies needed to fully understand its pathogenesis (Johansson et al. 2015; Kameda 2016).

Table 1. Molecular genetics, risk factor, and management of patients with different *RET* mutations. Table was modified from (Eng et al. 1996; Kouvaraki et al. 2005; Moore and Zaahl 2008; Raue and Frank-Raue 2009) and from www.cancer.net

Codon	609, 649, 768, 790, 791, 804, 891	611, 618, 620, 630, 631, 634	883, 918, 922
Risk Level (American Thyroid Risk Assessment)	1 (A, B, C)	2 (A, B, C)	3 (D)
MTC aggressiveness (cases)	High (100%)	Higher (98-100%)	Highest (98-100%)
MEN2 subtype	FMTC	MEN2A	MEN2B
Age of onset	Adults (>3-5 years)	>3-5 years	<1 year
Other endocrine tumours	Rarely	pHPT (5-10%), PHEO (50%)	PHEO (50%)
Other related features	Rarely	Hirschsprung's disease (50%) (Butter et al. 2007) Cutaneous Lichen Amyloidosis	Marfanoid Habitus (75-90%) Intestinal neuromas (Ganglioneuromatosis) (75-90%) Mucosal ganglioneuromas (95-98%) Muscle, joint, and spinal problems (95%)
Serum Calcitonin	>3-5 years	>3-5 years	Immediately
Prophylactic Thyroidectomy	5-10 years	Before or at 5 years	Immediately (preferably in the first months of life)

Despite all efforts towards improving the management of MEN2, the condition is still an underdiagnosed, or late diagnosed disease in many parts of the world. The pathogenesis of the disease has received less attention and thus less is known about it. Presently, molecular DNA diagnosis to identify *RET* mutations is mandatory for all MEN2 cases and for their relatives at risk for a predisposition to MEN2 (Toledo et al. 2006). This diagnostic procedure is progressively becoming a fundamental tool in early MEN2 diagnosis, enabling the currently most appropriate therapeutic and surgical management (Wells and Franz 2000). However, many cases of MEN2 are "sporadic" or apparently *de novo*, that is, the disease is found in individuals without any family history. This is reported in more than 50% of MEN2B patients, with 15% *de novo* cases reported in MEN2A patients and 10% in FMTC patients (Taieb et al. 2014). In these patients, the chance of an early diagnosis can be missed as there is no familial history until the onset of the disease. Early diagnosis is especially important for MEN2B which shows the earliest signs of malignant progression of MTC.

1.3 MEN Syndromes

1.3.1 Medullary Thyroid Carcinoma (MTC)

MTC results from a mutation in the *RET* gene (Nikiforov 2008; Lin 2011; Waguespack et al. 2011), contributes to about 5% of thyroid cancers and originates from the parafollicular cells (thyroid C cells) of the thyroid gland. This is known to be the first clinical manifestation reported in most patients because the gastrointestinal disturbances in MEN2B are usually missed (Brandi et al. 2001; King et al. 2006; Marini et al. 2006). Parafollicular C cells arise from the ultimobranchial cyst or body (UBB) during embryonic development of the foregut endoderm (Johansson et al. 2015) and differentiate into functional C cells once the UBB fuses with the thyroid primordium (Kusakabe et al. 2006; Kameda et al. 2007a). The C cells produce calcitonin, a hormone that regulates Ca^{2+} metabolism by lowering blood Ca^{2+} levels (Hazard 1977; Frendo et al. 1998), in opposition to the effects of Parathyroid Hormone (PTH; see below) (Poole and Reeve, 2005). C cell hyperplasia leads to an elevated levels of calcitonin and CGRP, as both are encoded by the same gene, causing diarrhoea, flushing, and itching (pruritis) in the affected patients (Lee and Norton 2000; Reich and Szepietowski 2007; Murota and Katayama 2017). C cell hyperplasia which is the increased number of

diffusely scattered C cells transforms over time to MTC with a distinct appearance of nests of C cells which infiltrates and distorts the thyroid follicles in the thyroid gland (Marini et al. 2006; Moline and Eng 2011). Total thyroidectomy is the treatment of choice after calcitonin evaluation of fine-needle biopsy to confirm MTC (Marini et al. 2006; Balachandran et al. 2013; Taieb et al. 2014).

1.3.2 Hyperparathyroidism (HPT)

Hyperparathyroidism is a benign tumour of the parathyroid gland due to hyperplastic process of parathyroid chief cells. This hyperplastic process involves the 4 parathyroid glands (multiple tumours) and precedes adenoma formation (Kouvaraki et al. 2005). In some patients it is recorded that both the hyperplasia and ademona may co-exist (Alevizaki 2013). The majority of HPT cases associated with MEN2A are commonly linked to exon 11 mutations specifically with the 634 codon mutation (C634R). Other mutations like codons 611, 618, and 620 on exon 10 have also been associated with HPT (Kraimps et al. 1996; Karga et al. 1998; Raue and Frank-Raue 2009). The parathyroid gland secretes parathyroid hormone (PTH) and hyperplasia of the parathyroid glands leads to overproduction of the hormone. Patients with HPT presents with slightly elevated blood calcium concentrations as well as higher blood levels of PTH. Most cases are initially asymptomatic and if not diagnosed early, these patients present with kidney stones and osteoporosis (Toledo et al. 2006). Total parathyroidectomy are usually performed when all 4 parathyroid glands are involved with autotransplantation in a nondominant forearm. On the other hand, partial or subtotal parathyroidectomy is the removal of only the affected gland (Toledo et al. 2006; Alevizaki 2013).

1.3.3 Pheochromocytoma (PHEO)

PHEO is a benign tumour of the NC-derived autonomic nervous system which involves mainly chromaffin cell hyperplasia of the adrenal gland. PHEO also develops in extra-adrenal medullary tissues such as the organ of Zukerkandl and they are referred to as extra-adrenal PHEO or paragangliomas (Neumann et al. 2002; Bryant et al. 2003; Lenders et al. 2005; Kahraman et al. 2011). These arise from the sympathetic nervous system or parasympathetic ganglia and are located at the head, neck (Whalen et al. 1992; Pacak et al. 2001) and mainly the abdomen (Erickson et al. 2001; Lenders et al.

2005). PHEO is a secondary characteristic feature of both MEN2A and MEN2B in humans with about 50% of patients developing PHEO although it is asymptomatic in most cases (Smith-Hicks et al. 2000; Pacak et al. 2001). Nevertheless, the chromaffin cell hyperplasia can result in over-activity of the 'fight-or-flight' response via release of excess catecholamines and metabolites. This can manifest as elevated blood pressure, fast/irregular heart rhythm and tremor. Currently, due to the risk of intraoperative hypertensive crisis, patients with MEN2B undergo assessment and screening for biochemical parameters to rule out PHEO before undergoing MTC thyroidectomy (Longo 2012; Balachandran et al. 2013). PHEO cases in MEN2B is categorised to be of a genetic (familial) predisposition but most cases of PHEO previously recorded have been sporadic cases. The former, however, has recently been suggested to be more frequent than sporadic cases (Pacak et al. 2001; Neumann et al. 2002; Bryant et al. 2003).

1.3.4 Intestinal Ganglioneuromas

Functional impairment of the intestine is the prominent and first feature of MEN2B and this occurs usually in the first weeks of life. In most cases, this is before the endocrine neoplasms manifest. Most patients describe constipation with alternating diarrhoea with other types of manifestations including projectile vomiting, abdominal pain and cramping, diverticulosis present in descending and sigmoid colon, and megacolon in severe cases. Despite their importance as the earliest diagnostic opportunity for detecting MEN2B, the nonspecific nature of these early intestinal symptoms is often ascribed to MEN2B only in retrospect. The release of humoral factors such as calcitonin by the hyperplastic C-cells is referenced as the cause of diarrhoea in these patients (Saad et al. 1984), but the role of dysfunction of the enteric nervous system (ENS) may also be involved.

Ganglioneuromatosis affects the entire gastrointestinal tract, from the oral cavity to the rectum (Lee and Norton 2000). In the oral cavity on the mucosal surface of the lips and on the tongue, multiple mucosal pseudo-polyps and bumps become progressively evident as a result of multiple ganglioneuromas (GN)/ganglioneurofibromas (GNf) (Sipple 1961; Brandi et al. 2001; Engiz et al. 2009; Martucciello et al. 2012). The ganglioneuromatosis of the ENS is marked by increased proliferation or hyperplasia of ganglion cells with hypertrophy and disorganization of the myenteric and submucosal

plexus (Yin et al. 2012). This causes defective peristalsis and poor contractility (Carney et al. 1976), and total intestinal obstruction as a result of a giant colonic ganglioneuroma occurs but is rare (Shocket and Teloh 1957; Moore and Zaahl 2008). These intestinal transit symptoms are similar to patients with Hirschsprung disease which is due to a defect in the *RET* gene in many cases (Amiel et al. 2008). The mutations in *RET* causing Hirschsprung disease leads to a loss-of-function of *RET* and thus the absence of intestinal ganglia. In contrast MEN2B-mutations provide a gain-of-function for *RET* leading to uncontrolled cellular proliferation (Pasini et al. 1995; Romeo et al. 1998).

1.4 Structure and Functions of the *RET* Gene and Protein

RET is a proto-oncogenic gene which encodes a receptor tyrosine kinase and has been mapped on chromosome 10q11.21 (Takahashi et al. 1989; Cote et al. 1995; Eng et al. 1996). The *RET* gene has 21 exons which encodes about 1096 amino acids which is translated into a transmembrane membrane protein serving as a receptor for members of the glial cell line-derived neurotrophic factor (GDNF) family of extracellular signalling molecules and its congeners neurturin, persephin and artemin. It forms part of a multicompetent receptor complex with other free and membrane-bound ligand-binding GDNF family co-receptors (GFRα1-4). The product of the *RET* gene is a transmembrane receptor protein which is made up of three functional domains, an extracellular domain with four cadherin-like repeats, a cysteine-rich region, and an intracellular tyrosine kinase region. The *RET* receptor encodes multiple tyrosine sites that upon phosphorylation regulate cell survival, proliferation, motility (via lamellipodia), chemotaxis and differentiation signals in early stage of embryonic development (Figure 1.1) (Murakumo et al. 2006).

There are 3 different isoforms of the protein *RET* after natural alternative splicing of the *RET* gene- *RET*51, *RET*43 and *RET*9 and these contain 51, 43 and 9 amino acids in their C-terminal tail, respectively (Myers et al. 1995). However, in human malignant cell lines and rat tissues, the *RET* proto-oncogene expresses four major mRNA species of different lengths which differ from each other in their 3' portions as a result of alternative polyadenylation and splicing of the mRNA (Tahira et al. 1990). *RET*9 and *RET*51 are the main isoforms synthesised in most cells and as such their biological roles are the most well studied *in vitro* and *in vivo* (Ichihara et al. 2004; Murakumo et al. 2006).

The *RET* gene was initially categorised as an oncogene but several additional and important functions during embryonic development and disease have since been discovered; ENS development, ureteric bud development, embryonic epithelial tube formation, neuron adhesion, NC cell migration and chemotaxis, caspase activation and posterior midgut development; (Pachnis et al. 1993; Avantaggiato et al. 1994; Tsuzuki et al. 1995; Trupp et al. 1997; Hearn et al. 1998; Young et al. 2001; Young and Newgreen 2001).

1.4.1 Molecular Genetics of MEN2

Mutations causing MEN2A are mostly found in the extracellular cysteine-rich 5' region domain of the *RET* gene. MEN2A patients have been identified to have *RET* missense mutations mainly in one of the six cysteine residues, 609, 611, 618 and 620 at exon 10 and 630 and 634 at exon 11 (Figure 1.1); all of which reside in the extracellular cysteine-rich domain with cysteine residue, codon 634 mutation representing approximately 85% of cases observed in MEN2A patients (Ichihara et al. 2004). The codon 634 mutation, particularly C634R, is associated with PHEO and/or primary HPT and has also been associated with about 30% of FMTC cases where FMTC cases in general are known to be distributed among the six cysteine residues. On the other hand, missense mutations in the intracellular domain of *RET*, such as codons 768, 790 and 791 at exon 13, codons 804 and 844 at exon 14 and codon 891 at exon 15 have been recorded in FMTC and some rare cases of MEN2A (Bolino et al. 1995). Contrastingly, most mutations causing MEN2B, if not all, are found in the intracellular tyrosine kinase receptor domain of the *RET* gene with more than 95% cases harbouring the M918T mutation at exon 16 and about 2-3% harbouring the A883F mutation at exon 15 (Table 1) (Marini et al. 2006; Toledo et al. 2006). About 30% cases of sporadic MTC tumours have been associated to the M918T MEN2B mutation whereas this is rare in the case of MEN2A-like mutations (Eng et al. 1994).

The missense mutations of MEN2A cases (also found in some FMTC patients) lead to the loss of one of the six cysteines localized in the extracellular domain. This impairment results in the atypical intra- or intermolecular disulfide bonds in the mutant protein as these cysteine residues are important in the formation of the tertiary structure of the RET protein. This bonding causes homodimerisation of the *RET* gene resulting in high levels of intrinsic tyrosine phosphorylation thereby constitutively activating the

RET protein (Asai et al. 1995; Coulpier et al. 2002). Missense mutations of MEN2B cases on the other hand do not lead to homodimerisation of the RET protein as their mutation is outside the cysteine rich region; methionine is substituted at codon 918 to threonine in the tyrosine kinase domain which is the activation loop of the RET protein (Hofstra et al. 1994; Asai et al. 1995). Although this mutation also leads to activation of intrinsic tyrosine kinase thereby constitutively activating *RET*, it is not as potent as MEN2A. This implies that the MEN2B mutation is much more than simply an activated *RET* Kinase as it is for MEN2A. The mutation rather alters the autophosphorylation sites and shifts the pattern of the intracellular proteins affecting selection of substrate (Hofstra et al. 1994; Liu et al. 1996). The increased autophosphorylation sites like Y1062 leads to the recruitment of the Shc adapter initiating further downstream signalling promoting cell survival, proliferation and differentiation (Coulpier et al. 2002; Murakumo et al. 2006).

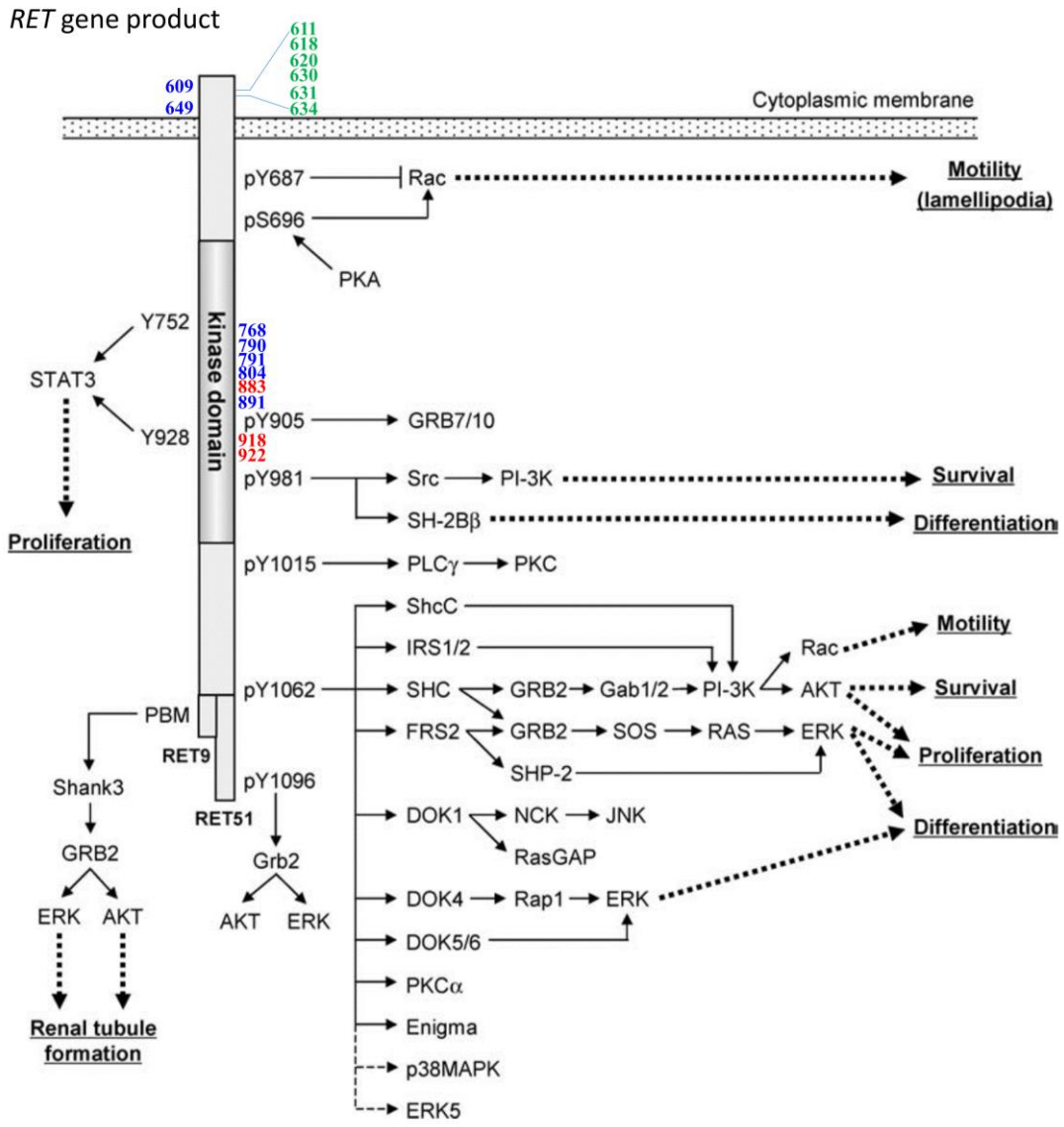

Figure 1.1 Intracellular signalling pathways mediated by *RET*. The "p" before amino acid residues means "phosphorylated". MEN2A, MEN2B and FMTC mutated codons are in green, red and blue respectively. Figure taken and modified from Murakumo et. al, 2006 (Murakumo et al. 2006)

1.5 Pluripotent stem cells

A cell that has the capability to self-renew, and to make cells from all three basic body (or germ) layers (ectoderm, mesoderm and endoderm) and to potentially produce any cell or tissue the body needs to construct and repair itself is termed as Pluripotent Stem Cell (PSC). PSCs cannot however form all extra-embryonic cell types. This state in development is not permanent but with recent research, PSCs can be isolated from early embryos and with the right supplementation of growth factors and culture conditions, they can be artificially maintained in a self-renewal state (Laslett et al. 2003; Draper et al. 2004; Hoffman and Carpenter 2005). The state of pluripotency is regulated by a

network of transcription factors namely OCT4 (POU5F1), SOX2, and NANOG (Boyer et al. 2005). Apart from these transcription factors, the pluripotency of PSC can be confirmed by cell surface markers like SSEA-4 (Rao et al. 2007), *in vitro* differentiation to all three embryonic germ lineages, whether they will form teratomas (tumor with tissue or organ components resembling normal derivatives of more than one germ layer) *in vivo* and whether they can contribute to chimera formation (De Los Angeles et al. 2016). PSC are categorised into two major types; embryonic stem cells (ESC) and induced pluripotent stem cells (iPSC). ESCs are derived from totipotent cells of the early mammalian embryo and are mainly isolated from the inner cell mass of blastocysts (Thomson et al. 1998). IPSC are somatic cells reprogrammed to pluripotency by forced expression of pluripotency transcription factors (see below) (Takahashi and Yamanaka 2006). The capabilities of PSC makes the hPSC a very important tool for the study of human development and establishing disease models *in vitro*, paving the way for better drug development.

1.5.1 Human Embryonic Stem Cells, hESC

The first hESC was derived by James A. Thomson (Thomson et al. 1998) from a donated human blastocyst generated by *in vitro* fertilization in 1998. Further work has standardised and made the derivation and maintenance of hESC more robust and efficient (Cowan et al. 2004; Mai et al. 2007; Bradley et al. 2016). These established hESCs have been confirmed for their pluripotency as assessed by multiple assays and their capability to differentiate into cell derivatives of all three germ layers when grown in required growth factors and supplements. In the field of regenerative medicine, hESCs are of great importance as they have demonstrated the differentiation ability of hESC to various disease-relevant cell types and in cell replacement therapies including spinal cord injury, macular degeneration and others (Kao et al. 2008; Paspala et al. 2011; Zhu et al. 2012b; Liu et al. 2013; Rajamohan et al. 2013; Wang et al. 2013a; Kimbrel and Lanza 2015; Pen and Jensen 2017).

The pluripotency state of hESC is maintained via signalling pathways regulated by OCT4, SOX2 and NANOG (Boyer et al. 2005). These pathways include the TGF-β (Tumour Growth Factor beta) pathway which promotes NANOG and OCT4 expression via SMAD2/3 whiles suppressing differentiation by inhibiting BMP signalling via SMAD1/5/8. FGF signalling activates some canonical pathways involved in

pluripotency including PI3K/Akt (Phosphoinositide 3-kinase/Protein Kinase B), MAPK/ERK (Mitogen-activated protein kinases/ Extracellular signal–regulated kinases), Wnt (int/Wingless family), and IGF (Insulin-like Growth Factor) through activation of PI3K pathway (James et al. 2005; Vallier et al. 2005; Xu et al. 2005; Bendall et al. 2007; Vallier et al. 2009). Other variables like epigenetic modifications (DNA methylation, histone modifications and chromatin structure) and microRNAs also regulates the maintenance of pluripotency (Bernstein et al. 2003; Hattori et al. 2004; Tsuji-Takayama et al. 2004).

The traditional method for maintaining hESCs is culturing them on mouse embryonic fibroblasts (MEF) grown on gelatin-coated surfaces and maintained in culture medium containing Fetal Bovine Serum (FBS). Maintaining the genetic stability of hESCs is very important and studies show that routine dissection of undifferentiated areas and manual transfer for subsequent passage is an adequate culture condition for hESCs (Thomson et al. 1998; Reubinoff et al. 2000). Some concerns have been raised regarding the variability and labour intensive aspects of this method and most importantly xeno-contamination. In view of that, the need has arisen for feeder-free, xeno-free culture conditions and also using serum-free chemically defined culture medium (Cobo et al. 2008). To avoid the undefined and variable FBS component, Knockout Serum Replacement (KSR) is currently used, supplemented with FGF (Thomson et al. 1998; Schwartz et al. 2011; Kaur et al. 2013). Many laboratories developed multiple maintenance conditions involving extracellular matrix proteins such as matrigel, fibronectin, laminin or vitronectin combined with chemically defined media, such as E8 medium (Stem Cell Technologies) and mTeSR medium (Stem Cell Technologies) with or without additional growth factor supplementation such as FGF; to establish adequate environments for the culture of hESC. Currently, the use of vitronectin substrates combined with either E8 or mTeSR media has been found to be effective in maintaining hPSC for over 30 passages (Braam et al. 2008; Chen et al. 2011; Wang et al. 2013b; Badenes et al. 2015; Badenes et al. 2016).

1.5.2 Human Induced Pluripotent Stem Cells, iPSCs

There are many technical limitations and ethical issues associated with hESC derivation (Lo and Parham 2009) and as such an alternative approach to studying pluripotency was very much sought after. This alternative approach will also offer great advantages to the

study of diseases and further provide an advanced platform for drug testing using patient-derived iPSC. This was not achieved until 2006 when Takahashi and Yamanaka identified four transcription factors OCT4, SOX2, KLF4, and cMYC (now referred to as Yamanaka Factors or OSKM) which when overexpressed in mouse fibroblasts induces a mesenchymal-to-epithelial transition, inducing pluripotency in these cells (Takahashi and Yamanaka 2006). Not long after the release of this finding, others have demonstrated the generation of iPSCs from human fibroblasts. These iPSCs show similar characteristics to hESC in terms of morphology, gene expression of pluripotency markers and the capability to differentiate *in vitro* to cell types of all three germ layers and also to form teratomas *in vivo* (Takahashi et al. 2007; Yu et al. 2007; Park et al. 2008). To improve the efficiency of reprogramming, a lot of research has been done to finely adjust the pluripotency transcription factors with other epigenetic regulating factors as a cocktail (Nakagawa et al. 2008; Wernig et al. 2008; Nakagawa et al. 2010). Others have generated iPSC from cell types including peripheral blood, keratinocytes, pancreatic B cells and neural progenitor cells (Aasen et al. 2008; Shi et al. 2008; Stadtfeld et al. 2008; Loh et al. 2009). Since hiPSCs are similar to hESCs, in order to support their pluripotency and self-renewal capacity the same culture conditions for hESCs are used to maintain and expand hiPSCs.

The first reprogramming studies done by Yamanaka and others used viral based systems including retroviral and lentiviral vectors to generate iPSCs. However, for major safety concerns of viral transgenic genomic integrations and potential mutagenesis and tumorigenicity (Okita et al. 2007), reprogramming using non-integrating episomal vectors, preferably Sendai virus, have been widely adopted as a preferred method for iPSC induction (Fusaki et al. 2009; Yu 2009; Yu et al. 2009; Zhang et al. 2009; Malik and Rao 2013). Others include piggyback transposition viruses (Kaji et al. 2009), excisable lentivirus (Soldner et al. 2009) and RNA based system (Warren et al. 2010; Schlaeger et al. 2015). On the other hand, direct delivery of transcription factor proteins has been achieved using lipofectamine, nanoparticles and electroporation (Bhise et al. 2013; Schlaeger et al. 2015).

Although studies confirm some overlapping variations with no marked differences between hESC and hiPSC (Guenther et al. 2010; Newman and Cooper 2010; Bock et al. 2011; Koyanagi-Aoi et al. 2013), other studies point to differences between hESC and hiPSC not only in the DNA methylation pattern but also in differentiation potential, and gene expression (Chin et al. 2009; Doi et al. 2009; Lister et al. 2011; Kyttala et al.

2016). Thus the variability and differences between hESC and hiPSC are very controversial (Liang and Zhang 2013; Carcamo-Orive et al. 2017; Kilpinen et al. 2017). A typical variability is the bias of some hESCs and hiPSCs towards a specific lineage in differentiation (Osafune et al. 2008) and these have been attributed to long-term maintenance in culture with hESCs (Baker et al. 2007) and to a number of factors including differentiation protocols, donor based differences (Kim et al. 2011; Kajiwara et al. 2012) and residual epigenetic memory of tissue of origin (Kim et al. 2010). In a nutshell, this shows the need for a careful design of experiments and rigour in handling of hPSCs. This applies to both hESCs and hiPSCs with much emphasis on hiPSCs in the aspect of disease modelling where the need for generation of several cell lines from patients with their corresponding controls are needed in order to attain concrete findings and conclusions relevant to the disease of interest.

1.6 Gene Editing

Around the second half of the twentieth century, alteration of the genome became possible with the arrival of molecular biology and this has seen rapid progress to date (Capecchi 2005; Berg and Mertz 2010). In particular, the laborious technique, cost ineffective aspect, variability and time consumption involved to generate even one transgenic animal is now much more efficient, cost effective and time saving with the advent of programmable engineered nucleases (PENs) (Durai et al. 2005; Christian et al. 2010; Miller et al. 2011; Skarnes 2015).

PENs are novel technologies developed to efficiently target and modify a specific allele in the genome by deleting nucleotides generating a knockout of that specific gene; or, with the presence of a DNA donor generating a mutation of interest or inserting a gene of interest in the genome. These PENs, the zinc finger nucleases (ZFNs), the transcription activator-like effector nucleases (TALENs) and the clustered regular interspaced palindromic repeats (CRISPR)/Cas9 system, have been used extensively in generating and correcting mutations in cells of plants (Zhang et al. 2010b; Zhang et al. 2013; Shan et al. 2014), humans (Carroll 2008; Hockemeyer et al. 2011; Cong et al. 2013; Hou et al. 2013; Mali et al. 2013; Yang et al. 2013; Ma et al. 2017), rodents (Geurts et al. 2009; Goldberg et al. 2010; Brown et al. 2013; Davies et al. 2013; Shao et al. 2014; Zhang et al. 2014b), monkeys (Shen 2013; Niu et al. 2014), fish (Ekker 2008; Huang et al. 2011; Auer and Del Bene 2014; Ota et al. 2014; Shin et al. 2014), chicken (Park et al. 2014; Veron et al. 2015; Abu-Bonsrah et al. 2016), fly (Bibikova et al. 2003;

Bassett and Liu 2014; Gokcezade et al. 2014) and worm (Wood et al. 2011; Chen et al. 2013) *in vitro* and *in vivo*, to generate transgenic cells, animals and plants.

1.6.1 CRISPR/Cas9 Gene Editing

CRISPR was discovered in 2012 as an immune defence in bacterium *Streptococcus pyogenes* against viral attack and was adapted as a PEN system for gene editing (Jinek et al. 2012). There are two elements that constitute this system; the CRISPR RNA and the CRISPR-associated protein (Cas9) which is an endonuclease. In *S .pyogenes*, the CRISPR RNA component has two types of RNA; the trans-activating, tracrRNA and the targeting crRNA which forms a base-paired structure which has now been combined into one single guide RNA (sgRNA) or guide RNA (gRNA) (Jinek et al. 2012; Ran et al. 2013) (Figure 1.2). The sgRNA forms a complex with the Cas9 enzyme and guides the Cas9 to its predetermined genomic DNA target to form a heteroduplex where the Cas9 initiates a double-strand cut or break (DSB) at the target site. DSBs in the genome are repaired by the same inbuilt cellular repair pathways, non-homologous end-joining (NHEJ) or homology-directed repair (HDR) and such processes too are initiated by the same ubiquitous breaks made by ZFNs, TALENs and CRISPR/Cas9s (Figure 1.2).

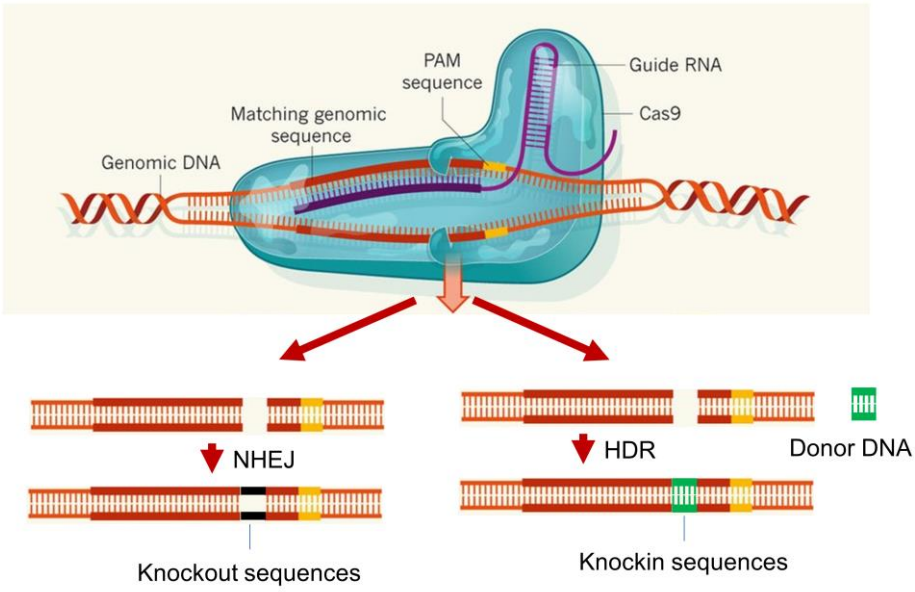

Figure 1.2 CRISPR/Cas9 targeting system showing the various DNA repairs. The CRISPR/Cas9 forms a complex with the guide RNA and creates a double strand break in the genome. This double strand break is repaired by two natural mechanism in cells, NHEJ and HDR. The donor DNA is used as template to introduce a specific mutation and insert a new gene intop the genome. Figure modified from (Tu et al. 2015)

The specificity to the target, ease of design and use, efficiency and reproducibility of CRISPR/Cas9 when compared to other PENs has made it one of the most used PEN for genome engineering.

Others have replaced the cutting activity of Cas9 with DNA methylating or histone modifying activities to perform an epigenetic modification by switching selected genes off or on at the target site on the genome without altering the genomic sequence. In this context, gene expression can be controlled without creating nucleotide changes in the DNA which will be heritable (Thakore et al. 2016).

The field of biomedical research has seen advancement in its research with the advent of CRISPR/Cas9 technology; however, one of the set-backs of CRISPR/Cas9 in clinical research is the issue of off-target effects (genome editing at unintended target sites) (Cradick et al. 2013; Fu et al. 2013). Subsequent studies using whole-genome sequence analysis and using the nickase form of the Cas9 enzyme have shown that the CRISPR/Cas9 system can be used with minimal to no off-target effects thereby increasing its specificity (Pattanayak et al. 2013; Cho et al. 2014; Shen et al. 2014; Kim et al. 2015; Kleinstiver et al. 2016a; Slaymaker et al. 2016).

1.7 Aims of the Thesis

1. Generate an MEN2B disease human Embryonic Stem Cell (hESC) model using the CRISPR/Cas9 system by homology-directed repair, HDR.
2. Differentiate hESC to:

a) Sympathoadrenal Progenitors (SAPs) to chromaffin cells of the adrenal glands,

b) Enteric Neural Crest Cell (ENCC) and Enteric Neurons (ENs), and

c) Neuroendocrine cells such as Parafollicular cells of the thyroid.

3. Generate an MEN2B mutation in the chick embryo (chick model) using the CRISPR/Cas9 system by homology-directed repair, HDR.

1.8 Overview of the Thesis

Generating a model, *in vitro* and *in vivo*, of specific diseases plays a vital role in understanding the pathogenesis and further, in looking for better ways of therapeutic management (Lee et al. 2009; Mertens et al. 2015). With the above as a broad hypothesis, my main objective was to create the precise MEN2B causing mutation, M918T, in hESCs and differentiate them to the cell lineages affected in MEN2B patients. This would provide a valuable platform to study the pathogenesis of the

disease and also create a human cell resource for testing of pharmacological therapeutic agents. To accomplish this, we had to establish the various differentiation protocols for the affected cell lineages, thyroid C cells, adrenal chromaffin cells and enteric NC cells, glia and neurons.

I have described the genetic predisposition of the MEN2B disease and the affected tissue lineages. There are MEN2B disease models in mouse but utilizing hESCs and further studying the differentiation steps is lacking. Accordingly, the avian embryo which is easily accessible and cheaper than mouse and other models, remains unexplored. Chapter 3 deals with targeting the chicken genome *in vitro* and *in ovo* using the CRISPR/Cas9 system. We were able to generate the MEN2B mutation in the chicken which is M910T showing how conserved the sequence is between humans and the chicken. Although the *in vitro* targeting efficiency was high, the *in ovo* targeting efficiency was low so further studies would be required to improve the efficiency of targeting *in* ovo. This has been published in *Scientific Reports, 2016.*

One of the affected cell lineages is the adrenal chromaffin cells and although there were differentiation protocols for mouse adrenal chromaffin cells, we had to develop a protocol for differentiating hPSCs (both hESCs and hiPSCs) via NCPC/SAPs lineages to functional adrenal chromaffin cells. In Chapter 4, we showed the time-point differentiation stage and the effect of long term exposure of BMP2/FGF2 on SAP differentiation. We also functionally validated the cell lineages by performing HPLC, which was done by A/Prof Andrew Bjorksten at the Department of Anaesthesia and Pain Management, The Royal Melbourne Hospital. This has recently been accepted for publication in *Stem Cells Reports, 2017.*

Finally, in Chapter 5, I describe the development of a protocol to differentiate hESCs with and without the M918T mutation to thyroid C cells via a definitive endoderm intermediate, and analysed them by qPCR and ELISA. I also differentiated the hESCs to Enteric NCC, glia and neurons and analysed them by microscopy, qPCR and FACs analysis of cell live and death assay.

2 MATERIALS AND METHODS

2.1 Ethics Statement

All experiments were performed with the official approval from the Murdoch Children's Research Institute Animal Ethics Committee AEC650 and AEC677 and Institutional Biosafety Committee 226-2015 PC2 NLRD and in strict accordance with its guidelines and those of the Australian Code of Practice for the Care and Use of Animals for Scientific Purposes, 7th Edition 2004 and the Prevention of Cruelty to Animals Act, Victoria 1986. Human Stem Cell studies were performed in accordance with approval from University of Melbourne Human Ethics, ID 1545384, 1545394 and 0605017.

2.2 Single Guide RNA-CRISPR/Cas9 System and Single-Stranded Oligodeoxynucleotides (ssODN) Design and Construction

Potential target sites of exon 16 of the *RET* gene were predicted using crispr.mit.edu software in the human genome and two target sequences with lower than 1.0 predicted score for off-targets were chosen. To construct the sgRNA-CRISPR/Cas9 construct for

each target gene (as in (Abu-Bonsrah et al. 2016)), I annealed two complementary 24-bp (base pair) oligonucleotides ordered from Bioneer Company, South Korea with the 20-bp target sequence to generate a double-strand DNA (Deoxyribonucleic acid) with 4-bp overhangs on both ends and cloned into BsaI-digested px330-IRES-mCherry (IRES-internal ribosome entry site). Briefly, 3 µL each of the Forward Primer (FP) and Reverse Primer (RP), 1X NEB Buffer 2 and topped up to a total of 20 µL with ddH_2O (double distilled water) in a 0.2 mL PCR (Polymerase Chain Reaction) tube. Annealing was done in a Thermocycler with the following steps: 95°C for 5 minutes, 95°C for 60s, 85°C for 60s, 75°C for 60s, 65°C for 60s, 55°C for 60s, 45°C for 60s, 35°C for 60s and held at 25°C.

For transformation into DH5α *E. coli* competent cells, 4 µL of the annealed mixture was ligated in 1X T4 DNA Ligase Buffer and 0.5 units of T4 DNA ligase (Promega) for 1-2 hours and. The ligation mixture was transferred unto 60 µL competent cells and incubated for 20 minutes on ice. The cells were then heat shocked at 42°C for 1 min and placed back on ice to recover for 2-3 minutes. I then added 600 µL of plain LB (without ampicillin) to the cells and incubated at 37°C at 220 rpm for 45-60 minutes. The cells were then plated on ampicillin-LB agar plates and incubated at 37°C for 12-16 hours. Single colonies were picked into 5 mL of LB in 15 mL tubes and incubated at 37°C at 220 rpm for 12-16 hours.

To test for correctly ligated clones, I used the FP of the hU6 promoter, 5' TTCCCATGATTCCTTCATATTTGC 3' of the px330-IRES-mCherry vector and the RP of the 24bp oligonucleotide, sgRNA in a total volume of 15 µL of PCR mixture containing 1X Promega Green Master Mix, 1 µL of 5 pmole of hU6 FP and sgRNA RP and topped up with ddH_2O. The PCR mixture was placed in a thermocycler and run with the following steps: 95°C for 3 minutes, (95°C for 30s, 60°C for 30s, 72°C for 10s) x 35, 72°C for 5 minutes and held at 12°C. The expected amplicon of 230 bp was confirmed by running the PCR product on 1% Agarose gel.

Positive clones were selected and plasmid extraction was done using the AccuPrep Nano-Plus Plasmid Mini Extraction Kit (K-3111-Bioneer Company, South Korea) following manufacturer's instructions. Briefly, the overnight grown culture was centrifuged at 13000 rpm for 60 seconds to collect the *E. coli* and the media was removed by pipetting. Afterwards, 250 µL of Buffer 1 was added to the collected cells and completely resuspended by pipetting followed by the addition of 250 µL of Buffer 2. The tube was then inverted 3-5 times gently to avoid shearing of genomic DNA. I

then added 350 µL of Buffer 3 and immediately inverted the tube to mix 3-5 times gently to neutralise Buffer 2. The mixture was then centrifuged at 13000 rpm at room temperature for 60 seconds and I transferred the cleared lysate to the DNA binding column tube provided by the manufacturer. The column with the lysate was then centrifuge at 13000 rpm for 60 seconds. The flow-through was poured away and after re-assembling the columns, 700 µL of Buffer 4 was added to the column and centrifuge at 13000 rpm for 60 seconds. The flow-through was poured away and the column was dry spun after re-assembling to remove residual ethanol from Buffer 4. The DNA binding filter column was then transferred to a new 1.5 mL Eppendorf tube and allowed to stand for at least 60 seconds after adding 30-50 µL of Buffer 5 to the DNA binding filter column. The plasmid DNA was eluted by centrifugation at 13000 rpm for 60 seconds. The purified plasmid was aliquoted and 10 µL sent to Melbourne Translational Genomics and Sequencing Platform for Sanger sequencing to confirm the correct ligation of our intended 24 bp oligonucleotide.

Sequence-confirmed clones were retransformed into competent cells and plated on LB agar as described above and single colonies were picked and cultured in 100 mL LB broth at 37°C at 220 rpm for 12-16 hours. Plasmid extraction was done using the Plasmid Midi Extraction Kit (Bioneer Company, South Korea) and reprecipitated by the isopropanol/ethanol purification method. Briefly 1/3 volume of isopropanol was added to the plasmid solution in a 1.5 mL Eppendorf tube and inverted 4-5 times and centrifuged at 13000 rpm for 10 minutes at room temperature. The pellet was washed with 70% ethanol and briefly centrifuged at 13000 rpm for 5 minutes at room temperature. The pellet was allowed to dry and rehydrated in a 1X TE (Tris-EDTA) buffer and the DNA concentration was measured using the NanoDrop machine (Thermo Scientific).

I designed homology arms of at least 30 nucleotides (nt) on either side of the sgRNA target site and modified some of the guide RNA binding nucleotides to avoid rebinding of the gRNA-Cas9 complex after HDR has occurred. These nucleotide changes were confirmed to not create a sense mutation but rather a silent mutation; that is the amino acid remains unchanged since the nucleotide/amino code is redundant. (Example is Leucine-UUA, UUG, CUU, CUC, CUA and CUG). In total, I designed 74 nucleotides (base pairs) as the single strand oligonucleotide (ssODN) and ordered them from Bioneer Pacific.

Table 2. Oligonucleotides for sgRNA and ssODN. Letters in red are changed nucleotides.

Gene or locus		Sequence 5' to 3'
*RET (*M918T)	sgRNA #1	F: CCGGTCGGATTCCAGTTAAATGGA
		R: AAACTCCATTTAACTGGAATCCGA
	sgRNA #2	F: CCGGTCAATTGCCATCCATTTAAC
		R: AAACGTTAAATGGATGGCAATTGA
ssODN: tatgatcaaaaagggattcaattgccgtccacttgaccgggatccgaccctaaagagaagatggaataaagaca		

2.2.1 Single Guide RNA-CRISPR/Cas9 System Design and Construction against the Chicken Genome

Potential target sites were predicted using crispr.mit.edu software in the chicken genome and two to three target sequences with lowest predicted score for off-targets were chosen. I chose a range of genes in addition to *RET* to test the general applicability of this technique to the avian genome, which had not been systematically investigated previously. To construct the sgRNA-CRISPR/Cas9 construct for each target gene, I annealed two complementary 24-bp oligonucleotides (Bioneer Company, South Korea) with the 20-bp target sequence to generate a double-strand DNA with 4-bp overhangs on both ends and cloned into BsaI-digested px330-IRES-mCherry. Oligonucleotides are listed in Table 2.2.

Table 3. Oligonucleotides for sgRNA and ssODN against the chicken genome. Letters in red are changed nucleotides.

Gene or locus		Direction	Sequence 5' to 3'
RET exon 16	sgRNA #1	FP1	CCGGAGGGTCGGATACCTGTTAAA
		RP1	AAACTTTAACAGGTATCCGACCCT
	sgRNA #2	FP2	CCGGTCTATGGCCATCCATTTAAC
		RP2	AAACGTTAAATGGATGGCCATAGA
RET exon 10	sgRNA #1	FP1	CCGGTCACAATAACAGTTCTGTCT
		RP1	AAACAGACAGAACTGTTATTGTGA
KIAA1279	sgRNA #1	FP1	CCGGGCGGAACTTCTCGCACGCCG
		RP1	AAACCGGCGTGCGAGAAGTTCCGC
	sgRNA #2	FP2	CCGGCGGCGGCGACAAGATGGCGG
		RP2	AAACCCGCCATCTTGTCGCCGCCG
MBD3	sgRNA #1	FP1	CCGGGCACCTTTGACTTCCGCACG
		RP1	AAACCGTGCGGAAGTCAAAGGTGC
	sgRNA #2	FP2	CCGGGTCAAAGGTGCTCAGGTCCA
		RP2	AAACTGGACCTGAGCACCTTTGAC
EZH2	sgRNA #1	FP1	CCGGACACGTTTTCGCCAACAAAT
		RP1	AAACATTTGTTGGCGAAAACGTGT
	sgRNA #2	FP2	CCGGCTGAGAAAGGACCAATTTGT
		RP2	AAACACAAATTGGTCCTTTCTCAG
CDKN1β	sgRNA #1	FP1	CCGGCCCTACCCTGGAGCGCATGG

		RP1	AAACCCATGCGCTCCAGGGTAGGG
	sgRNA #2	FP2	CCGGCCGCGCCTCCATGCGCTCCA
		RP2	AAACTGGAGCGCATGGAGGCGCGG
Stathmin-like 2 exon 1	sgRNA #1	FP1	CCGGATTGCTGTTTTAGCCATGGT
		RP1	AAACACCATGGCTAAAACAGCAAT
	sgRNA #2	FP2	CCGG AGCGCCTGCACATCCCACCA
		RP2	AAACTGGTGGGATGTGCAGGCGCT
Stathmin-like 2 exon 3	sgRNA #1	FP1	CCGGTGAGGAGATCCAGAAAAAGC
		RP1	AAACGCTTTTTCTGGATCTCCTCA
	sgRNA #2	FP2	CCGGCGGCAGCCTCCAGCTTTTTC
		RP2	AAACGAAAAAGCTGGAGGCTGCCG
DGCR8 exon 2	sgRNA #1	FP1	CCGGGTCTTCGTGCACCCAAAACA
		RP1	AAACTGTTTTGGGTGCACGAAGAC
	sgRNA #2	FP2	CCGGCACTTGTTTCTCCATCAGAC
		RP2	AAACGTCTGATGGAGAAACAAGTG
HIRA	sgRNA #1	FP1	CCGGTATGGCTCCTGTCCTGAAAG
		RP1	AAACCTTTCAGGACAGGAGCCATA
TYRP1	sgRNA #1	FP1	CCGGACCATTGAGTCTCTGAGAAG
		RP1	AAACCTTCTCAGAGACTCAATGGT
ssODN (MEN2B-M910T): gatatatataaatgttttttttagggtcggatcccggtcaagtggacggccatagaatccctgtttgatcatatct			
ssODN (MEN2A-C612R): tgggcaagagcagatgacgacttacccttgatgtcatctttctcacgatagcaattttggcgtgggaagcagtaacaaatcccatgtcctgac			

2.2.2 Single Guide RNA-CRISPR/Cas9 Validation

HEK 293T cells were cultured in Dulbecco's Modified Eagle's medium (DMEM, Gibco-BRL, Rockville, MD, USA) supplemented with 10% FBS (In Vitro Technologies) and 1X penicillin (100 U/mL)/streptomycin (100 µg/mL) (GIBCO) at 37°C and 5% CO_2 in a humidified incubator and harvested using 0.025% trypsin/EDTA solution (Invitrogen). 12-16 hours before transfection, 4 X 10^4 cells were seeded in each well of a 12 well dish and transfection was done using Fugene HD (Roche, Branford, CT, USA) per manufacturer's instructions. To perform the transfection, the media was changed to DMEM supplemented with 10% FBS without penicillin and streptomycin and replaced in the incubator. A suspension of Opti-MEM (Gibco) and sgRNA-CRISPR/Cas9 DNA complex (100 µL and 500 ng respectively) was prepared in a 1.5 mL Eppendorf tube and 3X of the Fugene HD solution was added to the mixture. The DNA-Fugene complex was briefly vortexed and incubated at room temperature for 10 minutes. The complex was pipetted onto the cells and incubated at 37°C for 24 hours. Media change was done after 24 hours and cells were harvested for genomic DNA extraction 72 hours posttransfection.

2.2.2.1 DF-1 Cell Culture and Transfection

The chicken DF-1 cell (Lambeth et al. 2013) line was maintained and sub-passaged in DMEM, supplemented with 10% FBS and 1× penicillin/streptomycin, at 37 °C in 5% CO_2. Cells were seeded at 0.4-0.8 X 10^5 cells/well in 24-well plates, incubated for 4 hours, and then transfected with 1.5 μg CRISPR/Cas9 sgRNA targeting the specified gene or region and with or without 0.15 μg of puromycin expression vector using Lipofectamine 3000 (Invitrogen) according to the manufacturer's protocol with slight modifications. Briefly, 1 μL and 2 μL of Lipofectamine 3000 reagent was added to two different tubes with 25 μL of OPTI-MEM medium (Invitrogen) and briefly vortexed. Then a mixture of 1.5 μg of the CRISPR/Cas9-sgRNA plasmid (px330-IRES-mCherry), 0.15ug puromycin expression vector and 3 μL of p3000 reagent (Invitrogen) in 50 μL OPTI-MEM was made and then 25 μL of the p3000-DNA complex was then added to each of the Lipofectamine 3000 complex tubes and incubated for 5 minute at room temperature. The complex mixture was then gently pipetted into a well of a 24-well plate with DF-1 cells at about 60-80% confluency. After 24 hours post-transfection, the cells were treated with puromycin at a final concentration of 2 μg/mL for 2 days and the cells were allowed to recover for a day or two.

For HDR knock-ins, cells were transfected with 1.0 μg CRISPR/Cas9 sgRNA targeting the specified gene or region with 40 pmoles of ssODN and 0.15 μg of puromycin expression vector following the same protocol.

2.2.2.2 DT40 Cell Culture and Transfection

Cells of the chicken B cell line DT40 (Kim et al. 2013) were cultured in chicken medium composed of RPMI-1640 medium (Sigma Aldrich), 10% FBS, 1% chicken serum (Sigma) and penicillin/streptomycin, at 39 °C in 5% CO_2. A total of 1-2 X 10^7 cells were pelleted at 1500 rpm for 3 min at room temperature and the pellet was washed with PBS and pelleted again. The pellet was then resuspended in 600 μl PBS and after the addition of 30 μg of sgRNA-CRISPR/Cas9 plasmid and 3 μg of puromycin expression vector, the resuspension was placed in a BioRad 4mm electroporation cuvette. Electroporation was done using BioRad Gene Pulser II at 250V and 950 μF. After electroporation, cells were mixed with 10 ml of culture medium without penicillin/streptomycin and cultured for 12–24 hours. The cells were treated with puromycin at a final concentration of 2 μg/mL for a day and the cells were allowed to recover for 2-3 days.

2.2.3 Single Cell Clonal Analysis

Cells were trypsinized and plated in 96 well plates at average 0.3 cell/well and incubated at 37 °C for two weeks. Each well was then microscopically evaluated, and single cell-derived clones were selected and expanded into 24 well plates. Genomic DNA from each clone was extracted and T7E1 assay (Vouillot et al. 2015) was conducted as published. To confirm HDR of the ssODN, PCR amplicons were digested with 5 units of the restriction enzyme BamH1 (New England Biolabs) for more than 2 hours at 37°C and then analysed on 2% agarose gel by electrophoresis. PCR amplicons of BamH1 or T7E1 digested clones were cloned into a pGEM-T Easy vector (Promega, Madison, WI) and sequenced.

2.3 Human Pluripotent Stem Cells (hPSCs) Culture

All cells were maintained at 37°C with 5% CO_2 in a humidified cell culture incubator (Sanyo, MCO-19M). Aseptic techniques were followed for all procedures and handling of cells, including working and preparing reagents in class II biological safety cabinets (fume hood or hood; SCANLAF, Mars Safety Class 2) and disinfection of surfaces and equipment using 70% ethanol. Cultures were monitored regularly under Zeiss Primo Vert microscope with Axiocam. To reduce risk of contamination, a group of equipment including pipettes (Gilson) and pipet-aids (Drumond, Scientific) were dedicated for tissue culture and exclusively used for this purpose.

Human ESC line H9: extensively used cell line derived by WiCell institute from donated *in vitro* fertilized embryo.

Human ESC line HES3 and HES3-ENVY: cell line derived by ESI International.

Human ESC line MEL2: cell line derived by ESI International.

Human iPSC line 007: cell line derived and provided by A/Prof Alice Pebay (Hernandez et al. 2016).

2.3.1 Tissue Culture Materials and Reagents

2.3.1.1 Tissue Culture Plastics and Glassware

Tissue culture grade plastic items were obtained from Falcon. Products used in tissue culture that were not bought as tissue culture grade such as pasteur glass pipets, Eppendorf tubes and glass coverslips, were autoclaved in containers covered with aluminium foil and were subsequently unwrapped inside the hood for use. Alternatively,

items such as forceps were sterilized by dipping in 100% ethanol and dried inside the hood prior to use.

2.3.1.2 Matrix Molecules for Maintenance and Neural Differentiation of hESC

The adhesive matrix molecules to be used as *in vitro* substrates listed in Table 2.2 were received in liquid format, aliquoted and stored at – 20 °C. When needed, an aliquot was thawed and stored at 4 °C and used within 2-4 weeks.

Table 4. List of matrices used to coat dishes.

	Stock	Final	Supplier	Cat #
Fibronectin	5 mg/mL	10 µg/mL	In Vitro Tech	FAL356008
EHS Laminin	1 mg/mL	10 µg/mL	Invitrogen	23017-015
Poly-D-lysine	1 mg/mL	10 µg/mL	Sigma	P1024-50MG
Vitronectin XF	250 µg/mL	10 µg/mL	StemCell Technologies	0719

2.3.1.3 Buffers and Solutions

CellAdhere Dilution Buffer (StemCell Technologies, Catalog no: 07183) stored at 4°C.

Ethanol 100% AR denatured (Thermo Fisher Scientific, Catalog no: FNNJJ008).

Phosphate Buffered Saline, Ca++/Mg++ free (CMF-PBS) (Invitrogen, Catalog no: 14190-144).

Trypan Blue Solution (0.4%) (Sigma, Catalog no: T8154) was freshly diluted 1:2 in media or CMF-PBS for counting cells in a haemocytometer.

EDTA-CMF-PBS was prepared by diluting 50 µL of 0.5 M EDTA (GIBCO) in 50 mL of CMF-PBS in a 50 mL Falcon tube and stored at room temperature.

Water, Sterile Distilled (Invitrogen, Catalog no: 15230-162).

Mitomycin C (Sigma, Catalog no: M0503) was received as 2 mg lyophilized powder, reconstituted in 4 mls of ddH_2O to a stock concentration of 0.5 mg/ml, sterile filtered, aliquoted and stored at -20°C. Solution was diluted further in defined mouse embryo fibroblast (MEF) media to a final concentration of 10 µg/ml before adding to MEFs for mitotic inactivation.

2.3.1.4 Media and Supplements for hPSCs Maintenance and Neural Differentiation

Cell culture media was prepared routinely every week, sterile filtered through 0.22 µM filter unit (In vitro Technologies, Catalog no: COR431097) aliquoted and consumed within 1-2 weeks post supplementation. Unless specified, media was stored at 4°C and

pre-warmed in a 37 °C water bath prior to medium change. The following reagents were purchased in bulk, aliquoted under sterile conditions and stored at recommended temperatures: FBS, KSR, L-Glutamine, and Penicillin/Streptomycin.

Table 5. hPSC maintenance media for feeder culturing system (hPSC media).

	500 mL	Final conc	Supplier/Cat#
KnockOut™ DMEM/F-12	387.5 mL		LifeTechnologies 12660-012
Knockout Serum Replacement (KSR)	100 mL	20%	LifeTechnologies 10828-029018
L-Glutamine	5 mL	1%	LifeTechnologies 25030081
Pen/Strep Solution Pen = 5000 units/ml, Strep = 5000 μg/ml	2.5 mL	0.5%	LifeTechnologies 15070-063
10mM NEAA, 10 mM	5 mL	0.1mM (1%)	LifeTechnologies 11140050
FGF2, 50ug/ml		10 ng/mL	MiltenyiBiotec 130093842

Sterile filter, protect from light, store at 4 °C and use within 2-3 weeks. FGF2 was supplemented fresh into the media volume used each day; e.g. 1 μl of FGF2 stock (50 μg/ml) was added to 5ml HES media before adding to cells. Abbreviations: Nonessential amino acids (NEAA), Penicillin/Streptomycin (Pen/Strep), Fibroblast growth factor-2 (FGF2, previously termed bFGF), Catalogue number (Cat#), concentration (conc).

Table 6. Media for culturing MEF as feeder cells.

	500 mL	Final conc	Supplier/Cat#
DMEM	442.5 mL		LifeTechnologies
FBS	50 mL	10%	In Vitro Technologies IVT3008403
L-Glutamine	5 mL	1%	LifeTechnologies 25030081
Pen/Strep Solution Pen = 5000 units/ml, Strep = 5000 μg/ml	2.5 mL	0.5%	LifeTechnologies 15070-063

Sterile filter, protect from light, store at 4 °C and use within 2-3 weeks.

Table 7. Standard freezing medium for MEF.

	10 mL	Final conc
FBS	9	
Dimethyl sulfoxide (DMSO)	1	10%

Sterile filter and made fresh for every use.

Table 8. hPSC maintenance media for feeder-free culturing system.

	500 mL	Final conc	Supplier	Cat# (Kit- #05940)
TeSR™-E8™ Basal Medium	474 mL		StemCell Technologies	#05941
TeSR™-E8™ 20X Supplement	25 mL	1X		#05942
TeSR™-E8™ 500X Supplement	1 mL	1X		#05943

Sterile filter, aliquot it in 40mL, store aliquots in -20 °C and use within 6 months. To use, thaw an aliquot overnight at 4°C.

Table 9. Defined neural induction medium (N2B27 media).

	100 mL	**Final**	**Supplier**	**Cat #**
DMEM/F12 (1x)	47.25 mL		Life Technologies (Gibco)	21103-049
Neurobasal medium	47.25 mL			11320-033
N-2 supplement (100x)	1 mL	1%		17502-048
B-27 supplement (without Vitamin A, 50x)	1 mL	1%		12587-010
Insulin-Transferrin-Selenium-A (ITS-A) (100x)	1 mL	1%		51300-044
L-Glutamine (100x) .2M	1 mL	2 mM		25030-081
Pen/Strep Solution Pen = 5000 units/ml, Strep = 5000 µg/ml	0.5 mL	0.5%		15070-063
Glucose 30% (w/v)	1 mL	0.3%	Sigma-Aldrich	

Sterile filter, store at 4°C and use within 2-3 weeks.

Table 10. Neural basal medium (NBM media).

	500 mL	**Final**	**Supplier**	**Cat #**
Neurobasal medium	472.5 mL		Life Technologies (Gibco)	11320-033
N-2 supplement (100x)	5 mL	1%		17502-048
B-27 supplement (without Vitamin A, 50x)	10 mL	2%		12587-010
Insulin-Transferrin-Selenium-A (ITS-A) (100x)	5 mL	1%		51300-044
L-Glutamine (100x) .2M	5 mL	2 mM		25030-081
Pen/Strep Solution Pen = 5000 units/ml, Strep = 5000 µg/ml	2.5 mL	0.5%		15070-063

Sterile filter, store at 4 °C and use within 2-3 weeks.

Table 11. Small molecules and growth factors.

	Stock	Final	Vehicle	Supplier	Cat#
BMP2	10 µg/ml	50 ng/ml	ddH_2O	PeproTech	120-02-10
CHIR99021	20 mM	3 µM	DMSO	Tocris	4423
FGF2	50 µg/ml	20 ng/ml	ddH_2O	Miltenyi Biotec	130093842
SB431542	10 mM	10 µM	Ethanol	Tocris	1614
Y-27632	0.1 M	10 µM	ddH_2O	Tocris	1254
BMP4	50 µg/ml	500 pg/ml	Sterile 4 mM HCl	RnD Systems	314-BP-050

Abbreviations: Bone morphogenetic protein (BMP), basic fibroblast growth factor (FGF2), double distilled water (ddH_2O), Dimethyl sulfoxide (DMSO), Catalogue number (Cat#).

2.3.1.5 Growth Factors and Small Molecules

Growth factors and small molecules (Table 11) were received as lyophilized powder, and then were appropriately reconstituted per manufacturer's recommendations, aliquoted and stored at -80 °C for long-term storage. When aliquots of growth factors were thawed, they were stored at 4 °C and used within 2 weeks. For short-term storage, the small molecules were stored at -30°C rather than 4°C. Immediately before feeding cells, growth factors and small molecules were further diluted to the working concentrations in the appropriate cell culture medium.

2.3.2 Maintenance of hPSCs on MEF Feeders

Single clones obtained after gene editing of hPSCs were transferred onto feeders and maintained using the traditional method of culturing hPSC on inactivated MEF feeders.

2.3.2.1 Preparation of MEF Feeder Cells for hPSCs Maintenance

Freshly derived MEFs were expanded for a maximum of 4 passages, and then treated with mitomycin C for mitotic inactivation. Subsequently, the remaining inactivated MEFs were frozen down at -80°C before storing them in liquid N_2 tanks. With the maintenance of hPSC, I plated 8 x 10^4 MEFs per well of a 24 well plate and incubated them overnight to allow the feeders to settle before seeding the hPSC. The MEF medium was changed to hPSC medium prior to seeding hPSC.

2.3.2.2 Propagation of hPSCs on MEF Feeders

Every 5-7 days, I mechanically dissected hPSC colonies with tungsten needles and transferred them to dishes containing MEFs. This was performed inside the hood under Zeiss stereo microscope on a warm stage. The undifferentiated edges of colonies are normally cut into small pieces and transferred by P20 Gilson pipette into dishes with

MEF (typically 10 pieces of hPSC per organ culture dish); this was done to avoid differentiated parts of the colonies such as the dense centre. Cultures were then very carefully moved to the incubator and small pieces of the colonies were allowed to settle and attach well for one day. Medium change was performed daily starting from the second day following plating. Note that spontaneous differentiation and variability in the quality of hPSC are common problems in hPSC culture even when done under strict handling conditions.

2.3.3 Feeder-free Maintenance of hPSCs

Feeder-free culturing is an alternative and less laborious approach for propagation of hPSCs. Early in 2014 our laboratory transitioned to feeder-free culturing of hPSCs.

2.3.3.1 Vitronectin Coating

Vitronectin is a defined, xeno-free matrix that supports proliferation and maintenance of hPSC. Coating with vitronectin should be performed at least 2 hours prior to seeding hPSC. The protocol below was followed:

1. Thaw vitronectin overnight at 4°C and use within 2 weeks. Stocks are stored at -20°C.
2. Dilute vitronectin in CellAdhere Dilution Buffer (40 µl vitronectin in 1,000 µl buffer) and distribute into each organ culture dishes each with 300 µl.
3. Incubate coated dishes at 4°C overnight or at room temperature for 2 hours.
4. Prior to use, remove vitronectin solution and add 1ml of mTeSR media and then place dishes in the incubator till required.

2.3.3.2 EDTA-CMF-PBS Buffer Dissociation of hPSCs

Every 5-7 days, enzymatically dissociate hPSCs by using EDTA-CMF-PBS buffer. The culture media is removed and replaced by the EDTA-CMF-PBS buffer for 4-6 minutes. the rate of dissociation is observed under microscope. The buffer is then removed and replaced with culture media. The cells are lifted off by gently pipetting up and down to harvest the cells into a 15 mL Falcon tube and counted using the haemocytometer. The required number of cells are then seeded in a new vitronectin-coated dish with TESR™-E8™ complete media supplemented with 10 µM Y-27632 and incubated overnight. Medium change is performed daily starting from the second day following plating.

2.3.4 hPSCs Culture and CRISPR/Cas9 Transfection

Human PSCs were maintained in feeder-free conditions with TESR™-E8™ complete media on Vitronectin-coated plates. Cultures were passaged as needed using the EDTA-CMF-PBS buffer and maintained at 37°C and 5% CO_2 in a humidified incubator. For transfection, hESCs were cultured to 80%–90% confluence and harvested using the EDTA-CMF-PBS buffer for 4-6 minutes. The dissociation reagent was gently removed and 4 mL of media was gently added to harvest the cells into a 15 mL Falcon tube and 10 µL was counted using a haemocytometer under the microscope. About 70-80% of the cells were single cells. A total of 8 X 10^5 cells were transferred into a 50- mL Falcon tube and centrifuged at 200 g for 5 minutes at room temperature. The supernatant was gently removed and resuspended in 82 µL of Lonza Cell solution and 18 µL of the supplement (LONZA) and transferred into a 1.5 mL Eppendorf tube. An amount of three µg of the *RET* exon 16-targeting CRISPR/Cas9 plasmid, 40 pmole of the ssODN and 0.3 µg of a puromycin plasmid was added to the cell suspension. The DNA-cell suspension was then transferred into the electroporating cuvettes and electroporated using the Lonza recommended parameters (CB-150 program). 400 µL of TESR™-E8™ complete media was added to the electroporated cells and the cuvette was incubated at 37°C for 4-6 minutes to allow cell recovery, and then plated on vitronectin coated 6 well plates. Puromycin selection was started after 24 hours at 0.5µg/mL. Selection was only done for 24 hours and the cells were allowed to recover. Drug-resistant colonies were picked and, plated on irradiated MEF feeders in 24 well plates and cultured in KSR medium containing DMEM/F12 Glutamax (GIBCO), 20% Serum Replacement (GIBCO), mercaptoethanol, 1X non-essential amino acids, NEAA (GIBCO), penicillin (50 U/mL)/streptomycin (50 µg/mL) supplemented with 10 ng/mL of FGF2. Media change was done daily till colonies grew to a reasonable size where parts can be picked. Parts of the colonies were picked and genomic DNA was extracted and screened for HDR genomic modification. Positive clones were transferred into irradiated MEF feeder in a 6 well plate for second HDR screening and expansion. One or two colonies were picked after a few days and second HDR screening was done to confirm genomic modification. Positive clones were then processed for sequencing by cloning the PCR product into a pGEM-T Easy vector and sequenced using the T7 Forward Primer-5'-TAATACGACTCACTATAGGG-3'.

2.3.4.1 T7E1 Mutation Frequency Analysis

Colonies were handpicked and digested in nuclear lysis buffer (Promega, Madison, WI). Genomic DNA was extracted from hESC cells. The genomic DNA was extracted from the lysate by phenol-chloroform and recovered by isopropanol/ethanol precipitation. The genomic region encompassing exon 16 of the *RET* gene was amplified with a specific primer set (see Table 12). The amplicons were re-annealed to form a heteroduplex DNA structure after denaturation and then treated with 2.5 units T7E1 (New England Biolabs, Ipswich, MA) for 20 min at 37 °C and then analyzed by 2% agarose gel electrophoresis. Mutation frequencies were calculated as previously described (Guschin et al. 2010) based on the band intensities using Image J software and the following equation: mutation frequency (%) = 100 x (1-(1-fraction cleaved)$^{1/2}$), where the fraction cleaved is the total relative density of the cleavage bands divided by the sum of the relative density of the cleavage bands and uncut bands. To confirm target locus mutation, PCR amplicons were cloned into a pGEM-T Easy vector (Promega, Madison, WI) and sequenced.

With chicken related work, samples of cells (DF-1 cells or DT40 cells after transfection of each CRISPR/Cas9-sgRNA) and electroporated embryos and parts thereof were collected and digested in nuclear lysis buffer (Promega, Madison, WI) for genomic DNA extraction and analysed as above.

Table 12. Oligonucleotides for PCR for T7E1 Assay and sequencing for human and chicken genomes.

Gene or locus	**Sequence 5' to 3'**
RET exon 16 (Human)	F: ATCTCAGCAATCCACAGGAGGT
	R: CTCTACCGGAGCTTTCAGAACT
RET exon 16	F: AACAGATCATCTGTCAGCTTGTGT
	R: TCCTCAGATTTAATTAAATGGCA
RET exon 10	F: CTACTCCAGTGCTCAGAAATCCAT
	R: GTCTCCATGCACAAGTCAATATGC
KIAA1279	F: GCCAGGGCCCTCGAGTAACCGCG
	R: GCGCAGCCCCCGCCCACCTGGGC
MBD3	F: TGCACTTATTCTGCTAATTATGCTG
	R: TGGGACAGGCTTTGTTCTTGAGA
EZH2	F: ATGGCCTGTTAATTTGTAACTAAAAT

	R: TTGATTCAATCACATACAAATGTA
CDKN1B	F: TCGGCTGCTCCCCTCCGGAGCCG
	R: GCCTGAAGTAGAAGTCGGGCGAG
Stathmin-like 2 exon 1	F: GTGGATCAATATTTAATGCCCGGAG
	R: TGATCTCAGATCGTTAAAAGAGCC
Stathmin-like 2 exon 3	F: TAGTCTGTATTTCTGATCGTACACT
	R: CAAGTTGCTGAAAGAAAATAAACT
DGCR8 exon 2	F: GGGATCATTGGACATTTCTAGTTC
	R: ACAACAGATGAAGACAAAAAGCAC
HIRA	F: TGTAACTGTATCAGAATGGCCTCT
	R: CCAGAGAAAGTTCACTGATTTCCA
TYRP1	F: CTGGACTGGAGGTTTGTATTTCTT
	R: CTAGGTGCATTAAAATCAACATGC

2.3.4.2 Sequence-Specific PCR and Restriction Enzyme Digestion (RFLP-Restriction Fragment Length Polymorphism)

The PCR product (6-8 µL) was digested in 0.5 µL of the BamHI restriction enzyme (Promega, Madison, WI), 1X Reaction Buffer and topped up to 20 µL total volume with ddH_2O and incubated for 4-8 hours at 37 °C. Digested products were then analysed by 1.5% agarose gel electrophoresis. Successful homologous recombination would generate a BamHI site in the genomic DNA and will generate double bands recognisable by gel electrophoresis. Negative and positive clones were cloned into the pGEM-T Easy vector (Promega, Madison, WI) by running the undigested PCR product on a 1% agarose gel. The right product size was excised and eluted using the Gel Extraction Kit (Bioneer) following manufacturer's instructions. A volume of 7 µL of the eluted product was cloned into 1 µL of pGEM-T Easy vector (Promega, Madison, WI), 1X DNA ligase buffer and 1 µL of T4 DNA ligase (Promega, Madison, WI) in a 10 µL reaction and incubated for 1-2 hours at room temperature. The ligated product was transformed into *E.coli* and plasmid extracted as described above. The product was then prepared for sequencing as outlined below.

With modified chicken cells, PCR products for MEN2B HDR templates were digested in BamHI restriction enzyme (New England Biolabs, Ipswich, MA) and in EcoRV restriction enzyme (New England Biolabs, Ipswich, MA) for MEN2A/HSCR HDR experiments and processed as above.

2.3.4.3 Sequencing Analysis

The PCR products of positive clones were run on a 1% agarose gel and the correct band was excised and eluted using the Gel Extraction Kit (Bioneer) following manufacturer's protocol. Excised gel fragments were dissolved in 600 µL of Buffer 1 at 60°C for 8-10 minutes. The dissolved solution was then transferred into supplied tubes and centrifuged at 13000 rpm for 60 seconds. Collected solution was discarded and 500 µL of Buffer 2 was added and centrifuged twice at 13000 rpm for 60 seconds. The tube was then dry spun at 13000 rpm for 30-60 seconds to remove excess Buffer before adding 20-30 µL of the Elution Buffer. The tube was incubated for 60 seconds and then centrifuged at 13000 rpm for 60 seconds. Eluted products were cloned into the pGEM-T Easy vector (Promega, Madison, WI) per manufacturer's instructions. Briefly, 3 µL of the eluted product was added to 1 µL of the pGEM-T Easy vector, 1X of the T4 DNA Ligase Buffer and 1 µL of the T4 DNA Ligase and incubated for more than 2 hours. The ligation mixture was then transformed into DH5α *E. coli* competent cells and grown on ampicillin-LB agar plates treated with X-gal (5-bromo-4-chloro-3-indolyl-beta-D-galacto-pyranoside)-IPTG (isopropyl-beta-D-thiogalactopyranoside) overnight to screen for blue and white colonies. White colonies were selected and grown in Ampicillin-LB broth overnight for miniprep plasmid extraction using the AccuPrep Nano-Plus Plasmid Mini Extraction Kit (K-3111-Bioneer Company, South Korea). The purified plasmid was aliquoted and 10 µL sent to Melbourne Translational Genomics and Sequencing Platform for Sanger sequencing using the T7 promoter primer (5'-TAATACGACTCACTATAGGG-3').

2.3.4.4 Off-Target Prediction and Analysis

Potential *RET* gene off-targets were predicted using crispr.mit.edu software in the human genome. Off-target site with scores more than 1, or with 2 or more mismatches were chosen and amplified by PCR using the extracted genomic DNA as templates. The PCR products were first subjected to T7E1 cleavage assay as described above (Niu et al. 2014).

Table 13. Oligonucleotides for off-target PCR. Letters in red are mismatched bases.

Locus	Off-Target sequence	Sequence 5' to 3'	Product Size
chr3:+188082367	TGGGATTGGAGTTAAATGGAGAG	F: GAATCTTTTTGCTATCCCTGTCTT	555 bp
		R: AAAGCCTCACTCACACATCTACTG	
chr2:+1	ACTGGTTTCAGTTAAA	F:	551 bp

17598397	TGGATAG	CAGATTGTCTCCTAAAATGCTGTG R: GCTCAGTCACCAGATGCTATCTAA	
chr1:-198522915	TCAGATTTCAGATAAATGGACAG	F: CCACAGTCAAGAAGTCTGTTTTCA R: GTCTATCACAATGTAAGCACCACA	563 bp

Table 14. Oligonucleotides for off-target PCR against chicken genome. Letters in red are mismatched bases.

Gene or locus	Off-Target sequence	Sequence 5' to 3'
RET exon 16 OT	AGGGTCAGCCACCTGTTAAAGGG	F: AGCACTCGAGTCAGGAGACTTAAT
		R: ATTGGAGGACTTCTTGTCTAGGTG
RET exon 10 OT1	TCAAAATGACAGTTCTGTCTCAG	F: GAGAAACAGGAAAATAGGAACAGG
		R: CAGCTACTGTGACACTTGATTCAG
RET exon 10 OT2	CCATCATAACAGTTCTGTCTCAG	F: GACCTCAGCATAATCACATTGTTC
		R: TATCCTATGCTTTACACTCGTCCA
KIAA1279 OT	GTGGAACTTCTCGCACGCAGCGG	F: AAATAGGGGAGAAAAATGAGGAAG
		R: AATCCCGCTGGTAAAATATGTATG
CDKN1β OT	CAGCAACCTGGAGCGCATGGGAG	F: CAAGGTCACAAAGTCTCATTGTTC
		R: CGTTGTCTTCATCCTTAGGTTTTT
Stathmin-like 2 exon 1 OT1	AGCTCCTGCACATCCCACCTGGG	F: TTTAAAAGGTAGTCCTGCTGCTCT
		R: GAGATTTTGCAGTTTCACAGAAGA
Stathmin-like 2 exon 1 OT2	ATCGCCACCACATCCCACCAAGG	F: TCCACGAAAGTATGCTGAGATAAA
		R: CTGGGAAAAGGATTACATTCAGAG
Stathmin-like 2 exon 3 OT	TTATAAGATTCAGAAAAAGCTGG	F: CACCCACAGTCAACTTATTTTTGT
		R: AAATGAGAGTTCCACAATGCAGTA

2.3.4.5 Karyotyping

hESCs were cultured to 80%–90% confluence in vitronectin-coated T25 flasks and harvested using the EDTA-CMF-PBS buffer for 4-6 minutes. EDTA-CMF-PBS buffer was removed and replaced with TesR-E8 media and pipetted up and down gently to lift off the cells. Harvested cells were centrifuged at 200 g x 3 minutes and the pellet was washed with CMF-PBS and centrifuged again. This procedure was repeated for the second time. The supernatant was discarded and the pellet was stored at -30°C until sent

for karyotyping by single nucleotide polymorphism (SNP) array at the Victorian Clinical Genetic Service (MCRI, Parkville).

2.4 Neuroblastoma (NB) Cell Culture

Human neuroblastoma (NB) cell line, SK-N-BE(2)C (ECACC Nos 95011817) was grown in DMEM supplemented with 10% FBS and 1X penicillin/streptomycin (both Life Technologies, Carlsbad, CA, USA) and maintained in a humidified incubator at 37 °C with 5% CO2. Cells were then harvested for FACs analysis.

2.5 Coating Dishes with Laminin

The protocol below was followed:

1. Thaw an aliquot of laminin, store at 4°C and use within 3-4 weeks. Stocks are stored at -30°C.
2. Prepare a 1:100 dilution of laminin (final concentration of 10 μg/ml) in sterile CMF-PBS- of appropriate volumes (each organ culture dish requires 300 μl).
3. Add laminin solution to organ culture dishes and incubated at 4°C overnight.

2.5.1 Coating Dishes with Poly-D-Lysine and Laminin

Protocol below was followed:

1. Thaw aliquots of laminin and poly-d-lysine, store at 4°C and use within 3-4 weeks. Stocks are stored at -30 °C.
2. Prepare a 1:100 dilution of poly-D-lysine (final concentration of 10 μg/ml) in sterile CMF-PBS- of appropriate volumes.
3. Incubate in dish at room temperature for at least 30 minutes.
4. Remove poly-D-lysine and wash three times in CMF-PBS- and keep in last wash while preparing laminin solution.
5. Prepare, apply and incubate of laminin as above.
6. The next day, remove laminin and wash dishes in CMF-PBS three times and add neural induction or differentiation media.

2.5.2 Coating Dishes with Poly-D-Lysine and Fibronectin

Protocol below was followed:

1. Thaw aliquots of fibronectin and poly-D-lysine, store at 4°C and use within 3-4 weeks. Stocks are stored at -30 °C.
2. Treat as above but substituting fibronectin for laminin.
3. The next day, remove fibronectin and wash dishes in CMF-PBS- three times and add chromaffin differentiation media.

2.5.3 Coating Dishes with Matrigel

The protocol below was followed:

1. Thaw aliquots of matrigel (Corning-Cat number-354277) at 4°C on ice overnight. Stocks are stored at -30 °C according to manufacturer's instructions.
2. Prechill pipette tips and culture wares and place them on ice.
3. Prepare a 1:100 dilution of matrigel in cold DMEM/F12 on ice and transfer onto plates carefully to avoid bubbles.
4. Incubate at room temperature for at least 1 hour.
5. Remove matrigel solution and add DE or thyroid C cell differentiation medium.
6. OR Parafilm the dishes and incubate at 4°C overnight.

2.5.4 Neural Crest Progenitor Cell Induction-Wnt Activation and TGFβ (Transforming Growth Factor Beta) Inhibition

hPSCs were cultured to 80%–90% confluence and harvested using the EDTA-CMF-PBS buffer for 4-6 minutes. The buffer was gently removed and 2 mL of media was gently added to harvest the cells into a 15 mL Falcon tube and 10 µL was counted using a haemocytometer under the microscope. Cells were seeded at 2 X 10^4 into laminin-coated organoid culture dishes with TESR™-E8™ complete media supplemented with 10 µM Y-27632 and cultured at 37°C and 5% CO_2 in a humidified incubator overnight; this is recorded as day 0. On day 1, the media was changed to N2B27 media supplemented with 3 µM CHIR99021 and 10 µM SB-431542 and cultured at 37°C and 5% CO_2 in a humidified incubator for four days. Medium change was done on the 3rd

day. On day 5, the cells were harvested using the EDTA-CMF-PBS buffer for 4-6 minutes into a 15 mL Falcon tube and centrifuged at 200g for 3 minutes. The pellet was resuspended in NBM supplemented with 10 ng/mL BMP2 and 20 ng/mL FGF2 and plated in a 96 well ultra-low attachment plates. Media change was done every three days by removing about two-third of the old media and replacing it with fresh NBM with the supplements for 4–6 days. Neurospheres were then seeded in an 8-well or 12-well chamber slides (Ibidi, Germany) coated with fibronectin for immunostaining or dissociated using EDTA-CMF-PBS buffer before differentiated into chromaffin-like cells.

2.5.5 NCPC Induction- only Wnt Activation

hPSCs were cultured to 80%–90% confluence and harvested using the EDTA-CMF-PBS buffer for 4-6 minutes. The buffer was gently removed and 2 mL of media was gently added to harvest the cells into a 15 mL Falcon tube and 10 µL was counted using a haemocytometer under the microscope. Cells were seeded at 3 X 10^4 into laminin-coated organoid culture dishes or 1 X 10^4 in a well of a multidish 4 well Nunclon round dish with TESR™-E8™ complete media supplemented with 10 µM Y-27632 and placed cultured at 37°C and 5% CO_2 in a humidified incubator overnight; this is recorded as day 0. On day 1, the media was changed to N2B27 media supplemented with 3 µM CHIR 99021 and cultured at 37°C and 5% CO_2 in a humidified incubator for four days. Media was replaced on the 3rd day. On day 5, the cells were harvested using the EDTA-CMF-PBS buffer for 4-6 minutes into a 15 mL Falcon tube and centrifuged at 200 g for 3 minutes and the pellet was resuspended in DM (Differentiation Medium (DM) DMEM/F12, 1X Glutamax, 2% B27, 0.5% BSA, 1X penicillin/streptomycin (GIBCO) supplemented with 500 pg/mL recombinant human BMP4 (hBMP4-R&D systems) and seeded for 2 days in a 96 well ultra-low attachment plates. The cells were then seeded in an 8-well or 12 Well chamber slides coated with fibronectin for differentiation or dissociated using EDTA-CMF-PBS buffer before being differentiated into chromaffin-like cells.

At various time-points, cells were harvested for RNA extraction and Real-Time PCR/quantitative PCR (qPCR) analysis whiles the other cells were plated for immunofluorescence and FACs analysis.

2.5.6 Chromaffin-like Cell Differentiation

For differentiation of NCPC toward chromaffin-like cells, neurospheres were harvested and dissociated using the EDTA-CMF-PBS buffer for 4-6 minutes. Dissociated cells were centrifuged and the cells were plated in 96 well ultra-low attachment plates in DM supplemented with 500 pg/mL (and 50 pg/mL) hBMP4 with or without 10 mM dexamethasone (Sigma-Aldrich) and 100 nM Phorbol 12-myristate 13-acetate (PMA, Millipore) and also 10 mM dexamethasone (Sigma-Aldrich) and 100 nM Phorbol 12-myristate 13-acetate (PMA, Millipore) only. Cells were then cultured at 37°C and 5% CO_2 in a humidified incubator for 6-9 days. Media change was done every 2-3 days by removing 2/3 of the medium and replacing it with a freshly made medium with supplements. For immunofluorescence, differentiated cells were briefly dissociated by pipetting up and down 3-5 times and plated for 3-4 hours on human plasma fibronectin-coated μ-slide 8-well or 12-Well Chamber slides.

For differentiation of GD2-sorted NCPC-derived SAP-like cells towards chromaffin-like cells, GD2+ cells were differentiated for 6-9 days on poly-D-lysine/fibronectin coated μ-slide 8 well dish in DM medium supplemented with 10 mM dexamethasone (Sigma-Aldrich) and 100 nM Phorbol 12-myristate 13-acetate (PMA, Millipore) with or without 500 pg/mL hBMP4.

2.5.7 NCPC Induction-Wnt Activation and TGFβ Inhibition to Enteric Neural Progenitor Cells

hPSCs were cultured to 80%–90% confluence and harvested using the EDTA-CMF-PBS buffer for 4-6 minutes. The buffer was gently removed and 2 mL of media was gently added to harvest the cells into a 15 mL Falcon tube and 10 μL was counted using a haemocytometer under the microscope. Cells were seeded and differentiated as previously described in 2.5.5. On day 5, the cells were harvested using the EDTA-CMF-PBS buffer for 4-6 minutes into a 15 mL Falcon tube and centrifuged at 200 g for 3 minutes. The pellet was resuspended in NBM supplemented with 50 ng/mL BMP2, 20 ng/mL FGF2 and 50 nM RA and plated in a 96 well ultra-low attachment plates. The plates were then centrifuged at 200 g for 3 minutes to collect the cells at one point and later cultured in the incubator for 7 days. Media was topped up on day 4. On day 12, neurospheres were then seeded 3 spheres per well of a 12-well chamber slides or 4-5 spheres per well of an 8-well chamber slides or 48 well plate coated with laminin

overnight for the cells to attach before differentiation. On day 13, media was changed to NBM supplemented with 10 μM RA or 100 nM RA plus 25 nM ET-3 (Sigma) or with 25 ng/mL human recombinant GDNF (R&D systems) for 6, 9 and 12 days. Media change was done every 2-3 days.

On day 19, 22, or 25, cells for RNA extraction were harvested and cells for immunofluorescence staining were fixed and stained following the protocols outlined below.

2.6 Thyroid C Cell Differentiation

2.6.1 Defintive Endoderm Differentiation and Differentiation to Thyroid C Cell-like Cells

hESCs were cultured to 80%–90% confluence and harvested using the EDTA-CMF-PBS buffer for 4-6 minutes. The buffer was gently removed and 2 mL of media was gently added to harvest the cells into a 15 mL Falcon tube and 10 μL was counted using a haemocytometer under the microscope. Cells were seeded at 0.5 X 10^4 into matrigel-coated organoid culture dishes with TESR™-E8™ complete media supplemented with 10 μM Y-27632 and cultured at 37°C and 5% CO_2 in a humidified incubator overnight; this is recorded as day 0. On day 1, the media was changed to DMEM/F12 supplemented with 0.5% FBS, 1X penicillin (100 U/mL)/streptomycin (100 μg/mL) and 100 ng/mL HumanKine Activin A (Miltenyi Biotec- 130-097-608) and cultured at 37°C and 5% CO_2 in a humidified incubator for 5 days. Medium was replaced on the 3rd day. On day 6, the cells were harvested using the EDTA-CMF-PBS buffer for 4-6 minutes into a 15 mL Falcon tube and centrifuged at 200g for 3 minutes and seeded on laminin coated μ-slide 8 well dish and cultured in DMEM/F12 supplemented with 10% FBS, 1X ITS and/or 2 ng/mL IGF-1 (Insulin-like growth factor 1) or 3 ng/mL of RA or both IGF-1 and RA for 6 days. Media change was done every other day. On day 12, the cells were cultured in DMEM/F12 supplemented with 10% FBS, 1X ITS-A without any supplements for additional 3 days.

2.6.2 Thyroid C Cell Differentiation Using Organoid Cultures

hESCs were harvested as above and seeded at 1 X 10^4 cells per well in matrigel-coated 8-well chamber slides for immunofluorescence or 48 well plate for RNA extraction. These cells were cultured in TESR™-E8™ complete media supplemented with 10 μM

Y-27632 and cultured at 37°C and 5% CO_2 in a humidified incubator overnight. This day was recorded as day 0. On day 1, the media was removed and the cells were briefly washed with CMF-PBS before culturing them in DMEM/F12 supplemented with 0.5% FBS, 1X ITS-A and 1X penicillin (100 U/mL)/streptomycin (100 μg/mL) and 100 ng/mL of Activin A. The cells were maintained at 37°C and 5% CO_2 in a humidified incubator for 5 days. Medium change was done on day 3 with fresh medium plus supplements. On day 6, media was changed to DMEM/F12 supplemented with 10% FBS, 1X ITS-A and 2 ng/mL IGF-1 for 6 days. On day 12, the cells were cultured in DMEM/F12 supplemented with 10% FBS, 1X ITS-A, and 1X penicillin (100 U/mL)/streptomycin (100 μg/mL) without any supplements for additional 3 days. On day 15, cells for RNA extraction were harvested and cells for immunofluorescence staining were fixed and stained following the protocols outlined below.

2.6.3 Thyroid C Cell Differentiation Using EB (Embryoid Bodies) Generated with Polyvinyl Alcohol (PVA)

hESCs were harvested as above and seeded at 1 X 10^4 cells per well in 96 well ultra-low attachment plates in DMEM/F12 supplemented with 0.5% FBS, 1X ITS-A, 0.5% PVA and 100 ng/mL of Activin A and recorded as day 1. The cells were maintained at 37°C and 5% CO_2 in a humidified incubator for 5 days. Medium change was done on day 3 with fresh media plus supplements. On day 6, many cells formed embryoid body (EB)-like spheres; these spheres were seeded at 3-4 spheres per well in vitronectin-coated 8-well chamber slides and 48 well plates and cultured in DMEM/F12 supplemented with 10% FBS, 1X ITS-A, 1X penicillin (100 U/mL)/streptomycin (100 μg/mL) and 2 ng/mL IGF-1 without PVA for 6 days (i.e. to day 12). On day 12, the cells were cultured in DMEM/F12 supplemented with 10% FBS, 1X ITS-A and 1X penicillin (100 U/mL)/streptomycin (100 μg/mL) without any supplements for additional 3 days. On day 15, cells for RNA extraction were harvested and cells for immunofluorescence staining were fixed and stained following the protocols outlined below.

2.6.4 Thyroid C Cell Differentiation Using Matrigel Scaffold Cultures

hESCs are harvested as above and 1 X 10^5 cells was resuspended in 35% of matrigel in DMEM/F12 supplemented with 0.5% FBS, 1X ITS-A and seeded in two wells of a 96 well plate and placed in the incubator 37°C for 60-90 minutes for the gel to cast before

topping the well up with DMEM/F12 supplemented with 0.5% FBS, 1X ITS-A, 1X penicillin (100 U/mL)/streptomycin (100 μg/mL) and 100 ng/mL of Activin A and cultured at 37°C and 5% CO_2 in a humidified incubator for 5 days. Media change was done every other day. On day 6, media was changed to DMEM/F12 supplemented with 10% FBS, 1X ITS-A, 1X penicillin (100 U/mL)/streptomycin (100 μg/mL) and 2 ng/mL IGF-1 for 6 days. Media change was done every day. After 7 days (i.e. day 12), the cells were cultured in DMEM/F12 supplemented with 10% FBS, 1X ITS-A and 1X penicillin (100 U/mL)/streptomycin (100 μg/mL) without any supplements for additional 3 days. On day 15, cells for RNA extraction were harvested and cells for immunofluorescence staining were fixed, cryosectioned and stained following the protocols outlined below.

2.7 *In Vivo* Transplantation of hPSC-derived Neural Crest Progenitor Cells (NCPC)

GFP-expressing ENVY-hESC cells were differentiated to NCPCs (see (Hotta et al. 2009)) and transplanted *in ovo* between the neural tube and somites at somite-level 16-24 of quail embryonic day 2 (QE2). (Somite level 18-24 is defined as the 'adrenomedullary' level (Le Douarin and Teillet 1974)). Incubation was continued for 4-5 days in a 65% humidified egg incubator at 38°C. The region (between the upper and lower limb) of migration of cells to the kidney and adrenal region were excised and fixed, embedded and cryosectioned as outlined below. Human cells were identified with antibody to GFP.

2.7.1 Organ Culture and CAM (Chorio-Allantoic Membranes) Grafts of hPSC-derived NCPCs

Neurospheres (aggregates of NCPCs) were incubated with Calcein AM cell-permeant dye (1/2000- ThermoFisher) per manufacturer's instruction for 20-30 minutes and washed twice with CMF-PBS; this aids implantation by making the implant visible. QE2 quail embryos were harvested and a tissue rectangle of the somites 14-24 trunk region was cut out and labelled neurospheres (resuspended in air-buffered Ham's F12 supplemented with 5% E4 quail embryonic extract, 10% FBS, 1X pen-strep) were implanted *in situ* as above. These were grown in the above medium in a humidified incubator at 38°C. After 24 hours, tissues were checked microscopically to confirm that the calcein-labelled implant cells had attached to the tissue and also to check whether

some of the implanted cells have started migrating out into the tissue. For organ culture, these were continued *in vitro* for a further 3 days. Alternatively, to achieve extended time and greater growth the ensemble was transferred to CE8 (Chick Embryonic day 8) chick embryo CAM and grown for an additional 8 days in a 65% humidified egg incubator at 38°C according to our previous protocol (Zhang et al. 2010a). Grafts were excised and fixed, embedded and cryosectioned as outlined below. Human cells were identified with mouse antibody to human nuclear antigen (HNA) and to human mitochondria (refer to section 2.8.1.1, Table 15).

2.8 Fixing, Embedding and Sectioning of Neural Crest Progenitor Cells and Tissues

Protocol below describes preparation and cryosectioning of neurospheres and tissues:

Fixing: collect neurospheres/tissues in PBS in Eppendorf tube and make sure they settle in the bottom.

Wash twice in PBS and add 4% PFA in PBS and incubate at room temperature 20 -30 minutes. Remove 4% PFA and wash twice in PBS. Add 20% sucrose in PBS to infiltrate neurospheres/tissues and incubate at 4 ºC overnight; infiltration is adequate when neurospheres/tissues sink to the bottom.

Embedding: fill Tissue-Tek Cryomold Biopsy moulds (10 x 10 x 5mm) with Tissue-Tek optimum cutting temperature (OCT) compound (both from ProSciTech, Thuringowa, Australia) and label appropriately. Transfer neurospheres to an organ culture dish containing OCT and using forceps further transfer each NSP individually to the OCT-filled mould. Using a needle, push neurospheres to the bottom of the block. With the tissues, transfer the tissues to the cryomould and remove excess sucrose from the tissues. Fill the cryomold with OCT and allow specimens to settle. Freeze block in a dry ice-cooled isopentane till the transparent OCT turns into white, mark with pen where neurospheres are located then proceed with sectioning or for long-term storage, store blocks at -80 ºC.

Sectioning: transfer blocks on dry ice to the cryostat. Place block inside the cryostat and set it to -30 ºC. Label 10 poly-L-lysine coated Superfrost slides (Thermo Fisher, Catalog no: MENSF41296SP) prior to sectioning. Cut sections between 18-20 µm and place in the bottom left corner of the first slide followed by the second section in the same position in the second slide up to the 5th slide. Then position the second round of sections in the bottom right corner to each slide sequentially and then move to middle

left position followed by middle right position and fifth round on top left position followed by top right position of slides producing at least 6 sections on each slide. Dry slides at room temperature for an hour and store at 4°C overnight and then proceed with immunostaining or store at -80 ºC for long-term storage.

2.8.1 Immunocytochemistry/Immunofluorescence

Cells were fixed with 1-4% paraformaldehyde for 15 min at room temperature and washed three times with PBS. The cells were then permeabilised for 30 minutes with 0.2% Triton-X and 1% horse serum in PBS with 0.2% azide and blocked with 3% horse serum in CMF-PBS azide for 30 minutes. The cells were then washed once with CMF-PBS azide and stained with primary antibodies per manufacturer's instructions and incubated at 4 °C overnight. Antibodies are listed in Table 15 below. Cells were then washed three times with CMF-PBS with a 5-minute interval between CMF-PBS changes. For detection, cells were incubated with respective fluorochrome-conjugated secondary antibodies for 2-3 hours at room temperature (see Table 15). Residual secondary antibodies were removed and washed twice with CMF-PBS before counterstaining the nuclei with 10 ng/mL 4',6- diamidino-2-phenylindole dihydrochloride (DAPI, Sigma-Aldrich). Cells were then mounted in glycerol mounting medium with antifade 1,4-diazabicyclo[2.2.2]octane (DABCO; Sigma Aldrich) and viewed using Zeiss LSM 780 confocal microscope (Carl-Zeiss-Strasse, Oberkochen, Germany).

2.8.1.1 Primary, Secondary and Isotype Antibodies

Table 15. Primary, secondary and isotype antibodies used in this thesis.

Primary antibodies	Target type	Host / Isotype	Company	Dilution
Anti-Human SOX10	NC lineage (not neurons)	Goat Polyclonal	R&D systems	1:200
Anti-p75NTR (D4B3) XP® Rabbit mAb #8238	NC lineage	Rabbit polyclonal	Cell Signalling	1:1,500
Anti-HNK1	NC lineage	Mouse IgM	MCRI	1:200
Anti-AP2α (3B5)	NC lineage	Mouse IgG2b	DSHB	1:200
Anti-GD2 (clone 14.G2a)	SAP marker	Mouse IgG_{2a}	BD Biosciences	0.5 µg / $1x10^6$ cells
Anti-MASH1/Achaete-scute homolog 1 antibody (ab38556)	SAP marker	Rabbit polyclonal	Abcam	1:500
Anti-Peripherin (clone 8G2)	SAP &. neuron	Mouse IgG	Millipore	1:500

	marker			
Anti-SA1	SAP lineage marker	Mouse IgG	DSHB	1:20
Anti-B2B1	Symp. neuron lineage	Mouse IgM	DSHB	1:20
Anti-Neurofilament Heavy antibody (NF421)	Neurite marker	Mouse IgG1	Abcam	1:500
Anti-Neurofilament M (145 kDa) Antibody	Neurite marker	Rabbit polyclonal	Millipore	1:2,000
Anti-TH	Neuron CA synth. enz.	Chicken polyclonal	Abcam	1:1,500
Anti-TH	Neuron CA synth. enz.	Rabbit polyclonal	Novus Biologicals	1:1,500
Anti-Chromogranin B (ab12242)	Neuroendocrine marker. LDCV	Rabbit polyclonal	Abcam	1:700
Anti-Chromogranin C (ab12241)	Neuroendocrine marker. LDCV	Rabbit polyclonal	Abcam	1:700
Anti-PNMT	Chromaffin-spec. adrenaline enzyme	Rabbit polyclonal	ThermoFisher Sci.	1:700
Anti-Chromogranin A (CPTC-CHGA-2)	Chromaffin/Sym. Neuronal lineage/neuroendocrine cells	Mouse Monoclonal	DSHB	1:10
Anti-FOXA2 antibody [EPR4466]	Endodermal Lineage	Rabbit monoclonal	Abcam	1:200
Anti-Human Nuclear Antigen antibody [235-1] (ab191181)	Human-specific marker	Mouse monoclonal IgG	Abcam	1:200
Anti-Mitochondria antibody [113-1] (ab92824)	Human-specific marker	Mouse monoclonal IgG	Abcam	1:1,500
Mouse IgG negative Isotype control (SC-2025)		Mouse IgG	Santa Cruz	1:500
Rabbit IgG negative Isotype control (SC-2027)		Mouse IgG	Santa Cruz	1:1,500
Secondary antibodies		**Host / Isotype**	**Company**	**Dilution**
Anti-Goat IgG:Alexa 488		Donkey	ThermoFisher Sci.	1:1,000
Anti-Goat IgG:Alexa 594		Donkey	ThermoFisher Sci.	1:1,000
Anti-Goat IgG:Alexa 647		Donkey	ThermoFisher	1:1,000

		Sci.	
Anti-Sheep IgG:Alexa 594	Donkey	ThermoFisher Sci.	1:1,000
Anti-Rabbit IgG Alexa 488	Donkey	ThermoFisher Sci.	1:1,000
Anti-Rabbit IgG Alexa 594	Donkey	ThermoFisher Sci.	1:1,000
Anti-Rabbit IgG Alexa 633	Goat	ThermoFisher Sci.	1:1,000
Anti-Mouse IgG-specific:Alexa 488	Goat	ThermoFisher Sci.	1:1,000
Anti-Mouse IgM- specific:Alexa 488	Goat	ThermoFisher Sci.	1:1,000
Anti-Mouse IgG+M Alexa 594	Donkey	Mol. Probes (A21203)	1:1,000
Anti-Mouse IgG Alexa 647	Donkey	ThermoFisher Sci.	1:1,000
Anti-Mouse IgG Alexa 568	Donkey	ThermoFisher Sci.	1:1,000
Anti-Chick IgY Dylight 488	Donkey	Jacksons Immunoresearch	1:500
Anti-Rabbit IgG Cy5	Donkey	Jacksons Immunoresearch	1:500
Anti-Chick IgY Alexa 488	Goat	ThermoFisher Sci.	1:1,000
Anti-Chick IgY Alexa 568	Goat	ThermoFisher Sci.	1:1,000

Abbreviations: TH-Tyrosine Hydroxylase, SA-Sympathoadrenal, GD2-Ganglioside 2, PNMT-Phenylethanolamine N-methyltransferase, B2B1- Carbohydrate epitope globoseries B2B1, LDCV- Large Dense Core Vesicles

2.8.2 Whole Mount Staining and Immunohistochemistry of Chicken Embryos

Embryos were harvested 2 days post electroporation (E3.5) and sagittally dissected, fixed in 4% paraformaldehyde in PBS at 4°C overnight then washed in PBS three times. Embryos were blocked and permeabilised with 3% horse serum and 0.2% Triton-X100 in PBS/azide for 1 hr. Control cryostat 18 µm sections of chick embryo and post-natal mouse brain (as antibody positive-control) were also used. Rabbit anti-DGCR8 antibody (Abcam-ab82876) and mouse anti-mCherry (DSHB, Iowa City) at 1:200 and 1 :100, respectively were applied in 1% horse serum and 0.1% Triton-X in PBS azide and

incubated on a rocker at 4°C overnight. The human DGCR8 immunogen (N-terminal amino acids 180-229) was 89% identical to the predicted chick amino acid sequence, with all changes conservative. Washing with PBS was done for 3 hours with changes every 30 minutes on a rocker at 4°C. Secondary antibodies were donkey anti-rabbit Alexa Fluor 488 for mouse sections (Life Technologies-1:1000) and donkey anti-rabbit Cy5 plus donkey anti-mouse IgG Alexa Fluor 568 for whole mounts (Jacksons Immunoresearch-1:500 and 1:1000, respectively) and 500 ng/mL (1 in 100 of 50 ug/mL stock) DAPI was applied and incubated for 3 hours on the rocker at 4°C. Embryos were washed with PBS three times and mounted using DABCO/glycerol mounting medium. Confocal microscopy was performed using the Zeiss LSM 780 confocal microscope.
For cryostat sections, fixed embryo heads (E5.5) were placed in 30% sucrose in PBS overnight, embedded in Tissue Tek OCT Compound Medium in Tissue Tek cryomoulds and frozen in dry ice-cooled isopentane. Eighteen µm sections were cut transversely using a Leica CM 1900 cryostat microtome and collected on Superfrost microscope slides (Biolab Scientific, Auckland, NZ) coated with poly-l-lysine. Mouse post-natal brains were also fixed, sectioned, mounted and stained as above.

2.8.3 Nuclear Dyes

DAPI was received as a powder, reconstituted in sterile H_2O to a stock concentration of 1 mg/ml, aliquoted and stored at -30ºC. Thawed aliquot in use was stored at 4ºC from which appropriate volume was taken and diluted 1:3000 in sterile H_2O and applied to immunostained samples at the end of the protocol, incubating for 3-5 minutes at room temperature.

2.8.4 Blocking Solutions

Horse Serum (ThermoFisher Scientific, Catalog no: SH303963) stocks were stored at -30ºC in 1 mL aliquots. Thawed aliquot was stored in 4ºC and used within couple of days. Normal goat serum (ThermoFisher Scientific, Catalog no PCN5000) stocks were stored at -30ºC in 1 mL aliquots. Thawed aliquot was stored in 4ºC and used within couple of days. These sera were used as blocking solution at 1-10% diluted in CMF-PBS.

2.8.5 Quantification Analysis of Immunostaining Data

Method described here is for quantification of markers that have nuclear and cytoplasmic expression. Quantification was performed using the free Fiji Image J ZEN imaging software (NIH). For immunofluorescence cell counts (e.g. αTH+, PNMT+, NF+, CgB+), Olympus IX70 and confocal images were selected and analysed using the Zeiss Image Analyser and ImageJ. The number of fields counted varied from 3 to 10, and images were blinded among counters. For each marker, minimum 3 independent experiments with minimum 10 random images from each experiment were analyzed. Total number of DAPI nuclei was used as the total number of cells in a field. With the DAPI channel and one other channel, (Green or Red or Far-red), the cells in a field were counted. The ratio of the different colours to DAPI was calculated as follow:

1. Save images of immunostaining data as black and white and JPEG format.
2. Open images of marker of interest. For each image do the following:
3. Run Image > Adjust > Threshold.
4. Manually set threshold to exclude background then click apply.
5. Run Edit > Invert.
6. Run Analyze > Set Measurements and select “Integrated density”.
7. Run Analyze > Measure. A "Result" window will come up with “Integrated density” value.
8. Document results in an excel document.
9. Save images and results.
10. Repeat steps 1-9 for corresponding DAPI images.
11. Calculate ratio for each image of marker of interest relative to matched DAPI image: Integrated density value of marker of interest/ Integrated density value of corresponding DAPI.
12. Calculate the average to obtain the percentage of expression for marker of interest.

13. Do same steps above for each independent experiment and perform statistics at the end.

2.8.5.1 Relative Pixel Quantification

Standard confocal images were selected and analysed using the Zeiss Image Analyser. Region of interest was selected with the Free-Hand tool and choosing the DAPI channel, the cells in a field were counted and relative pixel quantification was calculated following a previous publication (Oriol Arqués 2012). Relative fluorescence intensity was calculated by normalising the mCherry and DGCR8 expression to DAPI intensity.

2.9 *In Vivo* Electroporation

Eggs from a cross breed *White Leghorn x Black Australorp* were commercially purchased (Research Hatchery, Victoria). *In vivo* electroporation were performed as previously described (Sato et al. 2002; Yokota et al. 2011; Simkin et al. 2014). The CRISPR/Cas9 *DGCR8* exon 2 targeting construct was co-electroporated with pT2K-CAAGGS-EGFP (termed Tol2-GFP) and pCAGGS-T2TP (transposase) (Sato et al. 2007) at 6:6:1.5 µg/µL ratio respectively. The plasmid mixture was prepared and coloured with 2% Fast Green and then microinjected forward from the 3-4 somite level of the neural tube into the hind and midbrain of E1.5 chicken embryos. Electric pulses of 10.5 V, 50 ms duration were delivered 3 times bilaterally with 175-ms intervals. Chicken embryos were harvested 2 and 4 days post-electroporation and processed for immunostaining and cell sorting.

2.10 Flow Cytometry

Neurospheres (NCPC aggregates) were harvested using the EDTA-CMF-PBS buffer for 4-6 minutes into a 15 mL Falcon tube and centrifuged at 200 g for 5 minutes. The pellet was then resuspended in 5 mLs of NBM media and 10 µL was counted using a haemocytometer under the microscope. Mouse IgM B2B1 antibody and rabbit p75NTR antibody (for all antibody source and administration details, see Table 15 above) was used to indirectly label the cells for 30 minutes on ice. Cells were spun down and washed with CMF-PBS and then followed by the respective secondary antibodies, donkey anti-rabbit Alexa Fluor 594 and donkey anti-mouse IgM Alexa Fluor 488 for 30 minutes in the dark. The cells were washed with CMF-PBS and additionally directly labelled with mouse IgG GD2 antibody: Alexa Fluor® 647 for 30 min on ice in the

dark. For HNK1 and SA1 analysis, mouse HNK1 IgM antibody and mouse SA1 IgG antibody were used co-labelled with rabbit p75NTR antibody as above. Goat anti-mouse IgG-specific: Alexa Fluor 647 and goat anti-mouse IgM-specific Alexa Fluor 488 were used to label the cells since these distinguish between the IgG and IgM primary antibodies. Mouse serum and rabbit IgG for isotype staining (1:500, Jackson Immunoresearch) was used to gauge the degree of non-specific binding of antibody. The cells were washed with CMF-PBS, pelleted and resuspended in CMF-PBS containing 2% FBS and strained (40 μm mesh; BD Falcon; Becton, Dickinson and Company) and FACS sorted using the BD FACs Aria Fusion Cell Sorter (Becton, Dickinson and Company, Franklin Lakes, NJ), with separation based on secondary antibody, DAPI and live cell staining.

The p75NTR NCPC marker was used to gate for GD2, B2B1, SA1 and HNK1 analysis. The cells were washed once with CMF-PBS and centrifuged at 200 g for 5 minutes. The cells were then stained with goat anti-mouse IgG (H+L) Alexa Fluor 647 secondary antibody and incubated on ice for 30 minutes. After incubation, the cells were washed once with CMF-PBS and again with Ham's F12 media supplemented with 5% FBS and centrifuged at 200 g for 5 minutes. The pellet was suspended in Ham's F12 media supplemented with 5% FBS and strained through a 40 μm cell strainer (BD Falcon) and FACS sorted using the BD FACS Aria cell sorter.

To detect intracellular proteins, cells fixed with 1% PFA were permeabilized with 0.1% Triton-X in 1% horse serum, blocked with 1% horse serum, and incubated with primary antibodies in blocking buffer at 4°C overnight. After washing with CMF-PBS and centrifuging, appropriate secondary antibodies were added for 1 hour and cells were washed and events were acquired with BD FACS X-20 Fortessa. Data was analysed using CellQuest (both from BD Biosciences) and FCS Express 4 Flow (Denovo Software).

For live and death cell assay analysis, cells were harvested as above and stained with Calcein-AM and Propidium Iodide following manufacturer's instructions. Briefly, 1:2000 dilution of Calcein-AM (ThermoFisher Scientific) with 1:10,000 dilution of Propidum Iodide (Sigma Aldrich) was made by dissolving them in the culture medium and incubated at 37°C for 20-30 minutes. Cells were washed 3 times with CMF-PBS and centrifuged at 200 g for 3 minutes. The pellet was then resuspended in FACs buffer, 2% FBS in CMF-PBS and strained (40 μm mesh; BD Falcon; Becton, Dickinson and Company) before events were acquired with BD FACS X-20 Fortessa. Data was

analysed using CellQuest (both from BD Biosciences) and FCS Express 4 Flow (Denovo Software).

For chicken embryonic cells, cell suspensions from harvested embryos were made using 0.5% w/v Dispase II (Roche, Switzerland) and 0.1% w/v CLSAFA Collagenase (Worthington, USA) at 37°C in Hams F12 solution for 5-10 minutes. The enzyme reaction was stopped by adding 2X volume of the above suspension of PBS with 10% FBS. The digested cells were pelleted and resuspended in PBS containing 2% FBS and strained (40 μm mesh; BD Falcon; Becton, Dickinson and Co., Franklin Lakes, NJ) and FACS sorted using the BD Influx Cell Sorter, with separation based on GFP and mCherry fluorophores.

2.11 Faglu Fluorescence of Catecholamines

Differentiated NCPCs were fixed in Faglu mixture following published protocol (Furness et al. 1977; Furness et al. 1978), to convert catecholamines to a fluorescent compound. Briefly, differentiated cells were washed twice with CMF-PBS and fixed in Faglu mixture of 4% PFA and 0.5% glutaraldehyde (electron microscopy grade) in 0.1 M phosphate buffer, pH 7.0 for 1-2 hours at room temperature. Faglu mixture was then removed and the cells were washed thrice in CMF-PBS. The cells were then permeabilised as described above for combination with conventional immunostaining. The Faglu signal was detected using the 488-filter set of the Zeiss LSM 780 confocal microscope.

2.11.1 High Performance Liquid Chromatography for Catecholamine Detection

Differentiated cells for high performance liquid chromatography (HPLC) were prepared per previously published protocol (Saxena et al. 2013). Briefly, harvested cells (20,000 cells) were homogenized in 250 μL sonication buffer consisting of 0.1 M acetic acid (Sigma), and 2% EDTA (GIBCO). Qsonica sonicator (Newtown, CT, USA) was used to sonicate the cells on ice with 3 bursts (5 sec each) at 50% amplitude, at 25 s intervals. Sonicated lysate was centrifuged for 5 min at 10,000 rpm and the supernatant was used to analyze catecholamines by HPLC with fluorescence detection. The manual derivatizations were performed as described previously (van der Hoorn et al. 1989). For the derivatization, 10 μL of 1M KOH (to neutralise the acetic acid) was added to 40 μL

of sample, which was followed by 68 µL of solution R1 (potassium ferricyanide: acetonitrile containing 10 µM isoprenaline as internal standard, 1,000:80) and 38 µL of solution R2 (1,2-diphenylethylediamine:bicine, 600:300). Incubation was for 45 minutes at 37 °C. Injection volume was 100 µL.

For chromatography, the column was 15 cm x 3.9 mm Waters Symmetry C18 and the mobile phase was 35% acetonitrile in 50 mM sodium acetate at pH 6.8 and run at 2 ml/min. The run-time under these conditions was 60 minutes for each sample. Detection was by fluorescence at 350 nm excitation and 480 nm emission. This was performed by A/Prof Andrew Bjorksten at the Department of Anaesthesia and Pain Management, The Royal Melbourne Hospital.

2.12 Neurospheres Size Measurements

Neurospheres were made from 4-5,000 cells seeded per well in a 96 well ultra-low attachment wells in NBM supplemented with 50 ng/mL BMP2, 20 ng/mL FGF2 and 50 nM RA for NCPC/VNCC differentiation. On the other hand, NCPC/VNCs were cultured as neurospheres in NBM supplemented with 25 ng/mL GDNF for ENCC/EN/Enteric glia differentiation. To compare the size of MEN2B hESC-derived VNCC and differentiated ENCCs versus control H9 hESCs-derived VNCC, for each independent experiment (n=3), brightfield images were randomly taken for at least 8 neurospheres for each condition using Zeiss Axio Observer z1 florescence microscope and ZEN imaging software. Image J software was used to measure the largest diameter of each neurosphere.

2.13 Proliferation Assay

The proliferation rate of hESCs and differentiated cells was assessed by adding 5 and 10 µM EdU (Click-iT Plus EdU Alexa Fluor 488 Imaging Kit, ThermoFisher Scientific) to the culturing medium of hESCs and differentiated cells respectively for 4-8 hours. Cells were then fixed with 4% PFA for 5-10 minutes. EdU staining was performed per manufacturer's instructions as follows. After fixing, the PFA was removed and the cells were washed 3 times with CMF-PBS and then permeabilised for 30 minutes with 1% Horse serum and 0.1% Triton-X in CMF-PBS-Azide. The cells were then washed 3 times with CMF-PBS and a mixture of the EdU reaction cocktail (430 µL of 1X Click-

iT reaction buffer, 20 µL $CuSO_4$, 1.2 µL Alexa Fluor 488 picoyl azide and 50 µL Reaction buffer additive) was added to the cells and incubated for 30 minutes in the dark at room temperature. The reaction cocktail was removed and then washed with 1% Horse serum in CMF-PBS Azide. Cells were then immunostained with the respective primary and secondary antibodies as outlined above in 2.8.1.

2.14 RNA Extraction and SYBR Green QPCR

Briefly, harvested cells were spun down at 13,000 g for 2 minutes and supernatants are removed and discarded. Pelleted cells are suspended in 200 µL Trizol reagent and pipetted several times. An equal volume of acid-phenol chloroform was then added and vortexed till a uniform mixture was attained; this is left on ice for 5-7 minutes. This extraction mixture was centrifuged at 15,000 g for 10 minutes at 4°C. The top clear layer was gently removed avoiding the other layers and transferred into a 1.5 mL Eppendorf tube with equal amount of isopropanol. The mixture was then gently mixed by rotating the tube up and down 4 times and centrifuged at 15,000 g for 10 minutes at 4°C. The supernatant was discarded and 3X volume of the isopropanol was added to the pellet. The tubes were gently flicked for 3-4 times and centrifuged 15,000 g for 10 minutes at 4°C. The supernatant was discarded and the pellet was left to dry with a KIMTEK tissue (Kimberly-Clark Professional, USA) covering it. The pellet was resuspended in 20 µL of DEPC (Diethyl pyrocarbonate) water (Bioneer Pacific, South Korea). Extracted RNA was digested with DNaseI (deoxyribonuclease-Promega) following the manufacturer's instructions to remove any residual DNA. A total volume of 20µL, 1 µg of extracted RNA, 1X RNase Free DNaseI Reaction buffer, 1µL of DNaseI enzyme and topped up with DEPC water, was incubated at 37°C for 30 minutes and after addition of 1X DNaseI Stop Solution, the mixture was then incubated at 65°C for 10 minutes. Complementary DNA (cDNA) was synthesized using the Bioline SensiFAST™ cDNA Synthesis Kit (Bioline Australia: BIO-65054). Briefly, 30 ng total RNA was converted into cDNA following manufacturer's directions. A total volume of 20 µL, 30 ng of DNase1-treated RNA, 5X TransAmp Buffer, 1µL of Reverse Transcriptase and topped up with DEPC water, was incubated at 25°C for 10 minutes (primer annealing), 42°C for 15 minutes (reverse transcription), 85°C for 5 minutes (inactivation) and on hold at 4°C in a thermal cycler. For qPCR analysis, reactions were performed using cDNA converted from 30 ng of RNA, 5 nM of each primer (Forward

and Reverse Primer) and AccuPower® 2X GreenStar Master Mix Solution (Bioneer-South Korea) in a total volume of 10 µL in a 384 well plate (Bio-Rad, Australia). The plates were run on the LightCycler® 480 Instrument II (Roche Molecular Diagnostic) at 95°C for 10 minutes- 1 cycle, 95°C for 10 seconds, 60°C for 10 seconds and 72°C for 15 seconds-45 cycles and data were obtained using the recommended instrument settings. Data were extracted using the Absolute maximum as recommended by the manufacturer. Primers for qPCR analysis are listed in below. *β2M, GAPDH* and *RPL32* were used for data normalization where it is stated. Controls were used as a calibration standard and relative gene expression changes were calculated using the $2^{-\Delta\Delta CT}$ method. For chick-related experiments, extracted RNA was digested with DNaseI (Promega) following the manufacturer's instructions to remove any residual DNA. QPCR was performed to confirm the expression of *DROSHA, Neurogenin 2, Pax6, YPEL1,* and *DGCR8* genes in transfected modified embryonic cells from electroporated embryos. Briefly, 20 ng total RNA was converted into cDNA in the presence of SuperScript IV RT (Invitrogen) and random hexamers (Promega). Reactions were performed using cDNA converted from 10 ng of RNA, 250nM of each primer and 2X SYBR Green qPCR Master Mix (Promega) and topped up with Nuclease-Free water to a total volume of 20 µl. Primers for qPCR analysis are listed below. *ACTB* and *RPL32* were used for data normalization. mCherry-/GFP- sorted cells from each embryo were used as a calibrator and relative fold changes were calculated using the $2^{-\Delta\Delta CT}$ method.

Analysis of data:

Apply $2^{-\Delta\Delta CT}$ method to analyse data as follow:

1. On the Roche LightCycler machine the software manually set threshold above baseline during linear phase to capture cycle threshold (CT) values under. Export Abs Max data to Microsoft Excel for analysis.

2. Manually check integrity of triplicate CT values and exclude CT values above 38.

3. Calculate average of each triplicate CT values.

4. Calculate ΔCT values i.e. normalizing target genes CT values to the average CT values of the house keeping genes.

5. Calculate ΔΔCT values i.e. normalising ΔCT values of samples of interest to matched ΔCT values of control samples.

6. Calculate fold change by $2^{-(\Delta\Delta CT)}$ and perform appropriate statistical method.
7. Transfer gene expression data to Prism to generate graphs.

2.14.1 Semi-Quantitative RT-PCR

RNA extraction and cDNA synthesis were carried out and cDNA was synthesized using the Bioline SensiFAST™ cDNA Synthesis Kit (BIO-65054) as described above. Briefly, 30 ng total RNA was converted into cDNA following manufacturer's directions. Samples were diluted in nuclease free water in 1:1 ratio before performing the PCR reaction. Reactions were performed using 1 µL of diluted cDNA, 50 nM of each primer and 1X of GoTaq® Green Master Mix (Promega-M712) in a total volume of 12 µL. PCR products were run on a 1% agarose gel and analysed by gel doc. Primers for PCR analysis are listed in Supplementary. *RPL32* was used for data normalization. Cultured hPSCs and control cells (cultured with only the differentiation medium without supplements) were used as a calibration standard and relative gene expression changes were calculated using the (%) = 100 x (1-(1-fraction cleaved)$^{1/2}$) method.

Table 16. List of Taqman probes used for qPCR reactions.

Probes	Target type	Product size	Company	Accession Number
HOXA2	Hindbrain positional	107	ThermoFisher Sci.	Hs00534579_m1
HOXA5	Vagal positional	127	ThermoFisher Sci.	Hs00430330_m1
HOXA7	Trunk positional	131	ThermoFisher Sci.	Hs00600844_m1
HOXA10	Trunk positional	52	ThermoFisher Sci.	Hs00172012_m1
HOXB6	Trunk positional and Chromaffin cells specification	89	ThermoFisher Sci.	Hs00980016_m1
HOXB7	Trunk positional	66	ThermoFisher Sci.	Hs04187556_m1
HOXB8	Trunk positional and Noradrenergic specification	85	ThermoFisher Sci.	Hs00256885_m1
TFAP2α	NC lineage	73	ThermoFisher Sci.	Hs01029413_m1
TUBB3	Neuronal	134	ThermoFisher Sci	Hs00801390_s1
NEFH	Neuronal	149	ThermoFisher Sci	Hs00606024_m1
CDH1	Cell-to-cell adhesion protein	80	ThermoFisher Sci	Hs01023895_m1
CDH2		66	ThermoFisher Sci	Hs00983056_m1
FOXA1	Endodermal Marker	59	ThermoFisher Sci	Hs04187555_m1
FOXA2	Definitive Endodermal Marker	66	ThermoFisher Sci	Hs00232764_m1
RET		83	ThermoFisher Sci	Hs01120030_m1

PTEN		135	ThermoFisher Sci	Hs02621230_s1
ERBB3		62	ThermoFisher Sci	Hs00176538_m1
S100β	Glia marker	96	ThermoFisher Sci	Hs00902901_m1
ERBB4		64	ThermoFisher Sci	Hs00955522_m1
TOP2α	Proliferation Marker	81	ThermoFisher Sci	Hs01032137_m1
CASP3	Apoptotic Marker	100	ThermoFisher Sci	Hs00234387_m1
CASP8	Apoptotic Marker	124	ThermoFisher Sci	Hs01018151_m1
SOX10	NC lineage	102	ThermoFisher Sci	Hs00366918_m1
HOXD4	Trunk positional	149	ThermoFisher Sci	Hs00429605_m1
β2M	Housekeeper	64	ThermoFisher Sci.	Hs00187842_m1
GAPDH	Housekeeper	93	ThermoFisher Sci.	Hs02758991_g1

Table 17. Oligonucleotides used for qPCR reactions targeting *Homo Sapiens*

Gene	Sequence 5' to 3'	Fluorescent probes with BHQ1	Product size
PHOX2B	F: ACGCCGCAGTTCCTTACAAA	CACGGCGGCCTCAACGAGAA	88 bp
	R: CTGGTGAAAGTGGTGCGGAT		
PNMT	F: GCCTACCTCCGCAACAACTA	GAAGCTGCGCTGCTTGGCGC	200 bp
	R: GTCATGGTGATGTCCTCAAAGT		
SOX10	F: TCTGGAGGCTGCTGAACGAA	TCATCGAGGAGGCTGAGCGGC	210 bp
	R: AAGTGGGCGCTCTTGTAGTG		
αTH	F: GTGTTCCAGTGCACCCAGTA	TCTCGCAGGACATTGGCCTGGCGT	196 bp
	R: ACCAGTACAGCGTGGACAGCTTCT		
DβH	F: GCCATCCATTTCCAGCTCCT	AGGCTCAAGGCTGGCGTCCTGT	139 bp
	R: TCCAGGCGTCCGCAAAATAG		
ASCL1	F: TCCCCCAACTACTCCAACGA	TCGCCGGTCTCATCCTACTCG	188 bp
	R: GCGATCACCCTGCTTCCAAA		
HAND2	F: GGCAGAGATCAAGAAGACCGAC	GGAGAAGAGGAAGAAGGAGCTGAACG	105 bp
	R: CGGCCTTTGGTTTTCTTGTCGTT		
MYCN	F: GAGAGGACACCCTGAGCGATTCA	ACGTGGTCACTGTGGAGAAGC	123 bp
	R: ATGTGGTGACAGCCTTGGTGTTGG		

β2M	F: TGCTGTCTCCATGTTTGATGTATCT	GGTTGCTCCACAGGTAGCTCTAGCAG	86 bp
	R: TCTCTGCTCCCCACCTCTAAGT		
SOX2	F: ATGGACAGTTACGCGCACAT		220 bp
	R: GCTGCGAGTAGGACATGCTG		
GAPDH	F: GTCTCCTCTGACTTCAACAGCG	CACCTTTGACGCTGGGGCTG	131 bp
	R: ACCACCCTGTTGCTGTAGCCAA		
NTRK3	F: CCGTACGAGAGGGTGACAAT	TGGCTCTGGATCACCCCTTCC	113 bp
	R: ATTGGTCTGGTGAGTGTTGATG		
NNAT	F: AGATACCAGATCCCTTCCCAAC	CAGGGTCGAGAGAGGAGGG	102 bp
	R: CGACTTTGTCCAGATCAGAATG		
TG	F: CCAGTGGCTTCTCTTCCTGACT	TGACATTGAGAGAGCCTTGGTGGG	155 bp
	R: CCTTGGAGGAAGCGGATGGTTT		
TSHR	F: GAGTTTCCTTCACCTCACACGG	ACCTTTCTTACCCAAGCCACTGC	114 bp
	R: CTGCTCTCATTACACATCAAGGAC		
RET	F: GAGGAGAGACTACTTGGACCTTG		200 bp
	R: GGGGACAGCGGTGCTAGAAT		
GATA3	F: TAACATCGACGGTCAAGGCAAC	GCCACGGTGCAGAGGTACCC	131 bp
	R: GTAGGGATCCATGAAGCAGAGG		

Abbreviations: DβH-Dopamine-β-Hydroxylase, GAPDH- Glyceraldehyde 3-phosphate dehydrogenase, β2M-Beta-2-microglobulin, HAND2- Heart And Neural Crest Derivatives Expressed 2

Table 18. Oligonucleotides used for qPCR reactions targeting *Gallus Gallus*

Gene or locus	Sequence 5' to 3'	Product size
DROSHA	F: CATGGATCAAGTGGGGGACT	100 bp
	R: GGCCTTTGCCTGTCGTTTTC	
NeuroG2	F: CACAACTACATCTGGGCGCT	175 bp
	R: GCGATAAAGTGCAGGCGTAG	
DGCR8	F: GCATGAATATATGCAACGAGTCC	75 bp
	R: GGCTCACTTGGGTTCTCACA	
ACTB	F: GTATGTGCAAGGCCGGTTTC	92 bp
	R: AACCATCACACCCTGATGTCT	
RPL32	F: GTTACGACCCATCAGCCCTTG	93 bp
	R: CATGATGCCGAGAAGGAGATGG	
PAX6	F: GCGCAGTATAAACGAGAGTGC	187 bp
	R: TCAGCATCCTTAGCTTGTCGT	
YPEL1	F: GAGCCCACCTAGCCAATCAC	132 bp
	R: ACAGCCCACATTTACCACAG	
STMN2	F: CGAGGAGAGGAGAAAGTCCCA	150 bp
	R: TGTTCCATTTTCAGTATCAGCTTT	
KIAA1279	F: CTACATCCAGGCCCAGAACA	141 bp
	R: CTGGGATCCAGGGGAGGATT	
MBD3	F: TCCAACCAAGCCAAAGGCAA	125 bp
	R: GGATCACTCTTCACCTTATTGCTG	
CNN1	F: ATAAGCTGGAGAACATTGGGAAC	97 bp
	R: GTGTTCTCGAAGAGGTCGTTG	

Abbreviations: CNN1- Calponin 1, MBD3- Methyl-CpG-binding domain protein 3, STMN2- stathmin 2, YPEL1- yippee like 1, PAX6- Paired box 6, ACTB- β-Actin, RPL32- ribosomal protein L32

2.15 Western Blotting

Brains from chick embryos (E6) were homogenised in 2mL of sample buffer for SDS-PAGE. Homogenates were sonicated for 40 sec and centrifuged at 13,000 rpm for 5min. The resulting supernatants were divided into 100 mL aliquots and stored at −80∘C. Protein concentration of 3.3% homogenates (w/v) in PBS was determined by the Pierce BCA Protein Assay Kit (ThermoFisher Scientific) using bovine serum albumin as a standard. Forty micrograms of each sample were analyzed by Western blotting. The

apparent molecular mass of DGCR8 was estimated by a prestained protein marker (Life Technologies). Control tissue was obtained from post-natal mouse brain.

2.16 Statistics

All experiments were conducted in triplicate. Statistical analyses were performed using Microsoft Excel and/or Prism (Version 6, GraphPad). All results are presented as mean ± standard error of the mean (SEM), unless specified. Pairs of data were compared using independent groups (unpaired) unpaired t test with Welch's correction. Nonparametric Mann–Whitney test, Krustal-Wallis test with Dunn's multiple comparison post-test, one-way analysis of variance (One-way ANOVA) and two-way analysis of variance (Two-way ANOVA) with Bonferroni post- test were also applied where appropriate. Changes were deemed significant if the p value was < 0.05. Statistical significance is indicated as follows: $*p < 0.05$, $**p < 0.01$, and $***p < 0.001$. Graphs were drawn using GraphPad Prism.

3 CRISPR/Cas9 Targets Chicken Embryonic Somatic Cells *in vitro* and *in vivo* and generates Phenotypic Abnormalities

3.1 Introduction

Avian embryos, chiefly the chicken (*Gallus gallus*) and quail (*Coturnix japonica*), have been a mainstay of vertebrate embryologic research for over a century (Mason 2008).

The avian embryo is easy to obtain cheaply in large numbers as a result of its commercial utility. Development of avian embryos is simple to synchronise, with little individual variation, and benefits from excellent tables of development. Because development is external, these embryos are accessible to experimental manipulation (Niswander 2008). The similarity in the general ontogeny and gene expression patterns between avian and mouse embryos, as well as those of other vertebrates, indicates that Aves can serve as an excellent model for the study of genetic, molecular and biochemical mechanisms in mammals including humans. Avian models have been especially useful in following developmental pathways, for example in tracking cell movements in morphogenesis, untangling inductive pathways and deciphering differentiation pathways; and these have been shown to be valid for other vertebrates (Le Douarin and Dieterlen-Lievre 2013). They have also been instructive in pathogenesis of embryonic diseases, and also physiology, behaviour and toxicology (Smith et al. 2012; Park et al. 2013).

Avian embryology has lagged in genetic research, partly because the commercial utility of poultry factored against collection of instructive mutants (as in the fly, fish and mouse), and partly because of the dearth of techniques to manipulate their genome. The introduction of *in vivo* transfection, particularly by electroporation and by viral vectors, changed this dramatically, and allowed a form of conditional mutagenesis that was cheap and rapid (Itasaki et al. 1999). Great ingenuity has enabled up- and down-regulation of genes to be achieved in avian embryos (Sauka-Spengler and Barembaum 2008), but these techniques largely involved adding extra genetic information in a non-targeted way, in the form of plasmids or miRNAs, either episomally, or by means that randomly integrate into the host genome (Takahashi et al. 2008).

Programmable engineered nucleases (PENs) are novel technologies developed to efficiently target and alter a specific allele in the genome. These PENs, the zinc finger nucleases (ZFNs), the transcription activator-like effector nucleases (TALENs) and the clustered regular interspaced palindromic repeats (CRISPR)/Cas9 system, have been used extensively in generating and correcting mutations in cells of plants(Shan et al. 2014), humans (Hou et al. 2013; Yang et al. 2013), rodents (Shao et al. 2014; Zhang et al. 2014b), monkeys (Shen 2013; Niu et al. 2014), fish (Auer and Del Bene 2014; Ota et al. 2014; Shin et al. 2014), fly (Bassett and Liu 2014; Gokcezade et al. 2014) and worm (Chen et al. 2013) *in vitro* and *in vivo,* to generate transgenic cells, animals and plants. Recently, Park *et al.* validated the efficiency of TALENs in generating knockout

chicken primordial germ cells (PGCs) (Park et al. 2014) and showed that TALENs can be used to efficiently modify the genomes of chickens. Here we utilise the recently described CRISPR/Cas9 system, which is a very simple but powerful tool in the editing *in vivo* of the genomes of mice (Long et al. 2016; Nelson et al. 2016), in knocking-out and knocking-in of sequences in chicken cells *in vitro* and *in vivo.*

3.2 Aims

Generate an MEN2B mutation in the chick embryo (chick and quail model) using the CRISPR/Cas9 system by homology-directed repair, HDR.

1. To validate the efficiency of NHEJ genomic modification using the CRISPR/Cas9 system in avian cells, DF-1 embryonic fibroblast and DT-40 B cell lines.
2. To validate the efficiency of HDR genomic modification using the CRISPR/Cas9 system in avian cells, DF-1 embryonic fibroblast and using ssODN as donor templates.
3. To assess the safety of the CRISPR/Cas9 system in avian cells by screening for off-target effects of the designed single guides in DF-1 embryonic fibroblast and DT40 B cell lines.
4. To validate the efficiency of genomic modification using the CRISPR/Cas9 system in avian embryos by *in vivo* electroporation.

3.3 Results

A recent report showed that the gene *Pax7* could be modified by CRISPR/Cas9 in the chicken embryo *in vivo* (Veron et al. 2015). To explore the general applicability of this technique, we investigated a range of chicken genes on both macrochromosomes and on the unusual avian microchromosomes. The genes chosen were *DROSHA, DICER, MBD3, KIAA1279, CDKN1B, EZH2, HIRA, TYRP1, STMN2, DGCR8* (Di George Critical Region8) and *RET* (Appendix S1-Table 1). These genes have roles in embryonic development and the pathogenesis of embryonic diseases.

3.3.1 The CRISPR/Cas9 System Mediates NHEJ and HDR Gene Disruptions in Chicken Cell Lines

We validated the activity of the CRISPR/Cas9 system by designing sgRNAs (Appendix S1-Table 2) targeting the translational initiation region (start codon) of *DROSHA, DICER, MBD3, KIAA1279, CDKN1B* and *EZH2.* We generated NHEJ-induced mutation by co-transfecting the sgRNA CRISPR/Cas9 construct with or without a puromycin resistance-expressing construct into the chicken fibroblastic DF-1 cell line, using Lipofectamine 3000 (Figure 3.1A). Genomic DNA was isolated after 72-96 hours and the frequency of induced mutation in the targeted locus was analysed using the T7E1 assay and DNA sequencing (Table 3 and Table 12). In puromycin-resistant cells, cleavage bands ranging between 15%-60% were visible in all target genes as calculated by Image J software. The mutation efficiency induced was, for example, 50-51% in *KIAA1279*, 26-49% in *CDKN1B*, 68% in *MBD3* (Figure 3.1A), 58% in *DICER* and 38% in *EZH2* genes (Appendix S1-S1B). We further characterised cleavage by sequencing and this showed different indels detected at all the target sites with various mutation sizes (Appendix S1-S1D). We also targeted *KIAA1279* and *CDKN1B* with a different transfection method in a different cell line, using electroporation of the chicken B cell DT40 cell line, with similar results (Figure 3.1B).

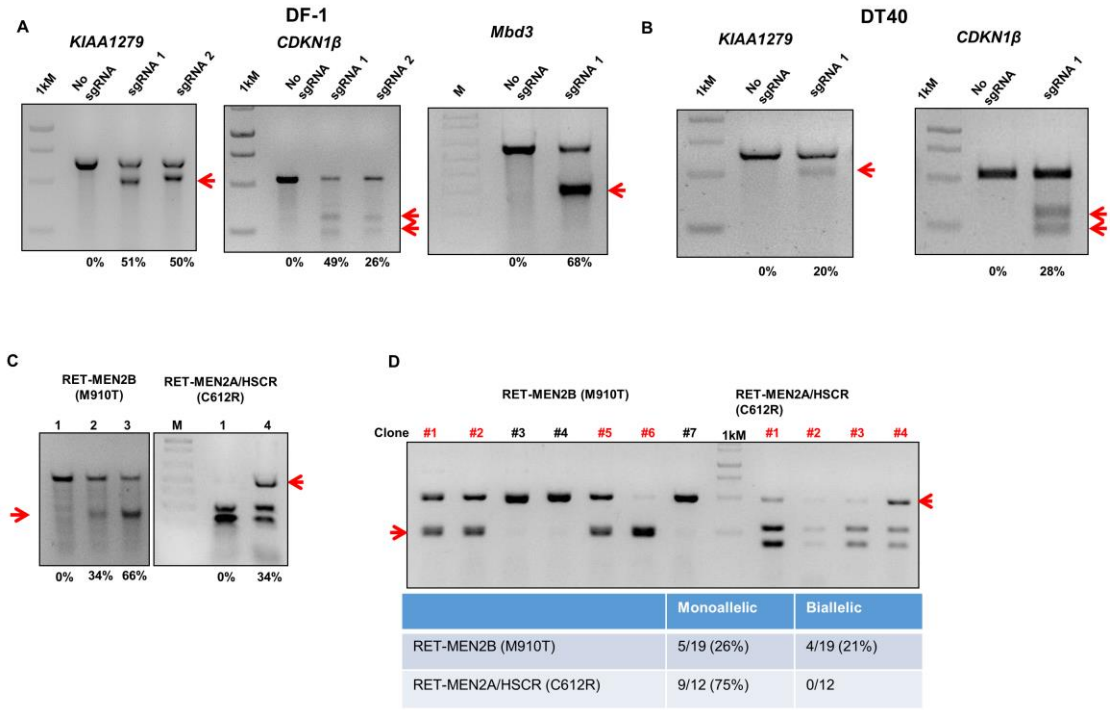

	Monoallelic	Biallelic
RET-MEN2B (M910T)	5/19 (26%)	4/19 (21%)
RET-MEN2A/HSCR (C612R)	9/12 (75%)	0/12

Figure 3.1 In vitro analysis of NHEJ and HDR genome modification (arrows) mediated by sgRNA-Cas9 system in chicken cell lines. (A) Frequency (%) of NHEJ mutation mediated by KIAA1279, Cdkn1b and Mbd3-targeting sgRNA-Cas9 system in chicken DF-1 cells by PCR and T7E1 assay. 1kM- 1 kbp DNA ladder, M- 100 bp DNA ladder. (B) Frequency (%) of NHEJ mutation mediated by KIAA1279 and Cdkn1b-targeting sgRNA-CRISPR/Cas9 system in chicken lymphoma B DT40 cells by PCR and T7E1 assay. (C) Representative gel from DF-1 cells transfected with the RET-targeting sgRNA-Cas9 and the ssODN showing efficient integration of the HDR-based BamHI and EcoRV sequence. The frequency of HDR is represented in percentages. 1-No sgRNA, 2- MEN2B sgRNA #1 plus ssODN, 3- MEN2B sgRNA #1 and #2 plus ssODN and 4- MEN2A/HSCR sgRNA 1 plus ssODN. (D) Representative gel for single cell clones derived from DF-1 cells transfected with the RET-targeting sgRNA-Cas9 and the ssODN for the MEN2B and MEN2A/HSCR HDR modifications respectively. The table shows the ratio of the monoallelic and biallelic HDR-based mutations detected with single cell clones and the overall efficiency in percentage: N = 19 for MEN2B and N = 12 for MEN2A/HSCR.

3.3.2 The CRISPR/Cas9 System Precisely Edits Genes in Chicken Cell Lines

Next, to test whether specific gene editing through HDR could be generated by the CRISPR/Cas9 system, we chose exons 10 and 16 of the *RET* gene which harbour, respectively, the mutation causing MEN2A and Hirschsprung disease (MEN2A/HSCR: C620R in humans and C612R in chickens) and MEN2B (M918T in humans and M910T in chickens) (Appendix S1-S1A) (Gimm et al. 1997; Smith et al. 1997). We designed ssODNs with restriction enzyme site creation and disruption and co-transfected the sgRNA-CRISPR/Cas9 construct with the ssODN and the puromycin construct into the DF-1 cell line, using Lipofectamine 3000. Genomic DNA was isolated from 72-96 hours post-transfected cells and the frequency of HDR-mediated genetic modification was analysed by digesting the PCR product with EcoRV and BamHI restriction

enzymes. The digested bands indicate the frequency of HDR-mediated genetic modification from the ssODN template, which ranged between 34-66% of puromycin-resistant cells (Figure 3.1C). Single clonal analysis shows the efficiency of biallelic and monoallelic HDR-mediated genetic modification by the CRISPR/Cas9 system as confirmed by gel and sequencing; 75% monoallelic with no biallelic for MEN2A/HSCR clones and 26% monoallelic and 21% biallelic for MEN2B clones (Figure 3.1D).

3.3.3 The CRISPR/Cas9 System Mediates Larger Genomic Deletions in Chicken Cell Lines

To see whether the CRISPR/Cas9 could also be used for large genomic fragment manipulation, we designed two sgRNAs targeting exon 1 and exon 3 of the *STMN2* gene spanning >24 kilobase pairs (kbps), exon 10 and exon 18 of the *RET* gene which spans >11 kbp, and exon 1 and 2 of *DGCR8* gene and exon 1 of *HIRA* genes spanning >75 kbps of the chicken genome (Table 3). We first co-transfected the two sgRNAs in DF-1 cells and analysed the targeted deletion by PCR after genomic DNA extraction. The PCR results (Figure 3.2A) shows that the CRISPR/Cas9 system can mediate large genomic deletions (frequency 15%) in chicken cells *in vitro* which is in concordance with published data for other species (Xiao et al. 2013; Ota et al. 2014; He et al. 2015). We then applied this approach to the chicken DT40 cell line, targeting the *STMN2* locus, and sequencing confirmed the >24 kbp deletion within this locus.

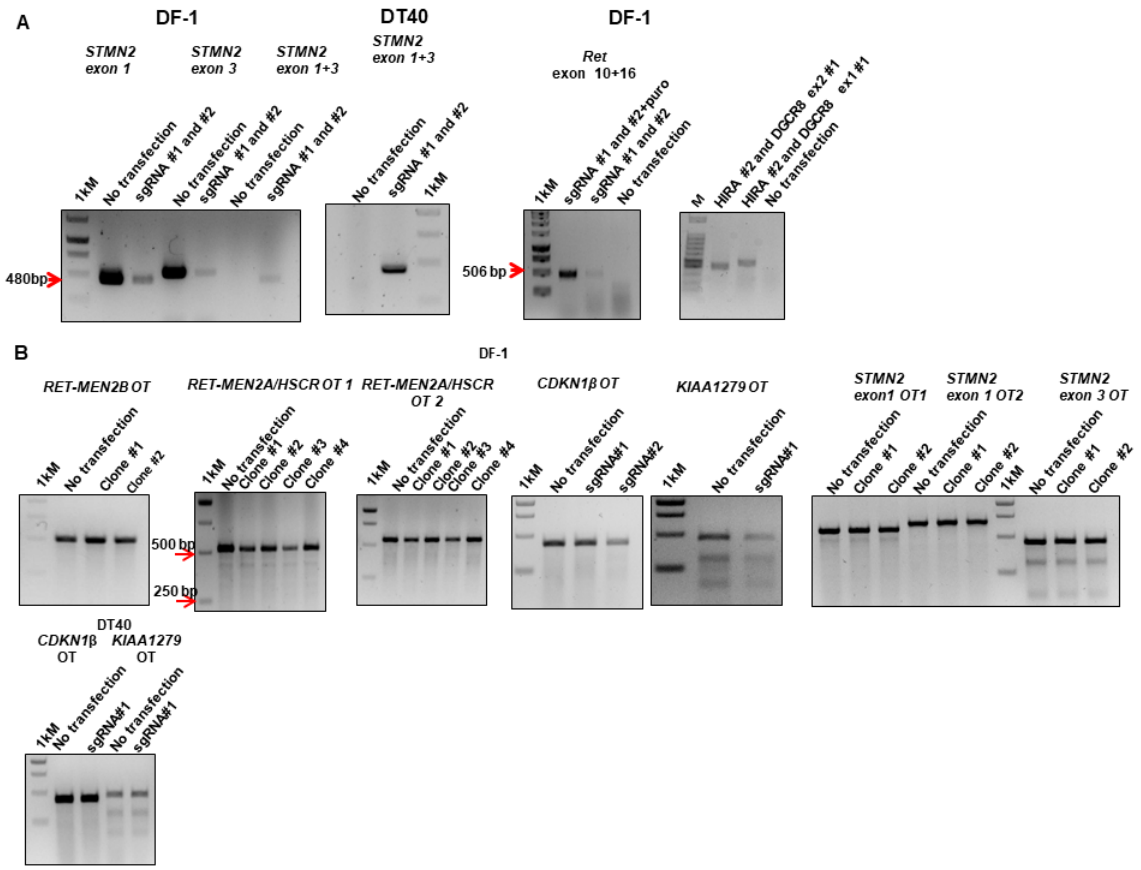

Figure 3.2 Targeted deletion of large genomic fragments and off-target effect analysis in chicken cells in vitro. (A) Representative gels showing the large genomic deletions within the STMN2 locus (>24 kbp) in chicken DF-1 and DT40 lymphoma B cells, and within the RET (>8 kbp) and HIRA-DGCR8 locus (>70 kbp). (B) Frequency of off-target effects mediated by RET-MEN2B and MEN2A/HSCR, CDKN1B, KIAA1279 and STMN2-targeting sgRNA-CRISPR/Cas9 system system in chicken DF-1 cells and CDKN1B and KIAA1279 -targeting sgRNA-CRISPR/Cas9 system in DT40 cells by PCR and T7E1 assay. 1kM- 1 kbp DNA ladder.

3.3.4 The CRISPR/Cas9 System Produces No Detectable Off-Target Effects in Chicken Cell Lines

Off-target mutagenesis remains a draw-back in the use of PENs, and in human cells the CRISPR/Cas9 system has been reported to have relatively high off-target effects compared to other PENs (Fu et al. 2013; Hsu et al. 2013; Pattanayak et al. 2013). Potential off-target sites with higher scores using the crispr.mit.edu software were selected and analysed by T7E1 assay in both the chicken DF-1 cells and the DT-40 cells of the *KIAA1279* and *CDKN1B*-targeting sgRNA-CRISPR/Cas9 constructs and that of the HDR experiments targeting *RET* in DF-1 cells (Figure 3.2B). There were no detectable off-target effects and these results suggest that chicken cells can potentially serve as a model for the use of the CRISPR/Cas9 nuclease, as opposed to in vitro off-targets being rare in human cells (Veres et al. 2014).

3.3.5 The CRISPR/Cas9 System Can Act Efficiently without Selection in Chicken Cell Lines

Drug selection cannot be used in *in vivo* applications so we investigated whether acceptable gene modification efficiency can be obtained without puromycin selection. Single gRNA activity and hence efficiency of mutation-induction can be affected by target locus location, chromatin structure, and nucleotide preferences (Doench et al. 2014). Our results show that drug selection for the CRISPR/Cas9 system in chickens is not a necessity but can however improve efficiencies for some sgRNAs with low targeting efficiencies (Appendix S1-S1C).

3.3.6 CRISPR/Cas9 Mediates Somatic Cell Modification in Chicken Embryonic Cells *In Vivo*

Genetic engineering techniques in chicken have been the genomic modification of PGCs with a germ-line transmission capacity using the lentiviral system (Motono et al. 2010; Park et al. 2010) or Piggybac transposon vector (Kubo et al. 2005; Park et al. 2010). Recent work by Park *et al.* showed that TALENs can efficiently generate knockout of targeted genes in chicken cells and in PGCs (Park et al. 2013; Park et al. 2014). We then tested the efficiency of the CRISPR/Cas9 system in introducing NHEJ mutations into the avian embryo by *in vivo* electroporation. *In vivo* electroporation is a useful tool for the study of spatio-temporal gene functions, since the manipulation of genes can be used to study the roles of such genes in a restricted region during specific developmental stages (Itasaki et al. 1999; Park et al. 2013).

We injected and electroporated the *DGCR8* exon 2-targeting sgRNA-CRISPR/Cas9 plasmid vectors incorporating mCherry marker *in vivo* into E1.5 embryo cranial neural tube, which transfects the brain and cranial NC (Appendix S1-S2A). DGCR8 is involved in miRNA processing and the targeted mutation should abrogate the gene function (Appendix S1-S2B). We also co-electroporated Tol2-GFP/transposase construct to indicate the trend and variability of transfection where NC cells migrate out of the neural tube to surround the brain and eye, and to branchial arch and facial mesoderm (Appendix S1-S2A). Note that for this technique, the distribution and number of transfected cells, as shown by the extent of GFP expressing cells, is variable (Simkin et al. 2014).

After embryo electroporation with the CRISPR/Cas9 construct, we analysed the hindbrain and midbrain by whole mount immunofluorescence for DGCR8 expression.

Since the mCherry plasmid is episomal, expression of mCherry is transient (Sato et al. 2007; Simkin et al. 2014), embryos were harvested after two days and immunostained with mCherry and DGCR8 antibodies (unelectroporated embryos, N = 8; electroporated embryos N = 24). Electroporated (i.e. mCherry-positive) cells in the midbrain, hindbrain and eye region showed a decrease in DGCR8 expression as determined by decrease in DGCR8 immunofluorescent intensity measured by pixel–count from confocal images (Figure 3.3A and B). It is important to mention that DGCR8 expression in postnatal mouse brain has a major nuclear location (Appendix S1-S4A), but mainly cytoplasmic location was observed in embryonic chick brain cells (Figure 3.3A). Subcellular heterogeneity of location has been reported for DGCR8 (Nakano et al. 2013). In addition DGCR8's binding partner Drosha also shows cytoplasmic as well as nuclear localisation (Link et al. 2016). The neuronal RNA-binding proteins HUC/D also have different localisation patterns in rodent and chicken cells (compare figures in Hao et al (Hao et al. 2016) and Rollo et al (Rollo et al. 2015)). Western blotting of postnatal mouse and embryonic chick brain showed identical DGCR8-immunoreactive protein bands of appropriate molecular weight (Appendix S1-S4B), in accord with the high predicted sequence homology between the two species.

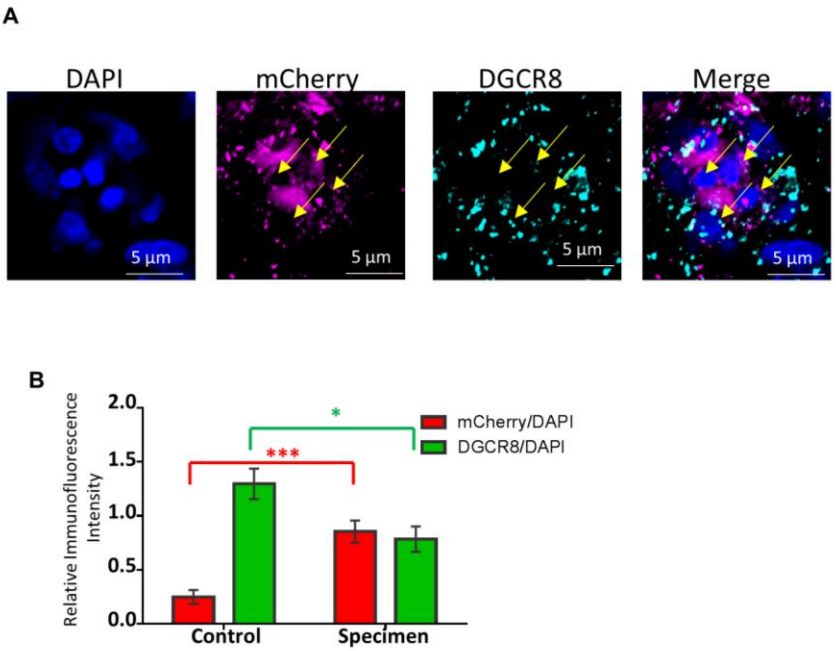

Figure 3.3 Protein expression 2 days after transfection with Dgcr8 CRISPR/Cas9 construct. (A) Immunofluorescence confocal images of single and merged channels of the indicated markers from whole mount staining of Dgcr8 mutant embryos, indicating reduced to no DGCR8 expression in transfected (mCherry+) cells (shown by yellow arrows). (B) Histogram of pixel counts on control embryos and DGCR8 mutants embryos relative to DAPI. A total of 540 cells and 542 (>=100

cells/embryo) were counted from 5 control and 6 electroporated embryos respectively. The low fluorescence in the mCherry waveband in controls is tissue autofluorescence. Scale bar: 5 µm. Error bars, mean±s.e.m. *P < 0.05, ***P < 0.001.

In addition, electroporated embryos were harvested after four days (N=34), along with controls (N=85), the latter to gauge the background effects of the techniques. The controls were sham-treated non-electroporated embryos (i.e. eggs opened, embryos visualised with India Ink, vitelline membrane nicked and eggs resealed; N=23), embryos electroporated but without plasmids (i.e. non-transfected; N=11), embryos electroporated and transfected with the benign Tol2-GFP/transposase plasmids (N=29), embryos electroporated with the Cas9 construct targeting the unrelated *STMN2* gene (N=14) and embryos electroporated with the empty Cas9 construct (Cas9 vector with no cloned guide sequence; N=8).

As expected, after 4 days mCherry fluorescence in wholemount embryos had declined to undetectable with the fluorescence stereomicroscope but we could FACs sort cells ($mCherry^{low}$ and $mCherry^{high}$) from the hindbrain. We performed T7E1 and qPCR analysis on these cells and showed a loss of *DGCR8* mRNA levels in $mCherry^{high}$ sorted cells which was confirmed by sequence analysis (Appendix S1-S2B). *DGCR8* sgRNA - CRISPR/Cas9 induced nucleotide deletions at the targeted locus with 1-5bp deletions and insertions leading, in most clones, to the generation of a stop codon which would result in nonsense-mediated decay of the *DGCR8* mRNA (Appendix S1-S2B). The qPCR results coupled with the sequence data suggest a drastic decrease in *DGCR8* gene expression in these brain cells during development, which could delay or disturb the growth of the midbrain as a whole. In addition the expression level of several other genes were analysed with findings consistent with previous findings (Appendix S1-S3A) (Boyer et al. 2006; Klein et al. 2007; Wang et al. 2007; Fan et al. 2013). Of the 34 *DGCR8*-targetted transfected embryos, 8 had a reduced head size and distorted morphology exemplified by major reduction of the midbrain (Figure 3.4A). They also showed a reduction in their eyes, aligning with the finding that miRNAs play an essential role in the differentiation of the retinal pigmented epithelium (Ohana et al. 2015). Furthermore, we compared the morphology of the hearts of the *DGCR8*-targetted embryos to the control embryos since in the mouse decreased DGCR8 expression results in a spectrum of malformations and reductions in cardiovascular development (Chapnik et al. 2012). We observed deformations in the heart and outflow tract in 14 embryos /34 total (41.2%) of the mutant group embryos. It is important to note that

none of the 85 control embryos had these cranial, retinal and cardiac abnormalities (Figure 3.4A and B).

These findings provide further support that the chicken embryo, a classical model of developmental biology, can be genetically modified *in vivo* in a targeted and sophisticated way to study disease models in developing embryos.

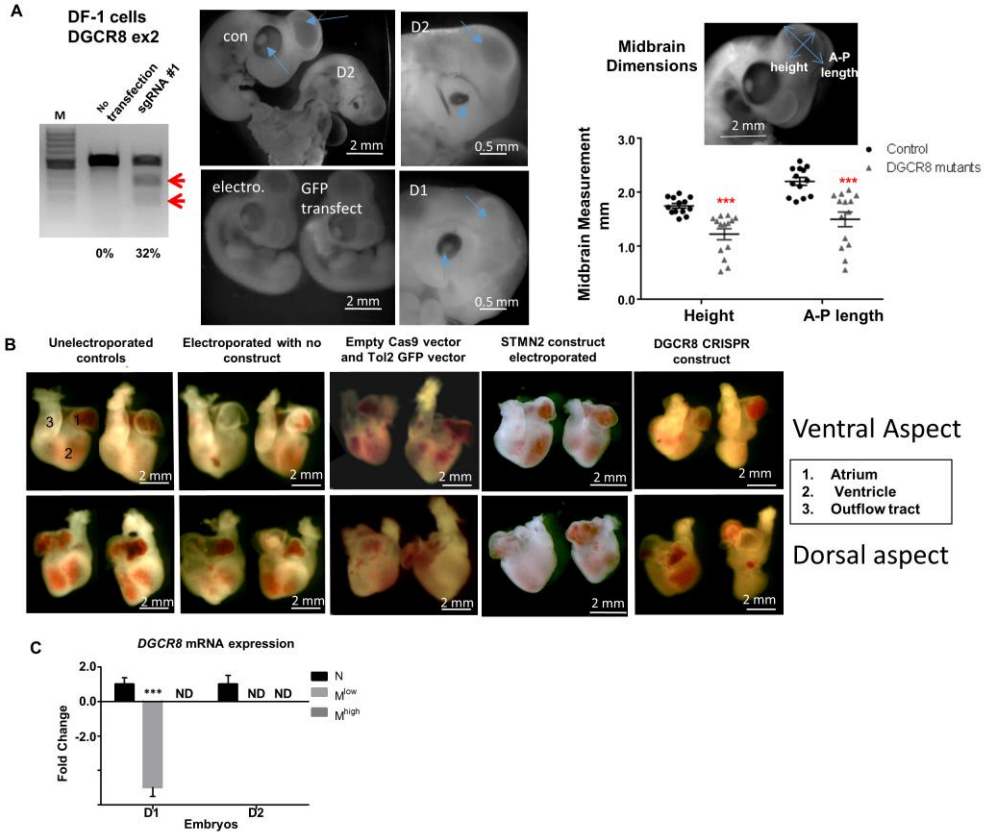

Figure 3.4 Somatic targeted genetic modification by CRISPR/Cas9 system in chickens 4 days after in vivo electroporation. (A) Frequency (%) of NHEJ mutation mediated by DGCR8-targeting sgRNA-CRISPR/Cas9 system in DF-1 cells by PCR. Red arrows indicate the NHEJ mutation created by the CRISPR/Cas9 system. M- 100 bp DNA ladder. Representative images of sham treated (con), electroporated untransfected embryos (electro.), Tol2 GFP transfected embryos (GFP transfect) with normal head development and DGCR8 CRISPR/Cas9 transfected embryos (D1 and D2) showing midbrain (open arrow) and eye (closed arrow) abnormalities. Graph shows the difference in the midbrain dimensions of DGCR8 mutant embryos compared to control embryos- N =14. (B) Representative image of the hearts of unelectroporated embryos, electroporated with no construct embryos, Tol2 GFP and empty Cas9 transfected embryos, STMN2 transfected embryos (negative control) showing normal heart development, and DGCR8 transfected embryos showing misshapen and reduced hearts. (C) qPCR analysis of cells isolated by FACS from DGCR8-targeted embryos demonstrating the reduced mRNA levels of DGCR8 in mCherry+ brain cells (M) relative to negatively sorted cells (N). Normalisation was done with ACTB and RPL32. ND-not detected. Error bars, mean±s.e.m. ***P < 0.001.

3.4 Discussion

The chick embryo is not only an excellent and reproducible system for embryonic developmental studies but also its accessibility and versatility makes it an alternative

model in research directly relatable to humans and other animals. We have shown that the CRISPR/Cas9 system can modify multiple genes on both avian macro- and microchromosomes at acceptable efficiency with or without selection, with no detectable off-target effects, a previously mentioned drawback in the use of the CRISPR/Cas9 system (Park and Han 2012).

The function of genes can be spatio-temporally studied using CRISPR/Cas9 system *in vivo* provided that selection is not required. A recent example uses viral delivery to the adult mouse brain (Swiech et al. 2015). Moreover, refinements to increase the efficiency (Chu et al. 2015) and limit the off-target errors (Kim et al. 2015; Kleinstiver et al. 2016b) are progressing rapidly. This means that for developmental studies, the advantages of the chick embryo as an accessible model and the convenience of *in vivo* electroporation at chosen developmental stages and locations can be combined with the power of CRISPR/Cas9 gene editing. We confirm this prediction here, extending the previous trial with *PAX7* (Veron et al. 2015).

In vivo transfection, including *in vivo* electroporation, affects a modest and variable proportion of cells (Simkin et al. 2014). This means that, as in many *DGCR8* electroporated embryos, a gross phenotype will not be observed in every instance since this depends on high mutational load (Sung et al. 2014; Shah et al. 2015). Despite this, functional effects of the genetic modification at the cellular level *in vivo* can be accurately gauged by imaging mutated cells and comparing with non-modified control cells in the same specimen. This requires markers of both the transfected cells and their otherwise similar control cells.

An interesting application of CRISPR/Cas9 editing would be the study of genes involved in nervous system development (Heidenreich and Zhang 2016), organogenesis and structural patterning. A specific application would be to modify genes for growth factor response, proliferation or differentiation in NC cells, for example gain-of-function MEN2 mutations of the RET gene (M910T and C612R) which induce a variety of neurocristopathies and developmental cancers (Zhang et al. 2014a). This can also be applied in studying clonal diversity and regulation during development as the MEN2B mutation is known to confer a higher proliferative ability to cells with the mutation. An example will be using this mutation to determine ENS superstar clones, which can disproportionately produce huge numbers of progeny during development. By one cell lineage tracing, it is shown that these superstars are normally generated stochastically and not predetermined; this could provide evidence for restriction of clonal diversity

and the variability in the penetrance of somatic mutations. Furthermore, it will also illuminate ENS clonal regulation during development especially in the distal colon which may make this part of the ENS unusually sensitive to somatic mutations. (Cheeseman et al. 2014; Newgreen et al. 2017; Zhang et al. 2018). In addition, targeting of primordial germ cells by CRISPR/Cas9 offers the hope of genetically engineering chicken models with any desired gene variant.

In conclusion, we have shown that transiently expressing the CRISPR/Cas9 construct can mediate genetic modification of avian embryonic somatic cells, reducing mRNA levels and generating phenotypes in the whole embryo. These results are in congruence with recent work also showing the efficiency of genome editing of postnatal mice using the CRISPR/Cas9 system (Long et al. 2015).

4 Generation of Functional Adrenal Chromaffin-like Cells from Human ES and iPS Cells

4.1 Introduction

Adrenal chromaffin cells, located in the adrenal gland and extra-adrenal locations, are NC derivatives (Le Douarin and Teillet 1974) and via SAPs they are closely related to sympathetic neurons in terms of lineage (Shtukmaster et al. 2013). These two cell types are mutually exclusive fates of SAPs. Chromaffin cells are biochemically and physiologically similar to sympathetic neurons but morphologically different (Huber et al. 2008; Huber et al. 2009). Both cell types produce enzymes including tyrosine hydroxylase (TH) and dopamine-β-hydroxylase (DβH) for catecholamine (CA) biosynthesis. The major CA for sympathetic neurons is noradrenaline since they lack the adrenaline synthesizing enzyme phenylethanolamine-N-methyltransferase (PNMT) while chromaffin cells secrete both nor- and adrenaline due to the presence of PNMT (Levitt et al. 1965). Chromaffin cells lack axons and dendrites, and they contain CA secretory large dense-core vesicles which, at 130–230 nm in diameter, depending on species, are larger than the <100 nm diameter dense-cored synaptic vesicles of sympathetic neurons (Teichberg and Holtzman 1973; Huber et al. 2009; Rosai 2011). These large dense-cored CA storage vesicles also possess Chromogranin A (CgA), Chromogranin B/Secretogranin I (CgB/SgI; predominant in human adrenal chromaffin cells), and Chromogranin C/Secretogranin II (CgC/SgII) (Trifaro 2002; Crivellato et al. 2008). Taken together the chromogranins have diverse functions as well as CA storage and release, being precursors of peptides which modulate vascular smooth muscle relaxation, mediate biosynthesis and release of insulin, inhibit glucose-stimulated insulin secretion by pancreatic beta cells, inhibit PTH secretion from parathyroid chief cells, stimulation of dopamine release from the striatum of the brain and the secretion of gonadotropin II from the anterior pituitary, as well as having bacteriolytic properties (Tatemoto et al. 1986; Cooper et al. 1990; Helle et al. 1993; Fischer-Colbrie et al. 1995; Taupenot et al. 2003).

The normal development of NC-derived cells through the SAP lineage to sympathetic neurons or adrenal chromaffin cells has been extensively studied especially in rodents and chicks (Anderson et al. 1991; Huber et al. 2002a; Howard 2005; Huber et al. 2005; Huber et al. 2008; Huber et al. 2009; Shtukmaster et al. 2013). In addition to the appearance of TH, DβH and PNMT as important differentiation markers, a number of other molecules are markers of autonomic developmental milestones. For example, p75NTR immunoreactivity is broadly indicative of early NC lineage (i.e. NCPCs), as is

HNK1 immunoreactivity although this is subject to species differences. The SA series of antibodies indicate SAPs (Carnahan and Patterson 1991b) and the B2B1 antibody, along with expression of neurofilament (NF), distinguishes a later stage, that is, sympathetic neuron lineage progression rather than chromaffin cell differentiation (Anderson et al. 1991). Cocaine- and amphetamine-regulated transcript (CART) peptides are also expressed in SAP lineage cells and highest CART expression marked sympathetic neuroblasts and neurons whereas its expression was low or absent in chromaffin cells even before the two populations become physically segregated. In contrast TH levels showed the inverse trend (Chan et al. 2016).

As well as their developmental and biochemical similarities to sympathetic neurons, adrenomedullary chromaffin cells show plasticity by being bipotential; they can express neuronal characteristics such as axon extension when cultured in the presence of FGF2 (Stemple et al. 1988), and RA and ascorbic acid (Vukicevic et al. 2012), and BMPs *in vivo* (Schneider et al. 1999).

Adrenal chromaffin cells, via secreted CAs, are central to the 'fight or flight' response. They also release enkephalins and enkephalin-containing peptides to produce analgesic effects (Livett et al. 1981; Hurley and Hammond 2001; Zhou et al. 2006; Jozan et al. 2007). Chromaffin cells also secrete neurotrophic growth factors notably FGF2, and also members of the transforming growth factor-β superfamily (TGFβ, GDNF), and neurotrophins (NT-4 and other unidentified neurotrophic components) (Date et al. 1994; Unsicker and Krieglstein 1996; Krieglstein et al. 1998; Schober et al. 1998; Schumm et al. 2004).

Pathologically, chromaffin cells are affected in the PHEO associated with MEN2A and MEN2B (Wells et al. 2013) and are also related to neuroblastoma development as they both originate from the SAPs (Szabo et al. 2012).

Because of their biochemical properties, chromaffin cells have been suggested as of clinical benefit in the treatment of neurodegenerative diseases such as Parkinson disease, in which dopaminergic neurons of the substantia nigra degenerate. Autologous intrabrain transplantation of adrenomedullary chromaffin cells raised early hopes of ameliorating Parkinson disease. Indeed, improvement of clinical symptoms after autologous adrenal medulla transplantation has been described in 390 patients from 1988 to 2001. The beneficial effects of these grafts were rapid but transient, since the

clinical improvements disappeared after 1–2 years, correlating with limited long-term survival of graft cells (Pappas et al. 1997).

Adrenomedullary chromaffin cell implants have also been suggested to alleviate intractable cancer pain (Pappas et al. 1997; Lazorthes et al. 2000; Drucker-Colin and Verdugo-Diaz 2004). Prospective phase II open clinical trials have been reported showing the feasibility of a cerebrospinal fluid (CSF) transplantation approach and its long-term safety using human adult adrenal medulla cells (Pappas et al. 1997; Bes et al. 1998; Lazorthes et al. 2000). However, the availability only of allogenic donor material was a limiting factor to the wider application of this approach (Zhou et al. 2006; Jozan et al. 2007).

There are many studies on the production of NCPCs from pluripotent cells, and the differentiation of these cells into autonomic neurons (Lee et al. 2007; Oh et al. 2016). In 2013, Saxena *et. al*, demonstrated production and isolation of SAPs from mouse Embryonic Stem (ES) cells by selecting for the expression of ganglioside GD2 (Saxena et al. 2013). Here, we describe modifications to this method applied to hESCs and hiPS cells to produce human adrenal chromaffin-like cells. A human cell resource will provide a platform to study normal development and physiology of these cells as well as provide insight into the mechanisms of diseases that involve the SA and adrenal chromaffin cell lineage, such as neuroblastoma and MEN2A and 2B. In addition, the potential capacity to produce these cells in large numbers from human autologous sources may assist in the clinical practices that have been hampered by the previous unavailability of donor material and also provide an initiative in regenerative therapies (Soto-Gutierrez et al. 2010; Fu et al. 2011).

4.2 Aims

Differentiate hPSCs to SAPs to chromaffin cells of the adrenal glands

1. To create a protocol for the differentiation of hPSCs to SAPs by modifying previously published protocols.
2. To analyse the time-point effect of BMP on SAP specification.
3. To analyse the positional identity of the derived SAPs
4. To differentiate the hPSC-derived SAPs to chromaffin-like cells *in vitro*.

5. To analyse the functional properties of the derived chromaffin-like cells by catecholamine secretion analysing techniques, Faglu and HPLC.
6. To assess whether the hPSC-derived SAPs will migrate and differentiate to chromaffin-like cells *in vivo*.

4.3 Results

4.3.1 Neural Crest Progenitor Cells differentiated from H9 hPSCs contain cells expressing markers of NCs and SAPs.

To generate NCPCs from hPSCs, we differentiated H9 hESCs into multipotent caudal (i.e. caudal to forebrain) neural progenitors (CNPs) by the 'dual inhibitor' tactic which inhibits TGFβ and GSK3β, the latter indirectly leading to Wnt activation. This was followed by FGF2 and BMP2 treatment to generate NCPCs as neurospheres. We refer to these cells as NCPC-xd, where x indicated the duration of FGF2/BMP2 treatment in days (Denham and Dottori 2011; Denham et al. 2015) (Figure 4.1A and Appendix S2-S1). To quantitate the efficiency of our differentiation protocol in generating NCPCs expressing NC markers, we FACs-analysed the dissociated cells, using p75NTR as a cell surface marker for NC cells. Most cells (89 ± 5%, N =5) were p75NTR+ (Figure 4.1B). We further investigated whether these differentiated cells expressed another NC marker, HNK1, and by FACs analysis, we showed that almost all of the p75NTR+ cells were HNK1+ (Figure 4.1B). Similar trends were seen in the HES3 and 007 iPSC-derived cells (Appendix S2-S3) with relative differences being discussed later.

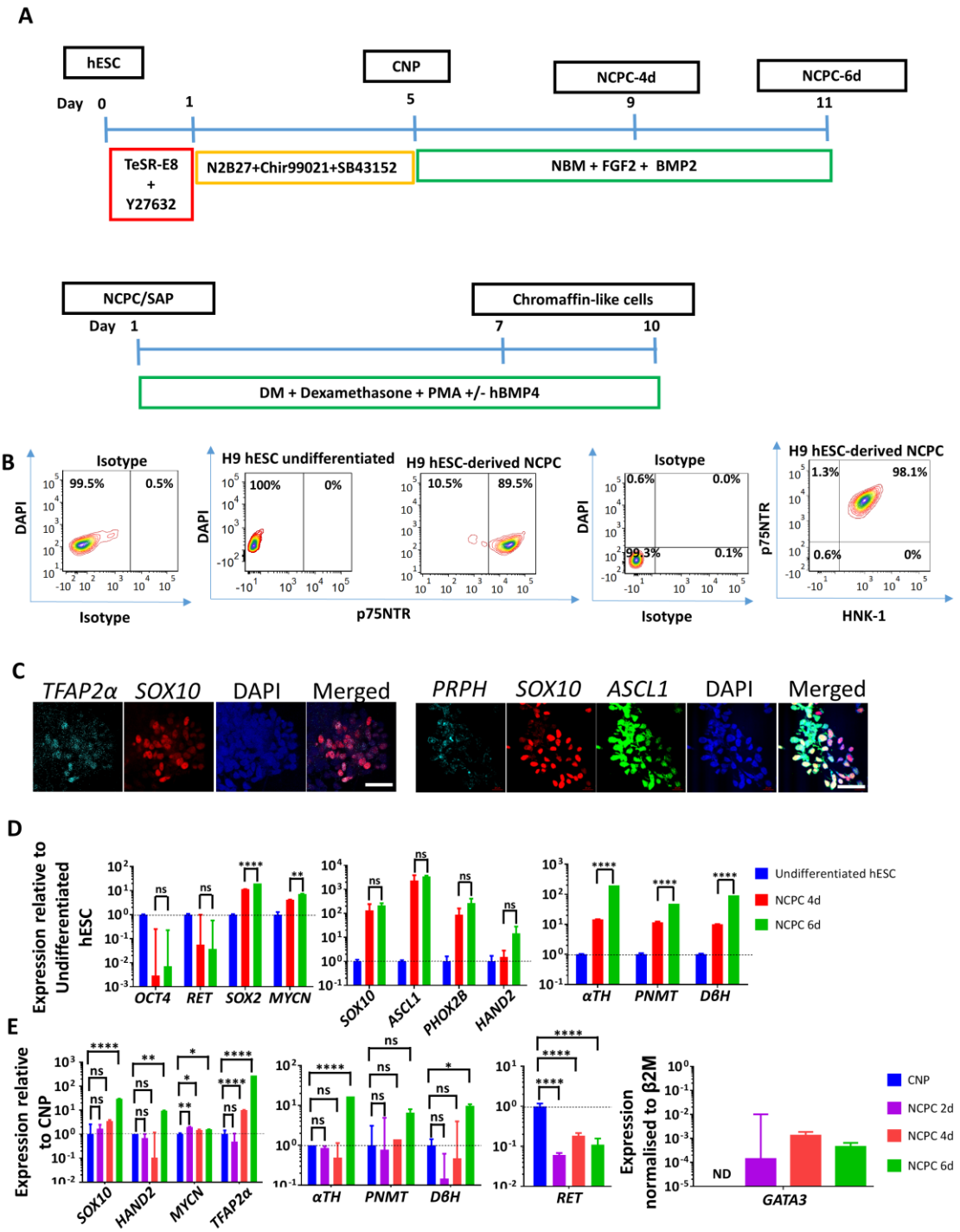

Figure 4.1 Characterisation of NCPC/SAPs derived from hESCs. (A). Schematic illustration of the summarised differentiation protocol of hESCs to NCPC/SAP-like cells and further to chromaffin-like cells. For detailed protocol, refer to Appendix S2-S1. (B) FACS analysis of NCPC-6d (ie. at day 11 of differentiation; Figure 4.1A) showing co-expression of the NCPC markers p75NTR and HNK1 at high frequency. Representative of 10 independent inductions of H9 cells. Non-specific antibody binding is shown as antibody isotype control. (C) Immunofluorescence of NCPC-6d cells with the NCPC and SAP markers SOX10, TFAP2α, ASCL1, PRPH. Note the co-expression of early NC markers TFAP2 and SOX10 and a trend for markers of lineage progression, ASCL1 and PRPH, to segregate from early NC marker SOX10. Scale bars: 50 µm. (D) qPCR analysis of NCPC-4d (total 9 days) and NCPC-6d normalized to undifferentiated hESC, showing upregulation of diverse NC/SAP markers. (E) Time point qPCR analysis NCPC-2d, NCPC-4d and NCPC-6d (day 7, 9 and 11 of differentiation respectively) normalized to CNP (day 5) showing NC/SAP

markers appear progressively. β2M-beta2microglobullin (housekeeping gene) ns- Not significant, *P < 0.05, **P < 0.01, ***P < 0.001, ****P < 0.0001. N ≥ 3 independent experiments; error bars represent mean ± SEM.

We analysed the NCPCs by immuno-fluorescence with antibodies to SOX10 and TFAP2α, two NC transcription factors, and to pro-neural markers ASCL1 and Peripherin (PRPH), which are expressed by SAPs (Huber et al. 2002a). The majority of the SOX10+ cells expressed TFAP2α, and ASCL1 and PRPH markers were elevated especially in the cells with lower SOX10 levels (Figure 4.1C). This parallels normal NC development, where neuronal differentiation is accompanied by reduction or loss of SOX10 expression (McKeown et al. 2005; Kelsh 2006).

As well as an early role in induction of the NC from the neural epithelium, the duration and concentration of BMP exposure has been shown to have effects on differentiation of SAPs (Schneider et al. 1999; Mizuseki et al. 2003; Huber et al. 2008; Saito et al. 2012). FGF2 has been reported as inducing pre-sympathetic neuronal differentiation of SAPs (Stemple et al. 1988; Carnahan and Patterson 1991b). We investigated whether there would be an effect of prolonging FGF2/BMP2 exposure (that is NCPC-6d compared to NCPC-4d). qPCR analysis showed, compared to the starting H9 hESC cells (see Figure 4.1A), a progressive upregulation of *SOX10*, and also a modest increase in *MYCN* expression, another marker for migratory NC cells and SAPs in animal models (Wakamatsu et al. 1997; Saxena et al. 2013; Mobley et al. 2015) (Figure 4.1D). The expression of *TFAP2α* also increased with exposure to FGF2/BMP2 from 4 days to 6 days as did the pro-neural transcription factors *ASCL1*, *HAND2* and *PHOX2B* (Figure 4.1D); see (Huber et al. 2005) for developmental correlates. Genes for CA transmitter synthesis enzymes α*TH*, *DβH* and the chromaffin cell-specific *PNMT* were all upregulated. Also the expression of *SOX2*, which is important in pluripotency and also specification of the neuroectoderm and maintenance of neural progenitor cells (Zhang and Cui 2014), was upregulated while the pluripotency gene *OCT4* was suppressed (Figure 4.1D).

Using the intermediate stage neuroectoderm-like CNP cells as a basis (see Figure 4.1A), the early NC genes *SOX10* and *MYCN* commenced their upregulation quickly (detectable in NCPC-2d cells) whereas the increase in the pro-neural gene *HAND2* and the CA synthesis enzyme genes, which reflect later differentiation of SAP lineages, were only apparent after 6 days of FGF2/BMP2 treatment (Figure 4.1E). The zinc finger transcription factor *GATA3* (with *ASCL1*, *PHOX2B* and *HAND2*) plays a role SAP

specification (Lim et al. 2000; Huber et al. 2005; Huber 2006; Moriguchi et al. 2006). *GATA3* mRNA expression, as assessed by qPCR, was detected after 2 days of NCPC/SAP lineage differentiation (NCPC-2d) and increased about 9-fold after 4 days (NCPC-4d) before decreasing slightly after 6 days (NCPC-6d) (Figure 4.1E).

RET, coding for the tyrosine kinase receptor for GDNF, is highly expressed in human neuroectoderm (Attie-Bitach et al. 1998), and expressed in aggregated SAPs at the dorsal aorta which forms the sympathetic primordia. The expression of *RET* is already detected in migrating SAPs populating the adrenal gland (Huber et al. 2002a; Allmendinger et al. 2003). However *RET* expression decreases as chromaffin cells differentiate, unlike the continued expression in sympathetic neurons (Huber et al. 2002a). In the present cells, compared to neuroectoderm-like CNPs, *RET* expression reduced after 2 days of NCPC/SAP lineage differentiation but later (NCPC-4d) increased 3-fold over NCPC-2d levels then reduced 1.7-fold when cultured for 2 more days (NCPC-6d) (Figure 4.1E).

SAP lineages express NFs as they differentiate into neurons and pre-chromaffin cells (Carnahan and Patterson 1991b; Huber et al. 2009). To follow neuronal properties, we dissociated, fixed and permeabilised NCPC-4d and NCPC-6d neurospheres and stained them with αTH and NF-200kDa antibodies and FACs analysed them. H9 hESCs expressed neither αTH nor NF, but about 25% of the NCPC/SAP population showed marginally increased expression of αTH with about 6-10% expressing NF-200kDa in both NCPC-4d and NCPC-6d (Figure 4.2A). The neuroblastoma line SK-N-BE(2)C expresses NF (Andres et al. 2013) and as a positive control, we analysed the expression of NF-200 kDa, αTH and also PNMT by FACs in this cell line (Appendix S2-S4) with very similar patterns to the NCPCs.

SA1 expression marks SAP lineages and increased expression marks pre-chromaffin cell differentiation (Carnahan and Patterson 1991b; Carnahan and Patterson 1991a; Lumb and Schwarz 2015). The results of FACs-analysed NCPCs showed that SA1 expression decreased from almost 80% of p75NTR+ cells of NCPC-4d to 66% of NCPC-6d (Figure 4.2B). The reduced proportion of SA1+ NCPCs with FGF2/BMP2 treatment lengthened from 4 days to 6 days is consistent with FGF2/BMP2 treatment priming the cells to an SAP state (Carnahan and Patterson 1991b) during the 4 day period with longer exposure disfavoring differentiation to pre-chromaffin cells (Stemple et al. 1988; Carnahan and Patterson 1991b) and favouring differentiation to neuronal

and other NC lineages. However the upregulation of *αTH, PNMT* and *DβH* expression by qPCR analysis and the pro-neuronal marker B2B1 by FACS indicates the cell population at day 6 is still heterogeneous (see Figures 4.1E, 4.5A).

4.3.2 H9 hESC-derived NCPC cells have a trunk neural crest positional identity

Antero-posterior positional information is important in NC development (Lee et al. 2005; Zhang et al. 2010a) and a major mediator is the *HOX* gene code (Nelms and Labosky 2010). We hypothesised that for trunk positional identity, consistent with SAPs, the hESC-derived NCPCs should express higher number trunk *HOX* genes (Huber et al. 2012) rather than the low number *HOX* genes, which are expressed at the cranial and vagal levels (Figure 4.2C, Appendix S2-S5). We performed qPCR analysis for *HOXA2, A5, A7, A10* and *HOXB1, B2, B4, B7* (Bhatt et al. 2013). We recorded upregulation of *HOXB7* expression over the 6 days of FGF2/BMP2 treatment relative to CNPs (Figure 4.2C). *HOXA10* expression was also upregulated in contrast to its low expression in vagal NCPC (Appendix S1-S5). Analyses of cranial *HOX* genes show a downregulation of *HOXB1* relative to CNP cells (Denham et al., 2015) and there was no significant upregulation of *HOXA2, HOXB2* and *B4* expression (Figure 4.2C). *HOXA5* expression, normally marking the vagal/trunk transition, was upregulated relative to CNP cells by the NCPC/SAP differentiation process but not to the degree seen in NCPCs with induced vagal properties (Appendix S2-S5).

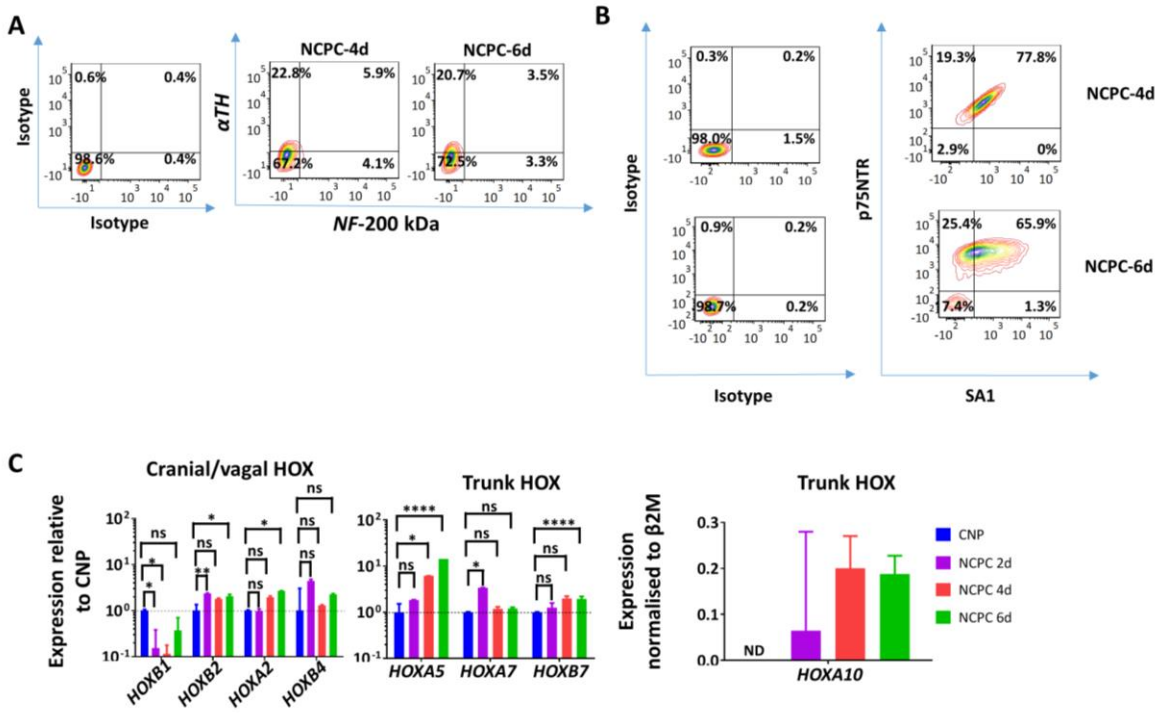

Figure 4.2 NCPC/SAPs derived from hESCs express adrenergic markers and possess the positional identity of mid-trunk NC cells (see 1A). (A) FACS analysis of differentiation of H9 NCPC-4d and NCPC-6d (both representative of 3 separations) with increase in cells with SAP adrenergic marker αTH and modest increase in neuronal marker NF-200 kDa. (B) FACS analysis of differentiation of NCPC-4d and NCPC-6d (both representative of 10 separations) with frequent expression of NCPC marker p75NTR and SAP marker SA1. (C) qPCR HOX gene analysis of CNP, NCPC-2d, NCPC-4d and NCPC-6d. CNP (hindbrain positional identity, low number HOX paralog) was used to normalize the expression except for HOXA10 which was normalized to β2M. NCPC/SAP induction is accompanied by decreased expression of lowest number and increased expression of higher number HOX paralogs. ND-not detectable, pooled from N = 4 different inductions each, PCRs in triplicate; error bars represent mean ± SEM. *P < 0.05, **P < 0.01, ***P < 0.001, ****P < 0.0001.

4.3.3 Differentiating hPSC-derived NCPCs to chromaffin cells

The paraortic tissue of the sympathetic localisation zone expresses BMP4 and distal to this the adrenal *anlage* is especially enriched in BMP4 as well as corticosteroids (Huber et al. 2008). Glucocorticoids were initially thought to be responsible for the transition of SAPs to chromaffin cells rather than to sympathetic neurons (Anderson 1993; Chung et al. 2011; Saxena et al. 2013) but a more nuanced view is now favoured (Unsicker et al. 2013) with the steroid hormones having a maintenance and proliferative role and BMP4 being a decisive cue for the differentiation of SAPs to chromaffin cells (Huber et al. 2008). BMP4 also plays a role in the early induction of neuronal and CAergic phenotype (Huber et al. 2002b; Huber et al. 2008), being instrumental in promoting the PNMT-mediated synthesis of adrenaline over noradrenaline. FGF2 is reported to drive SAPs to sympathetic neuron differentiation in the rat embryo (Anderson 1993). However, BMP4 is also reported to

be involved in the noradrenergic neuronal differentiation in the sympathetic ganglia *in vivo* in quail embryos (Schneider et al. 1999) and the timing of BMP4 exposure in the differentiation of SAP cells in quail is also important (Reissmann et al. 1996).

As human chromaffin differentiation from hPSCs has not being described, we developed a protocol (Figure 4.1A and Appendix S2-S1) based on that used for mouse cells (Saxena et al. 2013) and on work on human adrenal chromospheres (Santana et al. 2012). After treatment with FGF2/BMP2 (Figure 4.1A), we subjected the H9 hESC-derived NCPCs to differentiation *in vitro* for 6-9 days with 500 pg/mL human recombinant BMP4, or with dexamethasone plus PMA (Dex+PMA=DP), or with DP plus BMP4 (DPBMP4). (Note that BMP2 was used for the first stage of NCPC/SAP differentiation for consistency with our previous method (Denham et al. 2015), but BMP2 and BMP4 have similar effects for SAP lineage development (Reissmann et al. 1996)).

This extended treatment of NCPCs with BMP4 with or without DP resulted in upregulation of sympathetic/chromaffin markers αTH and CgB and, most importantly, of the chromaffin-restricted marker PNMT by immunofluorescence, thus demonstrating the chromaffin differentiation capacity of the hPSC-derived NCPCs (Figure 4.3A).

As outlined above regarding the timing of BMP in the differentiation of SAP cells from NC cells (Reissmann et al. 1996), we investigated the efficiency of differentiating chromaffin cells from dissociated NCPC-4d and NCPC-6d cells, the latter having a 2 day longer prior treatment with FGF2/BMP2. To quantitate the proportion of cells after additional BMP4 or DP or both, we used confocal images of αTH and CgB, reflecting the SAP lineage, and NF staining indicating neuronal differentiation. αTH expression was efficiently induced from both NCPC-4 and -6d cells in all conditions but DP plus BMP4 treatment of NCPC-4d cells resulted in a strikingly high proportion of cells that were CgB+ but fewer cells that were NF+ (i.e. neuronal) compared to NCPC-6d cells (Figure 4.3B left). However, with NCPC-6d as the starting point, BMP4 induced many more NF+ cells while CgB+ cells were reduced (Figure 4.3B right). DP had little effect on the already high proportion of CgB+ cells from NCPC-4d cells and reduced slightly the NF response. This is consistent with previous reports on the timing of BMP4 in initiating adrenergic neuron properties in SAPs during development and also the importance of BMP4 and corticoids in chromaffin differentiation (Reissmann et al. 1996; Huber et al. 2008).

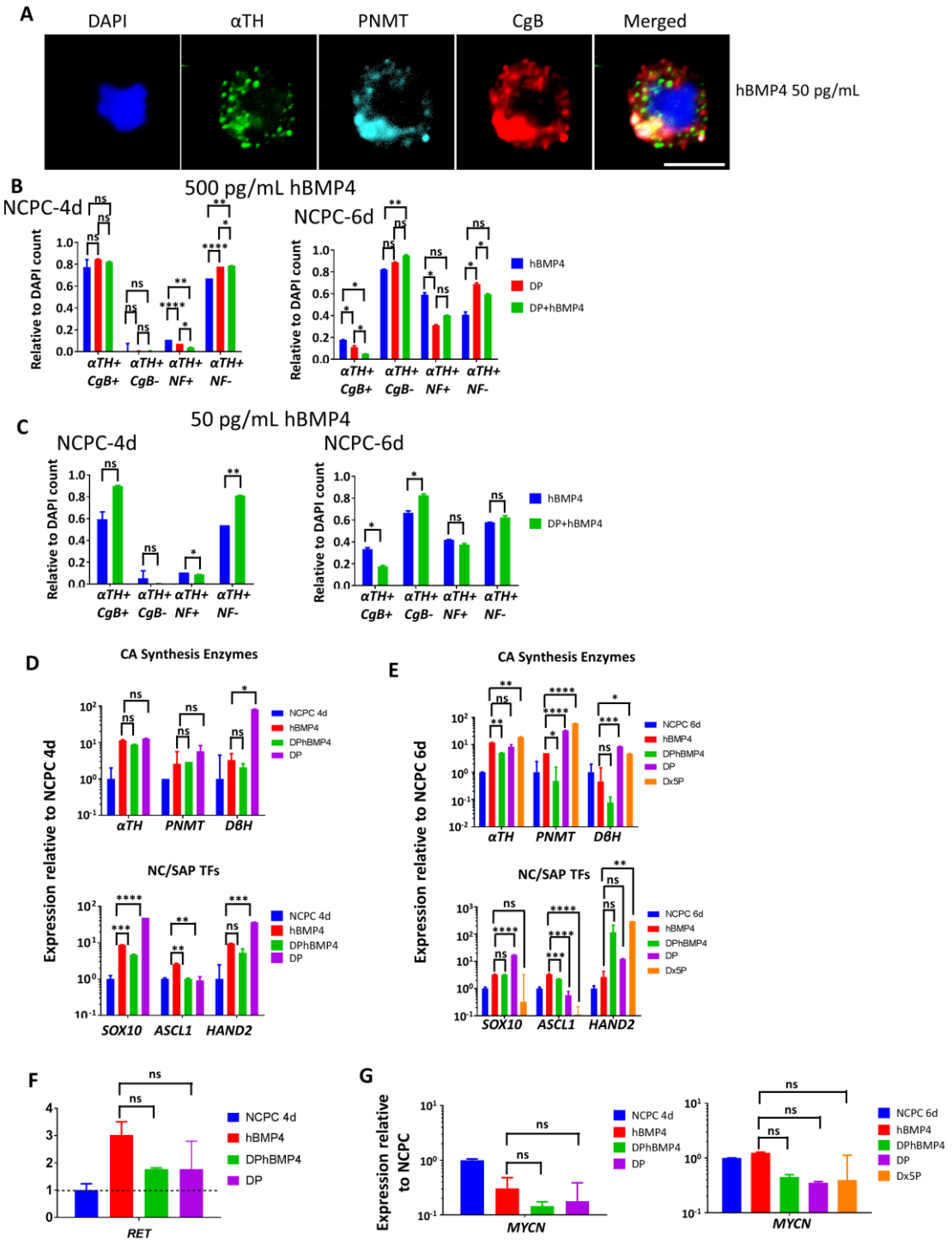

Figure 4.3 NCPC/SAPs derived from hESCs differentiate into chromaffin-like cells in vitro. (A) Immunofluorescence of H9 NCPC/SAPs differentiated with BMP4, showing co-expression of SAP markers αTH, chromaffin marker PNMT and storage vesicle marker Chromogranin B (CgB). Scale bar: 5 µm. (B, C) Immunofluorescence count of differentiation of NCPC-4d and NCPC-6d (see Figure 4.1A, Appendix S2-S1B) to chromaffin-like cells as stained for αTH, NF-200kDa and Chromogranin B (CgB) after 6 days of differentiation as in Figure 4.1A and S1B with high and low hBMP4 (500 and 50 pg/mL). Longer initial FGF2/BMP2 exposure resulted in a higher proportion of neuronal (NF+) and lower proportion of CgB+ SAP cells. DAPI stain was used to assess the total number of cells to normalize the other markers. N = 8, error bars represent mean ± SEM. (D,E) qPCR analysis of NCPC-4 days and NCPC-6 cells which were differentiated into chromaffin-like cells for 6 days. BMP-4 and corticosteroids increase chromaffin marker PNMT expression. NCPC-

4d and NCPC-6d cells were used to normalize the expression patterns of the various culture conditions. N = 4 independent experiments. (F) qPCR analysis of *RET* expression of NCPC-4d cells differentiated into chromaffin-like cells. N = 4 independent experiments (G) qPCR analysis of MYCN expression of NCPC-4d and NCPC-6d cells differentiated into chromaffin-like cells. N = 4 independent experiments: error bars represent mean ± SEM. ns- Not significant, *P < 0.05, **P < 0.01, ***P < 0.001, ****P < 0.0001.

The concentration of BMP4 influences SAP cell development *in vitro* and *in vivo* (Reissmann et al. 1996). Reducing the concentration of BMP4 from 500 pg/mL to 50 pg/mL decreased the proportion of CgB+ cells in BMP4-only treated conditions for both NCPC-4d and NCPC-6d cells, but NF+ cells were not greatly altered. The reduction of the proportion of CgB+ cells with low BMP4 in NCPC-4d starting cells was rescued by simultaneous addition of DP (Figure 4.3C) affirming the importance of the glucocorticoids in chromaffin differentiation (Anderson 1993; Chung et al. 2011; Saxena et al. 2013). We then confirmed that BMP4 at the low dose of 50 pg/mL activated its downstream signalling pathway by employing an antibody to phosphorylated SMAD1/5 in SAP-like cells identified by αTH immunoreactivity (Appendix S2-S6).

qPCR analysis of SAP and chromaffin markers showed upregulation of CA synthesis enzyme genes α*TH*, *DβH* and *PNMT* in cells derived from NCPC-4d under BMP4, DP and DPBMP4 conditions (Figure 4.3D). Analysis of CA synthesis enzymes as above on chromaffin-like cells differentiated from HES3 hESC and 007 iPSC-derived NCPC-4d showed a similar finding to chromaffin-like cells differentiated from H9 hESC-derived NCPC-4d under BMP4 and DPBMP4 conditions (Appendix S2-S2). In cells derived from NCPC-6d, DPBMP4 treated conditions resulted in less α*TH*, *DβH* and *PNMT* than in BMP4-only and DP-only treated conditions (Figure 4.3E). NC and SAP lineage transcription factor *HAND2* was also upregulated especially by DP, and *ASCL1* by BMP4, though this was relatively greater with the NCPC-4d cells than the 2 day older NCPC-6d starting cells.

Previous reports stated the importance of glucocorticoids in acquisition of adrenergic phenotypes of chromaffin cells (Hodel 2001), we therefore investigated this by qPCR for *αTH, PNMT, DβH, SOX10, ASCL1* and *HAND2*, comparing 10 mM and 50 mM dexamethasone. This 5-fold increase in dexamethasone led to a slight (not significant) increase in α*TH* and *PNMT* expression whereas *HAND2* was strongly increased and *ASCL1* and *SOX10* were reduced (Figure 4.3E). These markers have been validated in human adrenal chromaffin progenitor cells (Santana et al. 2012) and also

recently in mouse using genetic cell lineage tracing (Furlan et al. 2017), further confirming our differentiation protocol.

RET protein expression is extremely weak or undetectable by immunohistochemistry in most cells in the normal adrenal medulla (Allmendinger et al. 2003; Powers et al. 2003; Unsicker et al. 2005). To investigate this, we performed qPCR analysis of H9 hESC-derived cells under BMP4, DPBMP4 and DP treated conditions and there was no significant increase or decrease in *RET* mRNA expression of chromaffin-differentiated cells as compared to H9-derived NCPC-4d cells (Figure 4.3F). However, there was a reduction in *RET* mRNA expression in 007 iPSC and HES3 hESC-derived chromaffin-like cells under both conditions (Appendix S2-S7).

MYCN favours the differentiation of sympathetic neurons and acts against differentiation of adrenal chromaffin cells (Zhu et al. 2012a; Mobley et al. 2015). We analysed *MYCN* after BMP4 exposure by qPCR. Cells differentiated from NCPC-4d cells under BMP4, DP and DPBMP4 all showed less *MYCN* expression than the starting NCPC-4d SAP cells (Figure 4.3G) and this is consistent with the immunofluorescence count in Figure 4.3B showing a reduced percentage of neuronal αTH+/NF+ cells. In chromaffin-like cells derived from HES3 hESCs, DPBMP4 conditions showed less *MYCN* expression as compared to BMP4 only conditions whereas in 007 iPSC, both conditions showed less *MYCN* expression (Appendix S2-S7). On the other hand, cells differentiated from NCPC-6d cells under BMP4-only showed no decrease in *MYCN* expression but addition of DP, or DP alone, did decrease *MYCN* (Figure 4.3F). This was also reflected in the immunofluorescence count in Figure 4.3B. Taken together, these findings suggests that after 4 days of FGF2/BMP2, BMP4 alone, in the absence of FGF2, can divert SAPs away from neuronal differentiation and toward the chromaffin lineage whereas after 6 days of prior FGF2/BMP2 exposure, further exposure to BMP4 alone is relatively ineffective although glucocorticoids are still very important in differentiating SAPs toward chromaffin rather than neuronal lineages.

Rat, mouse and bovine adrenal chromaffin cells can both proliferate and transdifferentiate to neurons (Tischler et al. 1997; Sicard et al. 2007). Human chromaffin cells can transdifferentiate but display minimal proliferation antigens *in vivo* and do not respond to putative mitogens *in vitro* (Tischler and Riseberg 1993). Recently, a sub-population of adult human medullary cells selected by sphere formation ("chromospheres") displayed progenitor markers and could differentiate as both neurons

and chromaffin cells, although their ability to proliferate was unclear (Santana et al. 2012; Santana et al. 2013; Tischler 2013). To investigate the proliferative state of the present human pluripotent cell-derived chromaffin-like cells, we immunostained the 9 days BMP4DP cultures with Ki67 antibody. Most but not all of the cells in aggregates of αTH+/CgB+ cells showed no nuclear Ki67 so proliferation ability at this stage is likely to be minimal (Appendix S2-S8).

Based on the upregulation of PNMT by immunofluorescence and qPCR analysis, we hypothesised that the NCPCs (especially NCPC-4d) cells treated with BMP4 but deprived of FGF2 showing chromaffin differentiation will possess CAs including adrenaline. These cells were processed for Faglu-induced fluorescence (Furness et al. 1977) which directly converts CAs to a fluorescent product. These were co-immunostained for SAP marker CgB and chromaffin marker PNMT and observed by confocal microscopy. Most of the cells staining with Faglu, and therefore possessed CAs, co-stained with PNMT and CgB antibodies, consistent with adrenaline synthesis and storage (Figure 4.4A). To measure adrenaline directly, we performed HPLC with fluorescent detection on sonicated cell lysates of chromaffin-like cells differentiated from NCPCs (derived from H9 hESCs) with BMP4 only and with DPBMP4. HPLC detected both noradrenaline and adrenaline, with DPBMP4-treated cells showing moderately higher levels than BMP4-only treated cells (Figure 4.4B). The results also showed that lowering the BMP4 concentration from 500 pg/mL to 50 pg/mL reduced the concentration of CAs which corresponds with the data in Figure 4.3B and C.

To quantitatively validate the efficiency of the differentiation, we fixed and permeabilised the cells after 6 days of chromaffin differentiation, and stained them with antibodies to αTH, CgB and PNMT. FACs analysis of these stained cells showed that BMP4 alone can upregulate the expression of αTH, CgB and PNMT in differentiating cells with no significant difference in DP and DPBMP4 as we have already shown with the immunofluorescent counts (Figure 4.4C and see Figure 4.3B and C). *In vivo*, αTH+ adrenal chromaffin cells are both PNMT+ and PNMT- (Huber 2006). In our case about 30-40% of the cells expressed αTH+/PNMT+ markers of chromaffin cells (Figure 4.4D), using SK-N-BE(2)C as αTH+/PNMT- control and undifferentiated hESCs as αTH-/PNMT- control (Appendix S2-S4).

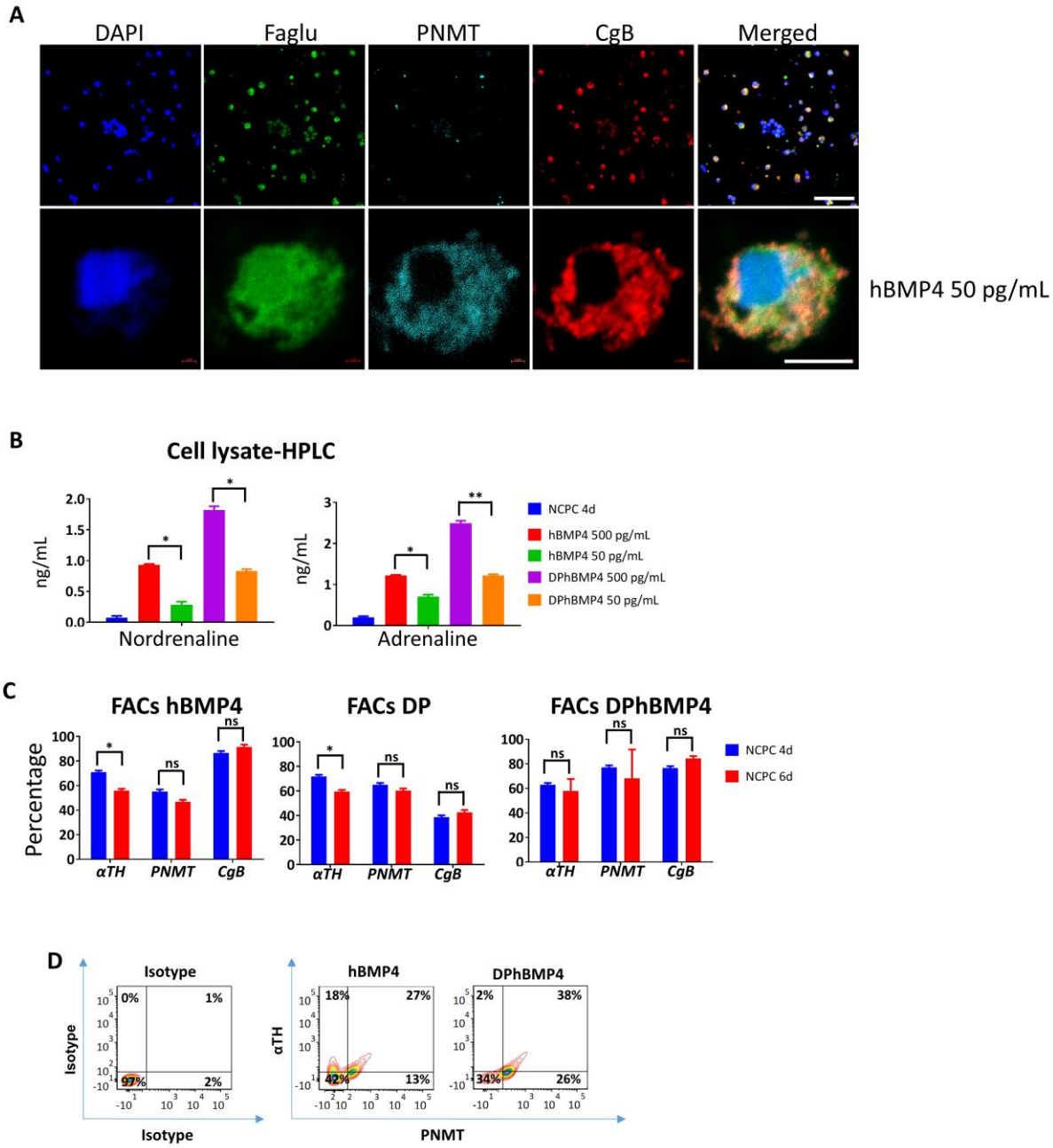

Figure 4.4 Chromaffin-like cells differentiated from NCPC/SAPs produce catecholamines. (A) Immunofluorescence of differentiated H9 NCPC-4d in differentiation medium (see Figure 4.1B) supplemented with DPhBMP4 (500 pg/mL) for 9 days with the chromaffin markers, PNMT, CgB and Faglu markers of CA synthesis and storage. Scale bars: 200 and 5 µm. (B) HPLC analysis of catecholamine content in lysates of chromaffin-like cells differentiated from NCPC-4d in differentiation medium (see Figure 4.1B) supplemented with hBMP4 (500 pg/mL), hBMP4 (50 pg/mL), DPhBMP4 (500 pg/mL) and DPhBMP4 (50 pg/mL). BMP4 and corticosteroid mimetic have a stimulatory effect particularly for adrenaline levels. ns- Not significant, *P < 0.05, **P < 0.01. N = 3 independent experiments. (C) FACS analysis of NCPC-4d and NCPC-6d differentiated to chromaffin-like cells as analysed using αTH, PNMT and CgB antibodies. The proportion of cells with various SA markers is similar under various chromaffin differentiation conditions. N = 8. (D) Representative FACS plot of NCPCs differentiated to chromaffin-like cells as analysed using αTH and PNMT antibodies. The plot suggests emergence of αTH+/PNMT- and αTH+/PNMT+ sub-populations in hBMP4 only conditions while addition of DP reduces the PNMT- sub-population. N = 8 independent experiments; error bars represent mean ± SEM.

4.3.4 Sorting for GD2 and B2B1 expression enriches for SAP-like cells

SAPs originate from the NC during development and are the origin of neuroblastoma and PHEO, for which GD2 ganglioside is a surface marker. GD2 is also useful for sorting SAP-like cells in the mouse model (Saxena et al. 2013). In addition, the B2B1 antibody has been used to detect committed sympathetic neuroblasts rather than the chromaffin cell lineage in the rat (Anderson et al. 1991; Carnahan and Patterson 1991b). We first asked whether these surface markers are expressed in differentiation of hPSC cells to NCPC cells. Our follow-up question was whether sorting NCPCs for these would improve the later differentiation of chromaffin-like cells.

We stained dissociated NCPC neurospheres with GD2 antibody to sort for SAPs and B2B1 antibody to separate cells that are already committed to the pre-sympathetic neuronal lineage. FGF2/BMP2 exposure for 4 days (NCPC-4d) gave GD2 expression in about 40% p75NTR+ H9-derived cells and less than 3% co-expression of GD2 and B2B1. After FGF2/BMP2 exposure was increased to 6 days (NCPC-6d), GD2 was expressed by all p75NTR+ cells with about 25% co-staining for B2B1 (Figure 4.5A). To test this finding in another cell line, we differentiated HES3-hESCs to NCPCs and analysed the expression of GD2 and B2B1 by FACs analysis. Similar to H9s, 24% of p75NTR+ HES3-derived NCPC-4d cells were GD2+ with about 3% co-expressing GD2 and B2B1. However, after 6 days of FGF2/BMP2 exposure a difference was noted in that over 90% p75NTR+ HES3-derived cells co-expressed GD2 and B2B1 (Appendix S2-S3). Differences in hPSC cell line behaviour is reported in other differentiation methods (Perrier et al. 2004; Hoffman and Carpenter 2005). This is consistent with our results in Figure 4.2B where the SA1+ population decreased after 6 days of FGF2/BMP2 exposure and also with previous reports where SAP cells lose SA1 expression as they start to express B2B1 (Anderson et al. 1991; Carnahan and Patterson 1991b).

An opposite trend was seen in the percentage of p75NTR expression which modestly reduced with duration of FGF2/BMP2 exposure at least in HES3 hESCs. In H9 cells, the total percentage of p75NTR+ cells reduced marginally being around 90% for NCPC-4d and 6d and with HES3 reduced from about 90% (4 days) to about 70 % (6 days) ($N = 5$ for 4 days and $N \geq 22$ for 6 days) (Figure 4.5B and Appendix S2-S3). As

the percentage of p75NTR reduced, GD2 and B2B1 co-expression increased and this inverse relation could be as a result of NCPC-like cells showing a FGF2/BMP2-duration dependent committment to neuroblastic differentiation indicated by an increase in B2B1 expression (see Figure 4.5A and Appendix S2-S3).

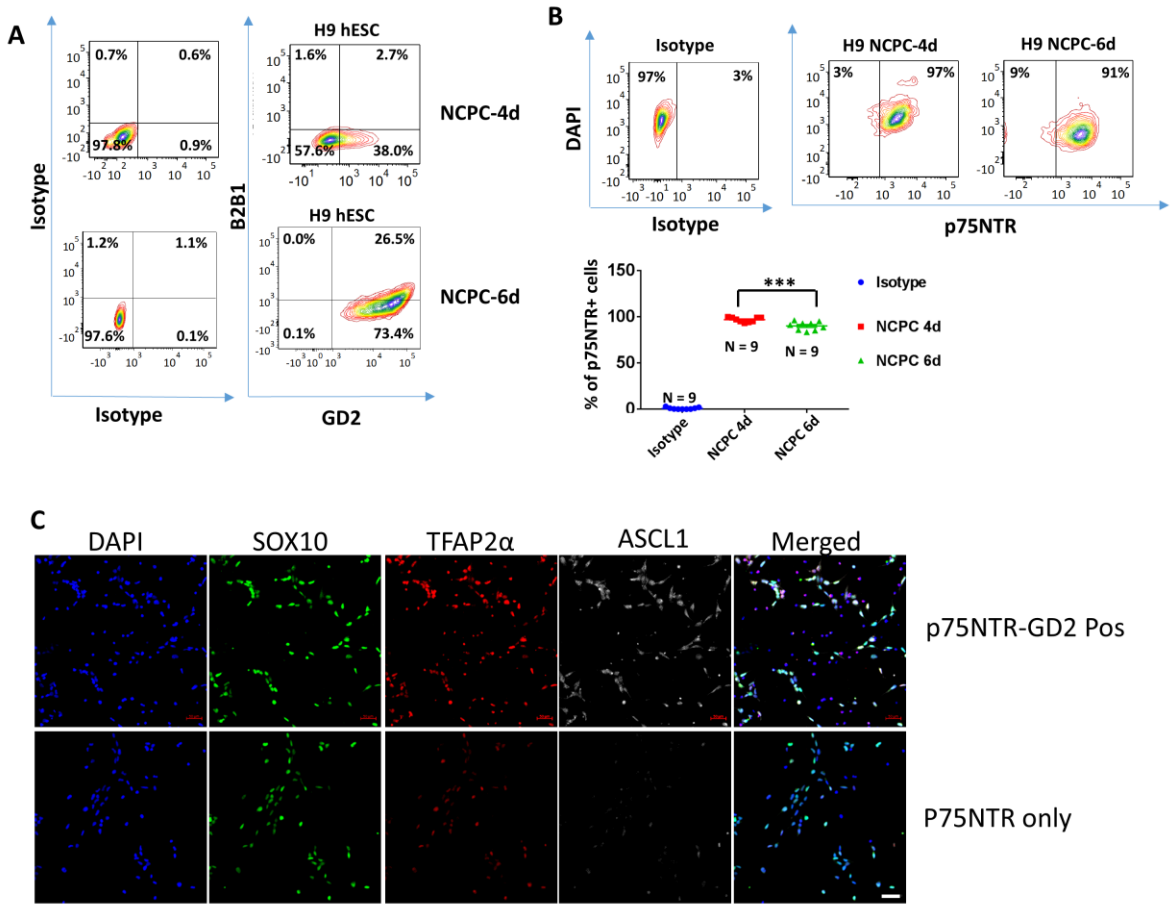

Figure 4.5 Characterisation of time-point differentiation of H9 hESCs into NCPC/SAP lineages with GD2 selection. (A) Representative FACS analysis of H9 hESC-derived NCPC-4d and NCPC-6d cells with SAP markers, B2B1 (neuroblast lineages) and GD2 (SAP lineages). The p75NTR positive population was used to gate and select for B2B1 and GD2 populations. NCPC-4d; N = 10 and NCPC-6d; N = 10 independent experiments. (B) Representative FACS analysis of NCPC-4d and NCPC-6d cells with the NCPC marker p75NTR showing uniformly high % expression of p75NTR. N=10 independent experiments. ***P < 0.001. (C) Immunofluorescence of differentiated cells at day 9 (see Figure 4.1B) of 75NTR/GD2 sorted cells and P75NTR-only sorted cells with NCPC markers SOX10 and TFAP2α, and SAP marker ASCL1, which is enriched by GD2 selection. Scale bar: 50 µm.

Immunofluorescence confirmed the expression of NC markers SOX10, TFAP2α and ASCL1 in the p75NTR/GD2-sorted NCPC population and TFAP2α and ASCL1 immunostaining was more intense than in p75NTR-only sorted populations (Figure 4.5C). Comparing GD2+ and GD2- sorted population by qPCR, showed the expected upregulation of NC and SAP genes as normalised to NCPC-4d and 6d (Figure 4.6A). For most markers at both 4 and 6 days NCPC/SAP induction the expression value for

GD2+ cells exceeded that for GD2- cells without attaining significance for individual markers (Figure 4.6A).

We differentiated the GD2- and GD2+ cells using the DP treatment for 6 days and analysed them by immunofluorescence with SAP and chromaffin markers, *αTH*, and *PNMT* and *PRPH* (Saxena et al. 2013). Differentiated GD2- and GD2+ cells expressed αTH, PNMT and PRPH with differentiated GD2+ cells being relatively more effective in level and proportion of expression as compared to differentiated GD2- cells (Figure 4.6B). This paralleled results using mouse cells (Saxena et al. 2013). We also analysed the differentiated cells by qPCR normalised to levels in NCPC-4d cells. GD2+ cells when differentiated with DP showed greater upregulation of *αTH, PNMT* and *DβH* as compared to GD2- cells and this increased between 6 and 9 days differentiation (Figure 4.6C). We conclude that sorting for GD2 expression after NCPC induction is an effective means of maximising chromaffin cell differentiation in the subsequent stage of differentiation.

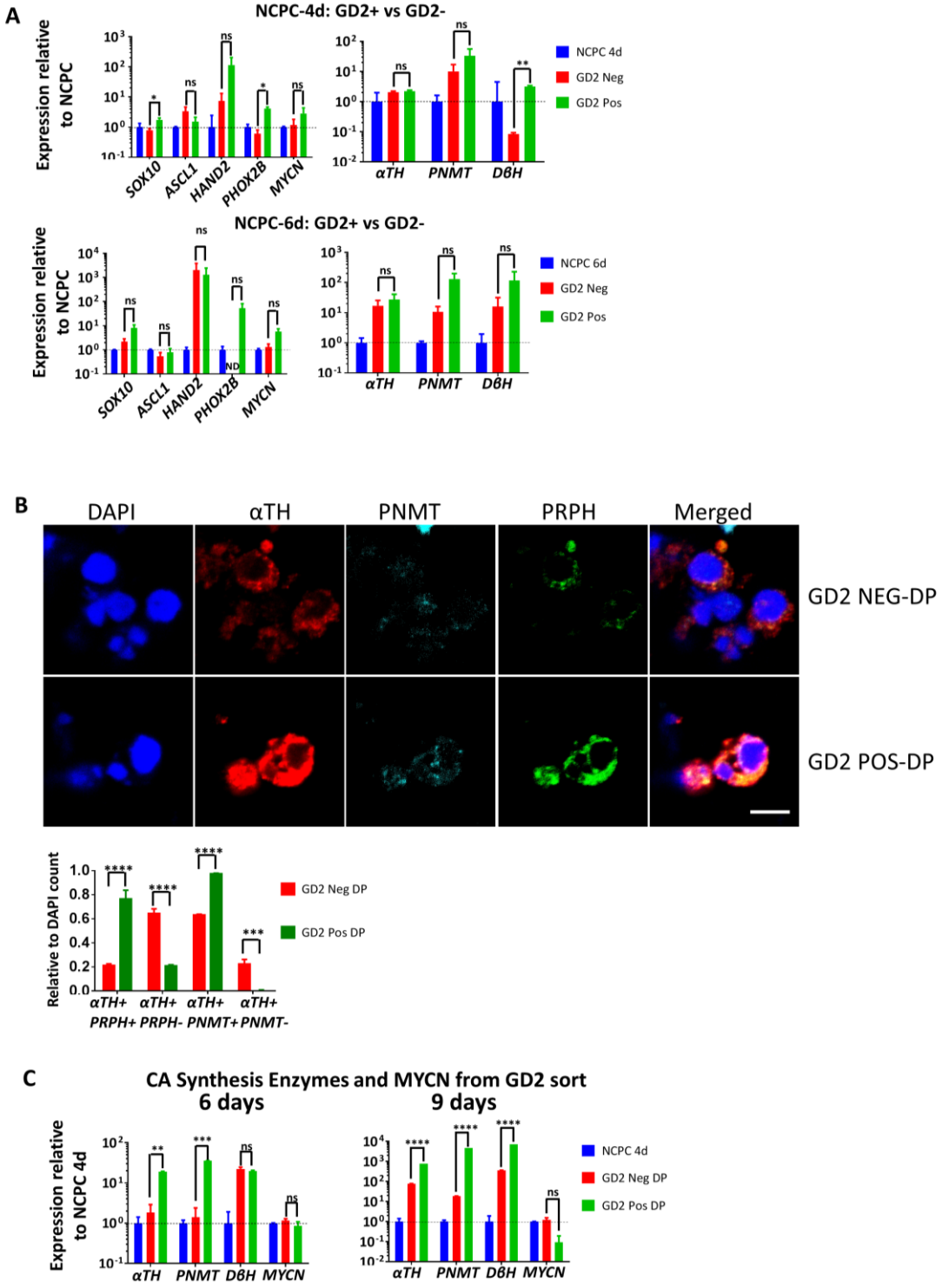

Figure 4.6 FACs sorting for GD2 enriches SAP-like cells. (A) qPCR analysis of p75NTR/GD2-sorted H9 NCPC-4d and NCPC-6d cells. GD2 Neg (p75+/GD2-) and GD2 Pos (p75+/GD2+) expression were normalized to the H9 hESC cells. N = 3 independent experiments. (B) p75NTR/GD2 (Positive and Negative-sorted) after 6 days of chromaffin differentiation in dexamethasone and PMA (DP) express SAP and chromaffin markers αTH, PNMT and PRPH (see Figure 4.1B). Scale bar: 5 µm. Immunofluorescence count of differentiated GD2 Neg and GD2 Pos cells shows GD2 selection favours PNMT expression. DAPI stain was used to count the total number of cells and to normalize the markers. N = 4 independent experiments. (C) qPCR analysis of GD2-sorted cells differentiated to chromaffin-like cells under DP cultured condition for 6 days and 9 days. NCPC-4d cells were used to normalize the expression. GD2 preselection augments

PNMT expression as well as other SAP markers. ND-not detectable, N = 4 independent experiments; error bars represent mean ± SEM. ns- Not significant, *P < 0.05, **P < 0.01, ***P < 0.001, ****P < 0.0001.

4.3.5 hESC-derived NCPC cells migrate *in vivo* and in CAM and organ culture to the suprarenal region and differentiate into cells expressing chromaffin markers

To assess whether hESC-derived NCPC cells would survive, migrate and differentiate into chromaffin-like cells *in situ*, we differentiated ENVY-HES3 cells, which express the GFP marker (Costa et al. 2005; Costa et al. 2007), along NCPC/SAP lines and transplanted them directly next to the neural tube in the 'adrenomedullary' level of E2 quail embryos *in vivo* and incubated the developing embryos for 4-5 days (Figure 4.7A). Cryosectioned tissues were immunostained for αTH, PNMT and GFP. Confocal analysis showed that human NCPC neurosphere GFP+ cells had survived, migrated away from the implant region and differentiated into αTH+ and PNMT+ cells. The human GFP+ cells had in general migrated to below the somitic vertebral cartilage where sympathetic tissues occur. Frequently αTH+ human cells were associated with quail host αTH+ cells. The sensitivity of the antibody to avian αTH would not be expected to be less than to human αTH because the antibody was raised against quail TH epitope, yet the human cells labelled more intensely. This suggests that the human cells had higher levels of this CA synthetic enzyme. Other cells were GFP+ but αTH-, or PNMT- (Figure 4.7B and Appendix S2-S10A). This is expected since the hESC-derived NCPCs are a mixed population of SAPs and other trunk NCPC cells. We could not find human cells (i.e. GFP+) directly adjacent to the mesonephric kidney of the host embryos which could be due to insufficient time *in vivo*, as colonisation of the suprarenal *anlage* commences around E5.5 in birds (equivalent to E12.5 in mouse) (Gut et al. 2005; Huber 2006). (Note: avian suprarenal gland does not have the medulla-cortex spatial organisation of the mammalian adrenal gland).

We also transplanted NCPCs derived from H9 hESCs to the excised 'adrenomedullary' level of E2 quail embryos and grew these combinations as organ-cultures *in vitro* for 3-4 days or as chorio-allantoic membrane (CAM) grafts for 8 days (refer to Figure 4.7A). Calcein AM-labelling of implanted cells was used to gauge whether the human cells were retained and had started migrating at 1 day. In these cases the tissue organisation was disturbed and histological section planes were difficult to define. Transplanted organ cultures left in culture for 3-4 days were analysed by whole

mount staining. Transplanted human cells in the quail tissue organ cultures were identified with anti-HNA; these co-expressed αTH and CgB and were surrounded by αTH and CgB-expressing HNA-negative quail cells (Figure 4.7C).

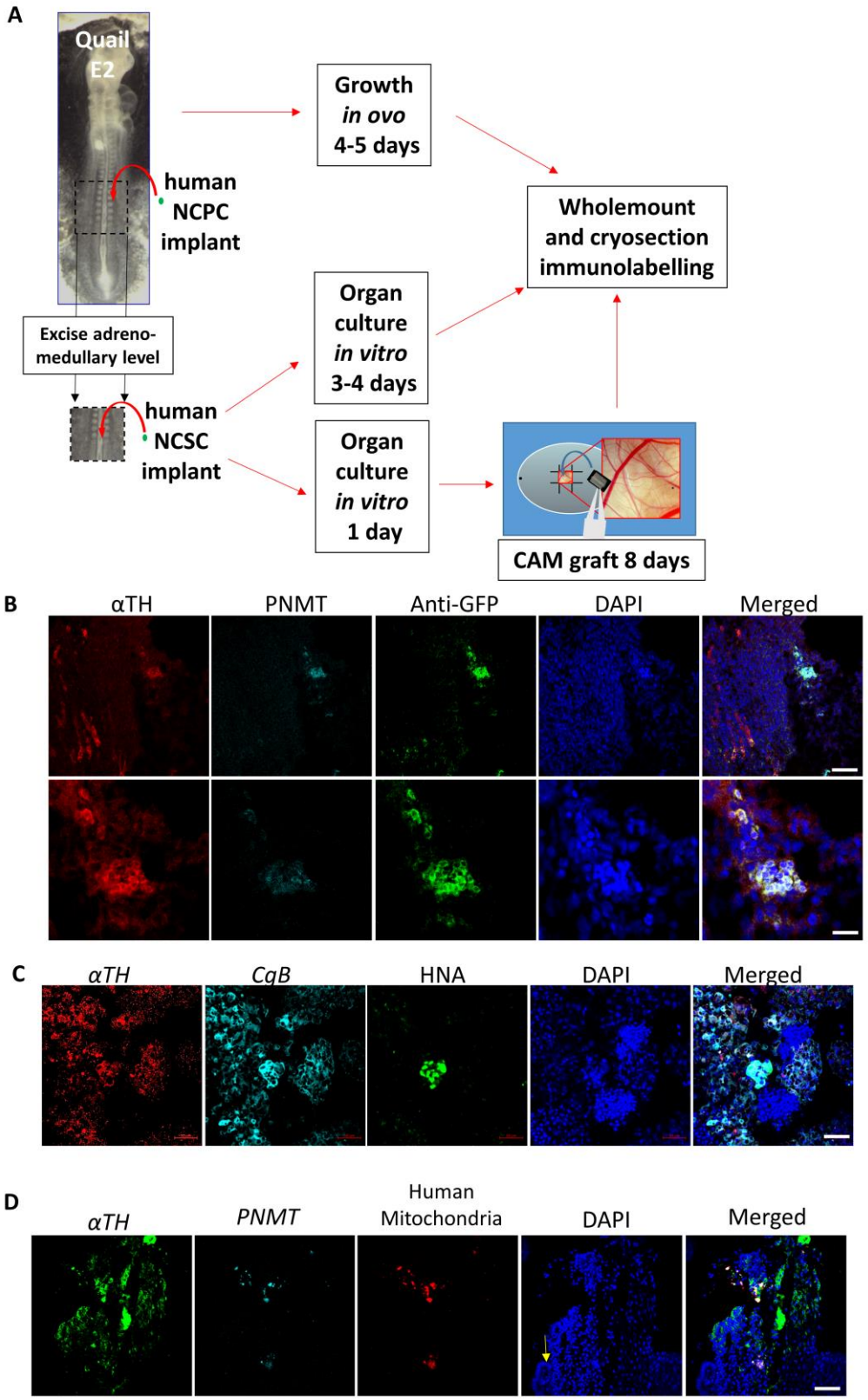

Figure 4.7 NCPC/SAP-like cells can integrate, migrate and differentiate in embryonic tissues. (A) Scheme of the transplantation of hESC-derived NCPCs in quail E2 (QE2) embryos and incubated in vivo or cultured in vitro or grown on CAM. (B) Immunofluorescence with chromaffin markers, αTH and PNMT of NCPC cells derived from ENVY-HES3 hESCs transplanted for 4 days in QE2 embryo. This frontal-oblique section is further ventral to the section shown in Supplementary Figure S10A. The human αTH+ cells associate with similar lineage host cells. Scale bars: 10 (lower) and 50 (upper) µm. (C) Immunofluorescence with chromaffin markers, αTH and CgB and human

cell-recognizing antibody, anti-Human Nuclear Antigen, of NCPC cells derived from H9 hESCs transplanted into QE2 tissue and cultured in vitro for 4 days. Scale bar: 50 µm. (D) Immunofluorescence with chromaffin markers, αTH and PNMT and human cell-recognizing antibody (anti-human mitochondria) of NCPC cells derived from H9 hESCs transplanted into QE2 tissue and cultured on CAM for 8 days. Section is through αTH-expressing tissue at margin of mesonephric kidney tissue (arrow). Scale bar: 50 µm.

To achieve extended time and greater growth of the grafted tissue, we used the CAM assay (Zhang et al., 2010). Excised tissues were cultured for 1 day *in vitro* as above before transfer to the chick embryo CAM for 8 days. CAM graft cryosections which had structures resembling renal tubules were processed for immunostaining for αTH, PNMT and human cells were identified with mouse anti-human mitochondria antibody. Transplanted human cells were found adjacent to tubular tissue in the CAM sections (Figure 4.7D), showed immunoreactivity for αTH and PNMT and were often associated with host αTH+ cells.

4.4 Discussion

There are previous reports on differentiation of NCPCs and SAP-like cells from human pluripotent cells (Lee et al. 2010a; Denham et al. 2015) and differentiation of sympathetic neurons (Oh et al. 2016), but the further differentiation of human pluripotent cells to chromaffin-like cells has not yet been described. Furthermore, previous reports have outlined the isolation, culturing and characterisation of human and bovine adrenal chromaffin cells (Santana et al. 2012; Santana et al. 2013; Tischler 2013). Here, starting from human pluripotent cells, we show the time-point of increment in SAP-like cell markers in NCPCs in relation to extended exposure to BMP2/FGF2, and the utility of sorting for GD2. We also analysed positional identity based on the *HOX* gene expression, and further differentiated the NCPCs to chromaffin-like cells as shown by a range of SAP markers and the specific chromaffin cell enzyme PNMT and its synthetic product adrenaline.

The differentiated NCPC/SAPs expressed markers, p75NTR, SOX10, ASCL1, HAND2, MYCN and PHOX2B, expressed by isolated and characterised human and bovine adrenal chromaffin cells (Santana et al. 2012; Santana et al. 2013; Tischler 2013) and genetic cell lineage tracing in mouse (Furlan et al. 2017), and GATA3 as shown in mouse ESC derived SAPs (Saxena et al. 2013) and human ESC-derived SAPs (Oh et al. 2016).

Our results suggest that the NCPC population is heterogeneous with about 50% being SAP-like cells as defined by protein, including transcription factor, expression. These could be differentiated into chromaffin-like cells with culture conditions that have been shown to play an important role in chromaffin cell development and differentiation (Huber et al. 2008; Santana et al. 2012; Santana et al. 2013; Saxena et al. 2013). This led to a greater proportion of cells expressing the chromaffin markers with low expression of neuroblast/sympathetic neuron markers. In addition, we have shown that BMP4 can more efficiently direct SAP-like cells to chromaffin cells *in vitro* when exposed at an earlier time-point during prior NCPC/SAP differentiation with FGF2/BMP2. This points to the necessity to reduce the duration of exposure to FGF2 to avoid sympathetic neuronal differentiation and to enable chromaffin differentiation and this is augmented by corticosteroid mimetics. Crucially these cells express PNMT and convert noradrenaline to adrenaline as assayed by HPLC. In addition, sorting the NCPCs on the basis of expression of the GD2 ganglioside improves the chromaffin cell purity. We have shown the SAP-like differentiation capacity of our differentiated hPSCs by *in vitro* differentiation into neurospheres and also shown their positional identity of the trunk axis, appropriate for SAP cells, by the increased expression of *HOX5-7* and *10*.

Overall, we consistently derived between 70-98% of cells expressing p75NTR which co-expressed HNK-1 in three tested cell lines (H9, HES3 hESCs and 007 iPSCs) using our differentiation protocol, with H9 hESCs and 007 iPSC outperforming HES3 hESCs. A similar pattern was seen in the subsequent chromaffin cell differentiation protocol where there were more cells expressing chromaffin markers in H9 hESC and 007 iPSC-derived cells than HES3-derived cells. There have been previous reports on differences in differentiation propensity between hPSC lines (Osafune et al. 2008; Melichar et al. 2011) .

Cells of NCPC spheres transplanted *in vivo* into the quail adrenomedullary axial level exhibited the morphology and properties of SAP-like cells by integrating, migrating and differentiating into cells expressing SAP (αTH, CgB) and chromaffin cell markers (PNMT). Typically these human cells were associated with quail host cells of the same lineage. This confirms the post-transplantation survival, integration and differentiation ability of the human NCPCs *in situ*.

In conclusion, the timing and duration exposure of human NCPCs and SAP-like cells to BMP4 and FGF2 *in vitro* is important in chromaffin-like cell differentiation and the presence of glucocorticoids promote a greater proportion of the differentiated cells expressing the adrenaline synthesis enzyme PNMT and becoming capable of converting noradrenaline to adrenaline. These cells have the potential for investigating differentiation of human chromaffin cell, for modelling specific diseases like phaeochromocytoma, for cell replacement strategies in neurodegenerative diseases and for pain management.

5 DIFFERENTIATION OF MEN2B AND CONTROL hESCs TO CELL TYPES AFFECTED IN MEN2B PATIENTS

5.1 Introduction

When a cancer is detected, every cell already has complex genetic (including epigenetic) changes, and the cancer cell population is heterogeneous (Tomlinson et al. 2002). This enormous variability conceals the key initiating mutations, and impedes searches for treatments (McGranahan and Swanton 2015). Numerous cell lines representing cancers of all cell lineages have been used for research but these reflect the cancer at and after detection (Vincent et al. 2015), not at initiation.

Cancer initiation is difficult to approach (Nguyen et al. 2015) but an ideal model would start with i) the normal human cell of origin, with ii) candidate initiating mutations. The former is problematic especially for paediatric cancers, where the cell of origin may be unobtainable post-natally. However this may now be overcome by using human pluripotent cell technology to produce facsimiles of the desired cell lineage (Lee et al. 2015; Gingold et al. 2016). The latter is now possible by introducing known mutations using programmable endonucleases such as CRISPR/Cas9 (Sanchez-Rivera and Jacks 2015).

Paediatric cancers often start as a developmental error (Parsons et al. 2011); examples are the MEN2A/2B. The onset of the latter (a rare but very aggressive and severe form of MEN2 see 1.1.1) is during the first year of life while the former (more common but less aggressive) starts between the age of 5 and 25 (Gujral et al. 2006; Raue and Frank-Raue 2009). Overall, the MEN2s affect 1 in every 30-35,000 live births (Marini et al. 2006) but have a restricted set of mutations in just one gene, *RET*. These affect SA and enteric (gut) NC-lineage cells and thyroid C cells, the latter being only recently shown to be of foregut endodermal entero-endocrine lineage (see 1.1.1). These lineages are limited to the embryonic/foetal period, and are unobtainable when these cancers are detected. The broad spectrum of affected lineages could explain why the MEN2s, especially MEN2B, are rare as they could be misdiagnosed due to the diversity of phenotypes (see Table 1) (Jones and Sisson 1983; Camacho et al. 2008; Lee et al. 2010b; Singer et al. 2014). Patients with MEN2A may present with Hirschsprung disease while patients with MEN2B also have mucosal neuromas, intestinal ganglioneuromas and a marfanoid habitus with skeletal deformations and joint laxity but without the vascular and ophthalmologic abnormalities of true Marfan syndrome. They often do not have a family history of the disease and harbour a *de novo* mutation.

5.2 Aims

To create the MEN2B mutation, M918T, in hESCs (H9, MEL2 and HES3) using the CRISPR/Cas9 system by homology-directed repair, HDR.

1. To karyotype all of the obtained clones for any aneuploidies.
2. To analyse the pluripotency state of the obtained clones by FACs and immunostaining.

Differentiate hESCs to:

a) Definitive Endoderm and to neuroendocrine cells such as thyroid C cells (Parafollicular cells of the thyroid) and analyse their functionality by ELISA.
b) Vagal Neural Crest-like Cells (VNCC) and to Enteric Neural Crest Cell (ENCC) and Enteric Neurons (ENs) and Enteric Glia-like cells.

5.3 Results

5.3.1 Generation of MEN2B-hESC cell lines by CRISPR/Cas9 targeted HDR

The majority of MEN2B mutations are diagnosed by single point autosomal transition in the tyrosine rich residue of the *RET* gene, A883F and M918T, with the latter driving the common and most aggressive outcome (Raue and Frank-Raue 2009). We chose H9 hESC cell lines that had a normal karyotype for electroporation. We co-electroporated the designed *RET* exon 16 targeting CRISPR/Cas9 construct with the ssODN and a puromycin expressing vector for selection by nucleofection. Nucleofection ensures a higher yield of transfected cells with a higher cell viability, a stable variability between experiments and also the ease of starting with a small number of cells was of great importance in designing the experiment (Zeitelhofer et al. 2007; Moore et al. 2010). Puromycin selection was done 24 hours post-electroporation at 0.5 µg/mL for another 24 hours and the cells were allowed to recover for 6-9 days with media change done every other day. Approximately 6 days after puromycin selection, puromycin resistant clones showing round edges were selected and plated on feeder cells for a week. Major parts of each of the expanding colonies were harvested and analysed by genomic DNA extraction and RFLP analysis to detect the mutation. Positive clones were further confirmed by Sanger sequencing. Sequencing results showed genetic modification of interest on only one allele (monoallelic) in all of the clones analysed (100%). Surprisingly, we did not detect any non-homologous end joining (NHEJ) event in the

sequence or any clone with the genetic modification on both alleles (biallelic) (Figure 5.1A). These clones were then karyotyped using the Illumina Infinium CoreExome-24 v1.1 and the clones that had no aneuploidies detected were further expanded and their pluripotency confirmed by FACs analysis and immunofluorescence for TRA-1-60 (Figure 5.1B) and NANOG (Figure 5.1C).

One of the setbacks of using the CRISPR/Cas9 has been off-target mutation effects (Cho et al. 2014), however, selection of sgRNAs with low off-target prediction and lowering the amount of the DNA transfected plays a critical role in reducing the risk of generating off-target changes (Kim et al. 2015; Kleinstiver et al. 2016a). The design of our sgRNAs was strictly per the suggestions of reducing off-target effects and so we hypothesised that there will be few or no off-target effects of our sgRNA. This prediction was born out because T7E1 assay analysis showed no detectable off-target effects as compared to the controls (Figure 5.1C).

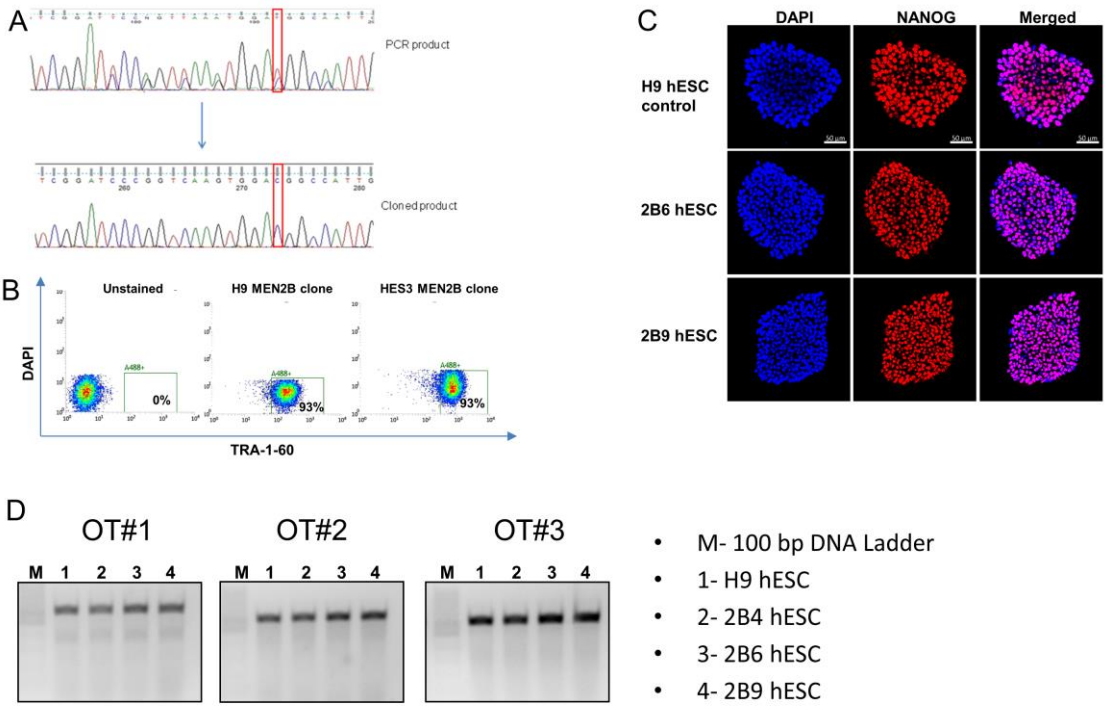

Figure 5.1 Generated M918T MEN2B hESCs maintain pluripotency and have no detectable off-target mutations. (A) Sanger sequencing of a representative MEN2B clone shows the precise conversion of ATG to ACG (coding for M→T amino acid change). (B) Representative FACs plot analysis of obtained MEN2B clones of two hES cell lines showing a high percentage of TRA-1-60 staining. (C) Representative image of two MEN2B clones showing the expression of NANOG, a pluripotency marker. Scale bar 50 µm. (D) T7E1 assay analysis of MEN2B hESC clones shows no detectable off-target effects.

Normally the RET protein undergoes dimerization when a ligand such as GDNF interacts with its co-receptor, in this case GFRα1, which in turn binds to the extracellular part of the RET protein. Dimerization of RET protein then promotes its activation by autophosphorylation (Airaksinen et al. 1999). A similar mechanism operates with three other RET ligands, neurturin, artemin and persephin and their respective co-receptors GFRα2, 3 and 4. *RET* activation drives many responses including cell survival, proliferation, differentiation, motility, renal tubule formation (Murakumo et al. 2006). Moreover *RET* activation upregulates *RET* gene expression. However, it is known that the *RET*-MEN2B mutation protein is at least partly independent of the ligand and does not require dimerisation to activate *RET* (Santoro et al. 1995) whiles others point out that dimerisation might still be necessary to maximally activate *RET* (Borrello et al. 1995). We therefore performed a qPCR analysis to test this self-upregulation hypothesis in the pluripotent state of the generated MEN2B clones. QPCR analysis of the expression of the *RET* gene showed a trend of increase in mRNA expression although the difference was not significant between H9 hESC controls and the MEN2B clones. One of the clones generated from the MEL2 hESC line showed a significant increase in *RET* mRNA expression with H3-20 clone from the HES3 hESC cell line showing a significant reduction in *RET* mRNA expression (Figure 5.2A). This variability or difference in *RET* mRNA expression behaviour could be attributed to the differences in the behaviour of the various hESC cell lines as already reported (Perrier et al. 2004; Hoffman and Carpenter 2005).

The activation of *RET* leads to the initiation of downstream pathways and an example is the PI3K pathway which promotes cell survival (Murakumo et al. 2006) and previous findings have shown the interaction between PTEN, a tumour suppressor gene and the PI3K pathway (Carracedo and Pandolfi 2008). QPCR assay of *PTEN* shows the increased expression of *PTEN* in most of the generated MEN2B clones. The increased expression of *PTEN* could be as a result of the slight increase in *RET* mRNA expression leading to an activation of the PI3K pathways thus initiating a negative feedback loop of *PTEN* upregulation. Furthermore, the expression of *RET* regulates neuronal differentiation (Bunone et al. 1995; Ikuno et al. 1995) so I investigated whether the created MEN2B mutation will affect the expression of the neural markers *TUBB3* and *S100β*. An increased expression of *TUBB3* mRNA in all of our generated MEN2B clones compared to the controls was recorded, whiles a moderate increase in *S100β* expression was recorded except in the H9 hESC-2B9 clone (refer to Figure 5.2A). I then

assayed one of the effects of *RET* activation, proliferation, by using the EdU assay (Murakumo et al. 2006). The MEN2B clones incorporated modestly but significantly more EdU as compared to the control hESC in 2 of the 3 MEN2B H9 clones. (Figure 5.2B), hence proliferation rate was increased indicating a functional response of the *RET* gene product by the incorporated M918T mutation. Note that these functional responses occur even in the ESC context where RET expression may be low level, compared to RET levels in RET expressing cell types (Takasato et al. 2014).

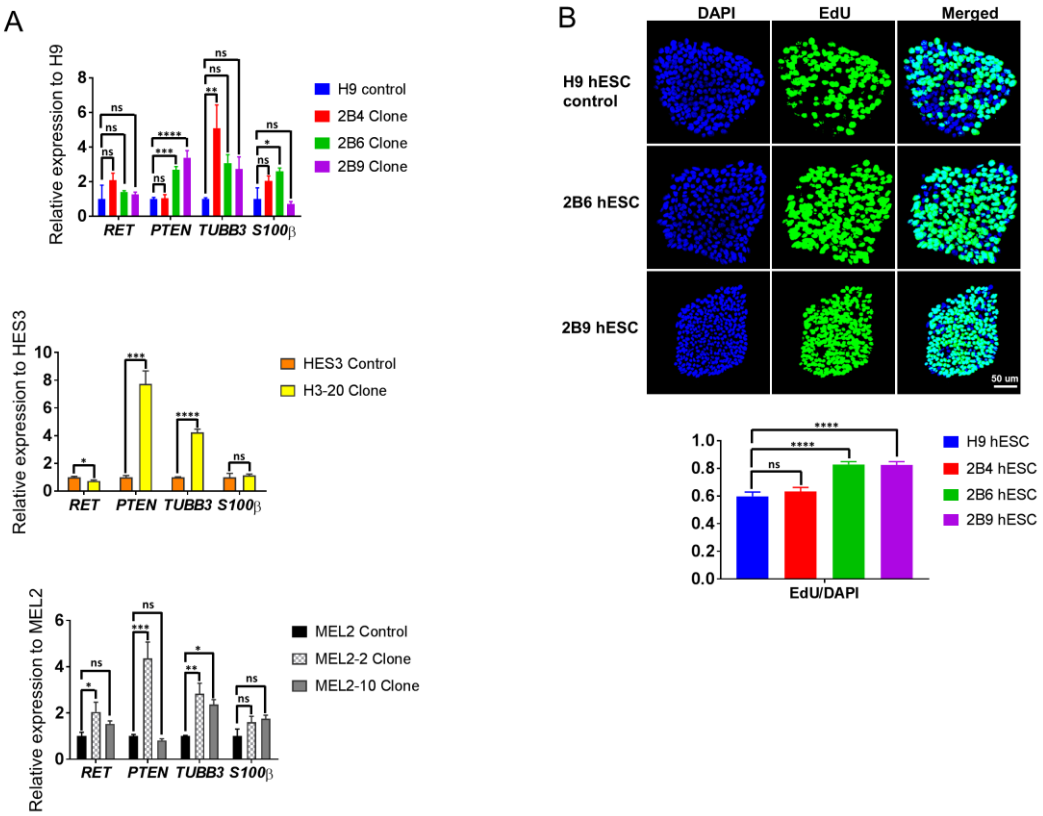

Figure 5.2 MEN2B clones proliferate faster than control cells. (A) QPCR analysis shows a slight increase in *RET* mRNA expression in both H9 hESC and MEL2 clones with a significant reduction recorded in the HES3 clone, H3-20. PTEN, TUBB3, and S100β mRNA expression increased in most of the MEN2B clones as compared to the controls. TUBB3 and S100β are markers for neuronal differentiation. (B) Representative image of EdU analysis showing the increased levels of EdU incorporation by MEN2B clones than control cells indicating their relatively higher proliferative ability. Scale bar 50 µm. N = 3 independent experiments; error bars represent mean ± SEM. ns- Not significant, *P < 0.05, **P < 0.01, ***P < 0.001, ****P < 0.0001.*

5.3.2 Differentiation of hESCs to endodermal thyroid C cell-like (parafollicular) cells

MTC is a key outcome of MEN2B, hence producing a human cell model for the C cell lineage is crucial for investigating the genesis of this aspect of the disease. Recent research has thrown light on the embryonic origin, development and differentiation of

mouse thyroid C cells *in vivo* proving that they originate from foregut endodermal cells (Johansson et al. 2015), and are not of NC lineage as previously thought (Le Douarin and Le Lievre 1970). We modified a previous published protocol for definitive endoderm (DE) differentiation induced by Activin A (D'Amour et al. 2005) by adding ITS to the media to support the growth of the cells in the presence of low FBS (Figure 5.3A). To test the efficiency of our DE differentiation from hESCs, we used the Sox17-mCherry hESC line and analysed the number of mCherry-expressing cells (i.e. expressing Sox17) on day 3 and day 5. We recorded about 30-40% of mCherry+ cells by day 3 with almost all cells (≥ 90%) expressing Sox17 by day 5 with the differentiation protocol (Figure 5.3B). We analysed the differentiated DE at day 5 for the expression of additional DE markers by qPCR, and we recorded an upregulation of most of the DE markers (Figure 5.3B). We then differentiated these cells into thyroid C cell-like cells in high FBS and supplementing the medium with or without IGF-1, RA, IGF-1+RA (Figure 5.3A) and analysed them after 6 days (day 12 in total). We used factors that have been used in neuronal differentiation of stem cells since our desired final result is a neuroendocrine cell type which shares many similarities to neural lineage cells, even though the similarities are via convergence rather than common descent (Brooker et al. 2000; Nieto-Estevez et al. 2016). We looked for conditions leading to an increased expression of *ASCL1*, and *CALCA*. *ASCL1* is a key proneural gene but also plays an important role in the development and differentiation of C cells and ASCL1 mutant mice lack C cells although the thyroid gland develops normally. CALCA encodes both calcitonin and CGRP by alternative RNA splicing. The development and migration of the UBB, the source of C cells (see 1.2.1), also depend on the expression of the paralogs of *HOX3,* an example is *HOXA3* (Kameda et al. 2007b; Kameda 2016). IGF-1 led to an increase in *ASCL1* and *CALCA* as compared to the other conditions and a comparable level of *HOXA3* expression was induced by both IGF-1 and RA (Figure 5.3C). We immunostained for E-cadherin, Procalcitonin and CGRP; these are markers expressed by C cells with Procalcitonin being restricted to the thyroid C cell lineage (Hazard 1977; Kameda et al. 2007b). We show that more than 40-50% of the cells differentiated co-express E-cadherin and Procalcitonin indicating that our differentiation protocol was generating thyroid C cell-like cells *in vitro* (Figure 5.4A and B).

Based on this, we differentiated the MEN2B-H9 hESC clones and the control H9 hESC via DE to thyroid C cell-like cells and analysed them by immunofluorescence and qPCR.

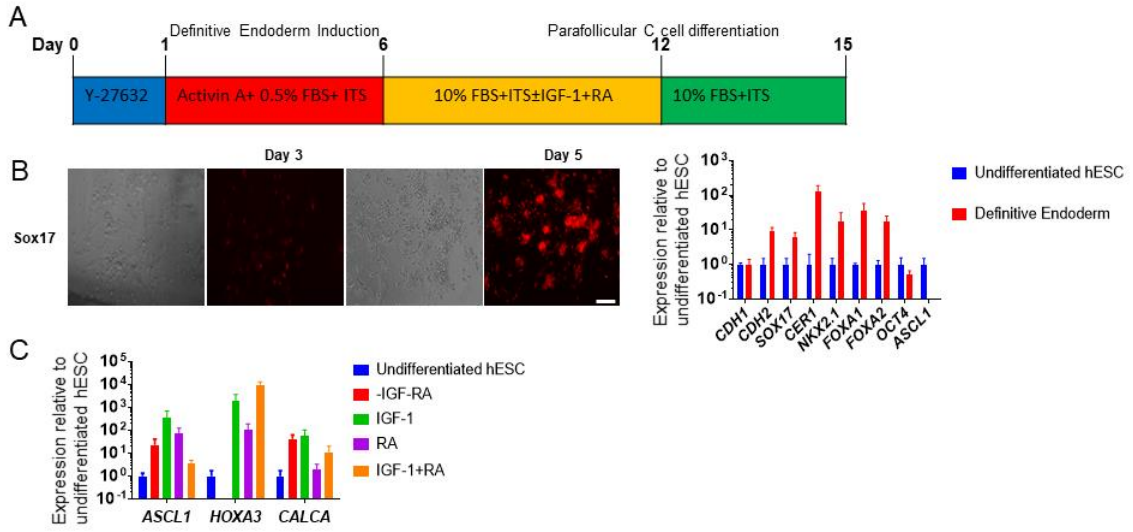

Figure 5.3 hESCs-derived DE precursors differentiate to C cell-like cells. (A) A schematic representation of the protocol for differentiating hESCs to DE and further to C cell-like cells. (B) Conventional microscopy showing the expression of mCherry at day 5 of differentiation towards the DE lineage. These cells have upregulated levels of DE markers, *FOXA2, FOXA1,* and *NKX2.1* and a downregulation of pluripotency marker, *hOCT4*. Scale bar is 200 µm. (C) QPCR analysis shows that IGF-1 treatment alone can promote the differentiation of DE lineage cells to C cell-like cells by the expression of 3 key markers, *ASCL1, HOXA3* and *CALCA*. –IGF-RA denotes no IGF and no RA

The distinctive function of thyroid C cells is the production of calcitonin, a hormone that regulates Ca^{2+} metabolism by lowering blood Ca^{2+} levels; so to further analyse the functionality of our differentiated cells, we stimulated the cells to secrete calcitonin into the medium by adding calcium chloride to the cells and analysed the medium by ELISA. The concentration of calcitonin secreted by thyroid C cell-like cells derived from MEN2B clones was higher than the control cells with 2B6 clone showing about 25% increase in concentration as compared to the control (Figure 5.4C).

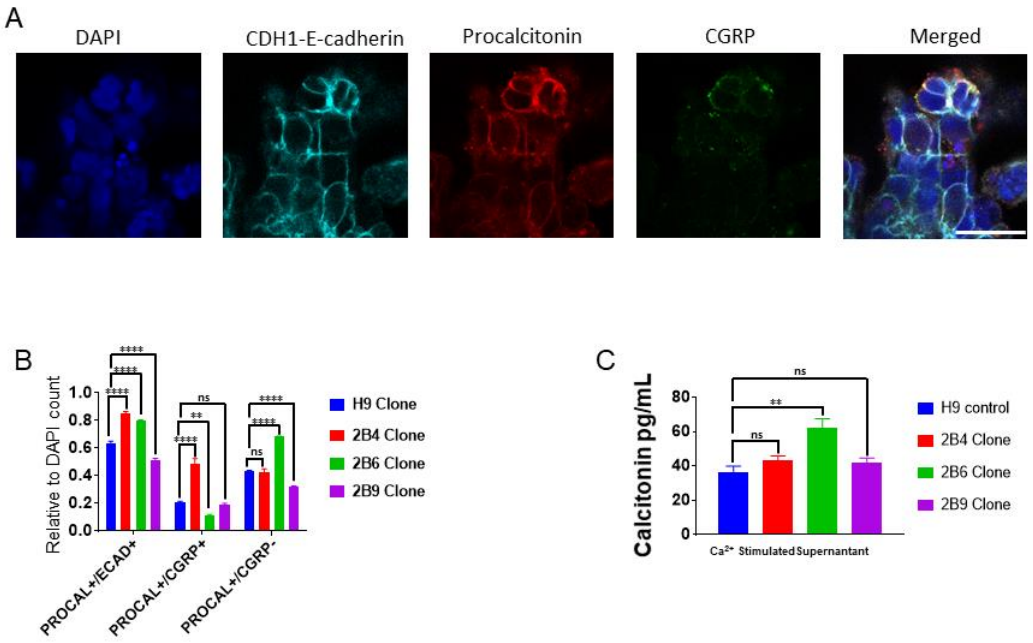

Figure 5.4 hESC-derived DE cells differentiated to C cell-like cells functionally produce calcitonin. (A) Differentiated C cell-like cells showing the expression of E-cadherin co-localising with PROCALCITONIN and CGRP, markers of C cells. Scale bar is 2 µm. (B) Immunofluorescent counts of differentiated H9 hESC controls and MEN2B-hESCs to C cell-like cells shows the increased number of PROCAL+/ECAD+ cells of the MEN2B clones, 2B4 and 2B6 except 2B9. N = 3 independent experiments (C) ELISA analysis of supernatant (culture medium) of differentiated thyroid C cell-like cells stimulated with 100 nM $CaCl_2$. N = 3 independent experiments; error bars represent mean ± SEM. ns- Not significant, **P < 0.05, **P < 0.01, ***P < 0.001, ****P < 0.0001.*

5.3.3 Differentiation of hESCs to vagal neural crest cells (VNCCs) and then to enteric neural crest cells (ENCC), enteric neurons (ENs) and enteric glia

Intestinal ganglioneuromatosis is in most cases, the first presenting feature of MEN2B patients and is therefore a key aspect of the MEN2B phenotype, but this is very often missed or misdiagnosed (King et al. 2006; Yin et al. 2006). We investigated whether the MEN2B mutation affects the survival, proliferation or differentiation of cells of the ENS in order to assess the reliability and validity of producing a human cell model for the intestinal ganglioneuromatosis of MEN2B. We modified previously published protocols and differentiated the hESCs first to vagal NC-like cells (VNCC) and further to ENCCs (Figure 5.5).

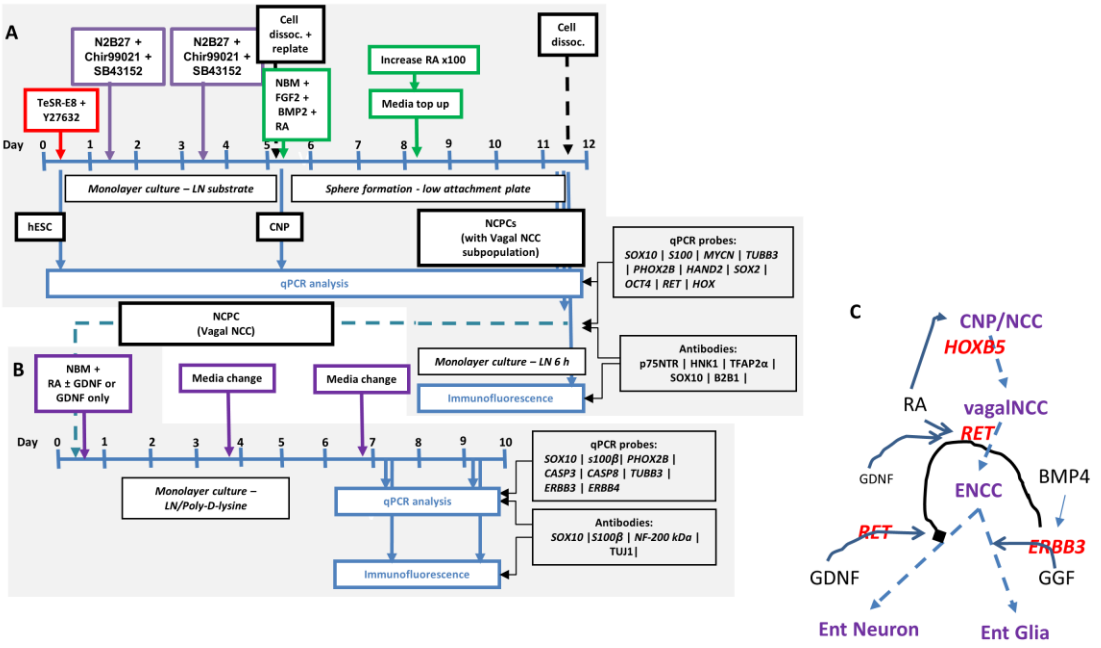

Figure 5.5 Detailed schematic illustration of the differentiation protocol of hESCs to Vagal NCC-like cells and to ENCC/ENs/Enteric Glia. (A) Illustration of the various differentiation via Wnt activation and TGFβ inhibition to generate multipotent caudal neuroprogenitors and further differentiation in BMP2/FGF2 supplemented with RA for positional identity to prime the cells toward a vagal NCC-like lineage. The cells are then analysed by qPCR analysis. (B & C) Illustration of the various differentiation steps required to generate ENCC/EN/Enteric glia-like cells from hESC-derived VNCC-like cells and the various genes and factors required for the downstream differentiation pathway (Obermayr et al. 2013).

We confirmed that our differentiated VNCCs express *SOX10*, *ASCL1*, *PHOX2B* and *TUBB3 (TUJ1)* by qPCR analysis and SOX10 and TUJ1 by immunostaining (Figure 5.6A). Relative to other axial level NCCs, VNCC has an increased expression of *HOXB5* (Kam and Lui 2015) (Figure 5.5C) and to further confirm the HOX identity of our differentiated VNCCs, we performed qPCR. The VNCC-like cells expressed higher levels of *HOXB5* as compared to *HOXB1-4* (*HOXB1-2* were conspiciously low but *HOXB3-4* were unaltered); which characterise more anterior levels of the NC (Figure 5.6B). We then further differentiated the cells using RA for 6 days, based on the observation in animal models that VNCCs require RA exposure to convert to ENC cells (Simkin et al., 2014). The cells were then immunolabelled for the expression of SOX10, S100β and NF-200 kDa. We recorded about 50% of SOX10+ cells co-expressing S100β indicating the presence of a mixture of enteric glia and ENC-like cells (ENCCs) in culture, since ENC cells and glia are both SOX10+ but only the latter express S100β. Additional staining of NF-200 kDa indicating the terminal differentiation into enteric neurons (Figure 5.6C).

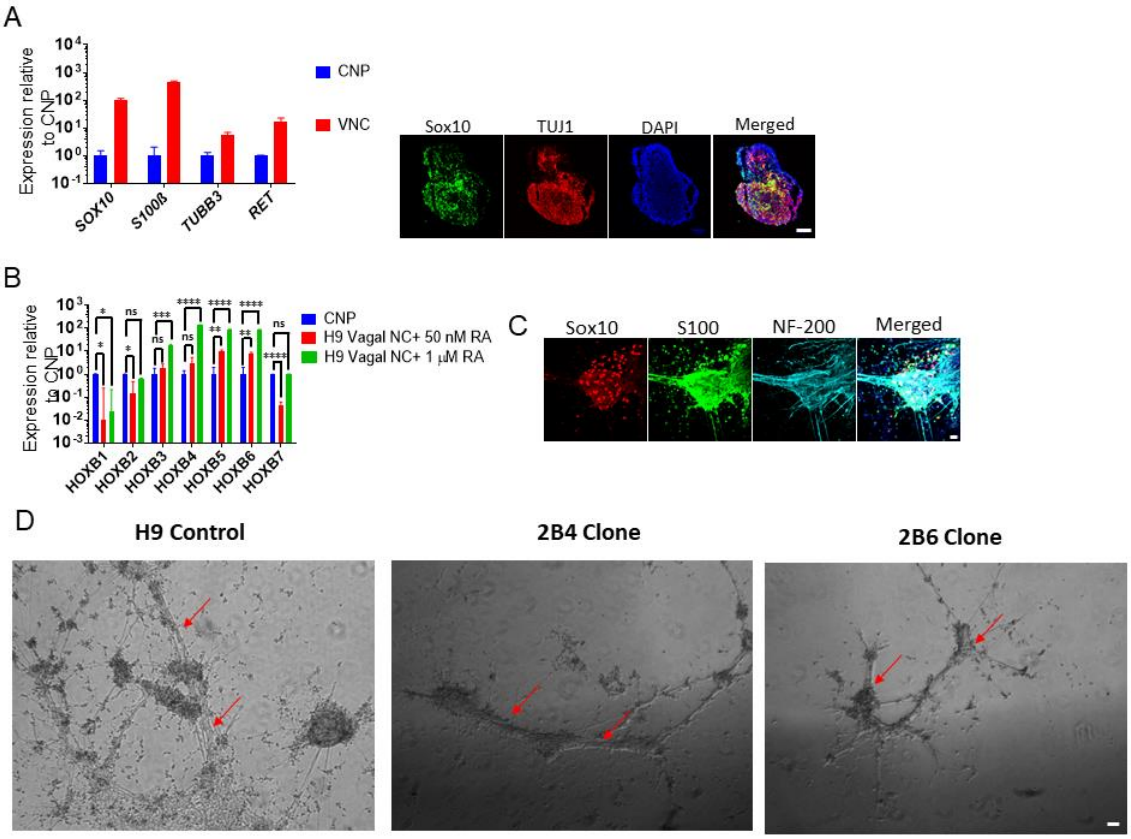

Figure 5.6 hESC-derived VNC-like cells differentiate into ENCC and Enteric glia-like cells. (A) QPCR analysis shows the increased expression of NC lineage markers gene, *SOX10, S100β, TUBB3* and *RET* after 7 days of BMP2/FGF2/RA exposure and cultured as neurospheres. The expression was normalised to housekeeping gene, *GAPDH* and further normalised (relative expression) to the multipotent caudal neuroprogenitors (CNP; 5 days after SBCHIR induction). Scale bar 100 µm. (B) QPCR analysis shows the HOX gene profiling of VNCC differentiation using different doses of RA treatment. Both conditions shows the increased expression of HOXB5, a VNCC HOX gene marker with 50 µM RA condition outperforming 1 µM RA treated condition as this condition leads to a reduced expression of Cranial NC HOX genes, HOXB1-2, relatively unaltered HOXB3-4 and trunk NC, HOXB7. Scale bar 100 µm (C) Immunostaining assay showing the co-staining of SOX10+/S100+ and S100+ only confirming the presence of Enteric glia-like cells, only SOX10+ staining, the presence of ENCC-like cells and NF-200 kDa, marking terminally differentiated neurons. (D) Brightfield image of hESC control and MEN2B-hESC clones differentiated to ENCC, Enteric glia and Enteric neuron-like cells showing the coarse appearance of the neurite outgrowth of the MEN2B clones, 2B4 and 2B6. Scale bar is 500 µm. N = 3 independent experiments; error bars represent mean ± SEM. ns- Not significant, **P < 0.05, **P < 0.01, ***P < 0.001, ****P < 0.0001.*

Next, the MEN2B clones were differentiated alongside the control H9 hESCs using the same differentiation protocol to VNCC and further to ENC cells, glia and neurons with RA treatment. In culture, we observed that the control H9-derived cells assembled in groups and showed a fine neurite outgrowth which both connected groups and projected onto the culture substrate. The cells of MEN2B clones also assembled in groups but showed bundled neurite outgrowth (Figure 5.6D). This characteristic of bundled neurite outgrowth resembles the ENS appearance in MEN2B patients where there is hypertrophy of nerve bundles (Martucciello et al. 2012). We then analysed the

expression of ENC cells, glia and neurons by qPCR and recorded an increased expression in *SOX10* and *S100*β, statistically significant in the 2B6 MEN2B mutant clone only as compared to the control line. The expression of *TUBB3* (neuronal marker) was moderately increased in the 2B6 clone but not significantly. *RET* expression remained unchanged with a decrease in apoptotic markers, *CASP3* and CASP8 in the MEN2B clones. We found a significant increase in the expression of *TOP2α*, a proliferative marker in the 2B6 clone (Figure 5.7A). PTEN plays a major role in the control of cell growth, proliferation and death and also in ENS development, and the expression of PTEN has been recorded to be low in intestinal ganglioneuromatosis (Puig et al. 2009). In our MEN2B clones, a decrease in *PTEN* mRNA expression was noted but not significant. Taken together, the MEN2B clones induced towards ENC cell differentiation *in vitro* showed an increased coherence especially of axons, decreased apoptosis markers and increase of a proliferative marker, consistent with intestinal ganglioneuromatosis of MEN2B patients (Martucciello et al. 2012).

5.3.4 GDNF rescues cell death of ENCCs, Enteric glia and Enteric neurons differentiated by RA

Some of the main functions of an activated *RET* is to promote cell survival (Murakumo et al. 2006) so we analysed the cell viability at the end of ENCC differentiation with RA by staining the cells with Calcein-AM for living cells and Propidium Iodide (PI) for dead cells. There was no significant difference between H9-ENS control cells and MEN2B clones in the percentage of dead cells *in vitro* with PI+ cells ranging from 12-18%. Clone 2B6 had more live cells as stained by Calcein-AM, 64.8% as compared to the control and other MEN2B clones. With GDNF known as the natural ligand for *RET* activation (Durbec et al. 1996; Jing et al. 1996; Trupp et al. 1996), we hypothesised that addition of GDNF for 3 days after 6 days exposure to RA would reduce the percentage of PI+ cells. RA induces the expression of TGF-β (Glick et al. 1991; Han et al. 1997) and GDNF becomes a potent neurotrophic factor in the presence of TGFβ by activating the PI3K pathway which is necessary for proliferation and survival (see Figure 1) (Krieglstein et al. 1998). The percentage of PI decreased by 21.4%, 31.6%, 39.2% and 38.7% in control, clone 2B4, 2B6 and 2B9 differentiation respectively (Figure 5.7B). This was also confirmed by analysing the mRNA expression of the apoptotic markers, *CASP3* and *CASP8* by qPCR, and it shows the decreased expression of these apoptotic markers in the presence of GDNF after RA induction (Figure 5.7B). This suggests that

the MEN2B mutation although it does not require GDNF to activate *RET*, GDNF still plays a very important role in the activation of the downstream pathways necessary for proliferation and survival, the PI3K pathway.

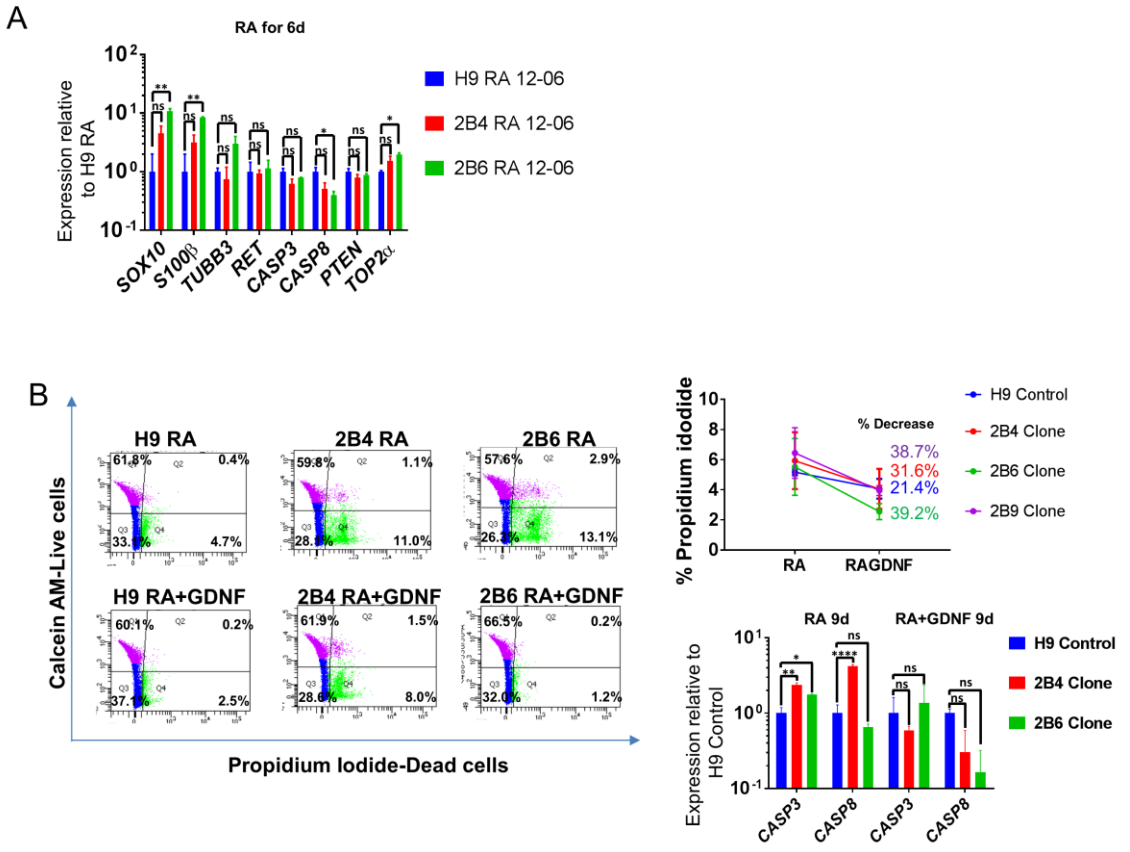

Figure 5.7 Cell death induced by RA can be rescued significantly in MEN2B differentiated cells by the addition of GDNF. (A) QPCR analysis shows an increase in SOX10 and S100β mRNA expression in both MEN2B clones (significant in the 2B6 clone) with an increase in TUBB3 expression only in the 2B6 clone. The expression of *RET* and *PTEN* remained unaltered with a slight decrease in CASP3 and CASP8 expression in both clones. Both clones had an increased expression of TOP2*α* mRNA expression. (B) Representative FACs plots show the high percentage of PI+ cells in the MEN2B clones when differentiated by RA only than the controls but this reduces more than 1.5-fold as compared to the controls when GDNF is added during differentiation. Cumulative graph showing the percentage of decrease after the addition of GDNF to the differentiation mix and a qPCR analysis showing the upregulation of apoptotic markers, *CASP3* and *CASP8* in RA only treated conditions as compared to RA plus GDNF conditions. N = 3 independent experiments; error bars represent mean ± SEM. ns- Not significant, **P < 0.05, **P < 0.01, ***P < 0.001, ****P < 0.0001.*

5.4 Discussion

MEN2B is a multifaceted disease which involves the endocrine tissues (thyroid and the adrenal gland) as well as extra-endocrine tissues like the oral mucosa and neural elements of the gastrointestinal tract, skeletal structures, and the eye in some cases. Modelling the *RET* mutant form in the human cell context could pave the way for the understanding of the pathogenesis of it, as well as other sporadic MTCs, and even

illuminate other diseases like Hirschsprung disease (where the ENS phenotype is the reverse of that in MEN2B).

We generated the M918T mutation of *RET* in H9 hESC, HES3 hESCs and MEL2 hESCs and these clones were karyoptically normal. We have shown that the M918T mutation in the pluripotent state did not alter expression of *RET* itself as well as several other genes, however, there was a functional effect of the mutation at this stage because proliferation rate of the mutated clones was increased.

We also generated a novel method for deriving *in vitro* thyroid C cell-like cells from hESC via a DE lineage intermediate. Functionally analysing these have shown that the M918T MEN2B clones produce a higher concentration of calcitonin as compared to the unaltered (control) hESCs. This was parallelled by generally higher proportion of cells immunoreactive for procalcitonin. This is consistent with the calcitonin and Ca^{2+} metabolic abnormalities of the FMTC aspect of the disease. We are currently generating a 3D model to more closely match the organ itself, for the testing of current drugs with the aim of achieving a better combination for management of MTCs and related thyroid cancers.

Intestinal ganglioneuromatosis in MEN2B patients, where there is over proliferation of neurons, glia and nerve fibres in the intestinal tract, presents as early evidence of the disease. Unlike FMTC, this ENS phenotype does not evolve to an invasive stage, but it may participate in the gastrointestinal functional disturbances of MEN2B. Mouse models of MEN2B fail to duplicate this ENS phenotype (Smith-Hicks et al. 2000), so a human model of this may be a model to identify markers and functions in this, as well as throwing light on Hirschsprung disease, where the *RET* mutation is a loss-of-function and the phenotype can be viewed as under-proliferation of the ENS. The generated MEN2B clones in an ENC differentiation context in culture mimic the characteristics of abnormally fasciculated neurite outgrowth in MEN2B cases as compared to the control. We have also shown that in the presence of GDNF, cell death in MEN2B clones is rescued to a greater proportion as compared to the degree of rescue in the control. This indicates that although the MEN2B mutation auto-activates *RET*, GDNF as a ligand is required for the full activation of *RET* and its downstream pathways, possibly via the normal RET allele. RET is known to be a dependency receptor in at least some contexts (Bordeaux et al. 2000), where possession of the receptor in the absence of ligand promotes apoptosis. Our next step is to differentiate the generated hESCs MEN2B lines to NCPCs/SAPs and then to adrenal chromaffin-like cells to further analyse whether

these cells will depict the phenotype of pheochromocytoma. PHEO is reported in 50% of MEN2B cases (Smith-Hicks et al. 2000; Pacak et al. 2001), so there is a 50-50% chance that these cells might not generate the pheochromocytoma phenotype *in vitro*. Therefore, we plan to FACs sort the generated NCPCs/SAPs from the hESCs MEN2B lines using the GD2/B2B1 antibody combination for a GD2+/B2B1- population and transplant these sorted cells into developing embryos as outlined in Chapter 4 (Abu-Bonsrah et al. 2018).

Overall, having a MEN2B human cell line is significant for further interrogating pathways mediating MEN2B pathogenesis within specific cell lineages.

6 DISCUSSION

The MEN2B disease affects SA and enteric (gut) NC-lineage cells and thyroid C cells (parafollicular cells) causing hyperplastic conditions which terminally progress to tumour of the adrenal gland (PHEO), hypergangliosis of the intestinal tract (ganglioneuromatosis) and tumour of the thyroid gland (MTC), the last of which progresses rapidly to a metastatic form. These three lineages were thought to have been derived from the NC thus MEN2B was considered a neurocristopathy but recent studies have shown that the latter cell type affected (thyroid C cells) are rather of the foregut endodermal entero-endocrine lineage (Johansson et al. 2015). The onset of the disease as early as 3 months indicates that these lineages are affected in the embryonic/foetal period. Since it is impossible to obtain human cells of these lineages at these stages, generating a cell model that can be maintained and differentiated to the various cell lineages affected would pave way to understanding the pathogenesis and finding better ways of intervening before the onset of the disease. Likewise it would be useful to establish an animal embryo research model that is tractable to new generation genetic manipulations such as CRISPR/Cas9 *in vivo*.

6.1 Generation CRISPR/Cas9 Modified Chicken Embryonic Cells *In Vitro* and *In Vivo*.

The chick embryo is one of the most widely used and accessible *in vivo* developmental models of higher vertebrates, with a wealth of background information especially on the NC system (Le Douarin and Chaya Kalcheim 1999). Before we started this project, there was no protocol or published article on the application of the CRISPR/Cas9 system to the avian embryo or to avian cells, so we had to first validate whether the CRISPR/Cas9 system used to modify mammalian cells (mouse and human), plant cells (Shan et al. 2014), and cells of fish (Auer and Del Bene 2014; Ota et al. 2014; Shin et al. 2014), fly (Bassett and Liu 2014; Gokcezade et al. 2014) and worm (Chen et al. 2013) *in vitro* and *in vivo,* would work in the chicken cells. Although a previous publication on the application of the TALEN gene editing method in the avian system was available (Park et al. 2014), it is worth noting that these systems are technically different and their activity in cells vary too. During the review of our manuscript entitled "CRISPR/Cas9 Targets Chicken Embryonic Somatic Cells *In Vitro* and *In Vivo* and generates Phenotypic Abnormalities" in *Scientific Reports,* a paper was published in *Developmental Biology* on the use of CRISPR/Cas9 system in modifying the neural

tube of chick embryos (Veron et al. 2015). Veron and colleagues used an integrating CRISPR/Cas9 construct and focussed on only one gene. We investigated 12 avian genes of developmental interest, and we used the transient electroporation vector which gave spatiotemporal control of the genetic modification *in vivo*. Through this project, we have been able to establish a protocol for targeting embryonic cells *in ovo* and we have been able to observe phenotypic abnormalities of the targeted embryos evaluated against a huge number of control experiments in which each element of the protocol was systematically omitted or changed. We showed that precisely targeting specific NC tube and NC lineages can generate phenotypic abnormalities in the avian embryo *in ovo* that closely resemble the abnormalities produced by genetic modification of the homologous gene in the same cell lineage in mouse models (Abu-Bonsrah et al. 2016). We have also shown that the CRISPR/Cas9 system can generate large deletions (>70 kbp) in the genome of chicken cells, as well as small indels and specific focal base changes.

One of the major aims of my PhD studies was to generate the MEN2B mutation in the RET protein (M918T in humans but M910T in chickens) in chicken cells and chick embryos. We were able to generate M910T in DF-1 cell lines with no detectable off-target effects, and validated the efficiency of the CRISPR/Cas9 system in developing embryos generating abnormal phenotypes in these embryos. The efficiency of generating NHEJ mutation (knockout mutations) was moderately higher than HDR and we recorded a low efficiency of M910T generated mutation in the electroporated embryos. With further improvements in the delivery of the CRISPR/Cas9 system and donor DNA in generating HDR mutations, we hope to set up a system to efficiently deliver both constructs (CRISPR/Cas9 and donor DNA) leading to a greater proportion of the cells being transfected. In future experiments, we will use a more efficient mode of delivering the CRISPR/Cas9 construct, and use the new variants of CRISPR/Cas9 systems, shown to be more efficient in genome editing (Ran et al. 2015; Zetsche et al. 2015). It should be remembered that the electroporation delivery system used here is itself of only moderate efficiency; our laboratory quantified this in the neural tube, a favoured electroporation site, as transfecting about 30% of potentially transfectable cells (Simkin et al. 2014). An example will be to clone the CRISPR/Cas9 system into the RCAS retroviral system as this has been widely used in delivering genes and other gene regulators in avians to improve the efficiency of targeting *in vivo* (Pao et al. 2003; von Werder et al. 2012). Furthermore, we will investigate whether AAV can infect chick

embryos due to its demonstrated deficiency in mouse embryos (Tabebordbar et al. 2016; Chan et al. 2017). Viral systems promise higher efficiency than electroporation but there may be loss of spatiotemporal fidelity. In the final analysis, choice of the *in ovo* transfection vehicle for CRISPR/Cas9 modification may rest on the relative value for the particular experiment of "hit rate" versus spatiotemporal discrimination.

6.2 Generation of Functional Adrenal Chromaffin-like Cells from Human Pluripotent Stem Cells.

The plasticity and functional benefits of producing neurotrophic and analgesic factors by human adrenal chromaffin cells makes them a valuable tool if large numbers of cells can be differentiated *in vitro*, particularly from autologous cell sources (Livett et al. 1981; Unsicker and Krieglstein 1996; Hurley and Hammond 2001; Schumm et al. 2004; Jozan et al. 2007).

Currently, there are few protocols describing the differentiation of hPSCs through the multipotent caudal neural progenitor (i.e. neuroepithelial) state and further to NCPCs and SAP-like cells, and our group was one of the first to establish one of these protocols (Lee et al. 2010a; Denham et al. 2015). Huang and colleagues have provided information of the generation of trunk-type human NCSCs (Huang et al. 2016), as opposed to focussing on cranial-like NCSCs. Before 2016, there was no detailed protocol on the differentiation of sympathetic neurons from hPSCs and Oh *et al* provided a detailed differentiation of sympathetic neurons from hPSCs where they utilised one of the most important functions of secreting CAs to stimulate cardiac muscles (Oh et al. 2016). They also demonstrated the importance of reciprocal interactions with cardiomyocytes in the further maturation of sympathetic neurons.

Adrenal chromaffin cells share a common progenitor with sympathetic neurons (Carnahan and Patterson 1991b; Shtukmaster et al. 2013) and it has shown that chromaffin cells can be differentiated to sympathetic neurons but not vice versa (Stemple et al. 1988; Ehrhart-Bornstein et al. 2009) thus making chromaffin cells an important cell lineage worth studying. On the other hand, the differentiation of chromaffin cells will throw more light on understanding the pathogenesis of PHEO which is reported in 50% of MEN2B cases (Smith-Hicks et al. 2000; Pacak et al. 2001). The advantage that chromaffin cells could provide in the field of pain therapy, Parkinson’s disease treatment and other therapies motivated investigations into

chromaffin cell isolation, culture and characterisation using human and bovine adrenal chromaffin cells (Santana et al. 2012; Santana et al. 2013; Tischler 2013).

In 2013, Beltinger's group published a protocol on differentiating mESCs to NCPC-like cells and further to chromaffin-like cells (Saxena et al. 2013). Differentiation of human SAP-like cells has been reported by Oh et al. (2016) but the protocol was identical to that used to generate sympathetic neurons. Chromaffin cell differentiation was as an apparently uncontrolled and little was stated about the efficiency of deriving chromaffin-like cells. Thus, combining our group's protocol of differentiating hPSCs to NCPCs, Beltinger's group differentiation protocol of chromaffin-like cell production from mouse NCPCs and the culturing protocol for human adrenal chromaffin cells, we developed a protocol of differentiation, isolation and culturing of human adrenal chromaffin cells from hESCs. To our knowledge, we are the first group to outline a detailed differentiation protocol of hPSCs to NCPCs and then to chromaffin-like cells.

In this project, starting from human pluripotent cells, using the dual-inhibitor method, we show the time-point of increment in SAP-like cell markers in NCPCs in relation to extended exposure to BMP2/FGF2, the utility of sorting for GD2 cell surface ganglioside, analysed positional identity based on the *HOX* gene expression, and further differentiated the NCPCs to chromaffin-like cells as shown by a range of SAP markers and the specific chromaffin cell enzyme PNMT and its synthetic product adrenaline. Of importance for optimal chromaffin lineage choice was: i) maintenance of BMP4 signalling, ii) timely cessation FGF2 signalling (to avoid driving SAPs towards an alternate sympathetic neuronal fate), and iii) provision of corticosteroid signalling.

6.3 Generation of Functional Thyroid C-like Cells from Human Pluripotent Stem Cells

There are various differentiation protocols for deriving endoderm, specifically definitive endoderm/anterior foregut endoderm from hESCs but there is no established differentiation protocol for thyroid C cells. Although there are protocols for the differentiation of thyroid follicular cells from hESCs (Antonica et al. 2012; Kurmann et al. 2015; Ma et al. 2015a; Ma et al. 2015b; Dame et al. 2017), it is important to note here that although these two lineages share some common transcription factors and later fuse together to form one organ, they originate from different routes (thyroid follicular cells from the median thyroid anlage and thyroid C cells from the 4th pharyngeal pouch)

and are controlled by specific transcription factors; an example is *ASCL1* which regulates C cell differentiation and *PAX8* which regulates follicular cell development (Nilsson and Fagman 2013; Nilsson and Fagman 2017). We have now developed a differentiation protocol for the differentiation of functional thyroid C cells *in vitro*. The differentiated thyroid C cell-like cells respond to Ca^{2+} by secreting calcitonin into the medium which was detectable by ELISA. We are currently using 3D format by differentiating the cells in a matrix (matrigel) to promote the differentiation of more thyroid C cell-like cells and finally to increase the number of calcitonin-secreting cells.

6.4 Creation of the MEN2B Mutation in Human Pluripotent Cells

We have successfully generated the MEN2B mutation, M918T, in three different hESC lines and all of the obtained and currently maintained clones are karyotypically normal. We have also shown that at the pluripotency state, although the gain-of-function mutation does not detectably increase the expression of *RET*, there is likely to be downstream signalling of the RET product since known RET functions occur: cell proliferation and increased expression of *PTEN*.

6.5 Effect of the MEN2B Mutation in Two Cell Lineages Differentiated from Human Pluripotent Cells

Two clones of the MEN2B-mutated hESCs differentiated along the C cell pathway showed an increased expression of C cell markers, E-cadherin and Procalcitonin, which suggests an increased number of differentiated C cells and this was reflected in the secretion of Calcitonin as assayed by ELISA. This resembles the disease state, where important elements of MTC are caused by elevated levels of calcitonin gene products.

We then differentiated the MEN2B clones to the NC lineage, specifically the vagal NC from which will be further differentiated to ENCCs, enteric glia and enteric neurons which are affected in ganglioneuromatosis. We have shown *in vitro* that control hESCs and the MEN2B clones differentiate into ENCC, enteric glia, and enteric neuron-like cells. In i*n vitro*, there were differences between control and MEN2B ENS-like cells which phenotypically resemble changes in MEN2B patients observed in rectal biopsy (Martucciello et al. 2012). Our results also demonstrate that although the MEN2B RET product can undergo autophosphorylation leading to an active RET without the presence of the ligand, GDNF, the addition of GDNF to ENCC, enteric glia and enteric neuron

differentiation can potentiate the effect of the auto-activated form of the MEN2B RET product.

6.6 Conclusions and Future Directions

The major aim of this thesis was to create the MEN2B mutation in the amenable avian model, and also to generate the M918T, MEN2B mutation in hESCs, characterise them and further differentiate them to the affected cell lineages in MEN2B patients (thyroid C cells, adrenal chromaffin cells and ENS cells).

In this study, we have successfully validated the efficiency of the CRISPR/Cas9 system in avian models both *in vitro* and *in vivo* and also create the MEN2B mutation, M910T in chicken cells and in the developing embryo. This was published in Scientific Reports in 2016. Improving the efficiency of this model will provide a major platform for studying and understanding disease pathogenesis in affected tissues growing in a normal environment; and a better understanding of how paediatric cancer develops and progresses before birth.

We have successfully generated three different hESCs MEN2B lines and characterised their pluripotency and analysed them karyotypically to confirm that they are genetically normal. We have also generated novel differentiation protocols for deriving both adrenal chromaffin cells and thyroid C cells from hPSCs. These provide valuable cellular platforms to gather information in the study of MEN2B and also neuroblastoma, as they both involve the same SA lineage. This section was published in Stem Cells Reports in January, 2018.

We show promising observations that we can model the MEN2B disease *in vitro* in the C cell (MTC) and ENS cell (ganglioneuromatosis) contexts and this can contribute to the investigation of better therapeutic drug combination in the management of the MEN2B patients to ensure a prolonged and normal life without debilitating surgeries and chemotherapies.

Future efforts will be to explore other methods to improve these established differentiation protocols to efficiently generate more thyroid C cells and combine differentiated thyroid C cells and thyroid follicular cells to form a thyroid organoid. We will also differentiate the generated hESCs MEN2B lines to NCPCs/SAPs and then to adrenal chromaffin-like cells to further analyse whether these cells will depict the phenotype of pheochromocytoma and also transplanted FACs sorted GD2+/B2B1-

population into developing embryos and further study the development of these cells. We will also explore other methods of improving the efficiency of our protocol in generating adrenal chromaffin cells and ENS cells *in vitro.* This will provide a platform to use the differentiation protocol to study diseases models like sporadic pheochromocytoma and other disease involving chromaffin cells or its precursors, SAPs. In the field of ENS, this protocol will also contribute to the study of ENS related diseases like Hirschsprung disease and also patients with Parkinsons disease as they also develop gastrointestinal problems.

REFERENCES

Aasen T, Raya A, Barrero MJ, Garreta E, Consiglio A, Gonzalez F, Vassena R, Bilic J, Pekarik V, Tiscornia G et al. 2008. Efficient and rapid generation of induced pluripotent stem cells from human keratinocytes. *Nature biotechnology* **26**: 1276-1284.

Abu-Bonsrah KD, Zhang D, Bjorksten AR, Dottori M, Newgreen DF. 2018. Generation of Adrenal Chromaffin-like Cells from Human Pluripotent Stem Cells. *Stem cell reports* **10**: 134-150.

Abu-Bonsrah KD, Zhang D, Newgreen DF. 2016. CRISPR/Cas9 Targets Chicken Embryonic Somatic Cells In Vitro and In Vivo and generates Phenotypic Abnormalities. *Scientific reports* **6**: 34524.

Airaksinen MS, Titievsky A, Saarma M. 1999. GDNF family neurotrophic factor signaling: four masters, one servant? *Molecular and cellular neurosciences* **13**: 313-325.

Alevizaki M. 2013. Management of hyperparathyroidism (PHP) in MEN2 syndromes in Europe. *Thyroid research* **6 Suppl 1**: S10.

Allmendinger A, Stoeckel E, Saarma M, Unsicker K, Huber K. 2003. Development of adrenal chromaffin cells is largely normal in mice lacking the receptor tyrosine kinase c-Ret. *Mechanisms of development* **120**: 299-304.

Amiel J, Sproat-Emison E, Garcia-Barcelo M, Lantieri F, Burzynski G, Borrego S, Pelet A, Arnold S, Miao X, Griseri P et al. 2008. Hirschsprung disease, associated syndromes and genetics: a review. *Journal of medical genetics* **45**: 1-14.

Anderson DJ. 1993. Molecular control of cell fate in the neural crest: the sympathoadrenal lineage. *Annu Rev Neurosci* **16**: 129-158.

Anderson DJ, Carnahan JF, Michelsohn A, Patterson PH. 1991. Antibody markers identify a common progenitor to sympathetic neurons and chromaffin cells in vivo and reveal the timing of commitment to neuronal differentiation in the sympathoadrenal lineage. *The Journal of neuroscience : the official journal of the Society for Neuroscience* **11**: 3507-3519.

Andres D, Keyser BM, Petrali J, Benton B, Hubbard KS, McNutt PM, Ray R. 2013. Morphological and functional differentiation in BE(2)-M17 human neuroblastoma cells by treatment with Trans-retinoic acid. *BMC neuroscience* **14**: 49.

Antonica F, Kasprzyk DF, Opitz R, Iacovino M, Liao XH, Dumitrescu AM, Refetoff S, Peremans K, Manto M, Kyba M et al. 2012. Generation of functional thyroid from embryonic stem cells. *Nature* **491**: 66-71.

Asai N, Iwashita T, Matsuyama M, Takahashi M. 1995. Mechanism of activation of the ret proto-oncogene by multiple endocrine neoplasia 2A mutations. *Molecular and cellular biology* **15**: 1613-1619.

Auer TO, Del Bene F. 2014. CRISPR/Cas9 and TALEN-mediated knock-in approaches in zebrafish. *Methods* **69**: 142-150.

Avantaggiato V, Dathan NA, Grieco M, Fabien N, Lazzaro D, Fusco A, Simeone A, Santoro M. 1994. Developmental expression of the RET protooncogene. *Cell growth & differentiation : the molecular biology journal of the American Association for Cancer Research* **5**: 305-311.

Badenes SM, Fernandes TG, Cordeiro CS, Boucher S, Kuninger D, Vemuri MC, Diogo MM, Cabral JM. 2016. Correction: Defined Essential 8 Medium and Vitronectin Efficiently Support Scalable Xeno-Free Expansion of Human Induced Pluripotent Stem Cells in Stirred Microcarrier Culture Systems. *PloS one* **11**: e0155296.

Badenes SM, Fernandes TG, Rodrigues CA, Diogo MM, Cabral JM. 2015. Scalable expansion of human-induced pluripotent stem cells in xeno-free microcarriers. *Methods Mol Biol* **1283**: 23-29.

Baker DE, Harrison NJ, Maltby E, Smith K, Moore HD, Shaw PJ, Heath PR, Holden H, Andrews PW. 2007. Adaptation to culture of human embryonic stem cells and oncogenesis in vivo. *Nature biotechnology* **25**: 207-215.

Balachandran K, Kamalanathan S, Gopalakrishnan S, Murugananadham K. 2013. Multiple endocrine neoplasia 2B: delayed presentation, rapid diagnosis. *BMJ Case Rep* **2013**.

Bassett AR, Liu JL. 2014. CRISPR/Cas9 and genome editing in Drosophila. *Journal of genetics and genomics = Yi chuan xue bao* **41**: 7-19.

Bendall SC, Stewart MH, Menendez P, George D, Vijayaragavan K, Werbowetski-Ogilvie T, Ramos-Mejia V, Rouleau A, Yang J, Bosse M et al. 2007. IGF and FGF cooperatively establish the regulatory stem cell niche of pluripotent human cells in vitro. *Nature* **448**: 1015-1021.

Berg P, Mertz JE. 2010. Personal reflections on the origins and emergence of recombinant DNA technology. *Genetics* **184**: 9-17.

Bernstein E, Kim SY, Carmell MA, Murchison EP, Alcorn H, Li MZ, Mills AA, Elledge SJ, Anderson KV, Hannon GJ. 2003. Dicer is essential for mouse development. *Nature genetics* **35**: 215-217.

Bes JC, Tkaczuk J, Czech KA, Tafani M, Bastide R, Caratero C, Pappas GD, Lazorthes Y. 1998. One-year chromaffin cell allograft survival in cancer patients with chronic pain: morphological and functional evidence. *Cell transplantation* **7**: 227-238.

Bhatt S, Diaz R, Trainor PA. 2013. Signals and switches in Mammalian neural crest cell differentiation. *Cold Spring Harb Perspect Biol* **5**.

Bhise NS, Wahlin KJ, Zack DJ, Green JJ. 2013. Evaluating the potential of poly(beta-amino ester) nanoparticles for reprogramming human fibroblasts to become induced pluripotent stem cells. *Int J Nanomed* **8**: 4641-4658.

Bibikova M, Beumer K, Trautman JK, Carroll D. 2003. Enhancing gene targeting with designed zinc finger nucleases. *Science* **300**: 764.

Bock C, Kiskinis E, Verstappen G, Gu H, Boulting G, Smith ZD, Ziller M, Croft GF, Amoroso MW, Oakley DH et al. 2011. Reference Maps of human ES and iPS cell variation enable high-throughput characterization of pluripotent cell lines. *Cell* **144**: 439-452.

Bolino A, Schuffenecker I, Luo Y, Seri M, Silengo M, Tocco T, Chabrier G, Houdent C, Murat A, Schlumberger M et al. 1995. RET mutations in exons 13 and 14 of FMTC patients. *Oncogene* **10**: 2415-2419.

Bordeaux MC, Forcet C, Granger L, Corset V, Bidaud C, Billaud M, Bredesen DE, Edery P, Mehlen P. 2000. The RET proto-oncogene induces apoptosis: a novel mechanism for Hirschsprung disease. *The EMBO journal* **19**: 4056-4063.

Borrello MG, Smith DP, Pasini B, Bongarzone I, Greco A, Lorenzo MJ, Arighi E, Miranda C, Eng C, Alberti L et al. 1995. RET activation by germline MEN2A and MEN2B mutations. *Oncogene* **11**: 2419-2427.

Boyer LA, Lee TI, Cole MF, Johnstone SE, Levine SS, Zucker JP, Guenther MG, Kumar RM, Murray HL, Jenner RG et al. 2005. Core transcriptional regulatory circuitry in human embryonic stem cells. *Cell* **122**: 947-956.

Boyer LA, Plath K, Zeitlinger J, Brambrink T, Medeiros LA, Lee TI, Levine SS, Wernig M, Tajonar A, Ray MK et al. 2006. Polycomb complexes repress developmental regulators in murine embryonic stem cells. *Nature* **441**: 349-353.

Braam SR, Zeinstra L, Litjens S, Ward-van Oostwaard D, van den Brink S, van Laake L, Lebrin F, Kats P, Hochstenbach R, Passier R et al. 2008. Recombinant vitronectin is a functionally defined substrate that supports human embryonic stem cell self-renewal via alphavbeta5 integrin. *Stem Cells* **26**: 2257-2265.

Bradley CK, Schaft J, Roy TK, Dumevska B, Peura TT. 2016. Derivation of Human Embryonic Stem Cell Lines from Vitrified Human Blastocysts. *Methods Mol Biol* **1307**: 1-23.

Brandi ML, Gagel RF, Angeli A, Bilezikian JP, Beck-Peccoz P, Bordi C, Conte-Devolx B, Falchetti A, Gheri RG, Libroia A et al. 2001. Guidelines for diagnosis and therapy of MEN type 1 and type 2. *The Journal of clinical endocrinology and metabolism* **86**: 5658-5671.

Brooker GJ, Kalloniatis M, Russo VC, Murphy M, Werther GA, Bartlett PF. 2000. Endogenous IGF-1 regulates the neuronal differentiation of adult stem cells. *Journal of neuroscience research* **59**: 332-341.

Brown AJ, Fisher DA, Kouranova E, McCoy A, Forbes K, Wu Y, Henry R, Ji D, Chambers A, Warren J et al. 2013. Whole-rat conditional gene knockout via genome editing. *Nature methods* **10**: 638-640.

Bryant J, Farmer J, Kessler LJ, Townsend RR, Nathanson KL. 2003. Pheochromocytoma: the expanding genetic differential diagnosis. *Journal of the National Cancer Institute* **95**: 1196-1204.

Bunone G, Borrello MG, Picetti R, Bongarzone I, Peverali FA, de Franciscis V, Della Valle G, Pierotti MA. 1995. Induction of RET proto-oncogene expression in neuroblastoma cells precedes neuronal differentiation and is not mediated by protein synthesis. *Experimental cell research* **217**: 92-99.

Butter A, Gagne J, Al-Jazaeri A, Emran MA, Deal C, St-Vil D. 2007. Prophylactic thyroidectomy in pediatric carriers of multiple endocrine neoplasia type 2A or familial medullary thyroid carcinoma: mutation in C620 is associated with Hirschsprung's disease. *J Pediatr Surg* **42**: 203-206.

Camacho CP, Hoff AO, Lindsey SC, Signorini PS, Valente FO, Oliveira MN, Kunii IS, Biscolla RP, Cerutti JM, Maciel RM. 2008. Early diagnosis of multiple endocrine neoplasia type 2B: a challenge for physicians. *Arquivos brasileiros de endocrinologia e metabologia* **52**: 1393-1398.

Capecchi MR. 2005. Gene targeting in mice: functional analysis of the mammalian genome for the twenty-first century. *Nature reviews Genetics* **6**: 507-512.

Carcamo-Orive I, Hoffman GE, Cundiff P, Beckmann ND, D'Souza SL, Knowles JW, Patel A, Papatsenko D, Abbasi F, Reaven GM et al. 2017. Analysis of Transcriptional Variability in a Large Human iPSC Library Reveals Genetic and Non-genetic Determinants of Heterogeneity. *Cell stem cell* **20**: 518-532 e519.

Carnahan JF, Patterson PH. 1991a. The generation of monoclonal antibodies that bind preferentially to adrenal chromaffin cells and the cells of embryonic sympathetic ganglia. *The Journal of neuroscience : the official journal of the Society for Neuroscience* **11**: 3493-3506.

Carnahan JF, Patterson PH. 1991b. Isolation of the progenitor cells of the sympathoadrenal lineage from embryonic sympathetic ganglia with the SA monoclonal antibodies. *The Journal of neuroscience : the official journal of the Society for Neuroscience* **11**: 3520-3530.

Carney JA, Go VL, Sizemore GW, Hayles AB. 1976. Alimentary-tract ganglioneuromatosis. A major component of the syndrome of multiple endocrine neoplasia, type 2b. *The New England journal of medicine* **295**: 1287-1291.

Carracedo A, Pandolfi PP. 2008. The PTEN-PI3K pathway: of feedbacks and cross-talks. *Oncogene* **27**: 5527-5541.

Carroll D. 2008. Progress and prospects: zinc-finger nucleases as gene therapy agents. *Gene therapy* **15**: 1463-1468.

Chan KY, Jang MJ, Yoo BB, Greenbaum A, Ravi N, Wu WL, Sanchez-Guardado L, Lois C, Mazmanian SK, Deverman BE et al. 2017. Engineered AAVs for efficient noninvasive gene delivery to the central and peripheral nervous systems. *Nature neuroscience* doi:10.1038/nn.4593.

Chan WH, Gonsalvez DG, Young HM, Southard-Smith EM, Cane KN, Anderson CR. 2016. Differences in CART expression and cell cycle behavior discriminate sympathetic neuroblast from chromaffin cell lineages in mouse sympathoadrenal cells. *Dev Neurobiol* **76**: 137-149.

Chapnik E, Sasson V, Blelloch R, Hornstein E. 2012. Dgcr8 controls neural crest cells survival in cardiovascular development. *Developmental biology* **362**: 50-56.

Cheeseman B, Zhang D, Binder B, Newgreen D, Landman K. 2014. Cell lineage tracing in the developing enteric nervous system: superstars revealed by experiment and simulation *J R Soc Interface* **11**: 20130815.

Chen C, Fenk LA, de Bono M. 2013. Efficient genome editing in Caenorhabditis elegans by CRISPR-targeted homologous recombination. *Nucleic acids research* **41**: e193.

Chen G, Gulbranson DR, Hou Z, Bolin JM, Ruotti V, Probasco MD, Smuga-Otto K, Howden SE, Diol NR, Propson NE et al. 2011. Chemically defined conditions for human iPSC derivation and culture. *Nature methods* **8**: 424-429.

Chin MH, Mason MJ, Xie W, Volinia S, Singer M, Peterson C, Ambartsumyan G, Aimiuwu O, Richter L, Zhang J et al. 2009. Induced pluripotent stem cells and embryonic stem cells are distinguished by gene expression signatures. *Cell stem cell* **5**: 111-123.

Cho SW, Kim S, Kim Y, Kweon J, Kim HS, Bae S, Kim JS. 2014. Analysis of off-target effects of CRISPR/Cas-derived RNA-guided endonucleases and nickases. *Genome research* **24**: 132-141.

Christian M, Cermak T, Doyle EL, Schmidt C, Zhang F, Hummel A, Bogdanove AJ, Voytas DF. 2010. Targeting DNA double-strand breaks with TAL effector nucleases. *Genetics* **186**: 757-761.

Chu VT, Weber T, Wefers B, Wurst W, Sander S, Rajewsky K, Kuhn R. 2015. Increasing the efficiency of homology-directed repair for CRISPR-Cas9-induced precise gene editing in mammalian cells. *Nature biotechnology* **33**: 543-548.

Chung KF, Qin N, Androutsellis-Theotokis A, Bornstein SR, Ehrhart-Bornstein M. 2011. Effects of dehydroepiandrosterone on proliferation and differentiation of chromaffin progenitor cells. *Mol Cell Endocrinol* **336**: 141-148.

Chung KF, Sicard F, Vukicevic V, Hermann A, Storch A, Huttner WB, Bornstein SR, Ehrhart-Bornstein M. 2009. Isolation of neural crest derived chromaffin progenitors from adult adrenal medulla. *Stem Cells* **27**: 2602-2613.

Cobo F, Navarro JM, Herrera MI, Vivo A, Porcel D, Hernandez C, Jurado M, Garcia-Castro J, Menendez P. 2008. Electron microscopy reveals the presence of viruses in mouse embryonic fibroblasts but neither in human embryonic fibroblasts nor in human mesenchymal cells used for hESC maintenance: toward an implementation of microbiological quality assurance program in stem cell banks. *Cloning and stem cells* **10**: 65-74.

Cong L, Ran FA, Cox D, Lin S, Barretto R, Habib N, Hsu PD, Wu X, Jiang W, Marraffini LA et al. 2013. Multiplex genome engineering using CRISPR/Cas systems. *Science* **339**: 819-823.

Cooper MJ, Hutchins GM, Israel MA. 1990. Histogenesis of the human adrenal medulla. An evaluation of the ontogeny of chromaffin and nonchromaffin lineages. *The American journal of pathology* **137**: 605-615.

Costa M, Dottori M, Ng E, Hawes SM, Sourris K, Jamshidi P, Pera MF, Elefanty AG, Stanley EG. 2005. The hESC line Envy expresses high levels of GFP in all differentiated progeny. *Nature methods* **2**: 259-260.

Costa M, Dottori M, Sourris K, Jamshidi P, Hatzistavrou T, Davis R, Azzola L, Jackson S, Lim SM, Pera M et al. 2007. A method for genetic modification of human embryonic stem cells using electroporation. *Nature protocols* **2**: 792-796.

Cote GJ, Wohllk N, Evans D, Goepfert H, Gagel RF. 1995. RET proto-oncogene mutations in multiple endocrine neoplasia type 2 and medullary thyroid carcinoma. *Bailliere's clinical endocrinology and metabolism* **9**: 609-630.

Coulpier M, Anders J, Ibanez CF. 2002. Coordinated activation of autophosphorylation sites in the RET receptor tyrosine kinase: importance of tyrosine 1062 for GDNF mediated

neuronal differentiation and survival. *The Journal of biological chemistry* **277**: 1991-1999.

Cowan CA, Klimanskaya I, McMahon J, Atienza J, Witmyer J, Zucker JP, Wang S, Morton CC, McMahon AP, Powers D et al. 2004. Derivation of embryonic stem-cell lines from human blastocysts. *The New England journal of medicine* **350**: 1353-1356.

Cradick TJ, Fine EJ, Antico CJ, Bao G. 2013. CRISPR/Cas9 systems targeting beta-globin and CCR5 genes have substantial off-target activity. *Nucleic acids research* **41**: 9584-9592.

Crivellato E, Nico B, Ribatti D. 2008. The chromaffin vesicle: advances in understanding the composition of a versatile, multifunctional secretory organelle. *Anatomical record* **291**: 1587-1602.

D'Amour KA, Agulnick AD, Eliazer S, Kelly OG, Kroon E, Baetge EE. 2005. Efficient differentiation of human embryonic stem cells to definitive endoderm. *Nature biotechnology* **23**: 1534-1541.

Dame K, Cincotta S, Lang AH, Sanghrajka RM, Zhang L, Choi J, Kwok L, Wilson T, Kandula MM, Monti S et al. 2017. Thyroid Progenitors Are Robustly Derived from Embryonic Stem Cells through Transient, Developmental Stage-Specific Overexpression of Nkx2-1. *Stem cell reports* **8**: 216-225.

Date I, Yoshimoto Y, Imaoka T, Miyoshi Y, Furuta T, Asari S, Ohmoto T. 1994. Effect of host age upon the degree of nigrostriatal dopaminergic system recovery following cografts of adrenal medulla and pretransected peripheral nerve. *Brain Res* **637**: 50-56.

Davies B, Davies G, Preece C, Puliyadi R, Szumska D, Bhattacharya S. 2013. Site specific mutation of the Zic2 locus by microinjection of TALEN mRNA in mouse CD1, C3H and C57BL/6J oocytes. *PloS one* **8**: e60216.

De Los Angeles A, Ferrari F, Xi R, Fujiwara Y, Benvenisty N, Deng H, Hochedlinger K, Jaenisch R, Lee S, Leitch HG et al. 2016. Corrigendum: Hallmarks of pluripotency. *Nature* **531**: 400.

Denham M, Dottori M. 2011. Neural differentiation of induced pluripotent stem cells. *Methods Mol Biol* **793**: 99-110.

Denham M, Hasegawa K, Menheniott T, Rollo B, Zhang D, Hough S, Alshawaf A, Febbraro F, Ighaniyan S, Leung J et al. 2015. Multipotent caudal neural progenitors derived from human pluripotent stem cells that give rise to lineages of the central and peripheral nervous system. *Stem Cells* **33**: 1759-1770.

Doench JG, Hartenian E, Graham DB, Tothova Z, Hegde M, Smith I, Sullender M, Ebert BL, Xavier RJ, Root DE. 2014. Rational design of highly active sgRNAs for CRISPR-Cas9-mediated gene inactivation. *Nature biotechnology* **32**: 1262-1267.

Doi A, Park IH, Wen B, Murakami P, Aryee MJ, Irizarry R, Herb B, Ladd-Acosta C, Rho J, Loewer S et al. 2009. Differential methylation of tissue- and cancer-specific CpG island shores distinguishes human induced pluripotent stem cells, embryonic stem cells and fibroblasts. *Nature genetics* **41**: 1350-1353.

Draper JS, Moore HD, Ruban LN, Gokhale PJ, Andrews PW. 2004. Culture and characterization of human embryonic stem cells. *Stem cells and development* **13**: 325-336.

Drucker-Colin R, Verdugo-Diaz L. 2004. Cell transplantation for Parkinson's disease: present status. *Cell Mol Neurobiol* **24**: 301-316.

Durai S, Mani M, Kandavelou K, Wu J, Porteus MH, Chandrasegaran S. 2005. Zinc finger nucleases: custom-designed molecular scissors for genome engineering of plant and mammalian cells. *Nucleic acids research* **33**: 5978-5990.

Durbec P, Marcos-Gutierrez CV, Kilkenny C, Grigoriou M, Wartiowaara K, Suvanto P, Smith D, Ponder B, Costantini F, Saarma M et al. 1996. GDNF signalling through the Ret receptor tyrosine kinase. *Nature* **381**: 789-793.

Ehrhart-Bornstein M, Chung KF, Vukicevic V, Bornstein SR. 2009. Is there a role for chromaffin progenitor cells in neurodegenerative diseases? *Mol Psychiatr* **14**: 2-4.

Ekker SC. 2008. Zinc finger-based knockout punches for zebrafish genes. *Zebrafish* **5**: 121-123.

Eng C, Clayton D, Schuffenecker I, Lenoir G, Cote G, Gagel RF, van Amstel HK, Lips CJ, Nishisho I, Takai SI et al. 1996. The relationship between specific RET proto-oncogene mutations and disease phenotype in multiple endocrine neoplasia type 2. International RET mutation consortium analysis. *Jama* **276**: 1575-1579.

Eng C, Smith DP, Mulligan LM, Nagai MA, Healey CS, Ponder MA, Gardner E, Scheumann GF, Jackson CE, Tunnacliffe A et al. 1994. Point mutation within the tyrosine kinase domain of the RET proto-oncogene in multiple endocrine neoplasia type 2B and related sporadic tumours. *Human molecular genetics* **3**: 237-241.

Engiz O, Ocal G, Siklar Z, Erdogan M, Kologlu M, Percinel S, Bilir P, Berberoglu M. 2009. Early prophylactic thyroidectomy for RET mutation-positive MEN 2B. *Pediatrics international : official journal of the Japan Pediatric Society* **51**: 590-593.

Erickson D, Kudva YC, Ebersold MJ, Thompson GB, Grant CS, van Heerden JA, Young WF, Jr. 2001. Benign paragangliomas: clinical presentation and treatment outcomes in 236 patients. *The Journal of clinical endocrinology and metabolism* **86**: 5210-5216.

Fan P, Chen Z, Tian P, Liu W, Jiao Y, Xue Y, Bhattacharya A, Wu J, Lu M, Guo Y et al. 2013. miRNA biogenesis enzyme Drosha is required for vascular smooth muscle cell survival. *PloS one* **8**: e60888.

Fischer-Colbrie R, Laslop A, Kirchmair R. 1995. Secretogranin II: molecular properties, regulation of biosynthesis and processing to the neuropeptide secretoneurin. *Prog Neurobiol* **46**: 49-70.

Frendo JL, Delage-Mourroux R, Cohen R, Pichaud F, Pidoux E, Guliana JM, Jullienne A. 1998. Calcitonin receptor mRNA expression in TT cells: effect of dexamethasone. *Mol Cell Endocrinol* **139**: 37-43.

Fu RH, Wang YC, Liu SP, Huang CM, Kang YH, Tsai CH, Shyu WC, Lin SZ. 2011. Differentiation of stem cells: strategies for modifying surface biomaterials. *Cell transplantation* **20**: 37-47.

Fu Y, Foden JA, Khayter C, Maeder ML, Reyon D, Joung JK, Sander JD. 2013. High-frequency off-target mutagenesis induced by CRISPR-Cas nucleases in human cells. *Nature biotechnology* **31**: 822-826.

Furlan A, Dyachuk V, Kastriti ME, Calvo-Enrique L, Abdo H, Hadjab S, Chontorotzea T, Akkuratova N, Usoskin D, Kamenev D et al. 2017. Multipotent peripheral glial cells generate neuroendocrine cells of the adrenal medulla. *Science* **357**.

Furness JB. 2000. Types of neurons in the enteric nervous system. *J Auton Nerv Syst* **81**: 87-96.

Furness JB, Costa M, Wilson AJ. 1977. Water-stable fluorophores, produced by reaction with aldehyde solutions, for the histochemical localization of catechol- and indolethylamines. *Histochemistry* **52**: 159-170.

Furness JB, Heath JW, Costa M. 1978. Aqueous aldehyde (Faglu) methods for the fluorescence histochemical localization of catecholamines and for ultrastructural studies of central nervous tissue. *Histochemistry* **57**: 285-295.

Fusaki N, Ban H, Nishiyama A, Saeki K, Hasegawa M. 2009. Efficient induction of transgene-free human pluripotent stem cells using a vector based on Sendai virus, an RNA virus that does not integrate into the host genome. *Proceedings of the Japan Academy Series B, Physical and biological sciences* **85**: 348-362.

Gammill LS, Roffers-Agarwal J. 2010. Division of labor during trunk neural crest development. *Developmental biology* **344**: 555-565.

Geurts AM, Cost GJ, Freyvert Y, Zeitler B, Miller JC, Choi VM, Jenkins SS, Wood A, Cui X, Meng X et al. 2009. Knockout rats via embryo microinjection of zinc-finger nucleases. *Science* **325**: 433.

Gimm O, Marsh DJ, Andrew SD, Frilling A, Dahia PL, Mulligan LM, Zajac JD, Robinson BG, Eng C. 1997. Germline dinucleotide mutation in codon 883 of the RET proto-oncogene in

multiple endocrine neoplasia type 2B without codon 918 mutation. *The Journal of clinical endocrinology and metabolism* **82**: 3902-3904.

Gingold J, Zhou R, Lemischka IR, Lee DF. 2016. Modeling Cancer with Pluripotent Stem Cells. *Trends in cancer* **2**: 485-494.

Glick AB, McCune BK, Abdulkarem N, Flanders KC, Lumadue JA, Smith JM, Sporn MB. 1991. Complex regulation of TGF beta expression by retinoic acid in the vitamin A-deficient rat. *Development* **111**: 1081-1086.

Gokcezade J, Sienski G, Duchek P. 2014. Efficient CRISPR/Cas9 plasmids for rapid and versatile genome editing in Drosophila. *G3* **4**: 2279-2282.

Goldberg AD, Banaszynski LA, Noh KM, Lewis PW, Elsaesser SJ, Stadler S, Dewell S, Law M, Guo X, Li X et al. 2010. Distinct factors control histone variant H3.3 localization at specific genomic regions. *Cell* **140**: 678-691.

Groves AK, LaBonne C. 2014. Setting appropriate boundaries: Fate, patterning and competence at the neural plate border. *Developmental biology* **389**: 2-12.

Guenther MG, Frampton GM, Soldner F, Hockemeyer D, Mitalipova M, Jaenisch R, Young RA. 2010. Chromatin structure and gene expression programs of human embryonic and induced pluripotent stem cells. *Cell stem cell* **7**: 249-257.

Gujral TS, Singh VK, Jia Z, Mulligan LM. 2006. Molecular mechanisms of RET receptor-mediated oncogenesis in multiple endocrine neoplasia 2B. *Cancer research* **66**: 10741-10749.

Gut P, Huber K, Lohr J, Bruhl B, Oberle S, Treier M, Ernsberger U, Kalcheim C, Unsicker K. 2005. Lack of an adrenal cortex in Sf1 mutant mice is compatible with the generation and differentiation of chromaffin cells. *Development* **132**: 4611-4619.

Han GR, Dohi DF, Lee HY, Rajah R, Walsh GL, Hong WK, Cohen P, Kurie JM. 1997. All-trans-retinoic acid increases transforming growth factor-beta2 and insulin-like growth factor binding protein-3 expression through a retinoic acid receptor-alpha-dependent signaling pathway. *The Journal of biological chemistry* **272**: 13711-13716.

Hao MM, Foong JP, Bornstein JC, Li ZL, Vanden Berghe P, Boesmans W. 2016. Enteric nervous system assembly: Functional integration within the developing gut. *Developmental biology* doi:10.1016/j.ydbio.2016.05.030.

Hattori N, Nishino K, Ko YG, Hattori N, Ohgane J, Tanaka S, Shiota K. 2004. Epigenetic control of mouse Oct-4 gene expression in embryonic stem cells and trophoblast stem cells. *The Journal of biological chemistry* **279**: 17063-17069.

Hazard JB. 1977. The C cells (parafollicular cells) of the thyroid gland and medullary thyroid carcinoma. A review. *The American journal of pathology* **88**: 213-250.

He Z, Proudfoot C, Mileham AJ, McLaren DG, Whitelaw CB, Lillico SG. 2015. Highly efficient targeted chromosome deletions using CRISPR/Cas9. *Biotechnology and bioengineering* **112**: 1060-1064.

Hearn CJ, Murphy M, Newgreen D. 1998. GDNF and ET-3 differentially modulate the numbers of avian enteric neural crest cells and enteric neurons in vitro. *Developmental biology* **197**: 93-105.

Heidenreich M, Zhang F. 2016. Applications of CRISPR-Cas systems in neuroscience. *Nature reviews Neuroscience* **17**: 36-44.

Helle KB, Marley PD, Angeletti RH, Aunis D, Galindo E, Small DH, Livett BG. 1993. Chromogranin A: secretion of processed products from the stimulated retrogradely perfused bovine adrenal gland. *Journal of neuroendocrinology* **5**: 413-420.

Hernandez D, Millard R, Sivakumaran P, Wong RC, Crombie DE, Hewitt AW, Liang H, Hung SS, Pebay A, Shepherd RK et al. 2016. Electrical Stimulation Promotes Cardiac Differentiation of Human Induced Pluripotent Stem Cells. *Stem cells international* **2016**: 1718041.

Hockemeyer D, Wang H, Kiani S, Lai CS, Gao Q, Cassady JP, Cost GJ, Zhang L, Santiago Y, Miller JC et al. 2011. Genetic engineering of human pluripotent cells using TALE nucleases. *Nature biotechnology* **29**: 731-734.

Hodel A. 2001. Effects of glucocorticoids on adrenal chromaffin cells. *Journal of neuroendocrinology* **13**: 216-220.

Hoffman LM, Carpenter MK. 2005. Characterization and culture of human embryonic stem cells. *Nature biotechnology* **23**: 699-708.

Hofstra RM, Landsvater RM, Ceccherini I, Stulp RP, Stelwagen T, Luo Y, Pasini B, Hoppener JW, van Amstel HK, Romeo G et al. 1994. A mutation in the RET proto-oncogene associated with multiple endocrine neoplasia type 2B and sporadic medullary thyroid carcinoma. *Nature* **367**: 375-376.

Hotta A, Cheung AY, Farra N, Vijayaragavan K, Seguin CA, Draper JS, Pasceri P, Maksakova IA, Mager DL, Rossant J et al. 2009. Isolation of human iPS cells using EOS lentiviral vectors to select for pluripotency. *Nature methods* **6**: 370-376.

Hou Z, Zhang Y, Propson NE, Howden SE, Chu LF, Sontheimer EJ, Thomson JA. 2013. Efficient genome engineering in human pluripotent stem cells using Cas9 from Neisseria meningitidis. *Proceedings of the National Academy of Sciences of the United States of America* **110**: 15644-15649.

Howard MJ. 2005. Mechanisms and perspectives on differentiation of autonomic neurons. *Developmental biology* **277**: 271-286.

Hsu PD, Scott DA, Weinstein JA, Ran FA, Konermann S, Agarwala V, Li Y, Fine EJ, Wu X, Shalem O et al. 2013. DNA targeting specificity of RNA-guided Cas9 nucleases. *Nature biotechnology* **31**: 827-832.

Huang M, Miller ML, McHenry LK, Zheng T, Zhen Q, Ilkhanizadeh S, Conklin BR, Bronner ME, Weiss WA. 2016. Generating trunk neural crest from human pluripotent stem cells. *Scientific reports* **6**: 19727.

Huang P, Xiao A, Zhou M, Zhu Z, Lin S, Zhang B. 2011. Heritable gene targeting in zebrafish using customized TALENs. *Nature biotechnology* **29**: 699-700.

Huang X, Saint-Jeannet JP. 2004. Induction of the neural crest and the opportunities of life on the edge. *Developmental biology* **275**: 1-11.

Huber K. 2006. The sympathoadrenal cell lineage: specification, diversification, and new perspectives. *Developmental biology* **298**: 335-343.

Huber K, Bruhl B, Guillemot F, Olson EN, Ernsberger U, Unsicker K. 2002a. Development of chromaffin cells depends on MASH1 function. *Development* **129**: 4729-4738.

Huber K, Combs S, Ernsberger U, Kalcheim C, Unsicker K. 2002b. Generation of neuroendocrine chromaffin cells from sympathoadrenal progenitors: beyond the glucocorticoid hypothesis. *Annals of the New York Academy of Sciences* **971**: 554-559.

Huber K, Franke A, Bruhl B, Krispin S, Ernsberger U, Schober A, von Bohlen und Halbach O, Rohrer H, Kalcheim C, Unsicker K. 2008. Persistent expression of BMP-4 in embryonic chick adrenal cortical cells and its role in chromaffin cell development. *Neural development* **3**: 28.

Huber K, Kalcheim C, Unsicker K. 2009. The development of the chromaffin cell lineage from the neural crest. *Autonomic neuroscience : basic & clinical* **151**: 10-16.

Huber K, Karch N, Ernsberger U, Goridis C, Unsicker K. 2005. The role of Phox2B in chromaffin cell development. *Developmental biology* **279**: 501-508.

Huber L, Ferdin M, Holzmann J, Stubbusch J, Rohrer H. 2012. HoxB8 in noradrenergic specification and differentiation of the autonomic nervous system. *Developmental biology* **363**: 219-233.

Hurley RW, Hammond DL. 2001. Contribution of endogenous enkephalins to the enhanced analgesic effects of supraspinal mu opioid receptor agonists after inflammatory injury.

The Journal of neuroscience : the official journal of the Society for Neuroscience **21**: 2536-2545.

Ichihara M, Murakumo Y, Takahashi M. 2004. RET and neuroendocrine tumors. *Cancer letters* **204**: 197-211.

Ikuno N, Shimokawa I, Nakamura T, Ishizaka Y, Ikeda T. 1995. Ret-oncogene expression correlates with neuronal differentiation of neuroblastic tumors. *Pathology, research and practice* **191**: 92-99.

Itasaki N, Bel-Vialar S, Krumlauf R. 1999. 'Shocking' developments in chick embryology: electroporation and in ovo gene expression. *Nature cell biology* **1**: E203-207.

James D, Levine AJ, Besser D, Hemmati-Brivanlou A. 2005. TGFbeta/activin/nodal signaling is necessary for the maintenance of pluripotency in human embryonic stem cells. *Development* **132**: 1273-1282.

Jinek M, Chylinski K, Fonfara I, Hauer M, Doudna JA, Charpentier E. 2012. A programmable dual-RNA-guided DNA endonuclease in adaptive bacterial immunity. *Science* **337**: 816-821.

Jing SQ, Wen DZ, Yu YB, Holst PL, Luo Y, Fang M, Tamir R, Antonio L, Hu Z, Cupples R et al. 1996. GDNF-induced activation of the Ret protein tyrosine kinase is mediated by GDNFR-alpha, a novel receptor for GDNF. *Cell* **85**: 1113-1124.

Johansson E, Andersson L, Ornros J, Carlsson T, Ingeson-Carlsson C, Liang S, Dahlberg J, Jansson S, Parrillo L, Zoppoli P et al. 2015. Revising the embryonic origin of thyroid C cells in mice and humans. *Development* **142**: 3519-3528.

Jones BA, Sisson JC. 1983. Early diagnosis and thyroidectomy in multiple endocrine neoplasia, type 2b. *The Journal of pediatrics* **102**: 219-223.

Jozan S, Aziza J, Chatelin S, Evra C, Courtade-Saidi M, Parant O, Sol JC, Zhou H, Lazorthes Y. 2007. Human fetal chromaffin cells: a potential tool for cell pain therapy. *Experimental neurology* **205**: 525-535.

Kahraman D, Goretzki PE, Szangolies M, Schade H, Schmidt M, Kobe C. 2011. Extra-adrenal pheochromocytoma in the organ of Zuckerkandl: diagnosis and treatment strategies. *Experimental and clinical endocrinology & diabetes : official journal, German Society of Endocrinology [and] German Diabetes Association* **119**: 436-439.

Kaji K, Norrby K, Paca A, Mileikovsky M, Mohseni P, Woltjen K. 2009. Virus-free induction of pluripotency and subsequent excision of reprogramming factors. *Nature* **458**: 771-U112.

Kajiwara M, Aoi T, Okita K, Takahashi R, Inoue H, Takayama N, Endo H, Eto K, Toguchida J, Uemoto S et al. 2012. Donor-dependent variations in hepatic differentiation from human-induced pluripotent stem cells. *Proceedings of the National Academy of Sciences of the United States of America* **109**: 12538-12543.

Kam MK, Lui VC. 2015. Roles of Hoxb5 in the development of vagal and trunk neural crest cells. *Development, growth & differentiation* **57**: 158-168.

Kameda Y. 2016. Cellular and molecular events on the development of mammalian thyroid C cells. *Developmental dynamics : an official publication of the American Association of Anatomists* **245**: 323-341.

Kameda Y, Nishimaki T, Chisaka O, Iseki S, Sucov HM. 2007a. Expression of the epithelial marker E-cadherin by thyroid C cells and their precursors during murine development. *The journal of histochemistry and cytochemistry : official journal of the Histochemistry Society* **55**: 1075-1088.

Kameda Y, Nishimaki T, Miura M, Jiang SX, Guillemot F. 2007b. Mash1 regulates the development of C cells in mouse thyroid glands. *Developmental dynamics : an official publication of the American Association of Anatomists* **236**: 262-270.

Kao CF, Chuang CY, Chen CH, Kuo HC. 2008. Human pluripotent stem cells: current status and future perspectives. *The Chinese journal of physiology* **51**: 214-225.

Karga HJ, Karayianni MK, Linos DA, Tseleni SC, Karaiskos KD, Papapetrou PD. 1998. Germ line mutation analysis in families with multiple endocrine neoplasia type 2A or familial medullary thyroid carcinoma. *European journal of endocrinology* **139**: 410-415.

Kaur J, Tilkins ML, Eckert R, Boucher S. 2013. Methods for culturing human embryonic stem cells in a xeno-free system. *Methods Mol Biol* **997**: 115-126.

Kelsh RN. 2006. Sorting out Sox10 functions in neural crest development. *BioEssays : news and reviews in molecular, cellular and developmental biology* **28**: 788-798.

Kilpinen H, Goncalves A, Leha A, Afzal V, Alasoo K, Ashford S, Bala S, Bensaddek D, Casale FP, Culley OJ et al. 2017. Common genetic variation drives molecular heterogeneity in human iPSCs. *Nature* doi:10.1038/nature22403.

Kim D, Bae S, Park J, Kim E, Kim S, Yu HR, Hwang J, Kim JI, Kim JS. 2015. Digenome-seq: genome-wide profiling of CRISPR-Cas9 off-target effects in human cells. *Nature methods* **12**: 237-243, 231 p following 243.

Kim J, Lo L, Dormand E, Anderson DJ. 2003. SOX10 maintains multipotency and inhibits neuronal differentiation of neural crest stem cells. *Neuron* **38**: 17-31.

Kim JH, Zhang T, Wong NC, Davidson N, Maksimovic J, Oshlack A, Earnshaw WC, Kalitsis P, Hudson DF. 2013. Condensin I associates with structural and gene regulatory regions in vertebrate chromosomes. *Nature communications* **4**: 2537.

Kim K, Doi A, Wen B, Ng K, Zhao R, Cahan P, Kim J, Aryee MJ, Ji H, Ehrlich LI et al. 2010. Epigenetic memory in induced pluripotent stem cells. *Nature* **467**: 285-290.

Kim K, Zhao R, Doi A, Ng K, Unternaehrer J, Cahan P, Huo H, Loh YH, Aryee MJ, Lensch MW et al. 2011. Donor cell type can influence the epigenome and differentiation potential of human induced pluripotent stem cells. *Nature biotechnology* **29**: 1117-1119.

Kimbrel EA, Lanza R. 2015. Current status of pluripotent stem cells: moving the first therapies to the clinic. *Nature reviews Drug discovery* **14**: 681-692.

King SK, Southwell BR, Hutson JM. 2006. An association of multiple endocrine neoplasia 2B, a RET mutation; constipation; and low substance P-nerve fiber density in colonic circular muscle. *J Pediatr Surg* **41**: 437-442.

Klein ME, Lioy DT, Ma L, Impey S, Mandel G, Goodman RH. 2007. Homeostatic regulation of MeCP2 expression by a CREB-induced microRNA. *Nature neuroscience* **10**: 1513-1514.

Kleinstiver BP, Pattanayak V, Prew MS, Tsai SQ, Nguyen NT, Zheng Z, Joung JK. 2016a. High-fidelity CRISPR-Cas9 nucleases with no detectable genome-wide off-target effects. *Nature* **529**: 490-495.

Kleinstiver BP, Pattanayak V, Prew MS, Tsai SQ, Nguyen NT, Zheng Z, Keith Joung J. 2016b. High-fidelity CRISPR-Cas9 nucleases with no detectable genome-wide off-target effects. *Nature* doi:10.1038/nature16526.

Kouvaraki MA, Shapiro SE, Perrier ND, Cote GJ, Gagel RF, Hoff AO, Sherman SI, Lee JE, Evans DB. 2005. RET proto-oncogene: a review and update of genotype-phenotype correlations in hereditary medullary thyroid cancer and associated endocrine tumors. *Thyroid : official journal of the American Thyroid Association* **15**: 531-544.

Koyanagi-Aoi M, Ohnuki M, Takahashi K, Okita K, Noma H, Sawamura Y, Teramoto I, Narita M, Sato Y, Ichisaka T et al. 2013. Differentiation-defective phenotypes revealed by large-scale analyses of human pluripotent stem cells. *Proceedings of the National Academy of Sciences of the United States of America* **110**: 20569-20574.

Kraimps JL, Denizot A, Carnaille B, Henry JF, Proye C, Bacourt F, Sarfati E, Dupond JL, Maes B, Travagli JP et al. 1996. Primary hyperparathyroidism in multiple endocrine neoplasia type IIa: retrospective French multicentric study. Groupe d'Etude des Tumeurs a Calcitonine (GETC, French Calcitonin Tumors Study Group), French Association of Endocrine Surgeons. *World journal of surgery* **20**: 808-812; discussion 812-803.

Krieglstein K, Henheik P, Farkas L, Jaszai J, Galter D, Krohn K, Unsicker K. 1998. Glial cell line-derived neurotrophic factor requires transforming growth factor-beta for exerting its

full neurotrophic potential on peripheral and CNS neurons. *The Journal of neuroscience : the official journal of the Society for Neuroscience* **18**: 9822-9834.

Kubo F, Takeichi M, Nakagawa S. 2005. Wnt2b inhibits differentiation of retinal progenitor cells in the absence of Notch activity by downregulating the expression of proneural genes. *Development* **132**: 2759-2770.

Kurmann AA, Serra M, Hawkins F, Rankin SA, Mori M, Astapova I, Ullas S, Lin S, Bilodeau M, Rossant J et al. 2015. Regeneration of Thyroid Function by Transplantation of Differentiated Pluripotent Stem Cells. *Cell stem cell* **17**: 527-542.

Kusakabe T, Hoshi N, Kimura S. 2006. Origin of the ultimobranchial body cyst: T/ebp/Nkx2.1 expression is required for development and fusion of the ultimobranchial body to the thyroid. *Developmental dynamics : an official publication of the American Association of Anatomists* **235**: 1300-1309.

Kyttala A, Moraghebi R, Valensisi C, Kettunen J, Andrus C, Pasumarthy KK, Nakanishi M, Nishimura K, Ohtaka M, Weltner J et al. 2016. Genetic Variability Overrides the Impact of Parental Cell Type and Determines iPSC Differentiation Potential. *Stem cell reports* **6**: 200-212.

Lambeth LS, Cummins DM, Doran TJ, Sinclair AH, Smith CA. 2013. Overexpression of aromatase alone is sufficient for ovarian development in genetically male chicken embryos. *PloS one* **8**: e68362.

Laslett AL, Filipczyk AA, Pera MF. 2003. Characterization and culture of human embryonic stem cells. *Trends in cardiovascular medicine* **13**: 295-301.

Lazorthes Y, Sagen J, Sallerin B, Tkaczuk J, Duplan H, Sol JC, Tafani M, Bes JC. 2000. Human chromaffin cell graft into the CSF for cancer pain management: a prospective phase II clinical study. *Pain* **87**: 19-32.

Le Douarin N. 1982. *The Neural Crest*. Cambridge University Press, Cambridge.

Le Douarin N, Le Lievre C. 1970. [Demonstration of neural origin of calcitonin cells of ultimobranchial body of chick embryo]. *Comptes rendus hebdomadaires des seances de l'Academie des sciences Serie D: Sciences naturelles* **270**: 2857-2860.

Le Douarin NM, Chaya Kalcheim C. 1999. *The Neural Crest*. Cambridge University Press, Cambridge.

Le Douarin NM, Dieterlen-Lievre F. 2013. How studies on the avian embryo have opened new avenues in the understanding of development: a view about the neural and hematopoietic systems. *Development, growth & differentiation* **55**: 1-14.

Le Douarin NM, Smith J. 1988. Development of the peripheral nervous system from the neural crest. *Annu Rev Cell Biol* **4**: 375-404.

Le Douarin NM, Teillet MA. 1973. The migration of neural crest cells to the wall of the digestive tract in avian embryo. *J Embryol Exp Morphol* **30**: 31-48.

Le Douarin NM, Teillet MA. 1974. Experimental analysis of the migration and differentiation of neuroblasts of the autonomic nervous system and of neurectodermal mesenchymal derivatives, using a biological cell marking technique. *Developmental biology* **41**: 162-184.

Lee DF, Su J, Kim HS, Chang B, Papatsenko D, Zhao R, Yuan Y, Gingold J, Xia W, Darr H et al. 2015. Modeling familial cancer with induced pluripotent stem cells. *Cell* **161**: 240-254.

Lee G, Chambers SM, Tomishima MJ, Studer L. 2010a. Derivation of neural crest cells from human pluripotent stem cells. *Nature protocols* **5**: 688-701.

Lee G, Kim H, Elkabetz Y, Al Shamy G, Panagiotakos G, Barberi T, Tabar V, Studer L. 2007. Isolation and directed differentiation of neural crest stem cells derived from human embryonic stem cells. *Nature biotechnology* **25**: 1468-1475.

Lee G, Papapetrou EP, Kim H, Chambers SM, Tomishima MJ, Fasano CA, Ganat YM, Menon J, Shimizu F, Viale A et al. 2009. Modelling pathogenesis and treatment of familial dysautonomia using patient-specific iPSCs. *Nature* **461**: 402-406.

Lee MJ, Chung KH, Park JS, Chung H, Jang HC, Kim JW. 2010b. Multiple Endocrine Neoplasia Type 2B: Early Diagnosis by Multiple Mucosal Neuroma and Its DNA Analysis. *Annals of dermatology* **22**: 452-455.

Lee NC, Norton JA. 2000. Multiple endocrine neoplasia type 2B--genetic basis and clinical expression. *Surgical oncology* **9**: 111-118.

Lee VM, Bronner-Fraser M, Baker CV. 2005. Restricted response of mesencephalic neural crest to sympathetic differentiation signals in the trunk. *Developmental biology* **278**: 175-192.

Lenders JW, Eisenhofer G, Mannelli M, Pacak K. 2005. Phaeochromocytoma. *Lancet* **366**: 665-675.

Levitt M, Spector S, Sjoerdsma A, Udenfriend S. 1965. Elucidation of the Rate-Limiting Step in Norepinephrine Biosynthesis in the Perfused Guinea-Pig Heart. *J Pharmacol Exp Ther* **148**: 1-8.

Liang G, Zhang Y. 2013. Genetic and epigenetic variations in iPSCs: potential causes and implications for application. *Cell stem cell* **13**: 149-159.

Lim J, Thiery JP. 2012. Epithelial-mesenchymal transitions: insights from development. *Development* **139**: 3471-3486.

Lim KC, Lakshmanan G, Crawford SE, Gu Y, Grosveld F, Engel JD. 2000. Gata3 loss leads to embryonic lethality due to noradrenaline deficiency of the sympathetic nervous system. *Nature genetics* **25**: 209-212.

Lin RY. 2011. Thyroid cancer stem cells. *Nature reviews Endocrinology* **7**: 609-616.

Link S, Grund SE, Diederichs S. 2016. Alternative splicing affects the subcellular localization of Drosha. *Nucleic acids research* **44**: 5330-5343.

Lister R, Pelizzola M, Kida YS, Hawkins RD, Nery JR, Hon G, Antosiewicz-Bourget J, O'Malley R, Castanon R, Klugman S et al. 2011. Hotspots of aberrant epigenomic reprogramming in human induced pluripotent stem cells. *Nature* **471**: 68-73.

Liu X, Vega QC, Decker RA, Pandey A, Worby CA, Dixon JE. 1996. Oncogenic RET receptors display different autophosphorylation sites and substrate binding specificities. *The Journal of biological chemistry* **271**: 5309-5312.

Liu Z, Zhou J, Wang H, Zhao M, Wang C. 2013. Current status of induced pluripotent stem cells in cardiac tissue regeneration and engineering. *Regenerative medicine research* **1**: 6.

Livett BG, Dean DM, Whelan LG, Udenfriend S, Rossier J. 1981. Co-release of enkephalin and catecholamines from cultured adrenal chromaffin cells. *Nature* **289**: 317-319.

Loh YH, Agarwal S, Park IH, Urbach A, Huo HG, Heffner GC, Kim KT, Miller JD, Ng KW, Daley GQ. 2009. Generation of induced pluripotent stem cells from human blood. *Blood* **113**: 5476-5479.

Long C, Amoasii L, Mireault AA, McAnally JR, Li H, Sanchez-Ortiz E, Bhattacharyya S, Shelton JM, Bassel-Duby R, Olson EN. 2015. Postnatal genome editing partially restores dystrophin expression in a mouse model of muscular dystrophy. *Science* doi:10.1126/science.aad5725.

Long C, Amoasii L, Mireault AA, McAnally JR, Li H, Sanchez-Ortiz E, Bhattacharyya S, Shelton JM, Bassel-Duby R, Olson EN. 2016. Postnatal genome editing partially restores dystrophin expression in a mouse model of muscular dystrophy. *Science* **351**: 400-403.

Longo DL. 2012. *Harrison's principles of internal medicine*. McGraw-Hill, New York.

Lumb R, Schwarz Q. 2015. Sympathoadrenal neural crest cells: the known, unknown and forgotten? *Development, growth & differentiation* **57**: 146-157.

Ma H, Marti-Gutierrez N, Park SW, Wu J, Lee Y, Suzuki K, Koski A, Ji D, Hayama T, Ahmed R et al. 2017. Correction of a pathogenic gene mutation in human embryos. *Nature* **548**: 413-419.

Ma R, Latif R, Davies TF. 2015a. Human embryonic stem cells form functional thyroid follicles. *Thyroid : official journal of the American Thyroid Association* **25**: 455-461.

Ma R, Morshed SA, Latif R, Davies TF. 2015b. Thyroid cell differentiation from murine induced pluripotent stem cells. *Frontiers in endocrinology* **6**: 56.

Mai Q, Yu Y, Li T, Wang L, Chen MJ, Huang SZ, Zhou C, Zhou Q. 2007. Derivation of human embryonic stem cell lines from parthenogenetic blastocysts. *Cell research* **17**: 1008-1019.

Mali P, Yang L, Esvelt KM, Aach J, Guell M, DiCarlo JE, Norville JE, Church GM. 2013. RNA-guided human genome engineering via Cas9. *Science* **339**: 823-826.

Malik N, Rao MS. 2013. A review of the methods for human iPSC derivation. *Methods Mol Biol* **997**: 23-33.

Marini F, Falchetti A, Del Monte F, Carbonell Sala S, Tognarini I, Luzi E, Brandi ML. 2006. Multiple endocrine neoplasia type 2. *Orphanet journal of rare diseases* **1**: 45.

Martucciello G, Lerone M, Bricco L, Tonini GP, Lombardi L, Del Rossi CG, Bernasconi S. 2012. Multiple endocrine neoplasias type 2B and RET proto-oncogene. *Italian journal of pediatrics* **38**: 9.

Mason I. 2008. The avian embryo: an overview. *Methods Mol Biol* **461**: 223-230.

Mathew CG, Chin KS, Easton DF, Thorpe K, Carter C, Liou GI, Fong SL, Bridges CD, Haak H, Kruseman AC et al. 1987. A linked genetic marker for multiple endocrine neoplasia type 2A on chromosome 10. *Nature* **328**: 527-528.

McGranahan N, Swanton C. 2015. Biological and therapeutic impact of intratumor heterogeneity in cancer evolution. *Cancer cell* **27**: 15-26.

McKeown SJ, Lee VM, Bronner-Fraser M, Newgreen DF, Farlie PG. 2005. Sox10 overexpression induces neural crest-like cells from all dorsoventral levels of the neural tube but inhibits differentiation. *Developmental dynamics : an official publication of the American Association of Anatomists* **233**: 430-444.

Mead TJ, Yutzey KE. 2012. Notch pathway regulation of neural crest cell development in vivo. *Developmental dynamics : an official publication of the American Association of Anatomists* **241**: 376-389.

Melichar H, Li O, Ross J, Haber H, Cado D, Nolla H, Robey EA, Winoto A. 2011. Comparative study of hematopoietic differentiation between human embryonic stem cell lines. *PloS one* **6**: e19854.

Mertens J, Wang QW, Kim Y, Yu DX, Pham S, Yang B, Zheng Y, Diffenderfer KE, Zhang J, Soltani S et al. 2015. Differential responses to lithium in hyperexcitable neurons from patients with bipolar disorder. *Nature* **527**: 95-99.

Milet C, Monsoro-Burq AH. 2012. Neural crest induction at the neural plate border in vertebrates. *Dev Biol* **366**: 22-33.

Miller JC, Tan S, Qiao G, Barlow KA, Wang J, Xia DF, Meng X, Paschon DE, Leung E, Hinkley SJ et al. 2011. A TALE nuclease architecture for efficient genome editing. *Nature biotechnology* **29**: 143-148.

Mizuseki K, Sakamoto T, Watanabe K, Muguruma K, Ikeya M, Nishiyama A, Arakawa A, Suemori H, Nakatsuji N, Kawasaki H et al. 2003. Generation of neural crest-derived peripheral neurons and floor plate cells from mouse and primate embryonic stem cells. *Proceedings of the National Academy of Sciences of the United States of America* **100**: 5828-5833.

Mobley BC, Kwon M, Kraemer BR, Hickman FE, Qiao J, Chung DH, Carter BD. 2015. Expression of MYCN in Multipotent Sympathoadrenal Progenitors Induces Proliferation and Neural Differentiation, but Is Not Sufficient for Tumorigenesis. *PloS one* **10**: e0133897.

Moline J, Eng C. 2011. Multiple endocrine neoplasia type 2: an overview. *Genetics in medicine : official journal of the American College of Medical Genetics* **13**: 755-764.

Moore JC, Atze K, Yeung PL, Toro-Ramos AJ, Camarillo C, Thompson K, Ricupero CL, Brenneman MA, Cohen RI, Hart RP. 2010. Efficient, high-throughput transfection of human embryonic stem cells. *Stem cell research & therapy* **1**: 23.

Moore SW, Zaahl MG. 2008. Multiple endocrine neoplasia syndromes, children, Hirschsprung's disease and RET. *Pediatric surgery international* **24**: 521-530.

Moriguchi T, Takako N, Hamada M, Maeda A, Fujioka Y, Kuroha T, Huber RE, Hasegawa SL, Rao A, Yamamoto M et al. 2006. Gata3 participates in a complex transcriptional feedback network to regulate sympathoadrenal differentiation. *Development* **133**: 3871-3881.

Motono M, Yamada Y, Hattori Y, Nakagawa R, Nishijima K, Iijima S. 2010. Production of transgenic chickens from purified primordial germ cells infected with a lentiviral vector. *Journal of bioscience and bioengineering* **109**: 315-321.

Mulligan LM, Kwok JB, Healey CS, Elsdon MJ, Eng C, Gardner E, Love DR, Mole SE, Moore JK, Papi L et al. 1993. Germ-line mutations of the RET proto-oncogene in multiple endocrine neoplasia type 2A. *Nature* **363**: 458-460.

Mundell NA, Labosky PA. 2011. Neural crest stem cell multipotency requires Foxd3 to maintain neural potential and repress mesenchymal fates. *Development* **138**: 641-652.

Murakumo Y, Jijiwa M, Asai N, Ichihara M, Takahashi M. 2006. RET and neuroendocrine tumors. *Pituitary* **9**: 179-192.

Murota H, Katayama I. 2017. Exacerbating factors of itch in atopic dermatitis. *Allergology international : official journal of the Japanese Society of Allergology* **66**: 8-13.

Myers SM, Eng C, Ponder BA, Mulligan LM. 1995. Characterization of RET proto-oncogene 3' splicing variants and polyadenylation sites: a novel C-terminus for RET. *Oncogene* **11**: 2039-2045.

Nakagawa M, Koyanagi M, Tanabe K, Takahashi K, Ichisaka T, Aoi T, Okita K, Mochiduki Y, Takizawa N, Yamanaka S. 2008. Generation of induced pluripotent stem cells without Myc from mouse and human fibroblasts. *Nature biotechnology* **26**: 101-106.

Nakagawa M, Takizawa N, Narita M, Ichisaka T, Yamanaka S. 2010. Promotion of direct reprogramming by transformation-deficient Myc. *Proceedings of the National Academy of Sciences of the United States of America* **107**: 14152-14157.

Nakano A, Onohara Y, Yokota S, Fujita H. 2013. DGCR8 Localizes to the Nucleus as well as Cytoplasmic Structures in Mammalian Spermatogenic Cells and Epididymal Sperm. *Journal of Histology* **2013**: 11.

Nelms BL, Labosky PA. 2010. In *Transcriptional Control of Neural Crest Development*, San Rafael (CA).

Nelson CE, Hakim CH, Ousterout DG, Thakore PI, Moreb EA, Castellanos Rivera RM, Madhavan S, Pan X, Ran FA, Yan WX et al. 2016. In vivo genome editing improves muscle function in a mouse model of Duchenne muscular dystrophy. *Science* **351**: 403-407.

Neumann HP, Bausch B, McWhinney SR, Bender BU, Gimm O, Franke G, Schipper J, Klisch J, Altehoefer C, Zerres K et al. 2002. Germ-line mutations in nonsyndromic pheochromocytoma. *The New England journal of medicine* **346**: 1459-1466.

Newgreen DF, Zhang D, Cheeseman BL, Binder BJ, Landman KA. 2017. Differential Clonal Expansion in an Invading Cell Population: Clonal Advantage or Dumb Luck? *Cells, tissues, organs* **203**: 105-113.

Newman AM, Cooper JB. 2010. Lab-specific gene expression signatures in pluripotent stem cells. *Cell stem cell* **7**: 258-262.

Nguyen LV, Pellacani D, Lefort S, Kannan N, Osako T, Makarem M, Cox CL, Kennedy W, Beer P, Carles A et al. 2015. Barcoding reveals complex clonal dynamics of de novo transformed human mammary cells. *Nature* **528**: 267-271.

Nieto-Estevez V, Defterali C, Vicario-Abejon C. 2016. IGF-I: A Key Growth Factor that Regulates Neurogenesis and Synaptogenesis from Embryonic to Adult Stages of the Brain. *Frontiers in neuroscience* **10**: 52.

Nikiforov YE. 2008. Thyroid carcinoma: molecular pathways and therapeutic targets. *Modern pathology : an official journal of the United States and Canadian Academy of Pathology, Inc* **21 Suppl 2**: S37-43.

Nilsson M, Fagman H. 2013. Mechanisms of thyroid development and dysgenesis: an analysis based on developmental stages and concurrent embryonic anatomy. *Current topics in developmental biology* **106**: 123-170.

Nilsson M, Fagman H. 2017. Development of the thyroid gland. *Development* **144**: 2123-2140.

Niswander L. 2008. Methods in avian embryology experimental and molecular manipulation of the embryonic chick limb. *Methods in cell biology* **87**: 135-152.

Niu Y, Shen B, Cui Y, Chen Y, Wang J, Wang L, Kang Y, Zhao X, Si W, Li W et al. 2014. Generation of gene-modified cynomolgus monkey via Cas9/RNA-mediated gene targeting in one-cell embryos. *Cell* **156**: 836-843.

Obermayr F, Hotta R, Enomoto H, Young HM. 2013. Development and developmental disorders of the enteric nervous system. *Nature reviews Gastroenterology & hepatology* **10**: 43-57.

Oh Y, Cho GS, Li Z, Hong I, Zhu R, Kim MJ, Kim YJ, Tampakakis E, Tung L, Huganir R et al. 2016. Functional Coupling with Cardiac Muscle Promotes Maturation of hPSC-Derived Sympathetic Neurons. *Cell stem cell* **19**: 95-106.

Ohana R, Weiman-Kelman B, Raviv S, Tamm ER, Pasmanik-Chor M, Rinon A, Netanely D, Shamir R, Solomon AS, Ashery-Padan R. 2015. MicroRNAs are essential for differentiation of the retinal pigmented epithelium and maturation of adjacent photoreceptors. *Development* **142**: 2487-2498.

Okita K, Ichisaka T, Yamanaka S. 2007. Generation of germline-competent induced pluripotent stem cells. *Nature* **448**: 313-U311.

Oriol Arqués IC, Stephan Tenbaum, Isabel Puig & Héctor G. Palmer. 2012. Standardized Relative Quantification of Immunofluorescence Tissue Staining. *Nature Protocol Exchange* doi:doi:10.1038/protex.2012.008.

Osafune K, Caron L, Borowiak M, Martinez RJ, Fitz-Gerald CS, Sato Y, Cowan CA, Chien KR, Melton DA. 2008. Marked differences in differentiation propensity among human embryonic stem cell lines. *Nature biotechnology* **26**: 313-315.

Ota S, Hisano Y, Ikawa Y, Kawahara A. 2014. Multiple genome modifications by the CRISPR/Cas9 system in zebrafish. *Genes to cells : devoted to molecular & cellular mechanisms* **19**: 555-564.

Pacak K, Linehan WM, Eisenhofer G, Walther MM, Goldstein DS. 2001. Recent advances in genetics, diagnosis, localization, and treatment of pheochromocytoma. *Ann Intern Med* **134**: 315-329.

Pachnis V, Mankoo B, Costantini F. 1993. Expression of the c-ret proto-oncogene during mouse embryogenesis. *Development* **119**: 1005-1017.

Pao W, Klimstra DS, Fisher GH, Varmus HE. 2003. Use of avian retroviral vectors to introduce transcriptional regulators into mammalian cells for analyses of tumor maintenance. *Proceedings of the National Academy of Sciences of the United States of America* **100**: 8764-8769.

Pappas GD, Lazorthes Y, Bes JC, Tafani M, Winnie AP. 1997. Relief of intractable cancer pain by human chromaffin cell transplants: experience at two medical centers. *Neurol Res* **19**: 71-77.

Park IH, Zhao R, West JA, Yabuuchi A, Huo H, Ince TA, Lerou PH, Lensch MW, Daley GQ. 2008. Reprogramming of human somatic cells to pluripotency with defined factors. *Nature* **451**: 141-146.

Park SH, Kim JN, Park TS, Lee SD, Kim TH, Han BK, Han JY. 2010. CpG methylation modulates tissue-specific expression of a transgene in chickens. *Theriogenology* **74**: 805-816 e801.

Park TS, Han JY. 2012. Genetic modification of chicken germ cells. *Annals of the New York Academy of Sciences* **1271**: 104-109.

Park TS, Kang KS, Han JY. 2013. Current genomic editing approaches in avian transgenesis. *General and comparative endocrinology* **190**: 144-148.

Park TS, Lee HJ, Kim KH, Kim JS, Han JY. 2014. Targeted gene knockout in chickens mediated by TALENs. *Proceedings of the National Academy of Sciences of the United States of America* **111**: 12716-12721.

Parsons DW, Li M, Zhang X, Jones S, Leary RJ, Lin JC, Boca SM, Carter H, Samayoa J, Bettegowda C et al. 2011. The genetic landscape of the childhood cancer medulloblastoma. *Science* **331**: 435-439.

Pasini B, Borrello MG, Greco A, Bongarzone I, Luo Y, Mondellini P, Alberti L, Miranda C, Arighi E, Bocciardi R et al. 1995. Loss of function effect of RET mutations causing Hirschsprung disease. *Nature genetics* **10**: 35-40.

Paspala SA, Murthy TV, Mahaboob VS, Habeeb MA. 2011. Pluripotent stem cells - a review of the current status in neural regeneration. *Neurology India* **59**: 558-565.

Pattanayak V, Lin S, Guilinger JP, Ma E, Doudna JA, Liu DR. 2013. High-throughput profiling of off-target DNA cleavage reveals RNA-programmed Cas9 nuclease specificity. *Nature biotechnology* **31**: 839-843.

Pen AE, Jensen UB. 2017. Current status of treating neurodegenerative disease with induced pluripotent stem cells. *Acta neurologica Scandinavica* **135**: 57-72.

Perrier AL, Tabar V, Barberi T, Rubio ME, Bruses J, Topf N, Harrison NL, Studer L. 2004. Derivation of midbrain dopamine neurons from human embryonic stem cells. *Proceedings of the National Academy of Sciences of the United States of America* **101**: 12543-12548.

Powers JF, Brachold JM, Tischler AS. 2003. Ret protein expression in adrenal medullary hyperplasia and pheochromocytoma. *Endocrine pathology* **14**: 351-361.

Puig I, Champeval D, De Santa Barbara P, Jaubert F, Lyonnet S, Larue L. 2009. Deletion of Pten in the mouse enteric nervous system induces ganglioneuromatosis and mimics intestinal pseudoobstruction. *The Journal of clinical investigation* **119**: 3586-3596.

Rajamohan D, Matsa E, Kalra S, Crutchley J, Patel A, George V, Denning C. 2013. Current status of drug screening and disease modelling in human pluripotent stem cells. *BioEssays : news and reviews in molecular, cellular and developmental biology* **35**: 281-298.

Ran FA, Cong L, Yan WX, Scott DA, Gootenberg JS, Kriz AJ, Zetsche B, Shalem O, Wu XB, Makarova KS et al. 2015. In vivo genome editing using Staphylococcus aureus Cas9. *Nature* **520**: 186-U198.

Ran FA, Hsu PD, Wright J, Agarwala V, Scott DA, Zhang F. 2013. Genome engineering using the CRISPR-Cas9 system. *Nature protocols* **8**: 2281-2308.

Rao RR, Johnson AV, Stice SL. 2007. Cell surface markers in human embryonic stem cells. *Methods Mol Biol* **407**: 51-61.

Raue F, Frank-Raue K. 2007. Multiple endocrine neoplasia type 2: 2007 update. *Hormone research* **68 Suppl 5**: 101-104.

Raue F, Frank-Raue K. 2009. Genotype-phenotype relationship in multiple endocrine neoplasia type 2. Implications for clinical management. *Hormones* **8**: 23-28.

Reich A, Szepietowski JC. 2007. Mediators of pruritus in psoriasis. *Mediators of inflammation* **2007**: 64727.

Reissmann E, Ernsberger U, Francis-West PH, Rueger D, Brickell PM, Rohrer H. 1996. Involvement of bone morphogenetic protein-4 and bone morphogenetic protein-7 in the differentiation of the adrenergic phenotype in developing sympathetic neurons. *Development* **122**: 2079-2088.

Reubinoff BE, Pera MF, Fong CY, Trounson A, Bongso A. 2000. Embryonic stem cell lines from human blastocysts: somatic differentiation in vitro. *Nature biotechnology* **18**: 399-404.

Rollo BN, Zhang D, Simkin JE, Menheniott TR, Newgreen DF. 2015. Why are enteric ganglia so small? Role of differential adhesion of enteric neurons and enteric neural crest cells. *F1000Research* **4**: 113.

Romeo G, Ceccherini I, Celli J, Priolo M, Betsos N, Bonardi G, Seri M, Yin L, Lerone M, Jasonni V et al. 1998. Association of multiple endocrine neoplasia type 2 and Hirschsprung disease. *Journal of internal medicine* **243**: 515-520.

Rosai J. 2011. The origin of neuroendocrine tumors and the neural crest saga. *Modern pathology : an official journal of the United States and Canadian Academy of Pathology, Inc* **24 Suppl 2**: S53-57.

Saad MF, Ordonez NG, Rashid RK, Guido JJ, Hill CS, Jr., Hickey RC, Samaan NA. 1984. Medullary carcinoma of the thyroid. A study of the clinical features and prognostic factors in 161 patients. *Medicine* **63**: 319-342.

Saito D, Takase Y, Murai H, Takahashi Y. 2012. The dorsal aorta initiates a molecular cascade that instructs sympatho-adrenal specification. *Science* **336**: 1578-1581.

Sakorafas GH, Friess H, Peros G. 2008. The genetic basis of hereditary medullary thyroid cancer: clinical implications for the surgeon, with a particular emphasis on the role of prophylactic thyroidectomy. *Endocrine-related cancer* **15**: 871-884.

Sanchez-Rivera FJ, Jacks T. 2015. Applications of the CRISPR-Cas9 system in cancer biology. *Nature reviews Cancer* **15**: 387-395.

Santana MM, Chung KF, Vukicevic V, Rosmaninho-Salgado J, Kanczkowski W, Cortez V, Hackmann K, Bastos CA, Mota A, Schrock E et al. 2012. Isolation, characterization, and differentiation of progenitor cells from human adult adrenal medulla. *Stem cells translational medicine* **1**: 783-791.

Santana MM, Ehrhart-Bornstein M, Cavadas C. 2013. Progenitor cells in chromospheres: in response to Arthur S. Tischler. *Stem cells translational medicine* **2**: 1020-1021.

Santoro M, Carlomagno F, Romano A, Bottaro DP, Dathan NA, Grieco M, Fusco A, Vecchio G, Matoskova B, Kraus MH et al. 1995. Activation of RET as a dominant transforming gene by germline mutations of MEN2A and MEN2B. *Science* **267**: 381-383.

Sasselli V, Pachnis V, Burns AJ. 2012. The enteric nervous system. *Developmental biology* **366**: 64-73.

Sato Y, Kasai T, Nakagawa S, Tanabe K, Watanabe T, Kawakami K, Takahashi Y. 2007. Stable integration and conditional expression of electroporated transgenes in chicken embryos. *Developmental biology* **305**: 616-624.

Sato Y, Yasuda K, Takahashi Y. 2002. Morphological boundary forms by a novel inductive event mediated by Lunatic fringe and Notch during somitic segmentation. *Development* **129**: 3633-3644.

Sauka-Spengler T, Barembaum M. 2008. Gain- and loss-of-function approaches in the chick embryo. *Methods in cell biology* **87**: 237-256.

Saxena S, Wahl J, Huber-Lang MS, Stadel D, Braubach P, Debatin KM, Beltinger C. 2013. Generation of murine sympathoadrenergic progenitor-like cells from embryonic stem cells and postnatal adrenal glands. *PloS one* **8**: e64454.

Schlaeger TM, Daheron L, Brickler TR, Entwisle S, Chan K, Cianci A, DeVine A, Ettenger A, Fitzgerald K, Godfrey M et al. 2015. A comparison of non-integrating reprogramming methods. *Nature biotechnology* **33**: 58-U230.

Schneider C, Wicht H, Enderich J, Wegner M, Rohrer H. 1999. Bone morphogenetic proteins are required in vivo for the generation of sympathetic neurons. *Neuron* **24**: 861-870.

Schober A, Wolf N, Huber K, Hertel R, Krieglstein K, Minichiello L, Kahane N, Widenfalk J, Kalcheim C, Olson L et al. 1998. TrkB and neurotrophin-4 are important for development and maintenance of sympathetic preganglionic neurons innervating the adrenal medulla. *The Journal of neuroscience : the official journal of the Society for Neuroscience* **18**: 7272-7284.

Schumm MA, Castellanos DA, Frydel BR, Sagen J. 2004. Improved neural progenitor cell survival when cografted with chromaffin cells in the rat striatum. *Experimental neurology* **185**: 133-142.

Schwartz PH, Brick DJ, Nethercott HE, Stover AE. 2011. Traditional human embryonic stem cell culture. *Methods Mol Biol* **767**: 107-123.

Selleck MA, Bronner-Fraser M. 1995. Origins of the avian neural crest: the role of neural plate-epidermal interactions. *Development* **121**: 525-538.

Shah AN, Davey CF, Whitebirch AC, Miller AC, Moens CB. 2015. Rapid reverse genetic screening using CRISPR in zebrafish. *Nature methods* **12**: 535-540.

Shan Q, Wang Y, Li J, Gao C. 2014. Genome editing in rice and wheat using the CRISPR/Cas system. *Nature protocols* **9**: 2395-2410.

Shao Y, Guan Y, Wang L, Qiu Z, Liu M, Chen Y, Wu L, Li Y, Ma X, Liu M et al. 2014. CRISPR/Cas-mediated genome editing in the rat via direct injection of one-cell embryos. *Nature protocols* **9**: 2493-2512.

Shen B, Zhang W, Zhang J, Zhou J, Wang J, Chen L, Wang L, Hodgkins A, Iyer V, Huang X et al. 2014. Efficient genome modification by CRISPR-Cas9 nickase with minimal off-target effects. *Nature methods* **11**: 399-402.

Shen H. 2013. Precision gene editing paves way for transgenic monkeys. *Nature* **503**: 14-15.

Shi Y, Do JT, Desponts C, Hahm HS, Scholer HR, Ding S. 2008. A combined chemical and genetic approach for the generation of induced pluripotent stem cells (vol 2, pg 525, 2008). *Cell stem cell* **3**: 119-119.

Shin J, Chen J, Solnica-Krezel L. 2014. Efficient homologous recombination-mediated genome engineering in zebrafish using TALE nucleases. *Development* **141**: 3807-3818.

Shocket E, Teloh HA. 1957. Aganglionic megacolon, pheochromocytoma, megaloureter, and neurofibroma; co-occurrence of several neural abnormalities. *AMA journal of diseases of children* **94**: 185-191.

Shtukmaster S, Schier MC, Huber K, Krispin S, Kalcheim C, Unsicker K. 2013. Sympathetic neurons and chromaffin cells share a common progenitor in the neural crest in vivo. *Neural development* **8**: 12.

Sicard F, Ehrhart-Bornstein M, Corbeil D, Sperber S, Krug AW, Ziegler CG, Rettori V, McCann SM, Bornstein SR. 2007. Age-dependent regulation of chromaffin cell proliferation by growth factors, dehydroepiandrosterone (DHEA), and DHEA sulfate. *Proceedings of the National Academy of Sciences of the United States of America* **104**: 2007-2012.

Simkin JE, Zhang D, Ighaniyan S, Newgreen DF. 2014. Parameters affecting efficiency of in ovo electroporation of the avian neural tube and crest. *Developmental dynamics : an official publication of the American Association of Anatomists* **243**: 1440-1447.

Singer K, Heiniger N, Thomas I, Worden FP, Menon RK, Chen M. 2014. Ectopic Cushing syndrome secondary to metastatic medullary thyroid cancer in a child with multiple endocrine neoplasia syndrome type 2B: clues to early diagnosis of the paraneoplastic syndromes. *Journal of pediatric endocrinology & metabolism : JPEM* **27**: 993-996.

Sipple JH. 1961. Association of Pheochromocytoma with Carcinoma of Thyroid Gland. *Am J Med* **31**: 163-&.

Skarnes WC. 2015. Is mouse embryonic stem cell technology obsolete? *Genome biology* **16**: 109.

Slaymaker IM, Gao L, Zetsche B, Scott DA, Yan WX, Zhang F. 2016. Rationally engineered Cas9 nucleases with improved specificity. *Science* **351**: 84-88.

Smith-Hicks CL, Sizer KC, Powers JF, Tischler AS, Costantini F. 2000. C-cell hyperplasia, pheochromocytoma and sympathoadrenal malformation in a mouse model of multiple endocrine neoplasia type 2B. *The EMBO journal* **19**: 612-622.

Smith DP, Houghton C, Ponder BA. 1997. Germline mutation of RET codon 883 in two cases of de novo MEN 2B. *Oncogene* **15**: 1213-1217.

Smith SM, Flentke GR, Garic A. 2012. Avian models in teratology and developmental toxicology. *Methods Mol Biol* **889**: 85-103.

Soldner F, Hockemeyer D, Beard C, Gao Q, Bell GW, Cook EG, Hargus G, Blak A, Cooper O, Mitalipova M et al. 2009. Parkinson's Disease Patient-Derived Induced Pluripotent Stem Cells Free of Viral Reprogramming Factors. *Cell* **136**: 964-977.

Soto-Gutierrez A, Yagi H, Uygun BE, Navarro-Alvarez N, Uygun K, Kobayashi N, Yang YG, Yarmush ML. 2010. Cell delivery: from cell transplantation to organ engineering. *Cell transplantation* **19**: 655-665.

Stadtfeld M, Brennand K, Hochedlinger K. 2008. Reprogramming of pancreatic beta cells into induced pluripotent stem cells. *Current Biology* **18**: 890-894.

Stemple DL, Mahanthappa NK, Anderson DJ. 1988. Basic FGF induces neuronal differentiation, cell division, and NGF dependence in chromaffin cells: a sequence of events in sympathetic development. *Neuron* **1**: 517-525.

Stuhlmiller TJ, Garcia-Castro MI. 2012a. Current perspectives of the signaling pathways directing neural crest induction. *Cell Mol Life Sci* **69**: 3715-3737.

Stuhlmiller TJ, Garcia-Castro MI. 2012b. FGF/MAPK signaling is required in the gastrula epiblast for avian neural crest induction. *Development* **139**: 289-300.

Sung YH, Kim JM, Kim HT, Lee J, Jeon J, Jin Y, Choi JH, Ban YH, Ha SJ, Kim CH et al. 2014. Highly efficient gene knockout in mice and zebrafish with RNA-guided endonucleases. *Genome research* **24**: 125-131.

Swiech L, Heidenreich M, Banerjee A, Habib N, Li Y, Trombetta J, Sur M, Zhang F. 2015. In vivo interrogation of gene function in the mammalian brain using CRISPR-Cas9. *Nature biotechnology* **33**: 102-106.

Szabo PM, Pinter M, Szabo DR, Zsippai A, Patocs A, Falus A, Racz K, Igaz P. 2012. Integrative analysis of neuroblastoma and pheochromocytoma genomics data. *BMC medical genomics* **5**: 48.

Tabebordbar M, Zhu K, Cheng JKW, Chew WL, Widrick JJ, Yan WX, Maesner C, Wu EY, Xiao R, Ran FA et al. 2016. In vivo gene editing in dystrophic mouse muscle and muscle stem cells. *Science* **351**: 407-411.

Tahira T, Ishizaka Y, Itoh F, Sugimura T, Nagao M. 1990. Characterization of ret proto-oncogene mRNAs encoding two isoforms of the protein product in a human neuroblastoma cell line. *Oncogene* **5**: 97-102.

Taieb D, Kebebew E, Castinetti F, Chen CC, Henry JF, Pacak K. 2014. Diagnosis and preoperative imaging of multiple endocrine neoplasia type 2: current status and future directions. *Clinical endocrinology* **81**: 317-328.

Takahashi K, Tanabe K, Ohnuki M, Narita M, Ichisaka T, Tomoda K, Yamanaka S. 2007. Induction of pluripotent stem cells from adult human fibroblasts by defined factors. *Cell* **131**: 861-872.

Takahashi K, Yamanaka S. 2006. Induction of pluripotent stem cells from mouse embryonic and adult fibroblast cultures by defined factors. *Cell* **126**: 663-676.

Takahashi M, Buma Y, Hiai H. 1989. Isolation of ret proto-oncogene cDNA with an amino-terminal signal sequence. *Oncogene* **4**: 805-806.

Takahashi Y, Watanabe T, Nakagawa S, Kawakami K, Sato Y. 2008. Transposon-mediated stable integration and tetracycline-inducible expression of electroporated transgenes in chicken embryos. *Methods in cell biology* **87**: 271-280.

Takasato M, Er PX, Becroft M, Vanslambrouck JM, Stanley EG, Elefanty AG, Little MH. 2014. Directing human embryonic stem cell differentiation towards a renal lineage generates a self-organizing kidney. *Nature cell biology* **16**: 118-126.

Tatemoto K, Efendic S, Mutt V, Makk G, Feistner GJ, Barchas JD. 1986. Pancreastatin, a novel pancreatic peptide that inhibits insulin secretion. *Nature* **324**: 476-478.

Taupenot L, Harper KL, O'Connor DT. 2003. The chromogranin-secretogranin family. *The New England journal of medicine* **348**: 1134-1149.

Teichberg S, Holtzman E. 1973. Axonal agranular reticulum and synaptic vesicles in cultured embryonic chick sympathetic neurons. *The Journal of cell biology* **57**: 88-108.

Thakore PI, Black JB, Hilton IB, Gersbach CA. 2016. Editing the epigenome: technologies for programmable transcription and epigenetic modulation. *Nature methods* **13**: 127-137.

Thomson JA, Itskovitz-Eldor J, Shapiro SS, Waknitz MA, Swiergiel JJ, Marshall VS, Jones JM. 1998. Embryonic stem cell lines derived from human blastocysts. *Science* **282**: 1145-1147.

Tischler AS. 2013. What happens in "chromospheres"? *Stem cells translational medicine* **2**: 1020.

Tischler AS, Powers JF, Shahsavari M, Ziar J, Tsokas P, Downing J, McClain RM. 1997. Comparative studies of chromaffin cell proliferation in the adrenal medulla of rats and mice. *Fundamental and applied toxicology : official journal of the Society of Toxicology* **35**: 216-220.

Toledo SP, dos Santos MA, Toledo Rde A, Lourenco DM, Jr. 2006. Impact of RET proto-oncogene analysis on the clinical management of multiple endocrine neoplasia type 2. *Clinics* **61**: 59-70.

Tomlinson I, Sasieni P, Bodmer W. 2002. How many mutations in a cancer? *The American journal of pathology* **160**: 755-758.

Trifaro JM. 2002. Molecular biology of the chromaffin cell. *Annals of the New York Academy of Sciences* **971**: 11-18.

Trupp M, Arenas E, Fainzilber M, Nilsson AS, Sieber BA, Grigoriou M, Kilkenny C, Salazar-Grueso E, Pachnis V, Arumae U. 1996. Functional receptor for GDNF encoded by the c-ret proto-oncogene. *Nature* **381**: 785-789.

Trupp M, Belluardo N, Funakoshi H, Ibanez CF. 1997. Complementary and overlapping expression of glial cell line-derived neurotrophic factor (GDNF), c-ret proto-oncogene, and GDNF receptor-alpha indicates multiple mechanisms of trophic actions in the adult rat CNS. *The Journal of neuroscience : the official journal of the Society for Neuroscience* **17**: 3554-3567.

Tsuji-Takayama K, Inoue T, Ijiri Y, Otani T, Motoda R, Nakamura S, Orita K. 2004. Demethylating agent, 5-azacytidine, reverses differentiation of embryonic stem cells. *Biochemical and biophysical research communications* **323**: 86-90.

Tsuzuki T, Takahashi M, Asai N, Iwashita T, Matsuyama M, Asai J. 1995. Spatial and temporal expression of the ret proto-oncogene product in embryonic, infant and adult rat tissues. *Oncogene* **10**: 191-198.

Tu Z, Yang W, Yan S, Guo X, Li XJ. 2015. CRISPR/Cas9: a powerful genetic engineering tool for establishing large animal models of neurodegenerative diseases. *Molecular neurodegeneration* **10**: 35.

Unsicker K, Huber K, Schober A, Kalcheim C. 2013. Resolved and open issues in chromaffin cell development. *Mechanisms of development* **130**: 324-329.

Unsicker K, Huber K, Schutz G, Kalcheim C. 2005. The chromaffin cell and its development. *Neurochemical research* **30**: 921-925.

Unsicker K, Krieglstein K. 1996. Growth factors in chromaffin cells. *Prog Neurobiol* **48**: 307-324.

Vallier L, Alexander M, Pedersen RA. 2005. Activin/Nodal and FGF pathways cooperate to maintain pluripotency of human embryonic stem cells. *Journal of cell science* **118**: 4495-4509.

Vallier L, Mendjan S, Brown S, Chng Z, Teo A, Smithers LE, Trotter MW, Cho CH, Martinez A, Rugg-Gunn P et al. 2009. Activin/Nodal signalling maintains pluripotency by controlling Nanog expression. *Development* **136**: 1339-1349.

van der Hoorn FA, Boomsma F, Man in 't Veld AJ, Schalekamp MA. 1989. Determination of catecholamines in human plasma by high-performance liquid chromatography:

comparison between a new method with fluorescence detection and an established method with electrochemical detection. *J Chromatogr* **487**: 17-28.

Veres A, Gosis BS, Ding Q, Collins R, Ragavendran A, Brand H, Erdin S, Cowan CA, Talkowski ME, Musunuru K. 2014. Low incidence of off-target mutations in individual CRISPR-Cas9 and TALEN targeted human stem cell clones detected by whole-genome sequencing. *Cell stem cell* **15**: 27-30.

Veron N, Qu Z, Kipen PA, Hirst CE, Marcelle C. 2015. CRISPR mediated somatic cell genome engineering in the chicken. *Developmental biology* **407**: 68-74.

Vincent KM, Findlay SD, Postovit LM. 2015. Assessing breast cancer cell lines as tumour models by comparison of mRNA expression profiles. *Breast cancer research : BCR* **17**: 114.

von Werder A, Seidler B, Schmid RM, Schneider G, Saur D. 2012. Production of avian retroviruses and tissue-specific somatic retroviral gene transfer in vivo using the RCAS/TVA system. *Nature protocols* **7**: 1167-1183.

Vouillot L, Thelie A, Pollet N. 2015. Comparison of T7E1 and surveyor mismatch cleavage assays to detect mutations triggered by engineered nucleases. *G3* **5**: 407-415.

Vukicevic V, Schmid J, Hermann A, Lange S, Qin N, Gebauer L, Chunk KF, Ravens U, Eisenhofer G, Storch A et al. 2012. Differentiation of chromaffin progenitor cells to dopaminergic neurons. *Cell transplantation* **21**: 2471-2486.

Waguespack SG, Rich TA, Perrier ND, Jimenez C, Cote GJ. 2011. Management of medullary thyroid carcinoma and MEN2 syndromes in childhood. *Nature reviews Endocrinology* **7**: 596-607.

Wakamatsu Y, Watanabe Y, Nakamura H, Kondoh H. 1997. Regulation of the neural crest cell fate by N-myc: promotion of ventral migration and neuronal differentiation. *Development* **124**: 1953-1962.

Wang H, Fang H, Dai J, Liu G, Xu ZJ. 2013a. Induced pluripotent stem cells for spinal cord injury therapy: current status and perspective. *Neurological sciences : official journal of the Italian Neurological Society and of the Italian Society of Clinical Neurophysiology* **34**: 11-17.

Wang Y, Chou BK, Dowey S, He C, Gerecht S, Cheng L. 2013b. Scalable expansion of human induced pluripotent stem cells in the defined xeno-free E8 medium under adherent and suspension culture conditions. *Stem cell research* **11**: 1103-1116.

Wang Y, Medvid R, Melton C, Jaenisch R, Blelloch R. 2007. DGCR8 is essential for microRNA biogenesis and silencing of embryonic stem cell self-renewal. *Nature genetics* **39**: 380-385.

Warren L, Manos PD, Ahfeldt T, Loh YH, Li H, Lau F, Ebina W, Mandal PK, Smith ZD, Meissner A et al. 2010. Highly Efficient Reprogramming to Pluripotency and Directed Differentiation of Human Cells with Synthetic Modified mRNA. *Cell stem cell* **7**: 618-630.

Wells SA, Jr., Franz C. 2000. Medullary carcinoma of the thyroid gland. *World journal of surgery* **24**: 952-956.

Wells SA, Jr., Pacini F, Robinson BG, Santoro M. 2013. Multiple endocrine neoplasia type 2 and familial medullary thyroid carcinoma: an update. *The Journal of clinical endocrinology and metabolism* **98**: 3149-3164.

Wernig M, Meissner A, Cassady JP, Jaenisch R. 2008. c-Myc is dispensable for direct reprogramming of mouse fibroblasts. *Cell stem cell* **2**: 10-12.

Whalen RK, Althausen AF, Daniels GH. 1992. Extra-adrenal pheochromocytoma. *J Urol* **147**: 1-10.

Wood AJ, Lo TW, Zeitler B, Pickle CS, Ralston EJ, Lee AH, Amora R, Miller JC, Leung E, Meng X et al. 2011. Targeted genome editing across species using ZFNs and TALENs. *Science* **333**: 307.

Xiao A, Wang Z, Hu Y, Wu Y, Luo Z, Yang Z, Zu Y, Li W, Huang P, Tong X et al. 2013. Chromosomal deletions and inversions mediated by TALENs and CRISPR/Cas in zebrafish. *Nucleic acids research* **41**: e141.

Xu RH, Peck RM, Li DS, Feng X, Ludwig T, Thomson JA. 2005. Basic FGF and suppression of BMP signaling sustain undifferentiated proliferation of human ES cells. *Nature methods* **2**: 185-190.

Yang L, Guell M, Byrne S, Yang JL, De Los Angeles A, Mali P, Aach J, Kim-Kiselak C, Briggs AW, Rios X et al. 2013. Optimization of scarless human stem cell genome editing. *Nucleic acids research* **41**: 9049-9061.

Yin H, Boyd T, Pacheco MC, Schonfeld D, Bove KE. 2012. Rectal biopsy in children with Down syndrome and chronic constipation: Hirschsprung disease vs non-hirschsprung disease. *Pediatric and developmental pathology : the official journal of the Society for Pediatric Pathology and the Paediatric Pathology Society* **15**: 87-95.

Yin M, King SK, Hutson JM, Chow CW. 2006. Multiple endocrine neoplasia type 2B diagnosed on suction rectal biopsy in infancy: a report of 2 cases. *Pediatric and developmental pathology : the official journal of the Society for Pediatric Pathology and the Paediatric Pathology Society* **9**: 56-60.

Yntema CL, Hammond WS. 1954. The origin of intrinsic ganglia of trunk viscera from vagal neural crest in the chick embryo. *The Journal of comparative neurology* **101**: 515-541.

Yokota Y, Saito D, Tadokoro R, Takahashi Y. 2011. Genomically integrated transgenes are stably and conditionally expressed in neural crest cell-specific lineages. *Developmental biology* **353**: 382-395.

Young HM, Hearn CJ, Farlie PG, Canty AJ, Thomas PQ, Newgreen DF. 2001. GDNF is a chemoattractant for enteric neural cells. *Developmental biology* **229**: 503-516.

Young HM, Newgreen D. 2001. Enteric neural crest-derived cells: origin, identification, migration, and differentiation. *Anat Rec* **262**: 1-15.

Yu J. 2009. Human induced pluripotent stem cells free of vector and transgene sequences (vol 324, pg 797, 2009). *Science* **324**: 1266-1266.

Yu J, Vodyanik MA, Smuga-Otto K, Antosiewicz-Bourget J, Frane JL, Tian S, Nie J, Jonsdottir GA, Ruotti V, Stewart R et al. 2007. Induced pluripotent stem cell lines derived from human somatic cells. *Science* **318**: 1917-1920.

Yu JY, Hu KJ, Smuga-Otto K, Tian SL, Stewart R, Slukvin II, Thomson JA. 2009. Human Induced Pluripotent Stem Cells Free of Vector and Transgene Sequences. *Science* **324**: 797-801.

Zeitelhofer M, Vessey JP, Xie Y, Tubing F, Thomas S, Kiebler M, Dahm R. 2007. High-efficiency transfection of mammalian neurons via nucleofection. *Nature protocols* **2**: 1692-1704.

Zetsche B, Gootenberg JS, Abudayyeh OO, Slaymaker IM, Makarova KS, Essletzbichler P, Volz SE, Joung J, van der Oost J, Regev A et al. 2015. Cpf1 Is a Single RNA-Guided Endonuclease of a Class 2 CRISPR-Cas System. *Cell* **163**: 759-771.

Zhang D, Brinas IM, Binder BJ, Landman KA, Newgreen DF. 2010a. Neural crest regionalisation for enteric nervous system formation: implications for Hirschsprung's disease and stem cell therapy. *Developmental biology* **339**: 280-294.

Zhang D, Ighaniyan S, Stathopoulos L, Rollo B, Landman K, Hutson J, Newgreen D. 2014a. The neural crest: a versatile organ system. *Birth defects research Part C, Embryo today : reviews* **102**: 275-298.

Zhang D, Osborne JM, Abu-Bonsrah KD, Cheeseman BL, Landman KA, Jurkowicz B, Newgreen DF. 2018. Stochastic clonal expansion of "superstars" enhances the reserve capacity of enteric nervous system precursor cells. *Developmental biology* doi:10.1016/j.ydbio.2018.01.020.

Zhang F, Maeder ML, Unger-Wallace E, Hoshaw JP, Reyon D, Christian M, Li X, Pierick CJ, Dobbs D, Peterson T et al. 2010b. High frequency targeted mutagenesis in Arabidopsis

thaliana using zinc finger nucleases. *Proceedings of the National Academy of Sciences of the United States of America* **107**: 12028-12033.

Zhang JH, Soerens AG, Wilson GF, Yu JY, Thomson JA, Kamp TJ. 2009. Human Induced Pluripotent Stem Cells Free of Vector and Transgene Sequences Undergo Cardiogenesis in Defined Conditions. *Circulation* **120**: S1123-S1124.

Zhang S, Cui W. 2014. Sox2, a key factor in the regulation of pluripotency and neural differentiation. *World journal of stem cells* **6**: 305-311.

Zhang Y, Vanoli F, LaRocque JR, Krawczyk PM, Jasin M. 2014b. Biallelic targeting of expressed genes in mouse embryonic stem cells using the Cas9 system. *Methods* **69**: 171-178.

Zhang Y, Zhang F, Li X, Baller JA, Qi Y, Starker CG, Bogdanove AJ, Voytas DF. 2013. Transcription activator-like effector nucleases enable efficient plant genome engineering. *Plant physiology* **161**: 20-27.

Zhou H, Aziza J, Sol JC, Courtade-Saidi M, Chatelin S, Evra C, Parant O, Lazorthes Y, Jozan S. 2006. Cell therapy of pain: Characterization of human fetal chromaffin cells at early adrenal medulla development. *Experimental neurology* **198**: 370-381.

Zhu S, Lee JS, Guo F, Shin J, Perez-Atayde AR, Kutok JL, Rodig SJ, Neuberg DS, Helman D, Feng H et al. 2012a. Activated ALK collaborates with MYCN in neuroblastoma pathogenesis. *Cancer cell* **21**: 362-373.

Zhu Y, Wan S, Zhan RY. 2012b. Inducible pluripotent stem cells for the treatment of ischemic stroke: current status and problems. *Reviews in the neurosciences* **23**: 393-402.

APPENDIX S1

Table 1: Genes mutated or detected in this study

Gene	Chicken c'some	Type, Function	Developmental expression/role	Human or rodent disease relationship	Present study
CDKN1B	1	Cyclin-dependent kinase inhibitor. Mediates G1 arrest.	Exp. ubiquitous. Leydig cell dev.	MEN4	NHEJ deletion DF-1 ±puromycin *in vitro.* Off-target screen DF-1, DT40 *in vitro.*
CNN1 Calponin1	30	Neg reg by DROSHA.	Cytoskeletal -related	Severe atrioventricular septal defects	Exp. level after *DGCR8* NHEJ deletion *in ovo.*
DGCR8	15micro	Complex & co-reg with DROSHA. miRNA processing.	Exp. wide esp. in neuroepithelium, palate, thymus, limbs.	DiGeorge critical region Het. reduced cell prolif^{n} and neurogenesis	Large transgenic deletion DF-1, DT40 *in vitro.* NHEJ deletion *in ovo.*
DICER	5	Ribonuclease III. miRNA processing.	Exp. ubiquitous esp. facial, pharyngeal arches and limb bud..	Up-reg. in melanoma Down-reg in breast carcinoma	NHEJ deletion DF-1 *in vitro.*
DROSHA	2	Ribonuclease III. miRNA processing. Complex & co-reg with DGCR8	Exp. ubiquitous esp. viscera.	Premature death Cachexia	NHEJ deletion DF-1 *in vitro.* Exp. level after *DGCR8* NHEJ deletion *in ovo.*
EZH2	2	Polycomb family. Regulation DNA methylation. Histone modification.	Exp. neuroepithelium, pharyngeal arches, myotome, later esp. testis. Lung, CNS and B cell dev.	Weaver syndrome	NHEJ deletion DF-1 ±puromycin *in vitro.*
HIRA	15micro	Histone cell cycle regulator.	Exp. esp. pharyngeal arches.	DiGeorge critical region	NHEJ deletion DF-1 ±puromycin *in vitro.* Large transgenic deletion DF-1 *in vitro.*
KIAA1279 (KIF1BP)	6	Regulation DNA methylation. Histone modification.	Exp. ubiquitous.	Goldberg-Shprintzen Hirschsprung	NHEJ deletion DF-1 ±puromycin *in vitro.* Off-target screen DF-1, DT40 *in vitro.* Exp. level after *DGCR8* NHEJ deletion *in ovo.*
NGN2	4	Regulated by DROSHA/DGCR8.	Exp. in neural tube, pharyngeal arches	PNET	Exp. level after *DGCR8* NHEJ deletion *in ovo.*
PAX6	5	Paired box homeotic TF. Regulated by DROSHA /DGCR8.	Exp. in neural tube, pharyngeal arches, eye.	Aniridia	Exp. level after *DGCR8* NHEJ deletion *in ovo.*
MBD3	28micro	NuRD complex subunit Chromatin alteration, epigenetic markers.	Exp. wide esp. in brain, pharyngeal arches, intestine	Siver-Russell syndrome	NHEJ deletion DF-1 ±puromycin *in vitro.* Exp. level after *DGCR8* NHEJ deletion *in ovo.*
RET	6	GF receptor tyrosine kinase	Exp. in PNS, CNS, kidney. Survival, proliferat^{n}, different^{n}.	MEN2A, MEN2B, Hirschsprung	HDR gene editing C612R, M918T DF-1 *in vitro.* Large intragenic deletion DF-1 *in vitro.*
STMN2	2	Target of MAPK8	Exp. CNS and PNS.	Alzheimer	Large intragenic deletion DF-1, DT40 *in vitro.*

		Regulation of microtubule stability	Neuronal growth.		NHEJ deletion *in ovo.* Exp. level after *DGCR8* NHEJ deletion *in ovo.*
TYRP1	Z	Tyrosinase-related protein-1, melanosomal tyrosinase	Exp. epidermal NCC, retina. Melanin biosynthesis.	Rufous oculocutaneous albinism	NHEJ deletion DF-1 ±puromycin *in vitro.*
YPEL1	15micro	Centrosomal/nucleolar Regulated by DROSHA /DGCR8	Exp. in pharyngeal arches.	DiGeorge critical region	Exp. level after *DGCR8* NHEJ deletion *in ovo.*

Gene data from: http://www.ncbi.nlm.nih.gov/gene/

Expression data from:

http://www.proteinatlas.org/search/

http://www.emouseatlas.org/emagewebapp/pages/emage_gene_browse.jsf

Disease data from: http://www.genecards.org/cgi-bin/carddisp.pl?gene=

miRNA target data: http://www.targetscan.org

http://www.microrna.org

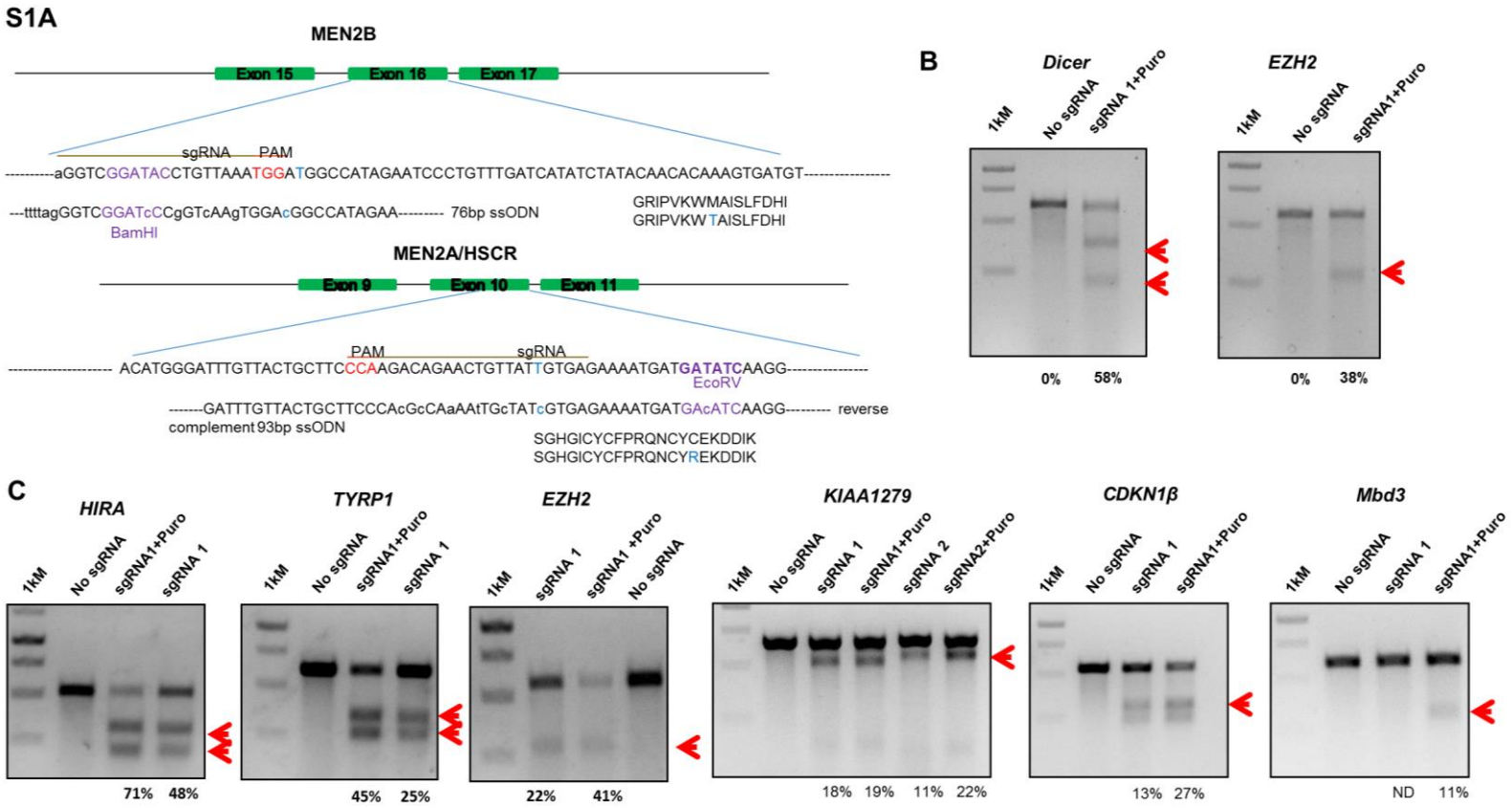

Appendix S1-S1. Related to Figure 3.1. (A)Diagram of sgRNAs targeting sites on exon 10 (MEN2A/HSCR) and exon 16 (MEN2B) of the RET gene and the corresponding ssODN. Exons are shown in green boxes with location of sgRNA and sequences of PAM in red. Created (BamHI) and disrupted (EcoRV) restriction enzyme site are in purple. Desired base pair correction and its corresponding amino acid is represented in blue. (B) Frequency (%) of NHEJ mutations mediated by Dicer and EZH2-targeting sgRNA-Cas9 system in DF-1 cells with puromycin selection, by PCR and T7E1 assay. (C) Frequency (%) of NHEJ mutations mediated by HIRA, TYRP1, EZH2, KIAA1279, CDKN1β, and Mbd3-targeting sgRNA-Cas9 system in DF-1 cells with and without puromycin selection by PCR and T7E1 assay. Arrow indicates the NHEJ mutation created by the CRISPR/Cas9 system. 1kM-1 kbp DNA ladder. ND=not detected.

S1D

Appendix S1-S1 (D). Related to Figure 3.1. NHEJ mutations in KIAA1279, CDKN1β and Mbd3 mediated by sgRNA-Cas9 in DF-1 cells. Red dashes and letters in red in the DNA sequences denote deleted nucleotides and inserted nucleotides respectively, and bold and underlined ATG indicates the translational initiation codon.

S1E

Appendix S1-S1 (E): Related to Figure 3.4. Sequence analysis of NHEJ mutation mediated by KIAA1279-targeting sgRNA-Cas9 system in chicken cells in ovo. Red dashes and letters in red in the DNA sequences denote deleted nucleotides and inserted nucleotides respectively, and bold and underlined ATG indicates the translational initiation codon in the gene.

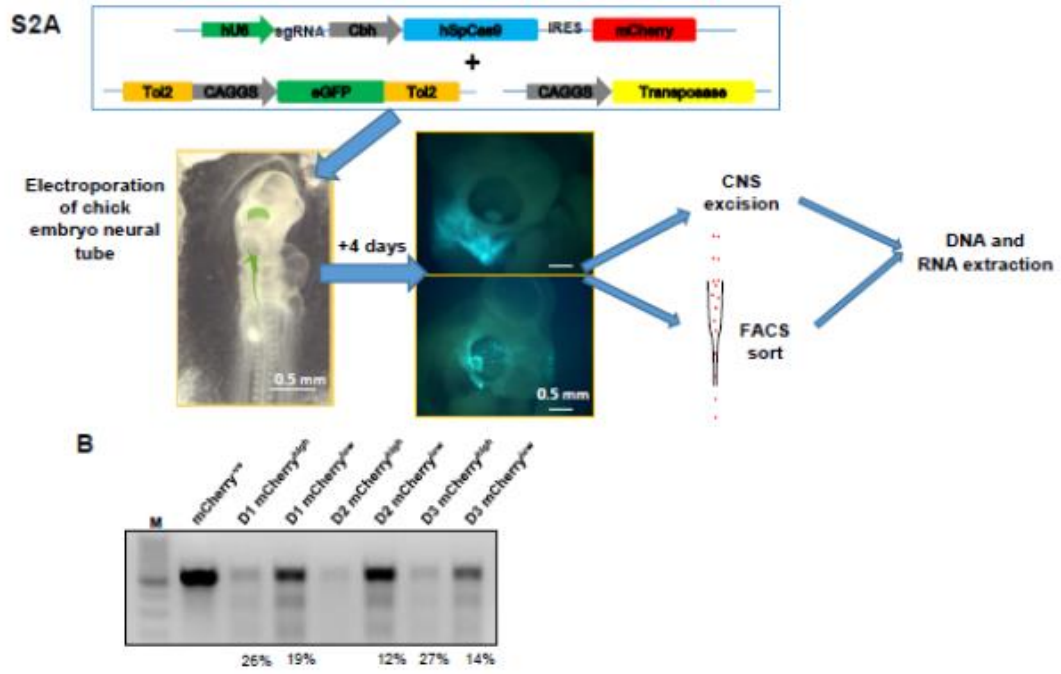

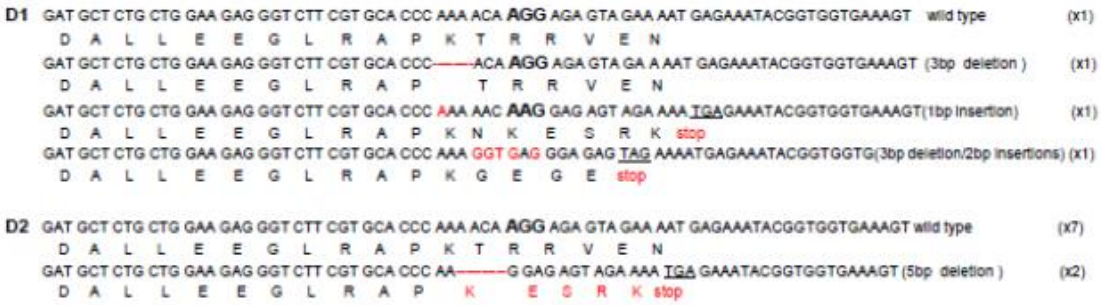

Appendix S1-S2. Related to Figure 3.3 and 3.4. (A) A schematic representation of the in ovo electroporation technique and FACs. The mCherry CRISPR/Cas9 and the Tol2-GFP/transposase plasmids were co-injected or injected separately into the neural tube lumen (shaded green) of E1.5 chick embryos and electroporated. Embryos were harvested at stage E5.5, dissociated by collagenase/dispase and sorted by FACs or, alternatively, surrounding tissues were removed leaving the CNS for analysis. Representative images showing the extent of the electroporation and distribution of GFP-labelled cells was variable. (B) Frequency of NHEJ mutation mediated by exon 2 of DGCR8-targeting sgRNA-CRISPR/Cas9 system in chick embryo by PCR and T7E1 assay and sequence analysis of cloned DGCR8-1 (D8-1) and D8-2 sorted cells. Red dashes and letters in red in the DNA sequences denote deleted nucleotides and inserted nucleotides respectively, and bold indicates the PAM sequence with underlined nucleotide indicating the stop codon. mCherrylow – mCherry low, mCherryhigh –mCherry high, mCherry-ve -mCherry negative, 1M- 100 bp DNA ladder, ND=not detected.

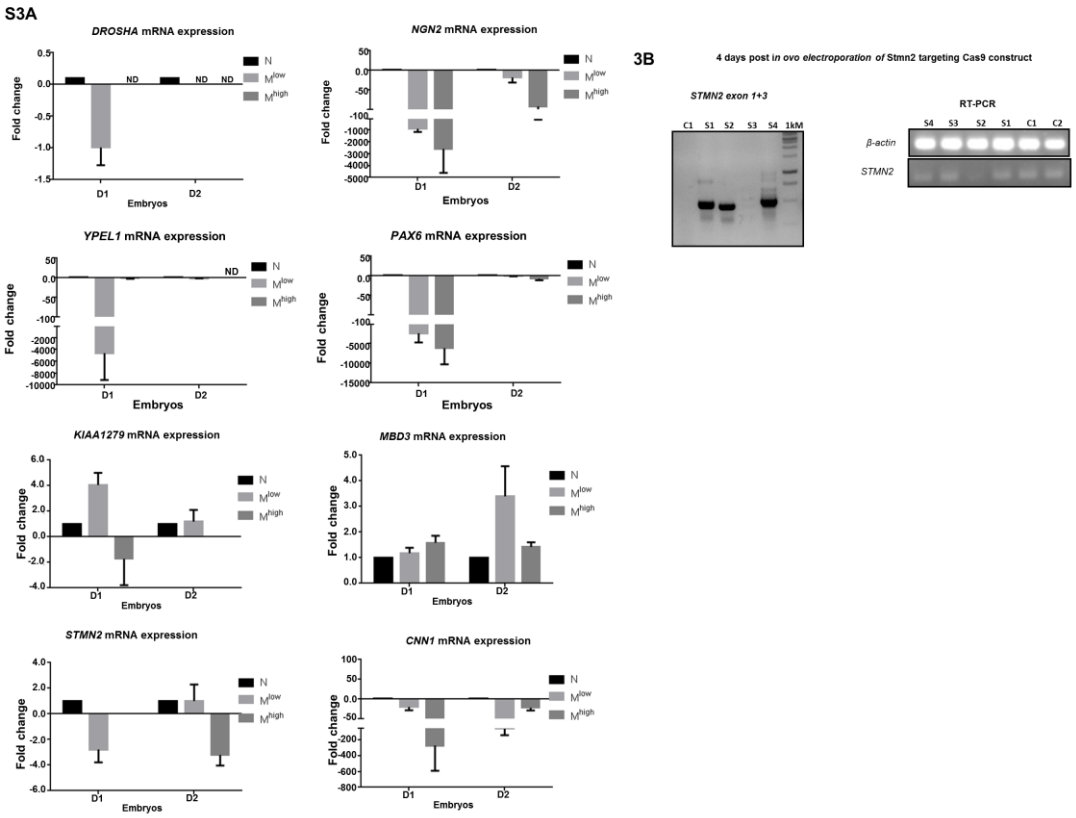

Appendix S1-S3. Related to Figure 3.4. (A) qPCR analysis of Dgcr8-targeted embryos demonstrating the reduced mRNA levels of neural (Neurogenin1, Pax6), cardiac outflow tract (Ypel1), smooth muscle cell (CNN1- positively regulated by DROSHA) genes in Dgcr8-targeted cells (ie. mCherry positive), relative to negatively sorted cells. Normalisation was done with ACTB and RPL32. N=mCherry negative cells, Mlow=mCherry low expressing cells, Mhigh=mCherry high expressing cells, (B) As a negative control to Dgcr8 mutant experiments, we electroporated embryos with the two sgRNA-Cas9 construct targeting the Stmn2 gene. The hindbrains were harvested and extracted genomic DNA and total RNA were analysed by PCR and RT-PCR respectively. Gel shows the frequency (%) of NHEJ mutation mediated by Stmn2-targeting sgRNA-Cas9 system in the hindbrain of chicken embryos by PCR and an RT-PCR analysis of Stmn2 mRNA levels of controls and samples. The chicken β-actin housekeeping gene was used as a reference point. ND- non detectable.

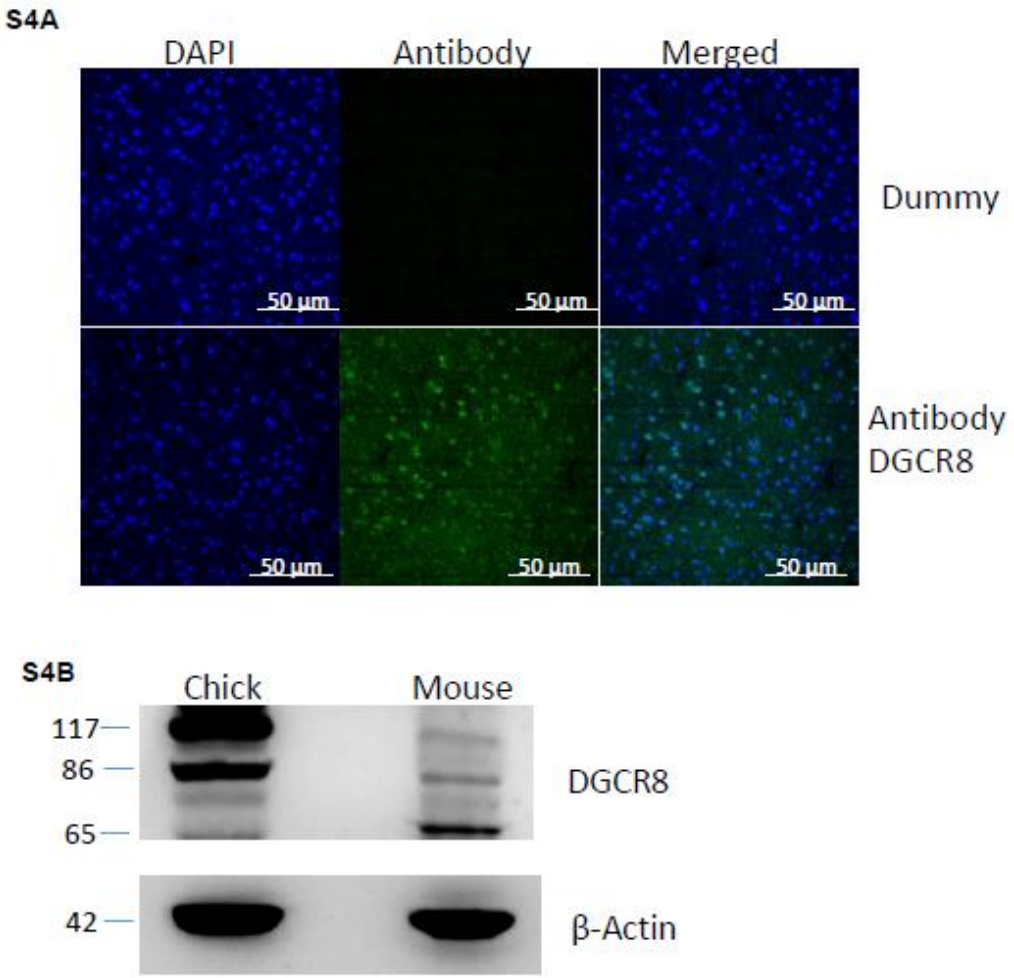

Appendix S1-S4. Related to Figure 3.3 and 3.4. (A) Immunofluorescence images of single and merged channels of the indicated markers from frozen sections of postnatal mouse brain. (B) Validation of the Anti-DGCR8 antibody on chick embryonic brains and postnatal mouse brain by western blot, showing expected 87 and 117 kD bands. The previously observed band at 65 kD has not been identified by the supplier (Abcam).

APPENDIX S2

Table 1. Primary and secondary antibodies, and probes.

Primary antibodies	Target type	Host / Isotype	Company	Dilution
Anti-Human SOX10	NC lineage (not neurons)	Goat Polyclonal	R&D systems	1:200
Anti-p75NTR (D4B3) XP® Rabbit mAb #8238	NC lineage	Rabbit polyclonal	Cell Signalling	1:1500
Anti-HNK1	NC lineage	Mouse IgM	MCRI	1:200
Anti-AP2α (3B5)	NC lineage	Mouse IgG2b	DSHB	1:200
Anti-GD2 (clone 14.G2a)	SAP marker	Mouse IgG_{2a}	BD Biosciences	0.5 µg / $1x10^6$ cells
Anti-MASH1/Achaete-scute homolog 1 antibody (ab38556)	SAP marker	Rabbit polyclonal	Abcam	1:500
Anti-Peripherin (clone 8G2)	SAP &. neuron marker	Mouse IgG	Millipore	1:500
Anti-SA1	SAP lineage marker	Mouse IgG	DSHB	1:20
Anti-B2B1	Symp. neuron lineage	Mouse IgM	DSHB	1:20
Anti-Ki67 (AFFN-KI67-3E6)	Proliferative marker	Mouse IgG2b	DSHB	1:50
Anti-Neurofilament Heavy antibody (NF421)	Neuron marker	Mouse IgG1	Abcam	1:500
Anti-Neurofilament M (145 kDa) Antibody	“	Rabbit polyclonal	Millipore	1:2000
Anti-TH	Neuron CA synth. enz.	Chicken polyclonal	Abcam	1:1500
Anti-TH	Neuron CA synth. enz.	Rabbit polyclonal	Novus Biologicals	1:1500
Anti-Chromogranin B (ab12242)	Neuroendocrine marker. LDCV	Rabbit polyclonal	Abcam	1:700
Anti-Chromogranin C (ab12241)	Neuroendocrine marker.	Rabbit polyclonal	Abcam	1:700

	LDCV			
Anti-PNMT	Chromaffin-spec. adrenaline enzyme	Rabbit polyclonal	ThermoFisher Sci.	1:700
Anti-Human Nuclear Antigen antibody [235-1] (ab191181)	Human-specific marker	Mouse monoclonal IgG	Abcam	1:200
Anti-Mitochondria antibody [113-1] (ab92824)	Human-specific marker	Mouse monoclonal IgG	Abcam	1:1500
Phospho-Smad1/5 (Ser463/465) (41D10)	BMP signaling	Rabbit monoclonal	Cell Signalling	1:100
Secondary antibodies		**Host / Isotype**	**Company**	**Dilution**
Anti-Goat IgG:Alexa 488		Donkey	ThermoFisher Sci.	1:1000
Anti-Goat IgG:Alexa 594		Donkey	ThermoFisher Sci.	1:1000
Anti-Goat IgG:Alexa 647		Donkey	ThermoFisher Sci.	1:1000
Anti-Sheep IgG:Alexa 594		Donkey	ThermoFisher Sci.	1:1000
Anti-Rabbit IgG Alexa 488		Donkey	ThermoFisher Sci.	1:1000
Anti-Rabbit IgG Alexa 594		Donkey	ThermoFisher Sci.	1:1000
Anti-Rabbit IgG Alexa 633		Goat	ThermoFisher Sci.	1:1000
Anti-Mouse IgG-specific:Alexa 488		Goat	ThermoFisher Sci.	1:1000
Anti-Mouse IgM- specific:Alexa 488		Goat	ThermoFisher Sci.	1:1000
Anti-Mouse IgG+M Alexa 594		Donkey	Mol. Probes (A21203)	1:1000
Anti-Mouse IgG Alexa 647		Donkey	ThermoFisher Sci.	1:1000
Anti-Chick IgY Alexa 488		Goat	ThermoFisher Sci.	1:1000
Anti-Chick IgY Alexa 568		Goat	ThermoFisher Sci.	1:1000

Appendix S2 Figures

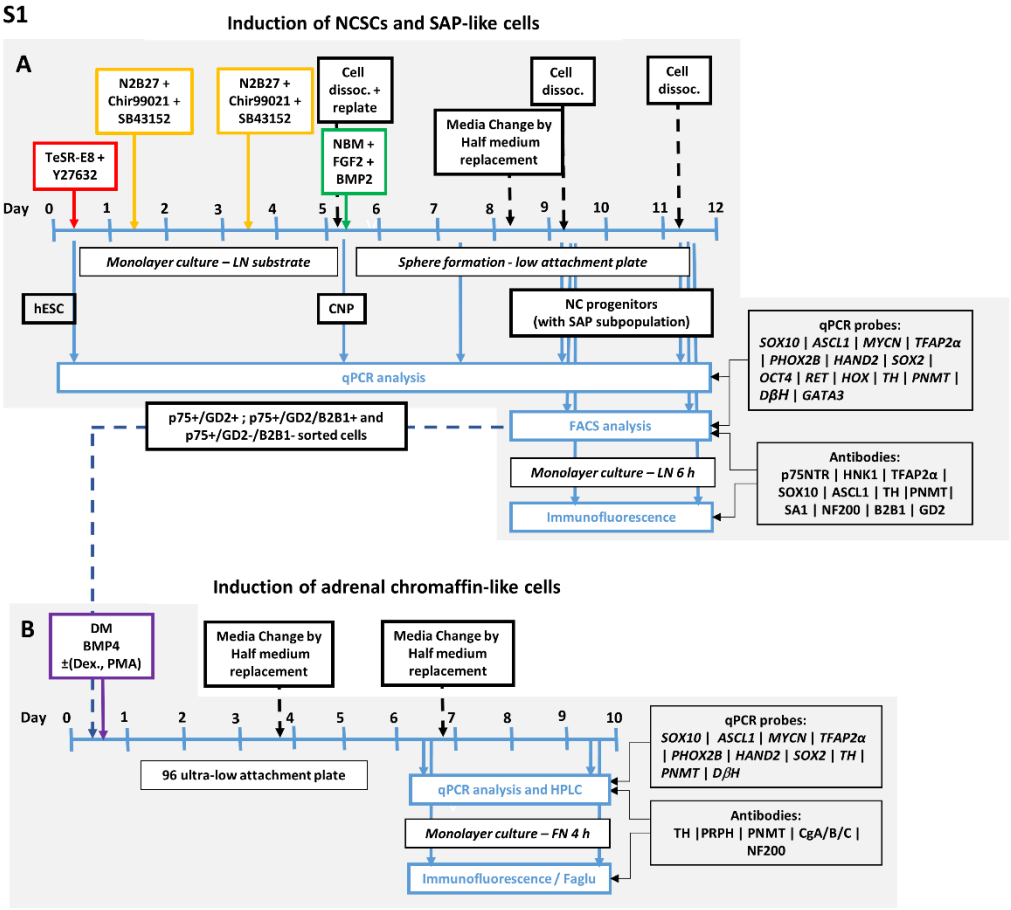

Appendix S2-S1A & B. Detailed schematic illustration of the differentiation protocol of hESCs to NCPC/SAP-like cells and further to chromaffin-like cells. Related to Figure 4.1.

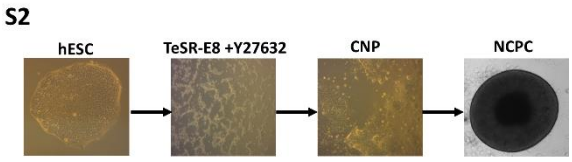

Appendix S2-S2. Bright-field images of stages of differentiation of hESCs into NCPC/SA-like cells. Related to time points in Figure 4.1 and Appendix S2-S1A.

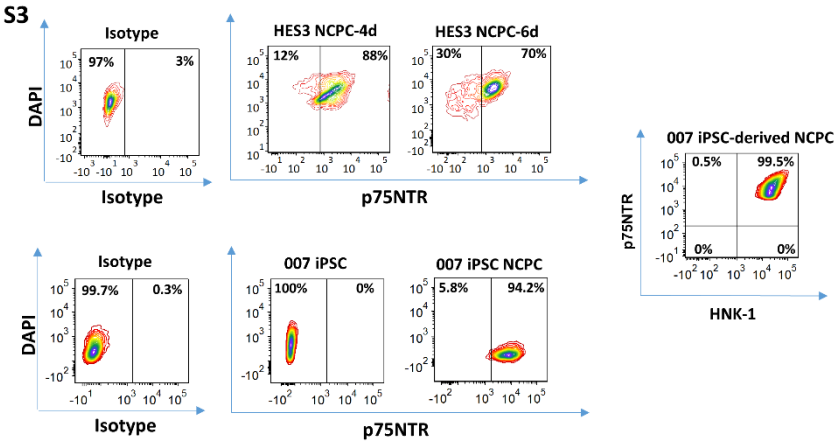

Appendix S2-S3. HES3 hESCs-derived and 007-iPSC-derived NCPC/SAP cells express NC markers similarly to H9 cells. Related to Figure 4.1B. FACS analysis at day 9 and 11 of differentiation of HES3 hESCs and day 9 only of 007 iPSC showing the expression of NCPC marker, p75NTR. The p75NTR positive population was used to gate for HNK-1 expression. Representative plots: Day 9; N = 10 independent experiments and Day 11; N = 10 independent experiments for HES3 hESC and Day 9; N=4 independent experiments for 007 iPSC.

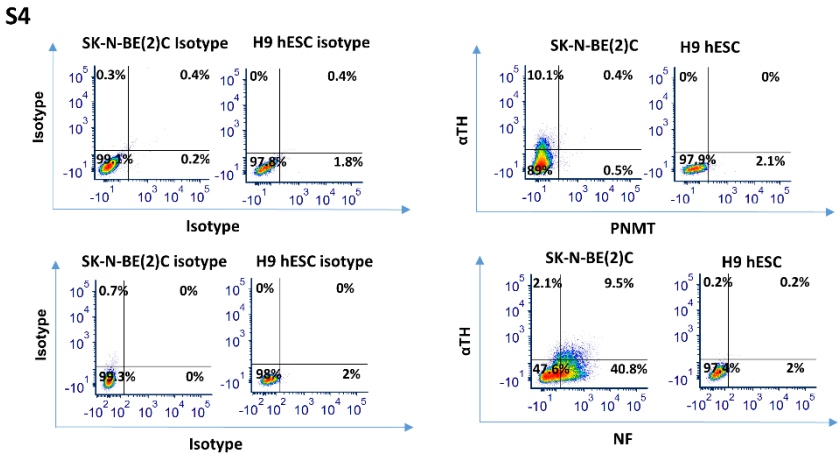

Appendix S2-S4. Neuroblastoma line SK-N-BE(2)C and negative control cells (H9 hESC) FACS analysed for αTH, NF-200 kDa and PNMT. Related to Figure 4.2 and 10. A representative FACS analysis of SK-N-BE(2)C showing the expression of αTH and NF-200 kDa with no expression of PNMT. H9 hESC showing no expression of αTH, NF-200 kDa and PNMT. DAPI was used to gate for cells. N = 3 independent experiments for both cell types.

S5

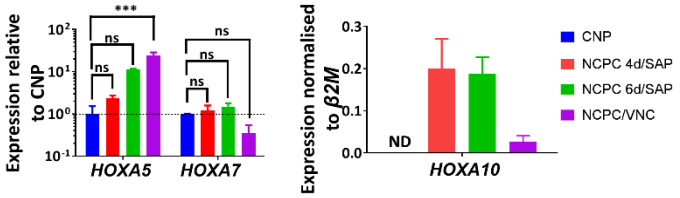

Appendix S2-S5. NCPC/SAP express higher number (trunk) HOX genes compared to NCPC/VNCC (vagal NC). Related to Figure 4.2. QPCR analysis of NCPC/SAP showing the increased expression of HOXA7 and HOXA10 trunk positional markers compared to Vagal NCPC with elevated HOXA5 vagal positional marker. ND: not detected. N = 3 independent experiments.

S6

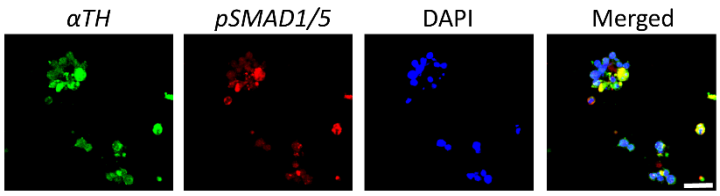

Appendix S2-S6. The downstream signaling effector of BMP4, SMAD1/5, is activated using 50 pg/mL of BMP4 in NCPC/SAP differentiation to chromaffin-like cells. Related to Figure 4.3. Immunofluorescence of chromaffin-like cells in vitro showing the expression of pSMAD1/5, and αTH. Scale bar 20 µm.

S7

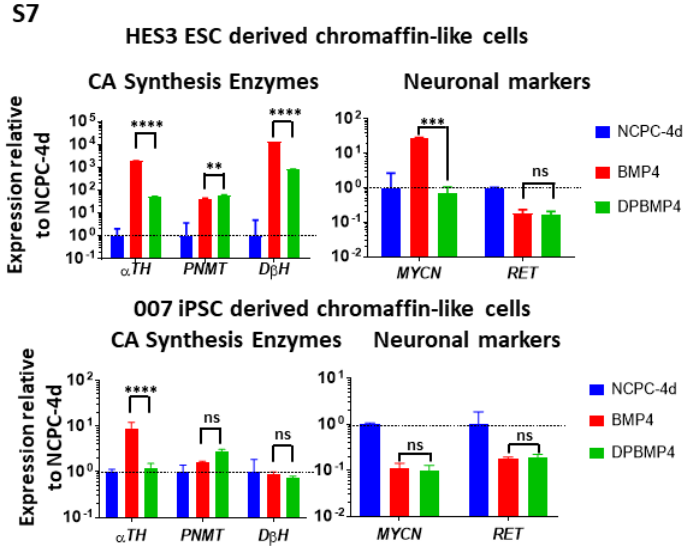

Appendix S2-S7. H9, HES3 hESCs and 007 iPSC-derived chromaffin-like cells express mRNA of catecholamine synthesizing enzymes and express low levels of RET. Related to Figure 4.3. QPCR analysis of HES3 hESCs and 007 iPSC-derived chromaffin-like cells showing the increased expression of CA enzymes and MYCN and RET expression. N = 3 independent experiments. Broadly αTH (especially with BMP4 alone) are upregulated similarly in HES3 and 007 cells but

DβH is elevated only in HES3 not 007 cells, and MYCN is downregulated in 007 cells but transiently upregulated in HES3s.

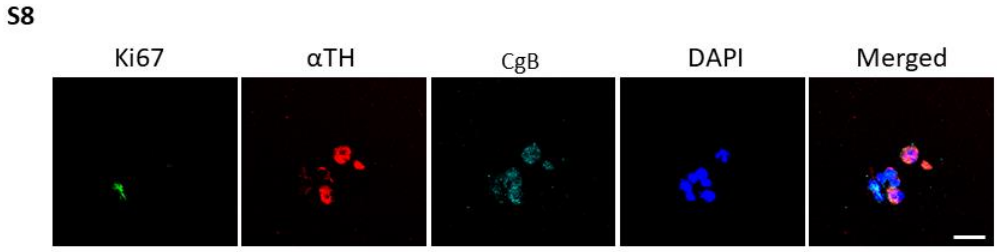

Appendix S2-S8. hESC-derived chromaffin-like cells have limited proliferative capacity. Related to Figure 4.3. Immunofluorescence of nuclear Ki67 in αTH+/CgB+ chromaffin-like in a cell aggregate after 9 days chromaffin differentiation. Note that Ki67 signal here is in cells with low αTH and CgB. Scale bar 20 µm.

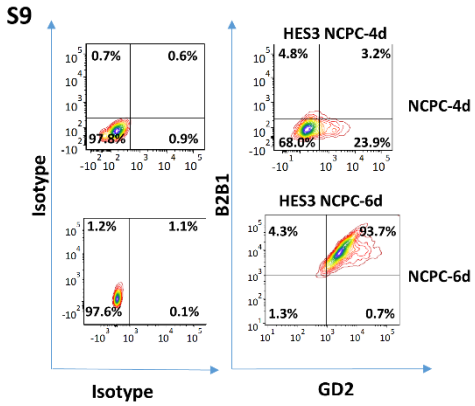

Appendix S2-S9. HES3 hESCs-derived NCPC/SAP cells express markers of NC and SAP lineages. Related to Figure 4.5. FACS analysis of NCSC-4d at day 9 and NCSC-6d at day 11 of differentiation of HES3 hESCs (initially gated by p75NTR expression). GD2 (SA lineage marker) appears in some cells initially but later, most cells are B2B1/GD2 double-positive. Day 9; N = 10 and Day 11; N = 10.

S10

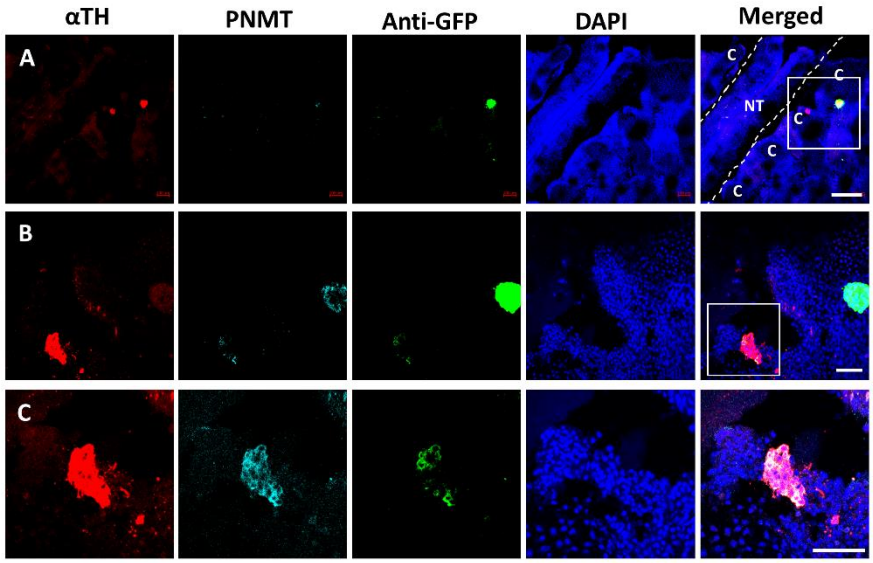

Appendix S2-S10. Transplanted NCPC/SAP cells in vivo integrate, migrate and differentiate into cells expressing chromaffin markers, αTH and PNMT. Related to Figure 4.7. (row A) Human GFP+ NCPC/SAP-like cells grafted into 2 day quail embryo trunk displace latero-ventrally and show SAP and chromaffin markers. Frontal-oblique section of ventral neural tube (NT) and somitic vertebral cartilage (C) in 4-day transplant. Scale bar 50 µm.

(row B) Boxed area in A is enlarged (next section ventral to A) to show human cells stained for αTH and PNMT and identified with anti-GFP. Scale bar 250 µm. (row C) Enlargement of area boxed in B showing co-expression of SAP and chromaffin markers. Scale bar 250 µm.